THE CLUSTER OF GALAXIES ABELL 1060

by

Robert John Smyth

PhD

University of Edinburgh

1980

ABSTRACT

This thesis describes the implementation and results of a programme of photometry of the relatively nearby southern cluster of galaxies and X-ray source, Abell 1060 = Hydra I.

Photographic photometry in B and V wavebands of galaxies in a $\sim$22 degree^2 region centred on this cluster have been obtained on the basis of measurements of four U.K. Schmidt telescope plates by the COSMOS measuring machine at the Royal Observatory, Edinburgh. The feasibility of using the COSMOS machine to derive reliable isophotal magnitudes of bright and faint galaxies is demonstrated.

Multiaperture photoelectric (U, B, V and R-band) photometry has been secured of sixteen galaxies in the field of the cluster, including seven NGC and IC systems. Besides providing photometric calibration, these observations permit the total magnitudes and colours of several galaxies to be derived.

The positions and magnitudes of over 5000 galaxies, supplemented in many cases by morphological classifications, by micrometric measurements of dimensions and alignment, and by redshift data, have been analysed to determine the static and dynamical properties of A1060. The cluster is symmetric, centrally condensed, and rich in disk galaxies; members segregate radially by morphological type, with spiral galaxies generally farthest from the centre.

The V-band luminosity function of A1060 has been constructed. It is similar in form but different in detail from those of other clusters. The colour-magnitude relation of early-type galaxies in

A1060 is outlined, and is shown to be inconsistent with one prediction of a standard theory of the morphological evolution of galaxies and clusters.

Visual searches for low surface brightness members of A1060 are described. It is suggested that fewer such galaxies exist than an extrapolation of the luminosity function for all galaxy types to faint magnitudes would predict.

Peculiar properties of four galaxies near the centre of the cluster are interpreted in terms of the influence of their environments. Three are anaemic spirals, for which there is strong evidence that an era of gas depletion has recently begun. The first-ranked member, N3311, is an extended system of low mean surface brightness, and may represent a D galaxy in the early stages of evolution. These observations suggest that the cluster Abell 1060 is relatively young in dynamical terms.

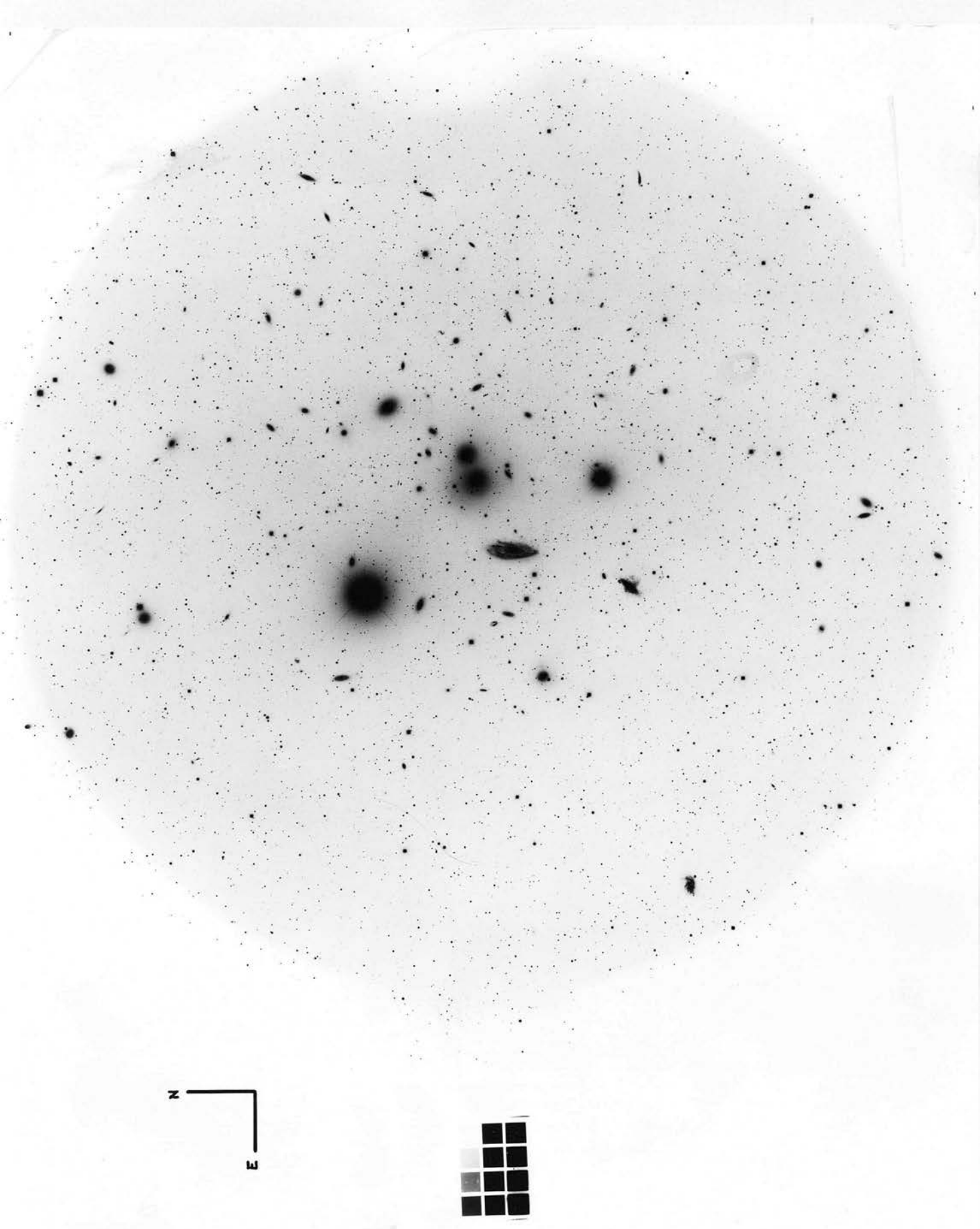

The cluster of galaxies Abell 1060. Photographed by M.G. Smith at the prime focus of the 4-metre reflector at Cerro Tololo Interamerican Observatory. The central 0.74 degree^2 of the cluster is represented, at a scale of 18.56 arcsec mm^{-1}. (For further particulars of plate 995, see page 169).

DECLARATION

This thesis has been composed entirely by the undersigned candidate and with the exception of some of the astronomical observations described in Chapter Four, all work presented herein is his own. (Regulation 2.4.15)

Most of the material presented in Chapter Four was published in Monthly Notices of the Royal Astronomical Society 190, 631 (1980) under the title "Multiaperture Photoelectric Photometry of Galaxies in the Hydra I Cluster", by R.J. Smyth and R.S. Stobie. (Regulation 2.4.11)

Signed: R.J. Smyth. Date: 12 March 1980.

CONTENTS

Learning without thought is labour lost;

Thought without learning is perilous.

- K'ung Fu-tzu (Confucius)

Analects. Bk. ii

CHAPTER 1

INTRODUCTION

1.1 The Clustering of Galaxies

The apparent congregation of galaxies in clusters, observable over immense distances down to the limiting magnitude of present sky surveys, is one of the most striking characteristics of the large-scale distribution of visible matter in the universe. Studies of galaxies and their clustering are consequently vital to our comprehension of the physical world.

The cataloguing and characterisation of galaxies was underway long before their true nature came to be generally recognised. Even the mere thirty-three verifiable extragalactic "nebulae" in the third and final catalogue of Messier (1781) suffice to illustrate a concentration of bright galaxies in a region of the sky that contains the constellations of Virgo and Coma Berenices. The much larger compilation of W. Herschel (1784), with more than a thousand truly extragalactic objects, revealed the apparent large-scale gradients in numbers of galaxies across the northern sky (due to optical obscuration in the plane of our own Galaxy); this compilation was the forerunner of the General Catalogue (J. Herschel 1864) which reveals several clusters (Waters 1873). At least four distinct groups, in Virgo, Ursa Major and two in Fornax, are apparent in the distribution of the nearby galaxies listed in the catalogue of Shapley & Ames (1932).

Recognition of the vast numbers of clusters came with the advent of photographic sky surveys of the northern hemisphere, in particular the Lick Observatory 20-inch Astrographic Survey as inspected by Shane and Wirtanen (Shane & Wirtanen 1954, 1967; Shane 1956; Shane, Wirtanen & Steinlin 1959; Kron & Shane 1974) and the National Geographical Society - Palomar Observatory Sky Survey. Stringent criteria became necessary in the study of large volumes of space in order to restrict selection to manageable numbers. Abell (1958) crudely characterised 2712 of the very richest clusters visible on Palomar plates, and from the same material Zwicky et al. (1961-8) catalogued some 9700 recognisable associations, representing an estimated 1.6×10^7 galaxies. Since the commissioning of the ESO and UK Schmidt telescopes, complementary surveys of the southern sky have been in progress, although specialised lists of southern clusters already exist (e.g. Duus & Newell 1977; Braid & MacGillivray 1978).

The surface distribution of galaxies as recorded by northern surveys has been subjected to statistical analysis since the 1950s (e.g. Neyman & Scott 1952). Correlation techniques involving angular separations have been developed by Peebles and his co-workers, and correlation functions determined which give the "excess" probabilities of finding 2-galaxy and 3-galaxy configurations (discussed by Fall et al. 1976). These functions vary as simple power laws of the angular scale, indicating no preferred scale of clustering at sizes up to 5 arc degrees. Clusters, therefore, may be only the high-density cores of extensive clouds of galaxies which may represent (cf. Soreira & Peebles 1977) substantially more than 80%

of all visible galaxies. Separate correlation analyses of the different morphological populations of galaxies reveals a greater clustering tendency among elliptical galaxies than other types (Davis & Geller 1976).

Important though statistical studies are, they are comparatively uninformative regarding the composition and dynamics of individual systems of galaxies. It has become increasingly evident in recent years that the location of a galaxy with respect to the centre of a cluster may play a significant part in determining its appearance and properties. A new classification scheme for galaxies was introduced by van den Bergh (1976) which explicitly recognised the existence of peculiar disk systems (anaemic spirals) that are often found in clusters. Strom & Strom (1977, 1978a,b,c,d, 1979a) have demonstrated that elliptical galaxies found in the cores of rich clusters where the density of galaxies is high tend to be of smaller characteristic size than those ellipticals of comparable central surface brightness that are found in the outskirts of clusters; they also find a corresponding variation of the disk colours of galaxies that are classified as SO types (Strom & Strom 1978e, 1979b).

1.2 Properties of Rich Clusters

The subject of rich clusters and their properties has been extensively reviewed by Abell (1975), Bahcall (1977a) and by van den Bergh (1977a). Some aspects are considered in later chapters, and only brief outlines of definitions of cluster size and type are necessary here.

By general acquiescence the term "rich cluster" has come to

mean any sufficiently populous grouping of galaxies comparable to those catalogued by Abell (1958). The apparent population of a cluster may depend on the surroundings relative to which it is viewed, but the structures of rich clusters do vary widely and several different classification schemes have been proposed. Shapley (1933) drew an analogy between loose, irregular systems of galaxies and open star clusters of this Galaxy; Abell (1965) uses the term irregular clusters, to distinguish them from the more centrally concentrated regular clusters. Bahcall (1977a) introduced an intermediate class to make the transition smoother. The regular, intermediate and irregular clusters correspond quite closely to the compact, medium-compact and open categories of Zwicky et al. (1961-8). Morgan (1961) and de Vaucouleurs (1961b) each suggested discriminating according to galactic content, but this in itself is not a satisfactory criterion because it is difficult or impossible to classify galaxies at the distance of remote clusters; the same objection may be raised to the scheme of Melnick & Sargent (1977). However, the composition of clusters appears to correlate with their form.

Rood & Sastry (1971; RS) proposed a useful morphological classification system for clusters which bears strong resemblance to the original Hubble scheme for galaxies; six classes are distinguished according to the projected distribution of the ten brightest members in each cluster. Bautz & Morgan (1970; BM) exploit the optical contrast of the brightest galaxy relative to other member galaxies in their five-part system, in which the dominance of the first-ranked member is greatest in type I clusters and least in type III. White (1978) has described an elaboration of the Bautz-Morgan system that

is applicable to poor as well as to rich clusters. The BM classification, although vulnerable to chance superpositons of non-members, is of special interest in connection with possible secular changes in the distribution of luminosity among brighter cluster members. In common with RS types, it is often supplemented with estimates of cluster richness on Abell's (1958) scale, for neither scheme incorporates a "population" parameter.

Clusters, like galaxies, have no definite boundary, and three general approaches have been made to the problem of defining cluster size. Zwicky et al. (1961-8) adopt the mean diameter of an isopleth that represents a fixed fraction of the field density around a cluster, but this definition is distance-dependent (Peach & Beard 1969; Noonan 1972). An alternative, applicable only to regular and symmetric clusters, is to fit functions with characteristic length scales to the projected number density profiles of galaxies. Although the isothermal (Emden) sphere model has usually been adopted, and is considered later in this thesis, previous representations have involved the de Vaucouleurs (1948) "$r^{\frac{1}{4}}$" law, Maxwellian (i.e. trivariate normal) distributions (Scott 1962), and King (1966) dynamical models (e.g. Rood et al. 1972). Each of the above represent the observed profiles almost equally well over the definable range of number density, which in clusters is a mere two decades because of the contaminating effects of non-members. Thirdly, specific mean projected distances between cluster members may be estimated (e.g. Noonan 1972; Austin & Peach 1974; Hickson 1977), which have the advantage that they do not depend on the structure of the cluster. Attempts have been made to exploit the apparent sizes of clusters, on

the assumption that rich clusters are of fixed dimensions, to determine the cosmological deceleration parameter of cosmological world models. They have not, however, been conspicuously successful (e.g. Bruzual & Spinrad 1978).

1.3 Cluster Luminosity Functions

The relevance of the frequency distribution of luminosities of galaxies that represent particular samples of space, to a wide range of extragalactic problems has been stressed by Schechter (1976). These distributions are termed luminosity functions and may be determined for individual clusters.

Luminosity distributions have in principle been available since very early times. The Herschelian symbols vB, B, F etc. were a rough attempt at the establishment of a nebular photometry. Ames (1923) published preliminary total magnitudes of 20 galaxies in the Virgo-Coma region, estimated by visual comparison with stellar images on photographic plates. The existence of a consistent local maximum in the numbers of bright members of the Virgo, Perseus and Ursa Major I clusters was commented on by Baade (1928).

A luminosity function for bright nearby galaxies that approximates a gaussian curve was derived by Hubble in the course of a famous study (Hubble 1936a,b). Doubts about its adequacy, however, followed Shapley's (1939) discovery of the Sculptor and Fornax dwarf members of the Local Group. Zwicky argued that no maximum in the luminosity function could exist, and presented evidence (Zwicky 1957) that the total number of galaxies per unit volume inside clusters

increased exponentially towards faint magnitudes. Subsequent studies (e.g. Abell 1976; Oemler 1974) have shown this to be a reasonable approximation, except at the bright end. Abell (1962, 1976) and Schechter (1976) have proposed alternative representations; these are contrasted with the Zwicky function in Figure 4 of Bahcall (1977a).

Three immediate questions concerning the luminosity functions of galaxies have yet to be answered. The first concerns which of the analytic representations is the most satisfactory; the second, whether it is constant from place to place in the universe (cf. Felten 1977); the third, whether it is constant in time. Universality of the luminosity functions of galaxies in rich clusters is an assumption implicit in, for example, the determination of the luminosity function of all galaxy systems from single galaxies to rich clusters (Bahcall 1979), otherwise the number of galaxies in a group in the range of the first few magnitudes (e.g. Abell 1958) would be a poor indicator of the total population of the group. Universality is obviously an attractive hypothesis, but recent photometry of rich clusters, and numerical simulations of their evolution, casts some doubt on the assumption. Further photometry of rich clusters to faint limits is required, and a substantial part of this thesis is devoted to the problem of photometry of one particular cluster that is sufficiently nearby for very faint members to be examined.

1.4 The Organisation of this Thesis

It has been found necessary to dispense with a strictly chronological approach to presentation.

In Chapter 2, the distribution of galaxies in and around the Abell 1060 cluster is considered on three scales: within a region of dimensions 45 by 23 arc degrees, on the basis of published data; in a smaller area encompassing ∿100 degree^2, examined on original photographic plates; and within a central ∿22 degree^2 that was scrutinised with the aid of the COSMOS machine. The structure of the cluster as inferred from these counts of galaxies is described, and the geometric parameters of the galaxies are investigated.

Chapter 3 presents a compilation of the radial velocities of galaxies in the field of this cluster. Additional redshifts of galaxies are determined from measurements of objective prism spectra.

Photoelectric photometry of galaxies in A1060 is detailed in Chapter 4. The (U - B) colour-magnitude relation for early-type galaxies in the cluster is derived and the total blue-band magnitudes of several members are estimated.

The derivation of photographic magnitudes of a large number of galaxies on the basis of measurements made by the COSMOS machine is discussed in some detail in Chapter 5. The photoelectric observations of Chapter 4 are shown to provide a satisfactory means of calibrating this photometry. The reliability of the V-band magnitudes is demonstrated by comparable reductions of a second plate.

In Chapter 6 an assessment of the combined photometric and optical information is presented. The luminosity function of A1060 is constructed and compared with those of other clusters. The properties of the brightest galaxy are discussed in terms of a theory

of evolution, and in terms of the previously constructed colour-magnitude diagram. Three peculiar spiral galaxies in the cluster are examined.

An account of a search for dwarf galaxies in the Hydra I cluster is given in Chapter 7.

In the eighth and final chapter, some previous results are employed to determine the average mass-to-luminosity ratio of the composition of the cluster; the main conclusions of previous chapters are summarised, and the implications discussed briefly.

The basic photometric data, morphological classifications and finding charts in respect of the brighter galaxies in the vicinity of A1060 are presented in a pair of Appendices that follow the main text.

Table 1.1

Abbreviations and Catalogues

Abbreviations

AM	Abell & Mihalas (1966)
CM	Coarse Measurement or Coarse Mode (re COSMOS)
COSMOS	Acronym for the system at ROE that measures the Co-Ordinates, Sizes, Magnitudes, Orientations and Shapes of images on photographic plates (Pratt 1977)
CTIO	Cerro Tololo Interamerican Observatory
ESO	European Southern Observatory
HMS	Humason, Mayall & Sandage (1956)
MM	Mapping Measurement or Mapping Mode (re COSMOS)
ROE	Royal Observatory, Edinburgh
RI	Relative Intensity
SAAO	South African Astronomical Observatory
SRC	Science Research Council of the U.K.
UKST(U)	United Kingdom Schmidt Telescope (Unit)
VVC	See RC2

Catalogues

a) Prefixes

3U	Giacconi et al. (1974)
4U	Forman et al. (1978)
2A	Cooke et al. (1978)
A	Abell (1958)
BS	Yale Catalogue of Bright Stars
IC ≡ I	Dreyer (1895, 1908)
MCG	Vorontsov-Velyaminov et al. (1962-8)
NGC ≡ N	Dreyer (1888)
SAO	Smithsonian Astrophysical Observatory Star Catalogue

b) Non-prefixes

CGCG	Zwicky et al. (1961-8)
RC1	de Vaucouleurs & de Vaucouleurs (1964)
RC2	de Vaucouleurs et al. (1976)
RNGC	Sulentic & Tifft (1973)

CHAPTER 2

STATIC PROPERTIES

2.1 A1060 Overviewed

The cluster of galaxies Hydra I, located at approximately α_{1950} = 10h 34m, δ_{1950} = -27^{o} 16' (revised estimates of position and redshift are quoted herein) is a relatively nearby southern cluster visible through a moderately rich star-field at a galactic latitude of $+26^{o}.5$. It appears to have been recorded as a group of nine galaxies during compilation of the New General Catalogue of Galaxies and Clusters of Stars (Dreyer 1888), and is the fifth entry among twenty-five in a list devoted to groups of galaxies drawn from both galactic hemispheres (Shapley 1933). In the standard catalogue of rich clusters found north of declination -27^{o} (Abell 1958), Hydra I is the unrepresentative 1060th of 2712; it is too southerly and too local for inclusion in the homogeneous subsample of this catalogue. Only two clusters belong to Abell's distance class D = 0, and of these A1060 has the lowest redshift. By contrast, Hydra II = A732 was for many years the cluster with the highest measured velocity of recession and many past allusions to the "Hydra cluster" refer to Hydra II (e.g. Allen 1973).

The distribution of galaxies in Hydra I was first investigated by Zwicky (1941, 1942), who emphasised its spherical symmetry and its structural similarity to the Coma = A1656 cluster, and quoted the first observational determination of its redshift (3950 km s^{-1} for the member NGC 3309). Zwicky determined the radial dependence of the

number density distribution of galaxies from counts on 0.5m Schmidt telescope plates, and estimated the structural index of the cluster on the isothermal sphere model to be four minutes of arc. His counts were later analysed by Sharov (1959) to deduce the three-dimensional structure of Hydra I. Kwast (1966) undertook independent counts of galaxies on 1.2m Schmidt plates, in two wavebands, and for the brighter systems confirmed Zwicky's estimate of the structural index. Noonan (1972) reanalysed all this data to derive a mean radius of the cluster of $\overline{r}_c \simeq 48$ minutes of arc.

Abell (1958) assigned to A1060 a richness class of R = 1, implying between 50 and 79 members within the two magnitude range faintwards of the third brightest member and within $4.6 \times 10^5/cz$ mm. $\simeq 103/z$ arcseconds of the cluster centre on the scale of the Palomar Sky Survey plates, where z denotes mean redshift. 51 galaxies were counted by Sandage & Hardy (1973) within an angular diameter of $137(1 + z^2)/z$ arcseconds and in the magnitude range from the third brightest galaxy in A1060 to $2\frac{1}{2}$ magnitudes fainter. Zwicky (1941) inferred "roughly 200" members in the range of the brightest three magnitudes from counts that covered some 50 square degrees in the vicinity, and suggested that this represented less than half the population of the cluster, which he considered to have a diameter of at least ten degrees.

Hydra I has been classified by Rood & Sastry (1971) as a type C and by Bautz & Morgan (1970) as a type III cluster, indicative of a core-halo structure with no dominant galaxies. Although the evident symmetry and central concentration of Hydra I (e.g. Kwast 1966;

Rudnicki 1967) is characteristic of rich regular clusters (Abell 1965), it also has properties more typical of irregular clusterings such as that in Virgo. Modern X-ray observations have confirmed (Ives & Sanford 1976) that A1060 (= 3U 1044-30 = 4U 1033-26 = 2A 1033-270) is a relatively weak source of X-ray emission, with a 2-10 kev luminosity $L_x \simeq 2 \times 10^{43}$ erg s^{-1} on the basis of both the third UHURU (Giacconi et al. 1974) and second Ariel V (Cooke et al. 1978) satellite observations (Gursky & Schwartz 1977; Bahcall 1977a). A discrete emitter at radio wavelengths has also been reported in the direction of the centre of A1060, which may be associated with either or both of the giant member galaxies N3309 and N3311 (Disney & Wall 1977).

Photographic photometry of bright members of the system of globular clusters centred on N3311 (Smith & Weedman 1976), supplemented by photometric parameters for the three brightest "elliptical" galaxies, were the basis of a recent estimate, Δ(Hya I) = 40.5(1 ± .10:) Mpc, of the distance of the Hydra I cluster (de Vaucouleurs 1977b). An arithmetic error and an underestimate of the total magnitude B_T of N3311 impair this determination, but it is unlikely to be in error by more than 40%. The working approximation Δ(Hya I) = 40 Mpc is adopted hereafter, except where otherwise implied by a stated value of the Hubble 'constant' H_o. For a cosmological recessional velocity of 3390 km s^{-1} (Chapter 3), Δ = 40 Mpc corresponds to a local value of H_o of 85 km s^{-1} Mpc^{-1}.

2.2 Visual Impressions of the Large-Scale Structure

Since an angular extent of 10^o (Zwicky 1941) corresponds to a linear

diameter of 7 Mpc at 40 Mpc, the question arises as to whether A1060 is part of a galaxy complex or supersystem such as those described by de Vaucouleurs (1971), of characteristic scale length $\Lambda \simeq 10$ Mpc.

A study of the surface distribution of galaxies brighter than the 13th magnitude in the catalogue of Shapley & Ames (1932) reveals a large ellipsoidal cloud complex containing galaxies of various types, at low galactic latitudes in Hydra (de Vaucouleurs 1956a,b). This cloud extends westwards from A1060 ($l = 270^{o}$, $b = +26^{o}$) and the Antlia group ($l = 273^{o}$, $b = +19^{o}$) across some 40^{o} in galactic longitude and 20^{o} in latitude, nearly parallel to the galactic plane. A plot of the distribution of the galaxies in this area that are listed in the Revised New General Catalogue (Sulentic & Tifft 1973) reveals all three associations (Figure 2.1).

Visvanathan & Griersmith (1979) have decomposed the main Hydra complex into clouds A and B with a velocity differential of 1400 km s^{-1}, the north-westerly cloud B with a redshift similar to that of A1060. However, an enlarged sample of redshifts drawn from Sandage (1978) suggests that this demarcation is artificial (inset, Figure 2.1). The mean velocity of recession of the Hydra cloud as a whole is about 2250 km s^{-1} relative to the Local Group, and most members are probably in the foreground of A1060 and the Antlia group. The loose N2997 group = G8 (de Vaucouleurs 1975) at $l = 250^{o}$, $b = +19^{o}$ is closer still, and is represented by the peak at $\sim$500 km s^{-1} in the frequency distribution of velocities.

To gain an independent insight into the large-scale structure

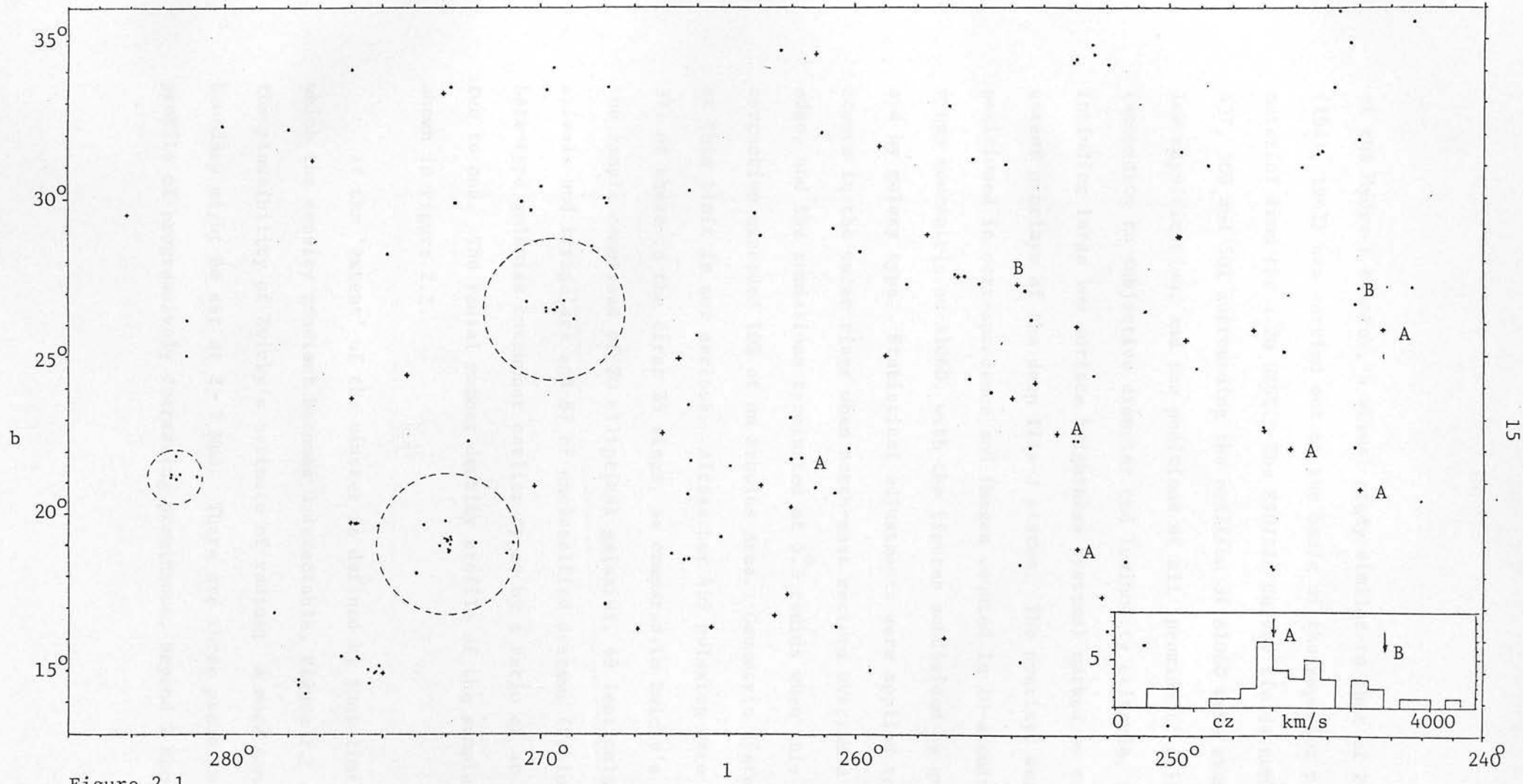

Figure 2.1

The surface distribution in galactic coordinates (l,b) of galaxies listed in the RNGC (Sulentic & Tifft 1973) which are visible in a 45° x 23° region encompassing the Hydra I cluster (269°,26°), Antlia group (273°,19°) and N3557 group (282°,21°). The Hydra cloud extends westwards from $l \simeq 275°$. The inset shows the frequency distribution of "indicative velocities" relative to the Local Group of those galaxies (outside the dotted circles, and shown as crosses in the plot) of known redshift. "A" refers to Hydra cloud A, "B" to cloud B after Visvanathan & Griersmith (1979).

of the Hydra I cluster, a visual study similar to that of Zwicky (1941, 1942) was carried out on the basis of the superior plate material from the 1.2m UKST. The ESO/SRC Survey fields number 436, 437, 500 and 501 surrounding the position of A1060 were examined at low magnification, and the positions of all 'prominent' galaxies (according to subjective diameter and luminosity criteria, and including large low surface brightness systems) marked on transparent overlays of the deep IIIa-J plates. The overlays were then positioned in correspondence and images counted in 10-arcminute rings concentric on A1060, with the figures subdivided by quadrant and by galaxy type. Statistical adjustments were applied to the counts in the outer rings when north-east sectors overran a field edge, and the summations terminated at $5^{\circ}.3$ radius when this correction exceeded 10% of an annulus area. Geometric distortion at this limit is not serious. Altogether 459 galaxies were recorded, 371 of these in the first 25 rings, as compared to Zwicky's 374; the sample comprised of 20 elliptical galaxies, 49 lenticulars, 303 spirals and irregulars and 87 of unclassified systems (Table 2.1). Late-type galaxies outnumber earlier types by a ratio of at least two to one. The radial number density profile of the sample is shown in Figure 2.2.

If the 'extent' of the cluster is defined by that limit at which the density gradient becomes undetectable, Figure 2.2 confirms the plausibility of Zwicky's estimate of radius; a more conservative boundary might be set at 2 - 3 Mpc. There are three peaks in the profile of progressively decreasing prominence, beyond 2 Mpc; all

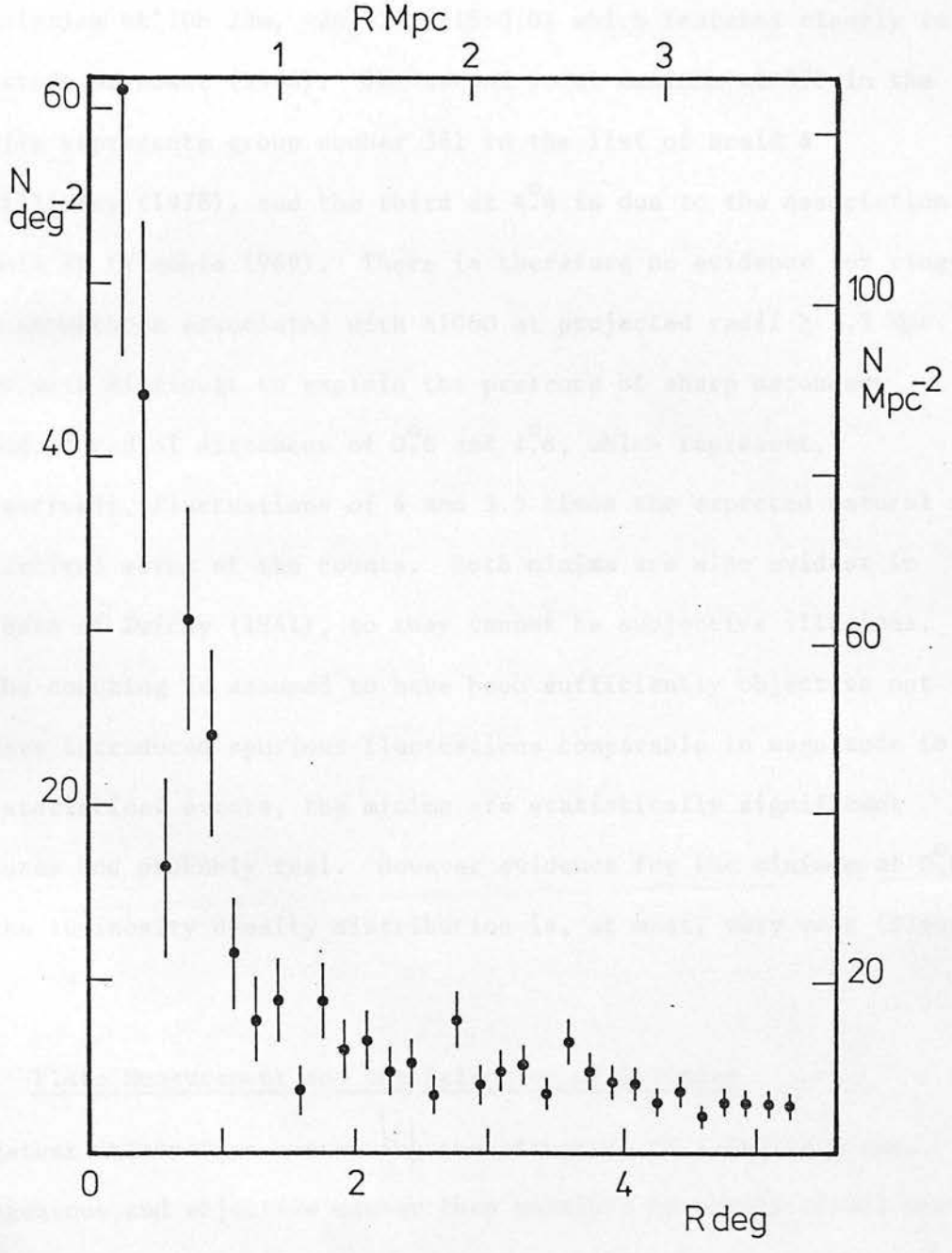

Figure 2.2

The radial surface density distribution of "prominent" galaxies within $5^{\circ}.3$ of the centre of A1060 as seen in projection. Discrete peaks in the profile beyond $\sim$1.5 Mpc are due to identifiable groups of galaxies.

are attributable to localised clusterings. The most obvious, at a projected separation of $2^{\circ}.75$ from the centre of A1060, is the group of galaxies at 10h 23m, -26° 24' (1950.0) which features clearly in the study of Kwast (1966). The second local maximum at $3^{\circ}.6$ in the profile represents group number 381 in the list of Braid & MacGillivray (1978), and the third at $4^{\circ}.4$ is due to the association Klemola 11 (Klemola 1969). There is therefore no evidence for ring-like structures associated with A1060 at projected radii $\gtrsim$ 1.5 Mpc. It is more difficult to explain the presence of sharp secondary minima at radial distances of $0^{\circ}.6$ and $1^{\circ}.6$, which represent, respectively, fluctuations of 4 and 3.5 times the expected natural statistical error of the counts. Both minima are also evident in the data of Zwicky (1941), so they cannot be subjective illusions. If the counting is assumed to have been sufficiently objective not to have introduced spurious fluctuations comparable in magnitude to the statistical errors, the minima are statistically significant features and probably real. However evidence for the minimum at $0^{\circ}.6$ in the luminosity density distribution is, at most, very weak (Figure 6.7).

2.3 Plate Measurement and the Selection of Galaxies

To gather information concerning the structure of A1060 in a more homogeneous and objective manner than possible by purely visual means, the COSMOS machine was assigned to measure the central $\sim$22 degree^2 of three short-exposure (B, V and R waveband) UKST plates on which were recorded the cluster and its surroundings. The particulars of the V and R plates are included in Table 5.1. Operating in its

Coarse Mode (CM), COSMOS measured the positions, extents, minimum transmissions (measures of maximum surface brightness), areas, and quadrants of the orientation of tens of thousands of images that registered on each plate, and transferred the information to magnetic tape for off-line access by computer.

Rapid separation of the parameter sets which refer to galaxies from those that refer to foreground "field" stars is usually attempted at this stage by the application of quantitative classification criteria which are optimised for each plate in question. Until recently such easily measurable gross parameters as image shape (Tyson & Jarvis 1979) or surface brightness (e.g. Oemler 1974) have been the only practicable discriminators of image type; see Godwin & Peach (1977) for some comments on the efficacy of these criteria. MacGillivray et al. (1976a) have shown that the most successful discriminator for the sorting of COSMOS CM data of individual plates is a plot of the logarithm of the image area against the minimum transmission in each image; galaxies and stars segregate by surface brightness, the demarcation varying with image size and frequently with position on the plate. Such variations can sometimes be adjusted for, but this was not the case for the plates of A1060. As a result the application of classification criteria determined for sample areas on each plate failed to sort galaxies from stars over the full areas of the scans with any reliability. Additional factors contributing to the low ($\sim$40%) success rate were the comparatively high proportion of blended star images recorded at this galactic latitude, some of which mimic the properties of galaxies, and the

relative granularity of the emulsions involved (Table 5.1). Following the precedents of Godwin & Peach (1977) and Dressler (1978b), the elimination of the stars was instead accomplished by visual inspection.

The dataset pertaining to plate R1347 was selected for sorting, as a compromise between the desirability of a faint limiting magnitude to detect low surface brightness galaxies on one hand, and conversely of a bright limit to minimize the generation of spurious shredded images within the haloes of bright objects, and which presented a manageable exercise in manual data handling, on the other. COSMOS detected 158000 images during measurement of this plate, 55000 of which were less than ten units (1 unit = 64 μm^2) in area and attributable mainly to grain clumping in the emulsion. The remainder were treated as valid images and displayed in the form of computer listings and finding charts.

Scott (1962) notes that the probability that a galaxy is identified and counted depends on, among other factors, the state of the observer at the time of counting. Sorting proceeded at the rate of roughly one square degree per thirteen hours, so to mitigate the effect of possible day-to-day variation of the identification criteria, the 49 sub-regions of the scan area were inspected in semi-random order, though tending from centre outwards. Coverage of different quarters of the scan was provided by four different IIIa-J plates; that representing the south-west was affected by atmospheric haze, whereas the plate of the north-east quarter had a denser sky background exposure and the images on it were slightly trailed. Offsetting

this patchwork inhomogeneity, however, was the gain of some 3^m in limiting magnitude and the high definition afforded by the IIIa-J plates, as compared to the 098 emulsion scanned by machine.

To check the repeatability of the selection of galaxies, 3 of the 49 sub-regions were re-examined after a lapse of some months, with the comparison plates rotated through 90^o relative to their original orientation. The original and secondary classifications of the images in each area are compared in Table 2.2. Whilst fewer galaxies and more objects of uncertain nature were recorded during the repeat sessions, the actual numbers of galaxies recognised are stable to within ∿10%. This implies a consistency of 99% in the visual sorting process, a success rate infrequently achieved by automatic image sorters except under favourable conditions. The automatic detection process, on the other hand, has a repeatability of much less than 99% for faint images, and moreover different observers are liable to apply different visual criteria to any selection task.

At the conclusion of this process, CM parameters for 5185 individual galaxies and 227 instances of image blends had been placed on a master card file. 54 additional images of galaxies were found to have been split into double or multiple components; area-weighted centroids were assigned to the low surface brightness systems in this category, and the locations of the remainder were estimated either by direct inspection of the plates, or by transformation of the coordinates listed during the course of independent photographic photometry (Chapter 5). A total of 220 images,

distributed widely throughout the scan area, were of uncertain classification and were excluded from further analysis.

Following the elimination of the foreground star component, visual inspection of plates was resumed in order to classify as many galaxies as possible within the framework of a simplified de Vaucouleurs (= revised 3-dimensional Hubble) system. An attractive feature of this scheme (see e.g., de Vaucouleurs 1959) is its additive property, whereby ever higher degrees of refinement of classification can be accommodated according to the suitability of the plate material. A simple numerical coding scheme was devised which took advantage of this fact, based on the system employed in the RC1 (de Vaucouleurs & de Vaucouleurs 1964), to facilitate later computer analysis of the morphological statistics. Those parameters which describe stage and DDO luminosity class were ignored, since only the brightest systems were photographed with sufficient resolution.

The microcmetric axis dimensions of all galaxies with measurable diameters ($\gtrsim 1\frac{1}{2}$ graticule divisions or $\gtrsim$ 10 arcsec) were also recorded during classification. More images were measured than could be classified; it was found to be particularly difficult to assign morphological types to overexposed disk systems at high inclinations to the line of sight, whereas the more lightly exposed non-IIIa-J emulsions were too coarse-grained to be of assistance. The preponderance of spiral galaxies in the classified sample is partly a reflection of the fact that they are the easiest type to identify out to moderate distances.

The projected distribution of the different types of galaxies is considered in Section 2.6.

2.4 The Surface Distribution of Galaxies

It is convenient to discuss the distribution of the ∿5500 galaxies recognised on plate R1347, in terms of apparent photographic magnitude. The method whereby magnitudes are estimated from CM data is described later in Section 5.6.

Figure 2.3 shows the surface distribution of galaxies which have V-band magnitudes at the 25th mag arcsec^{-2} isophote (V_{25}), or approximations thereof (as explained in Chapter 5), brighter than 17^m. This limit is chosen because at fainter magnitudes, the sample becomes significantly incomplete. Apart from the omission of small strips along the north and west boundaries, Figures 2.3 - 2.5 show approximately the full area of the CM scan. Note the high degree of symmetry in the central region of the cluster and the general decrease of surface density towards the edges of the field (Figure 2.3). This is a quantitative statement of what the charts in Appendix I make clear more qualitatively.

The indistinctness of the group of galaxies Klemola 13 (Klemola 1969) in Figure 2.3 deserves comment. This group is visible south preceding the core of Hydra I at an angular separation of only 0.8 Mpc, and is dominated by a large barred spiral and includes a pair of interacting galaxies. In the second finding chart in Appendix I, the group may be found at coordinates X = 14.9 cm, Y = 8.5 cm. Klemola 13 is also listed as the 378th entry in the catalogue of

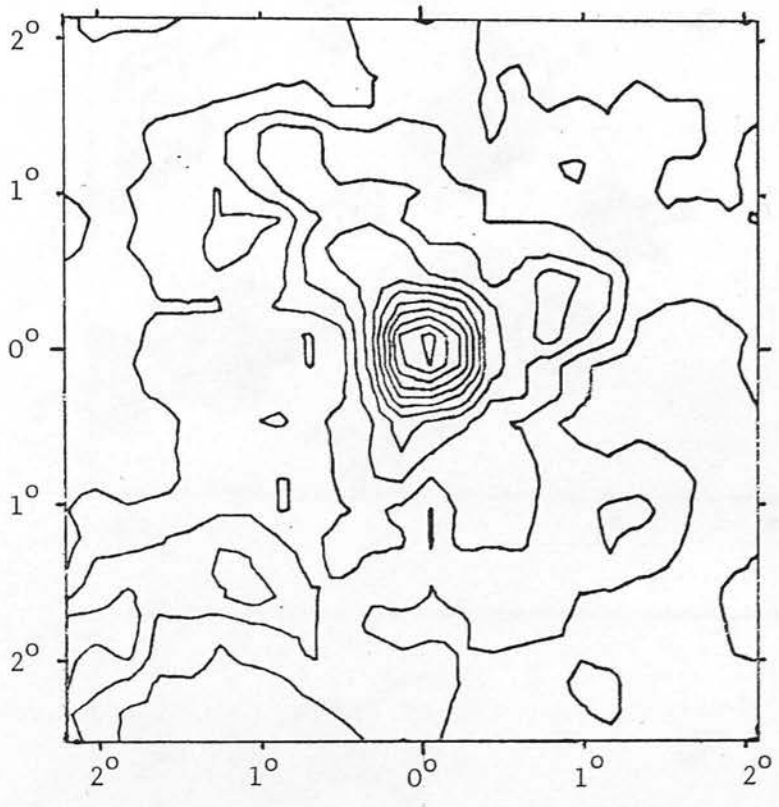

Figure 2.3

Isopleths of galaxies brighter than V_{25} = 17 in a region of dimensions $4^{\circ}.51 \times 4^{\circ}.85$ approximately. Contours are in steps of 20 galaxies degree^{-2} from 20 to 220 galaxies degree^{-2}.

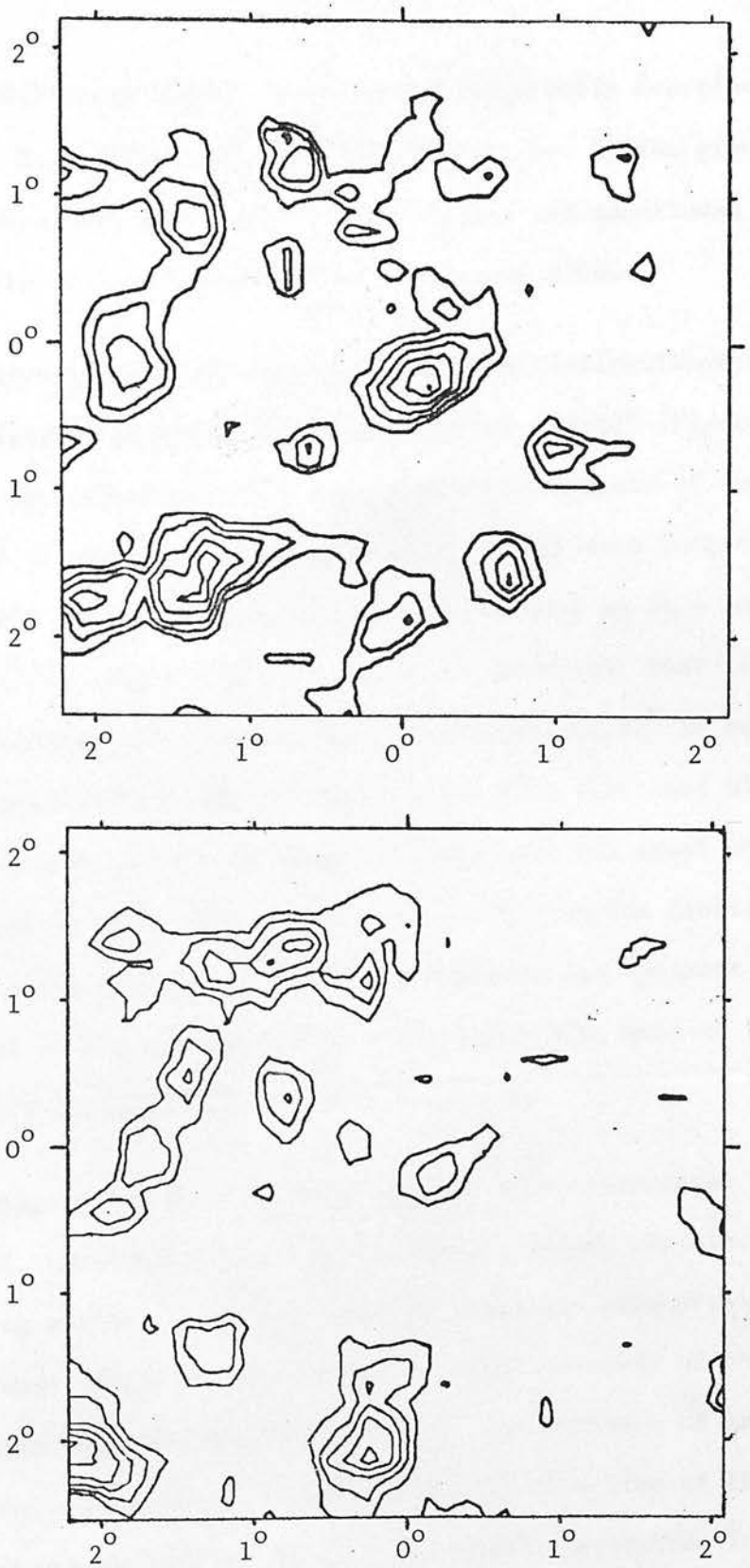

Figure 2.4 (top) Isopleths of 1387 galaxies of $17.0 < V_{25} \leq 18.2$ contoured in steps of 20 galaxies degree^{-2} from 100 to 200 galaxies degree^{-2}.

Figure 2.5 (bottom) Isopleths of 3257 galaxies fainter than $V_{25} = 18.2$, contoured in steps of 40 galaxies degree^{-2} from 200 to 360 galaxies degree^{-2}.

Braid & MacGillivray (1978), where it is incorrectly described as very rich. No redshifts of the brighter galaxies in the group have been published, but their apparent dimensions and magnitudes suggest that they lie at a distance similar to that of A1060.

At fainter magnitudes Hydra I cannot be distinguished relative to the density of galaxies in the surrounding "field" (Figure 2.4). To a first approximation the number density of members of the cluster and of the field (both considered later) each increase exponentially with magnitude, but the latter does so at a much faster rate (cf. Figures 6.3 & 6.4), with the result that field galaxies dominate the total population even before 17^m is reached. The most interesting feature in Figure 2.4 is a flattened cloud of galaxies, central in the diagram, which is only $0^\circ.2$ south preceding the position of A1060 and almost certainly behind the cluster. In Figures 2.4 and 2.5 other density enhancements are apparent mainly to the east of the central meridian through A1060, most of which probably lie at large line-of-sight distances.

At magnitudes still fainter ($\gtrsim 20^m$) than illustrated in Figure 2.5, extremely distant rich clusters become visible. Although very strong subjective effects tend to frustrate attempts to select a homogeneous sample of these faint clusters, a study of their distribution suggests two observations: the presence of greater optical obscuration in the (south-westerly) direction of the galactic plane, and the absence of strong intracluster absorption in A1060 (other than what is attributable to the individual bright cluster members). There is no indication that the number of galaxy

associations visible in the background are fewer along the line of sight through this cluster than outside it. Zwicky (e.g. 1957) has reported that galaxy clusters appear to be fewer in number behind intervening clusters than in other directions, but Abadi & Edmunds (1978) consider that this effect is due merely to problems of recognition.

To locate the position of the centre of the cluster the projected distributions of galaxies brighter than V_{25} = 15, 16 and 17^m were each smoothed and contoured in the manner of Figure 2.3, and the centres of symmetry of the isopleths estimated. This is essentially a refined version of the conventional procedure of defining the cluster centre by means of strip counts. The position of maximum number density in A1060 is at X = 126.8 ± 1.4 mm, Y = 142.8 ± 1.0 mm in the system of the COSMOS Coarse Mode measurements, and corresponds to the 1950.0 coordinates α = 10h 34m 17s ±6s, $\delta = -27^o$ 13'±1'. The two brightest galaxies in the cluster, N3309 and N3311, are located just 30 kpc immediately south of this position (cf. Figure 6.5). The centre of (luminous) mass in the cluster probably coincides with this giant binary.

There is evidence (e.g. MacGillivray et al. 1976b) that most or all distant, rich clusters of galaxies are elongated systems. The degree of apparent flattening of A1060 may be estimated by the iterative fitting of a series of ellipses to the surface density distribution illustrated in Figure 2.3. Stable (or mildly oscillating) solutions were obtained in which each ellipse assumed a shape and orientation most consistent with the distribution of galaxies that

it enclosed. The mean axial ratio of the best-fitting models was 0.87 ± 0.02, with no marked dependence on the proportion of the sample of galaxies bounded (that is, on the size of the ellipse). If it is maintained that A1060 has a disk-like structure, the disk must be aligned so as to present an almost face-on aspect.

The high degree of circular symmetry makes A1060 amenable to representation by the isothermal sphere model (cf. Zwicky 1942, 1957; Bahcall 1972, 1973a,b,c, 1974, 1975; Austin & Peach 1974 ; MacGillivray et al. 1976b). The density distribution in an infinite isothermal "gas" sphere of self-gravitating point masses (Emden 1907) as projected onto a plane has been tabulated by Zwicky (1957). He uses rather large increments in the radial variable to describe the profile to very great distances from the nucleus, but the central peak of the profile is not well defined, and some interpolation of his figures was necessary. A χ^2-minimising computer procedure was applied to fit the observed surface distribution of galaxies brighter than $V_{25} = 17$ to this projected Emden sphere (Figure 2.6).

The structural index of A1060 is $\beta = 2.1$ minutes of arc, corresponding to a core radius (Bahcall 1973a) of $R_c = 3\beta = 73$ kpc. If the innermost core of the observed distribution is excluded from the fit, the derived β increases by 20% to 2!5. Butcher & Oemler (1978) have carried out visual counts of galaxies in A1060 to an estimated limiting magnitude of $V \simeq 16.6$; a fit of their data to the standard projected sphere yields $\beta = 2!6$, which is in good agreement. The matching procedure is not particularly sensitive to the choice of cluster centre, but estimates of β may vary with the

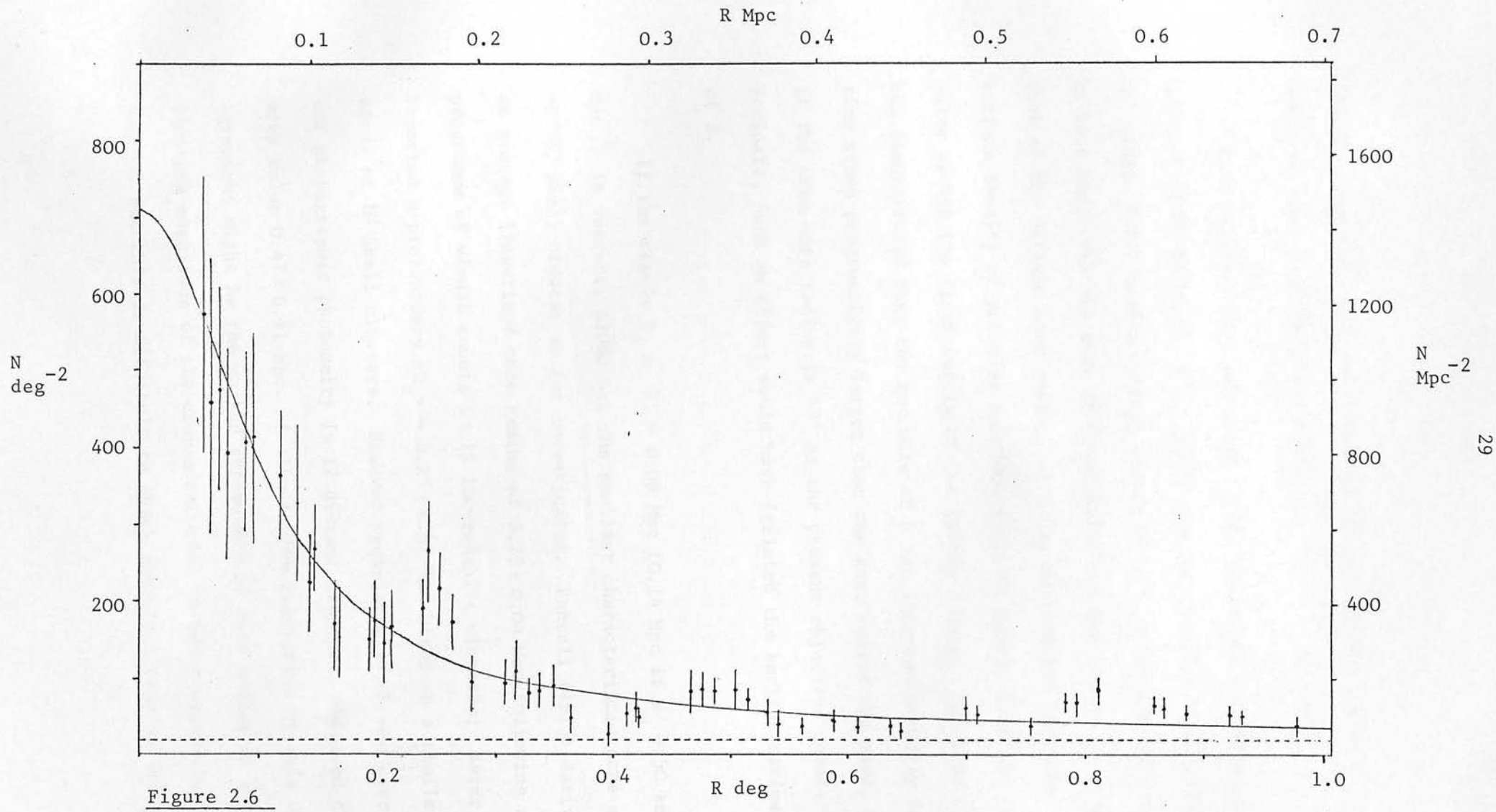

Figure 2.6

The radial surface density distribution of galaxies of $V_{25} < 17$ from counts in annuli of various widths, and the best isothermal sphere representation. The adopted background level is shown by the dotted line.

limiting magnitude (and completeness) of the counts, and with the choice of ring size (Quintana 1979).

Both Zwicky (1942) and Kwast (1966) estimated the structural index of A1060 to be $\beta = 4'$. Zwicky counted galaxies within rings 10' wide; Kwast used a central circle of 15' followed by 10' rings. In both cases the bin size or 'resolution' of the counts is about that of the derived core radius, with the implication that the surface density of galaxies in A1060 falls to nearly half its central value within the first circle of the Zwicky counts. Quintana (1979) has demonstrated that the estimate of β can increase markedly if ring sizes progressively larger than the core radius are used, and if the true core radius is $\sim 7'$ as the present objective counts indicate, such an effect would have inflated the earlier estimates of β.

If the result $R_c \simeq 7' = 0.08$ Mpc (0.14 Mpc if $H_o = 50$ km s^{-1} Mpc^{-1}) is correct, A1060 has the smallest characteristic core size of any Abell cluster so far investigated. Bahcall (1975) derived an average linearised core radius of 0.25 ± 0.04 Mpc following a programme of visual counts in 15 low-redshift clusters; Baier (1976) reported a preliminary $\langle R_c \rangle = 0.23 \pm 0.08$ Mpc based on a similar study of 10 Abell clusters. However Dressler (1978c), who carried out photographic photometry in 12 distant clusters, obtained the mean value 0.47 ± 0.11 Mpc. A clue to the resolution of this disagreement might be the marked dependence of core radius on the limiting magnitude of the counts recorded in two clusters by Quintana (1979), but this is difficult to check quantitatively in the present

case because very large statistical uncertainties in the density of galaxies in the core arise if the modest numbers of galaxies in A1060 are subdivided by magnitude range.

2.5 The Correction for Non-members

The redshifts of all but a very small number of galaxies in the sample are unavailable, so any correction intended to eliminate galaxies which are not members of A1060 must inevitably be statistical in nature. If the distribution of "field" (i.e. non-member) galaxies of all types within the volume of space surveyed is homogeneous and isotropic, then the number, $N(\leq m)$, of field galaxies brighter than apparent magnitude m varies as $N(\leq m) \propto 10^{0.6m}$. The constant of proportionality may be fixed by the requirement that the expression should agree with the number of field galaxies to a given limiting magnitude in the regions immediately beyond the boundary of the cluster.

The surface density of galaxies brighter than $V_{25} = 17$ in the scan area decreases from approximately 31 galaxies degree^{-2} at 0.91 Mpc from the cluster centre to 20 galaxies degree^{-2} at 1.56 Mpc. A similar decline of number density with increasing radial distance has been found for galaxies in the magnitude range $17 < V_{25} < 18$. Fainter than $V_{25} = 18$, the number distribution fluctuates strongly due to the presence of background clusters but shows no corresponding decrease from centre to edge. It is clear from these observations and from Figure 2.2 that there are still appreciable numbers of galaxies associated with A1060 at 1 to 1.5 Mpc from the centre, and

that to determine the field density, either photometrically calibrated number counts that refer to a wider local region must be considered (cf. Dressler 1978b,c) or some form of extrapolation to larger angular distances must be applied using the existing counts (cf. Butcher & Oemler 1978; Quintana 1979).

Neither the CGCG (Zwicky et al. 1961-68) nor the Lick Observatory galaxy counts (e.g. Shane & Wirtanen 1954) enumerate the distribution of galaxies in this region, but earlier estimates of the local field density exist. Shapley (1933) determined an average background density of 34.6 galaxies degree^{-2} to a limiting photographic magnitude, m_{pg}, of 17.3 for galaxies, over a nine square degree region excluding the cluster core. As this would correspond roughly to the annulus about Hydra I with inner and outer radii of 0.5 Mpc and 1 Mpc respectively, his figure is an overestimate. Zwicky (1941) found 2.8 galaxies degree^{-2} brighter than $m_{pg} \simeq 16$ at a projected distance of 5^{o} (3.5 Mpc). If it is assumed that both m_{pg} systems approximate the International photographic scale, then (Brown 1974)

$$B \simeq m_{pg} + 0.1 + 0.14(m_{pg} - 15)$$

where B is a blue-band magnitude presumably equivalent to the standard face-on magnitude B(O) defined in the RC1 (de Vaucouleurs & de Vaucouleurs 1964), which correspond to the $\sim$23.5th B mag arcsec^{-2} isophote in ellipticals and lenticulars and $\sim$24.5th B isophote for later types (Freeman 1976). With $B_{25} \simeq B$ and a mean colour index $\langle B^{c}_{25} - V^{c}_{25} \rangle = 1.1$ for lenticular galaxies at $V_{25} = 17$, it follows that

Shapley's counts imply $N(V_{25} \leq 17) \simeq 58$ galaxies degree^{-2} in this region, whereas Zwicky's imply $\sim$37 galaxies degree^{-2}. These figures are very uncertain, not least because the original estimates of limiting magnitude were crude. By contrast, Butcher & Oemler (1978) estimate that there are only 7 non-members per square degree brighter than magnitude 16.6 on V-band plates.

A fit of all galaxies of $V_{25} < 17$ to the Emden sphere model gives a value of 17.6 galaxies degree^{-2} at a projected radius of 5^{o}. With proper regard of the above considerations, an estimate of the background which exceeds this value slightly but which is less than the actual counts at a projected radius of 1.5 Mpc ($2^{o}.1$) is adopted, viz. 19 ± 6: galaxies degree^{-2} to $V_{25} = 17$, which corresponds to the logarithmic cumulative luminosity function

$$\log N(\leq V_{25}) = 0.6V_{25} - 8.921$$

for field galaxies in each square degree, as dimmed by extinction. For comparison, the function adopted by Sandage & Tammann (1976) [$\log N(\leq m) = 0.6m - 9.30$] predicts 7.2 galaxies degree^{-2} to this limit, after allowance for extinction ($A_V = 0.13$, Sandage 1973a) and for their use of total magnitudes ($\simeq V_{25} - 0^{m}.2$). The field correction of Bucknell et al. (1978) and previous papers in that series imply $N(\leq 17) = 19.4$ galaxies degree^{-2}, very close to the figure assumed here.

The adopted field correction predicts that at most, 276 of the 526 galaxies brighter than $V_{25} = 17$ and within 1.5 Mpc of the centre of A1060 are likely to be non-members. Since this subtracted

'background' tends to exceed the density of galaxies observed at the corners of the $\sim$22 degree^2 scan area, 250 is probably a minimum estimate of the number of systems associated with A1060. The relative contribution of this background to the observed number density of galaxies at V_{25} = 17 is illustrated in Figure 2.6 . Knowledge of the field correction at each magnitude is essential to the later discussion, in Section 6.2, of the cluster luminosity function.

2.6 The Radial Variation of the Cluster Composition

The surface distributions of the galaxies that are brighter than V_{25} = 17 (a few are fainter systems blended with a star image) and which belong to different morphological types is displayed in Figures 2.7 to 2.9 . Some galaxies which were not categorised on visual inspection and which happened to lie within the smaller scan area of the primary photographic photometry were identified as late-type systems on the basis of integrated B-V colour (Section 6.1). These were assigned to the spiral and irregular galaxy category, and marked by crosses in Figure 2.9 to distinguish them from visually classified systems. The distribution of the remaining unclassified galaxies brighter than 17^m is illustrated in Figure 2.10.

The differences of the distributions of the three recognised types of systems is striking. Elliptical galaxies form a rather compact central core superposed on an apparently distinct, homogeneous field distribution. The lenticulars do not exhibit this dichotomy, but instead are smoothly concentrated toward the centre of the cluster, and trail off towards the outskirts with no

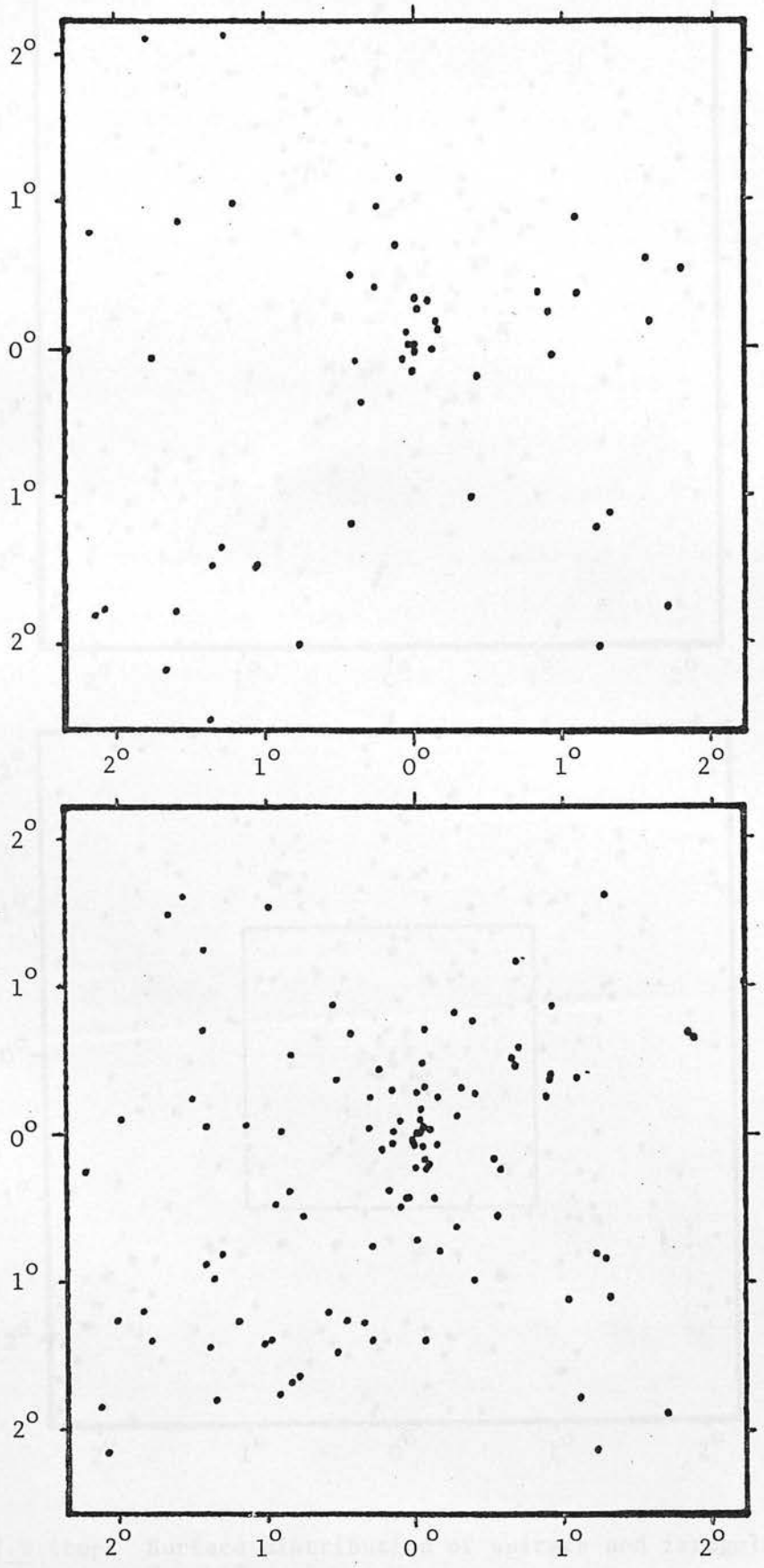

Figure 2.7 (top) Surface distribution of ellipticals, $V_{25} < 17$

Figure 2.8 (bottom) Surface distribution of lenticulars, $V_{25} < 17$

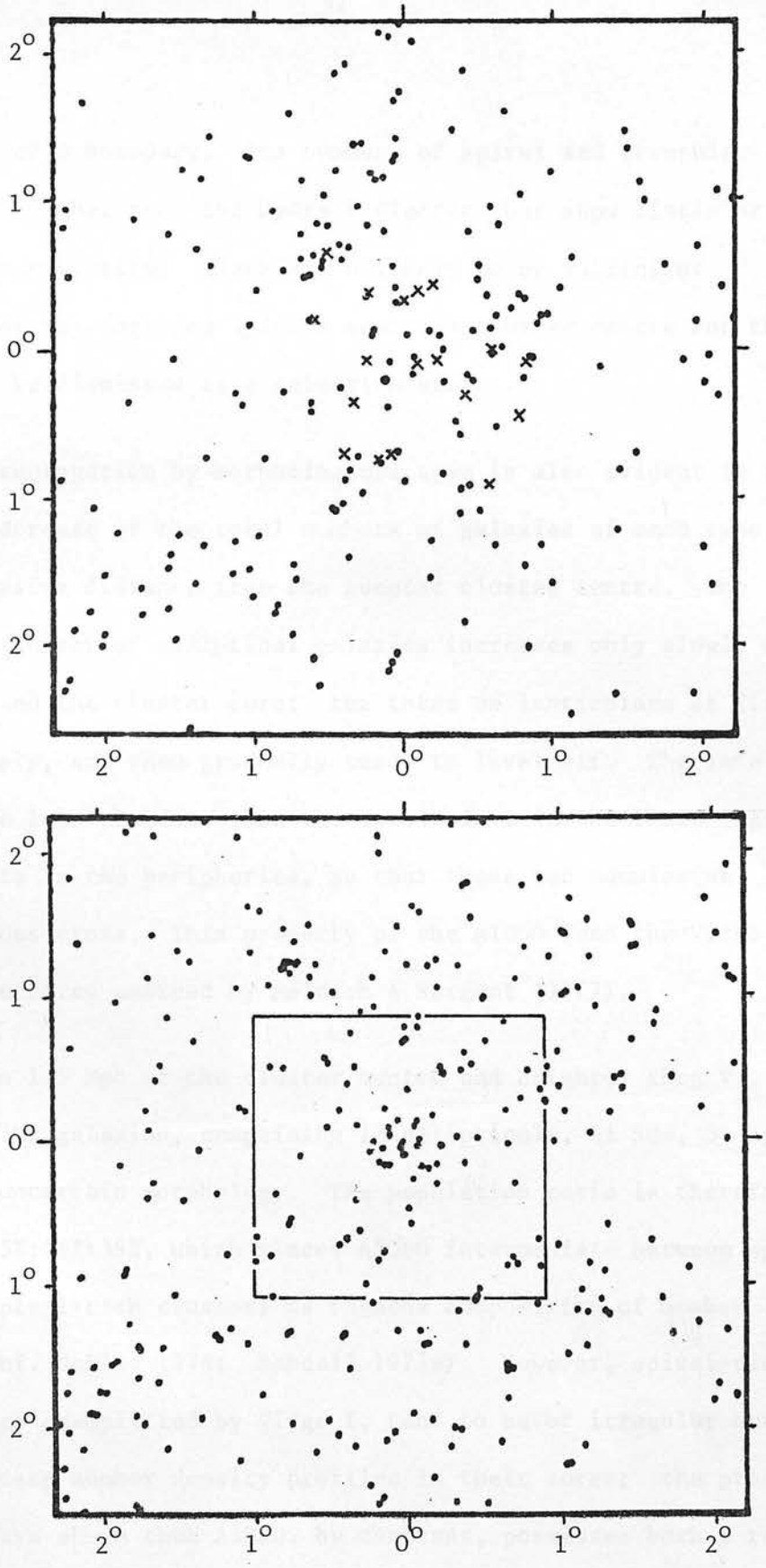

Figure 2.9 (top) Surface distribution of spirals and irregulars, $V_{25} < 17$.

Figure 2.10 (bottom) Surface distribution of unclassified galaxies, $V_{25} < 17$.

suggestion of a boundary. The numbers of spiral and irregular systems are higher near the Hydra I cluster, but show little or no central concentration; there are unlikely to be sufficient instances of unrecognised spirals near the cluster centre for this paucity to be dismissed as a selection effect.

This segregation by morphological type is also evident in the rates of increase of the total numbers of galaxies of each type with increasing distance from the adopted cluster centre. The cumulative number of elliptical galaxies increases only slowly with radius beyond the cluster core; the total of lenticulars at first rises steeply, and then gradually tends to level off. The late-type systems are less abundant than the lenticulars in the inner regions, but dominate in the peripheries, so that these two cumulative distributions cross. This property of the A1060 (and the Virgo I) cluster was first noticed by Melnick & Sargent (1977).

Within 1.5 Mpc of the cluster centre and brighter than $V_{25} = 15$ there are 102 galaxies, comprising 13 ellipticals, 41 SOs, 34 spirals and 14 of uncertain morphology. The population ratio is therefore E:SO:S = 15%:46%:39%, which places A1060 intermediate between spiral-poor and spiral-rich clusters as regards composition of member galaxies (cf. Oemler 1974; Bahcall 1977a). However, spiral-rich clusters, as exemplified by Virgo I, tend to be of irregular outline and lack steep number density profiles in their cores; the preceding sections have shown that A1060, by contrast, possesses both a regular structure and strong central condensation. The Hydra I cluster may therefore be classified as of intermediate type in the sense of Bahcall (1977a).

2.7 Geometric Parameters of the Galaxies

Supplementary information concerning the visual geometry of the brightest galaxies was collected on a manually controlled plate comparator. In this machine image acquisition and display are facilitated by a television system, and a teletype provides positional readout in steps of 12.5 microns over some 20 degree^2 of plate. Scanning in a boustrophedonic fashion, an initial finding list of over 500 bright galaxies was prepared. The axial diameters, D and d, and the orientations of the projected major axes were then determined for many of these images by the following procedure. The coordinates of each end of the major axis were noted, and next those of the minor axis: this supplied four points which defined an approximating ellipse, and the procedure was repeated. The ratio of the average lengths of the two semi-major and semi-minor axes defined the apparent ellipticity of the image. The projected orientation was taken to be the average of the mean major axis and mean minor axis orientations, the latter shifted into correspondence by the addition of 90°, weighted by axis length; the meridian passing through the cluster centre defined the axis of reference, angles increasing north through east. Arigo et al. (1978) have described a quadruple averaging procedure for the reduction of similar data, and their prescription was found to yield comparable figures for axis ratio and orientation.

For direct comparison with the above, a second set of values was derived with the plate rotated through 112°. This angle was chosen following Thompson (1976), to avoid unconscious biases which

can occur at multiples of 45^{o}. Not all galaxies in peripheral regions could be measured twice, because the accessible region of the plate varied with alignment. The internal errors in the data may be quantified by evaluating (cf. Hawley & Peebles 1975)

$$\Delta P = \tfrac{1}{2} < P_1 - P_2 > \quad \text{and} \quad \sigma(P) = \tfrac{1}{2} < (P_1 - P_2)^2 >^{\frac{1}{2}}$$

where the angular brackets < > denote average value and the subscripts 1 and 2 refer to the first and second determinations of parameter P respectively. For the axis ratios $R = d/D (\leq 1)$ and orientations ϕ determined for 167 galaxies at both plate alignments,

$$\Delta R = -0.01 \qquad \sigma(R) = 0.05$$
$$\Delta\phi = -0^{o}.81 \qquad \sigma(\phi) = 6^{o}.80$$

These indicate no important systematic disagreement of the two sets of measured shapes and orientations. The dispersion about the mean orientation, $\sigma(\phi)$, falls to $\sim 4^{o}$ if 33 images of apparent ellipticity $e = 10(1 - R)$ less than 2.5 are excluded.

When the axis ratios of non-spherical images with gradual luminosity gradients are measured by eye rather than by machine, their ellipticities tend to be overestimated (Holmberg 1946). To determine whether, and how seriously, the axis ratios derived from the above measurements with a manual plate comparator (R_3) and from micrometric axis diameters collated during galaxy classification (R_2) were biased, each set of apparent axis ratios was compared with the values (R_1) obtained from direct measurements of

the extents of the 25th V mag arcsec^{-2} isophotes of bright galaxies on contour plots. The ratios R_1 should be free from errors of the type described by Holmberg since the isophotal contours were constructed by machine from objective data. In analogy with the previous analysis, comparisons of 73 galaxies yielded

$$\langle R_2 - R_1 \rangle = -0.11 \qquad \langle (R_2 - R_1)^2 \rangle^{\frac{1}{2}} = 0.16$$

$$\langle R_3 - R_1 \rangle = 0.00 \qquad \langle (R_3 - R_1)^2 \rangle^{\frac{1}{2}} = 0.15.$$

These figures confirm that the micrometric measurements do suffer from a "Holmberg effect" which causes ellipticities to be overestimated by 1 unit on average. The data from the plate comparator appear to be unbiased, but because these measurements refer typically to contours of higher luminosity ($\lesssim$ 23.5 V mag arcsec^{-2}), the comparison is not strictly valid; the brighter isophotes of the galaxies may be more circular. The accuracy of the estimates of R_1 and R_2 is about ±0.1 for the brighter systems, deteriorating for smaller images.

The most extensive and hence useful body of axis ratio estimates is the set R_2. These were first corrected for the Holmberg effect by means of the expressions given in RC1:

$$R_c = .86R_2 - .14(1 - R_2)^6 + .14 \quad \text{for ellipticals}$$

$$= .81R_2 - .19(1 - R_2)^6 + .19 \quad \text{for other types,}$$

with the results

$$\langle R_c - R_1 \rangle = -0.02 \qquad \langle (R_c - R_1)^2 \rangle^{\frac{1}{2}} = 0.11$$

(74 systems),

which are clear improvements over the unadjusted quantities and fully justify the correction procedure.

The frequency distribution of ellipticities corresponding to the corrected axis ratios R_c for galaxies within 1.5 Mpc of the cluster centre is shown for each of three ranges of V_{25} magnitude in Figure 2.11. Apart from N3314, which consists of two spirals superposed in the line of sight, the sample representing the galaxies brighter than $V_{25} = 15$ is complete (upper histogram, Figure 2.11); fainter than this, omissions become progressively more numerous and contamination by non-members of A1060 more severe. The data for galaxies which satisfy $V_{25} < 16$ may usefully be compared with the frequency distribution, shown in Figure 4(a) of MacGillivray & Dodd (1979), of the apparent ellipticities of galaxies in the field of the rich cluster at $\alpha_{1950} = 00h\ 47m$, $\delta_{1950} = -29^{o}\ 46'$. That field is a square of side $\sim$3.2 Mpc at the distance of the cluster, of similar size to the 3 Mpc-diameter circular boundary applied here to A1060, if distances are scaled simply as the redshifts. A greater proportion of elongated ($e > 3$) systems are found in A1060, about 50% as compared to 40% in the other cluster. This indicates that the population of Hydra I is relatively richer in disk systems.

Strom & Strom (1979a) have reported a relatively greater incidence of flattened elliptical (E) galaxies in the visibly elongated cD cluster A401 than in the less flattened cD cluster A2670, and suggest that as a general rule, the flattening of a rich cluster may correlate with the shape of the member galaxies. At a very different scale, the average ellipticity of poorly populated galaxy

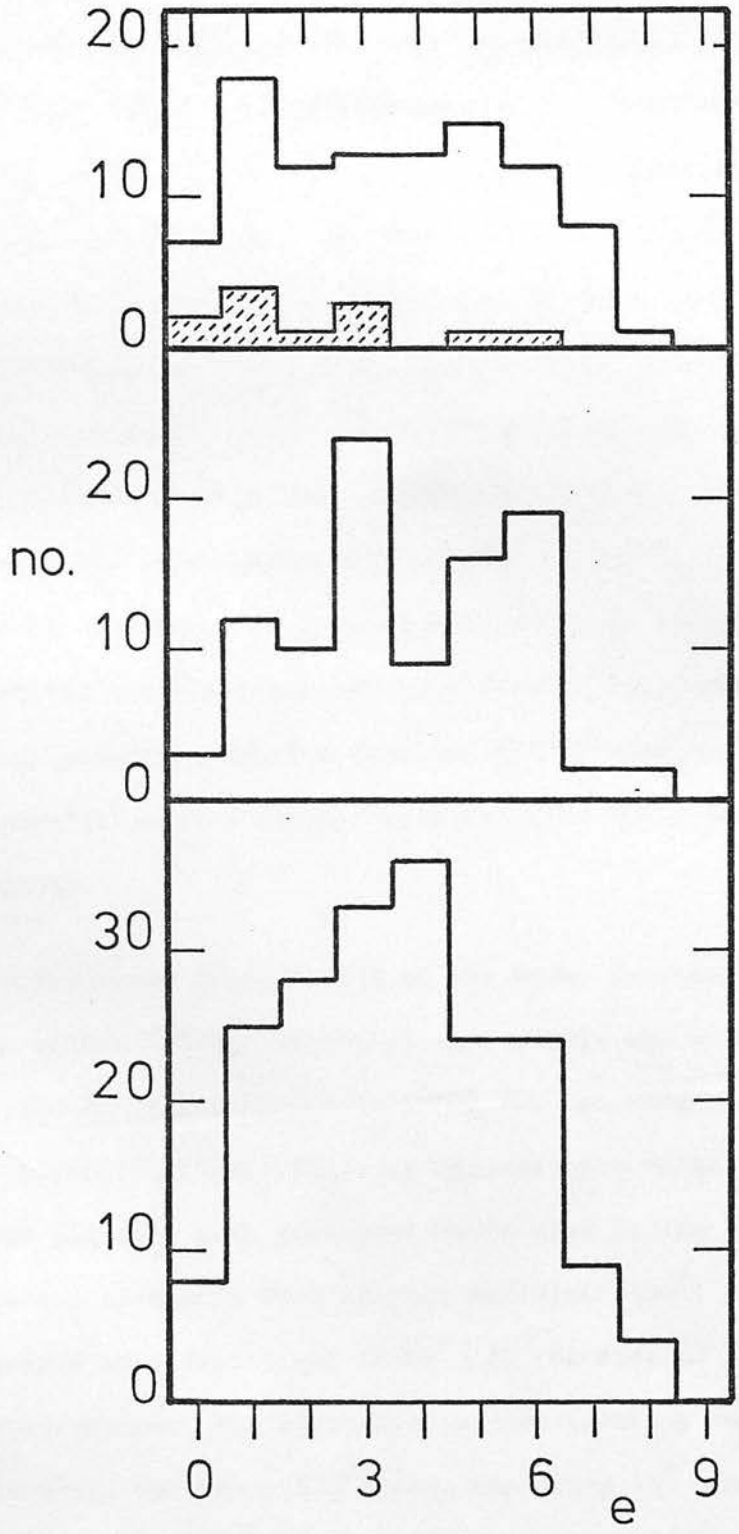

Figure 2.11

Frequency distributions of the ellipticities of those galaxies within 1.5 Mpc of the cluster centre and of magnitude (i) $V_{25} < 15$ (top; semi-hatched histogram represents E galaxies); (ii) $15 \leq V_{25} < 16$ (centre; completeness 92%); and (iii) $16 \leq V_{25} < 17$ (bottom; completeness 56%).

groupings is comparable to the mean for individual elliptical galaxies (Rood 1979). Both observations may constitute evidence that there exists some physical process which governs both the distribution of stars in a galaxy and the distribution of galaxies in an association. The population of E galaxies in A1060 which are brighter than $V_{25} = 15$, however, is barely sufficient for a meaningful comparison to be made with the frequency distributions of ellipticities of E galaxies in other clusters: the few Es in this sample are represented by the semi-hatched histogram in Figure 2.11. Inclusion of fainter E galaxies is the obvious remedy, but redshifts would be required to eliminate non-members. The relationship between cluster type and the flattening of the E galaxy population is a further consideration which has yet to be investigated.

The frequency distribution of the known orientations, ϕ, of galaxies within 1.5 Mpc of the cluster centre and with apparent axis ratios of less than 0.9 is shown for two ranges of V_{25} magnitude in Figure 2.12(a). There is apparently a relative deficiency of bright galaxies with projected major axes in the east-west plane (orientation eastwards from central meridian $\simeq 100^{\circ}$) and most systems are observed at orientations of $60^{\circ} \pm 20^{\circ}$ or else at right-angles to this direction. The impression of non-isotropy does not hold up statistically, however. A χ^2 test, employing 15° bins of ϕ, reveals the observed frequency histogram to be significantly non-random only at the 40% level, and on the modelled amplitude test (see Hawley & Peebles 1975, or Thompson 1976) the probability of a chance

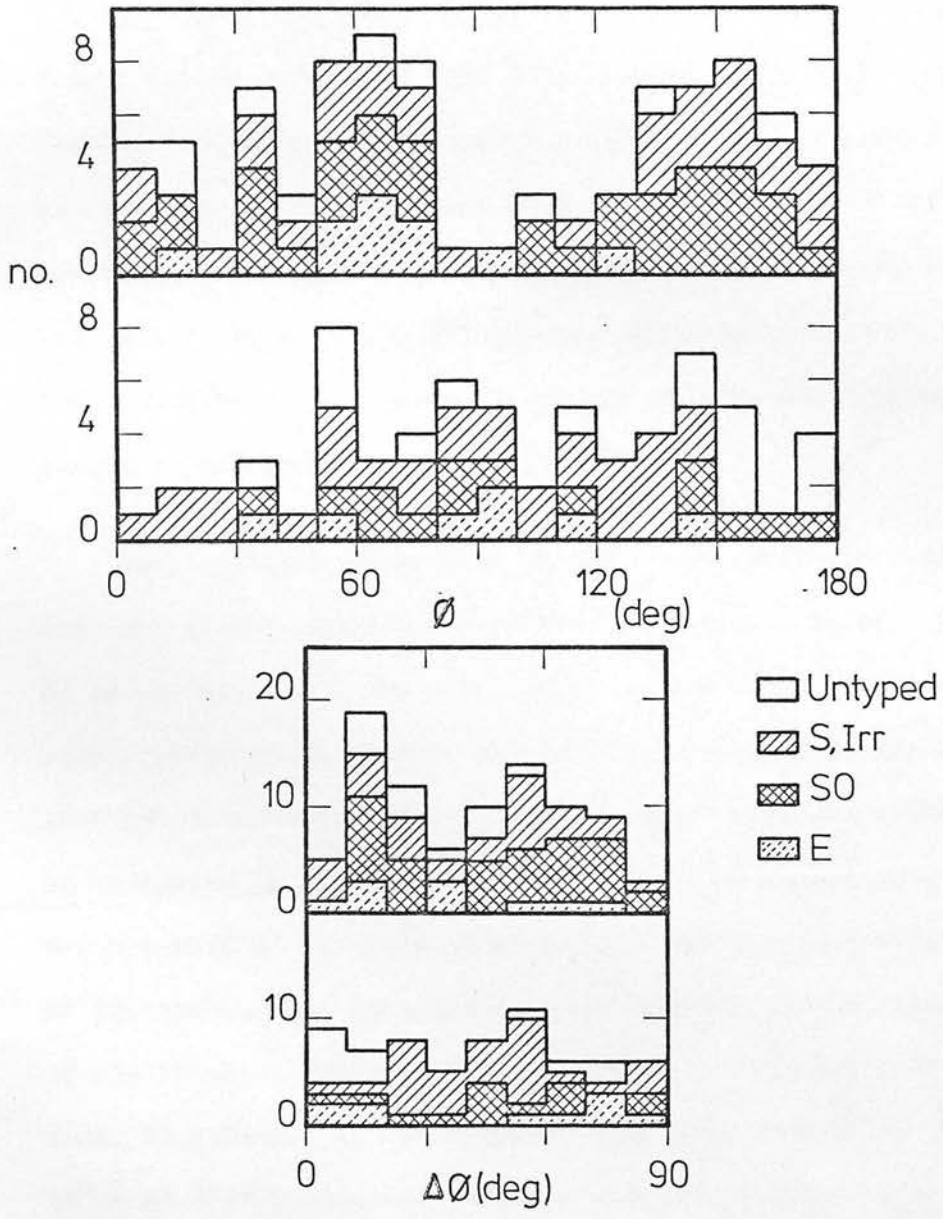

Figure 2.12 (a) (top)

Frequency distributions of orientations ϕ of those galaxies within 1.5 Mpc of the cluster centre and of magnitude (i) $V_{25} < 15$ (upper histogram; completeness 95%); and (ii) $15 \leq V_{25} < 16$ (lower histogram; completeness 41%)

Figure 2.12 (b) (bottom)

Frequency distributions of the radial position angles $\Delta\phi$ of the same samples (i) and (ii).

occurrence of this distribution is 66%, which is high. Nonetheless, it is worth mentioning that many galaxies in the cluster have approximately the same orientation as the brightest member, N3311 ($\sim 50^{o}$). N3308 and N3309 (Figure 6.5) are conspicuous examples of near-parallel alignment, and most of the bright E galaxies satisfying $V_{25} < 15$ have similar orientations. A second noteworthy point is the correspondence of the orientation of the cluster ($\sim 121^{o}$) as determined by iterative ellipse fitting, with the axis defined by the central four bright NGC galaxies numbers 3308, 3309, 3311 and 3312 ($\sim 130^{o}$) and also with the second peak in the frequency distribution of galaxy orientations ($\sim 150^{o}$).

The frequency histograms of the radial position angles, $\Delta\phi$, of the same galaxy samples are plotted in Figure 2.12(b). The angle $\Delta\phi$ is defined to be the orientation of the major axis of each galaxy with respect to the imaginary radius vector linking the centre of that galaxy to the centre of the cluster. Galaxies which appear to be elongated in the direction of the cluster centre have $\Delta\phi = 0^{o}$ and are said to be radially aligned. The frequency distribution of $\Delta\phi$ for the fainter galaxies sampled is emphatically random; that of the brighter systems is less readily interpreted, but the breakdown, 47 galaxies in the range $0^{o} \leq \Delta\phi \leq 44^{o}$ and 42 in the range $45^{o} \leq \Delta\phi \leq 89^{o}$, does not indicate that these galaxies are preferentially aligned either radially or tangentially.

Before discussing these results, it should be pointed out that they are based on two-dimensional, projected representations of the true spatial orientations and shapes of the galaxies and of their

distribution. A good example of the peculiar distortions which may result from projection effects is provided by the pair of lenticular galaxies numbers 22 and 38 in the list of Appendix II. Number 38 is an unusual system intermediate in appearance with regard to N128 and N7332 (depicted in the Hubble Atlas of Sandage, 1961); it consists of a box-shaped nuclear region within an envelope that resembles a peanut with pointed ends. The immediate neighbour, number 22, is a normal SO with a slightly elongated nucleus. It is evident from the appearance of the pair that they lie almost parallel to each other and nearly edge-on to the line of sight; yet, because their intrinsic major axes are foreshortened, they are assigned quite different values of ϕ. Thus although statistically the gross features of the spatial alignments in a large assembly tend to be preserved in projection, inferences regarding isolated cases are unreliable.

MacGillivray & Dodd (1979) have ventured that systematic radial alignment trends are more likely to be observed in clusters classified as early in the scheme of Bautz & Morgan (1970), viz. classes I, I-II and II, whereas a tendency of member galaxies to align with the apparent major axis of the cluster as a whole may be more common amongst clusters of later BM type. A special case of the latter effect may arise in clusters which are dominated by a highly luminous giant galaxy; this first-ranked member is often aligned with the apparent major axis defined by the positions of the fainter galaxies (Sastry 1968; Dressler 1978b; Green 1978). Thompson (1976) suggests that linear alignment of a cluster and its membership is more probable amongst highly elongated clusters in general, or in

types L (linear) and F (flattened) in the classification system of Rood & Sastry (1971), in particular.

The trends observed in A1060, even though they are not statistically impressive, provide a modicum of support for the above proposals. The exception is the special case: whilst a number of galaxies in excess of average are oriented in parallel with the apparent major axis of the first-ranked system, this axis does not coincide with the direction of elongation of A1060. The cluster is classified as of BM type III, and the bright galaxies in this area do show a mild preference to be aligned with the distributive elongation axis; at the same time, some of them are aligned roughly parallel to the direction defined by the central four NGC galaxies, as appropriate for a cluster of RS type L. Actually the classification of Hydra I is C on the RS system, but the direction of slight flattening appears to be well defined, and is stable even if the brightest galaxies are excluded.

Table 2.1

Visual counts of "prominent" galaxies within circular annuli of width 10 arcmin centred on A1060, broken down by galaxy type. 'Ring 1' is a circle of radius 10 arcmin.

E = elliptical galaxies, SO = lenticulars, S = spirals and irregulars, and U = untyped.

Ring No	E	SO	S	U	Total
1	3	4	3	0	10
2	0	8	3	5	16
3	2	6	7	4	19
4	0	0	5	5	10
5	0	3	15	6	24
6	1	3	12	7	23
7	2	1	6	4	13
8	0	1	7	2	10
9	1	2	4	6	13
10	0	1	5	0	6
11	2	3	7	4	16
12	1	0	11	0	12
13	0	0	11	3	14
14	0	2	7	2	11
15	0	0	8	5	13
16	0	1	7	1	9
17	1	3	14	4	22
18	0	0	12	0	12
19	0	1	12	2	15
20	2	1	12	2	17
21	0	1	9	2	12
22	1	1	20	2	24
23*	1	0	17	0	18
24*	1	0	13	2	16
25*	0	0	13	3	16
26*	2	1	6	3	12
27*	0	3	12	0	15
28*	0	1	8	0	9
29*	0	0	9	4	13
30*	0	1	11	1	13
31*	0	1	7	5	13
32*	0	0	10	3	13
	20	49	303	87	459

* ring overran a field edge.

Table 2.2

Comparison of the numbers of images, by category, as classified during the initial (A) and repeated (B) inspections of IIIa-J plates.

	Subregion 8		Subregion 19		Subregion 37	
	Centre 10h44m $-25^{o}45'$		Centre 10h30m $-26^{o}31'$		Centre 10h40m $-28^{o}45'$	
	(A)	(B)	(A)	(B)	(A)	(B)
(1)	1800	1806	2472	2477	2658	2659
(2)	100	95	137	120	201	194
(3)	9	6	1	14	2	6
(4)	4	6	6	5	4	6
(5)	0	0	1	1	1	1

Description of categories:

(1): stars and spurious images; (2): galaxies; (3): uncertain objects; (4): image blends; (5): dissociated images (single images recorded by the measuring machine in two or more discrete components).

CHAPTER 3

REDSHIFTS

Knowledge of the redshifts of a sample of galaxies in the field of any cluster is very valuable, because it provides the only reasonably reliable means of identifying those systems not gravitationally associated with major clustering, and because only redshifts can define the internal dynamics of a cluster. Both applications assume that the redshift is purely a Döppler effect. Controversial evidence for intrinsic quantised components in the redshifts of galaxies in the cores of clusters has been reviewed by Tifft (1974).

Redshifts are inferred from spectra, obtained either individually at high wavelength dispersion (spectrograms) or en masse at lower resolution (e.g. objective prism plates). All new redshifts reported in this chapter for galaxies in the field of A1060 have been obtained from prism plates, and are useful only in assessments of cluster membership. However, the opportunity has also been taken to reassess the velocity dispersion of the cluster, as defined by accurate radial velocities that are already in print. This is done in conjunction with estimates of the luminosities of the galaxies for which redshifts are available (Chapter 5).

3.1 Redshifts from Objective Prism Spectra

Very large numbers of galaxy spectra can be recorded simultaneously on fine-grain photographic plates exposed behind an objective prism, and in particular that of the U.K. Schmidt telescope (Nandy et al. 1977). The redshifts of early-type galaxies in the sample may be

estimated by comparison of the redshifted and rest-frame positions of characteristic features in the galaxy spectra, as recorded, for example, in graphical form (Cooke et al. 1977) or in digitized form, following measurements by the COSMOS machine (e.g. Nandy 1979). The integrated spectra of such galaxies - E, S0 and Sa/Sb - is dominated by emission from late-type stars which exhibit a sharp drop in intensity shortwards of about 4000Å in their rest frame. This "step" is sufficiently clear in low-dispersion prism spectra to serve as a redshift indicator.

UKST prism plate UJ4067P, an exposure centred on the Hydra I cluster, was used for this purpose. The particulars of UJ4067P are summarized in Table 3.1. Galaxies were initially selected for tracing on the basis of their apparent brightness (approximately $14.5 < V_{25} < 17.5$ in the notation of Chapter 5), position within the COSMOS CM scan area of the previous chapter (for identification purposes), and freedom from blending on the CM charts. In practice, spectral overlaps resulted in many rejections, whereas a few image blends were in fact successfully decomposed. Unfortunately an important area of plate 47 arcminutes wide and symmetric about the length of the central meridian through the cluster, was physically inaccessible to measurement on the microdensitometer. Consequently, no systems within 270 kpc of the cluster centre could be examined.

The spectra of 108 galaxies satisfying the luminosity, isolation and accessibility criteria were recorded; twenty of these were traced once or more during independent recording sessions. Calibration was provided by tracings of field stars. Nineteen

distinct lines and blends in the spectra of four stars, fitted to the dispersion curve of the UKST objective prism (Nandy et al. 1977), gave $\lambda_c = 5433 \pm 11\ (1 \pm .17)$(s.e.) Å as the value of the wavelength cutoff of the emulsion of plate UJ4067P. In turn, this fiducial mark fixed the wavelength of the 4000Å feature, defined in nine late-type stars, as $\lambda_{4000} = 3990 \pm 9\ (1 \pm .24)$(s.e.) Å, assuming zero error in λ_c. This figure is consistent with the published value of $\lambda_{4000} = 4010 \pm 30$ Å (Nandy et al. 1977). The wavelength cutoff for UJ4067P differs significantly from the value, 5360 ± 30 Å, of Nandy et al., but one should perhaps be wary of possible systematic external errors in the present work. The values of λ_{4000} and λ_c determined for UJ4067P were adopted on the grounds that they lead to internally consistent redshifts, a decision that avoids the spurious blueshifts that would otherwise result.

Of the recorded sample, sixty percent, spiral galaxies figuring prominently, lacked an unambiguous 4000Å feature and had to be discarded. The redshifts obtained for the remaining 43 galaxies are presented in Table 3.2. Nine of the listed values represent the means of repeated determinations, and the mean absolute internal error for these estimates is only $\langle|z|\rangle = 0.005$. A better indication of the accuracy of the redshifts would follow if they could be compared with independent measurements of a second prism plate or, preferably, a high-dispersion spectrogram obtained on some other telescope. As matters stand, the errors in the tabulated redshifts are probably less that ±0.02 (cf. Cooke et al. 1977).

Eight galaxies in Table 3.2 are identified as probable outlying members of A1060 on the evidence of their redshifts. Not one is fainter than $V_{25} = 16$, but the background would be expected to dominate at faint magnitudes in the outskirts of the cluster. The low density of cluster members in regions distant from the core of Hydra I would be accentuated in any sample of redshifts obtained by the procedure outlined above, because the proportion of late-type members in the cluster outskirts is higher and this class of galaxy does not exhibit the spectral features that permit redshifts to be determined on objective prism plates. Table 3.2, nevertheless, is sufficient to establish that two galaxy groupings which exist in this field have mean redshifts of $\sim$0.07 and 0.08 respectively, clearly identifying both as distant groups at seven times the distance of Hydra I.

3.2 The Velocity Dispersion

The mean velocity of recession and the internal velocity dispersion of A1060 has previously been estimated by Vidal & Peterson (1975), Faber & Dressler (1976, 1977) and by Rood & Dickel (1978). Harrison & Noonan (1979), however, have illustrated that considerable ambiguity exists in the interpretation of redshift data, so it seems worthwhile to repeat the velocity analysis below on the basis of previously published heliocentric redshifts and newly determined photographic magnitudes.

The information sources are listed in the References section to Table 3.3, which summarizes the existing redshift data for all

galaxies within a projected radius of 5 Mpc from the cluster centre. Weights inversely proportional to the square of the internal errors have been adopted in the calculations of velocity averages, after first converting the probable errors quoted by Ref. 1 and the mean errors of Refs. 4 and 5 to corresponding standard deviations as used by Ref. 3, and assigning, arbitrarily, an internal standard deviation of 75 km s^{-1} to the velocity estimates of Ref. 2. Where only one velocity is available the standard deviation of that determination has been substituted for the standard error of the mean, the latter an obviously uncertain quantity since multiple observations of any system are few.

The distribution of the averaged heliocentric redshifts (expressed as "indicative velocities", $cz_\odot$) is shown in Figure 3.1, which is evidently ambiguous. As a spatial distribution along the line of sight it may be distorted greatly by peculiar motions. The small sample does not present a classical gaussian velocity distribution (cf. Yahil & Vidal 1977), yet none of the redshift extremes differs by an amount, 2.5 or 3 times the standard deviation of the original velocity distribution, that would justify its elimination as a non-member. This casts doubt on the analysis of Rood & Dickel (1978) of Sandage's (1978) limited sample of galaxies in A1060, since Rood & Dickel reject three of his seven systems.* On the other hand, the line-of-sight depth of the sample would be large - $20(100/H_o)$ Mpc - if no peculiar motions were involved, and those bright spirals in the low-velocity tail of the distribution, including N3312, have redshifts similar to that of the foreground

* A1060 = Hydra I is misidentified as A732 = Hydra II due to a misprint in Sandage (1978).

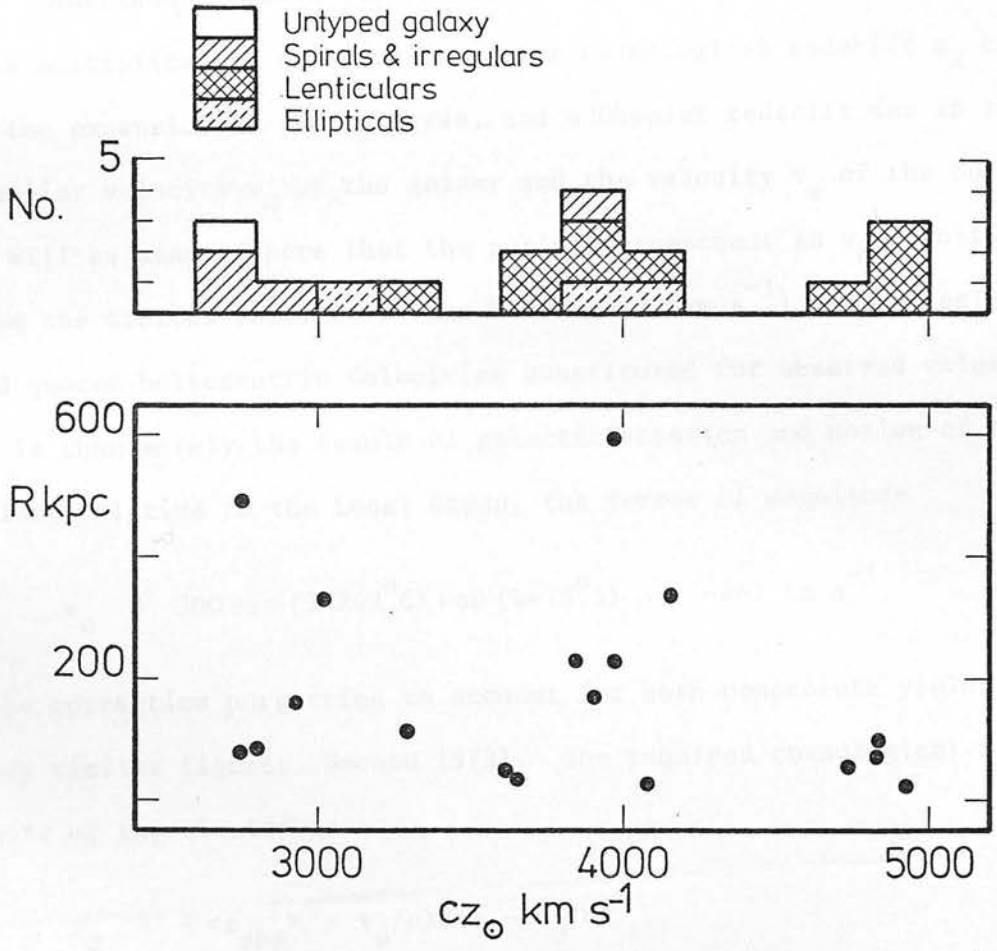

Figure 3.1

The distribution of the indicative heliocentric radial velocities listed in Table 3.3. R is the projected separation in kpc from the adopted cluster centre.

Hydra cloud (Chapter 2). For the present discussion, all galaxies in Table 3.3 will be treated as members of A1060.

Harrison & Noonan (1979) remark that any observable redshift z is a multiplicative combination of the cosmological redshift z_R caused by the expansion of the universe, and a Döppler redshift due to the peculiar velocity v_G of the galaxy and the velocity v_o of the observer. It will be assumed here that the periodic component in v_o resulting from the orbital velocity of the Earth ($\leq$ 30 km s^{-1}) can be neglected and quoted heliocentric velocities substituted for observed values; v_o is then merely the result of galactic rotation and motion of the galaxy relative to the Local Group, the former of magnitude

$$v_o = 300 \sin (l=269^{\circ}.6) \cos (b=26^{\circ}.5) = -267 \text{ km s}^{-1}.$$

(The correction purporting to account for both components yields a very similar figure: Noonan 1973). The required cosmological redshift of the cluster is

$$z_R = (\langle z_{obs} \rangle + v_o/c)/(1 - v_o/c)$$

where $z_{obs} \simeq z_o$, and the mean square dispersion of the radial velocities in the cluster is

$$S^2 \equiv \langle v_G^2 \rangle = (\langle z_{obs}^2 \rangle - \langle z_{obs} \rangle^2)/(1 + z_R)^2$$

in which the angular brackets $\langle\ \rangle$ denote mass-weighted values. The galaxy masses are calculated on the basis of absolute V_{25} luminosities and representative mass-to-light ratios of 5, 10 and 15 $M_{\odot}/L_{\odot}$ for spiral galaxies, lenticulars and ellipticals respectively. If

galaxies one and twelve in Table 3.1 are discounted because of conflicting redshift estimates and the remaining galaxies treated as cluster members, the recessional and dynamical parameters of Hydra I are

$$\langle z_{obs} \rangle = 0.01221 \pm 0.00042 \text{ (s.e.)},$$

$$z_R = 0.01131 \pm 0.00043 \text{ (s.e.)},$$

$$cz_R = 3390 \pm 129 \text{ km s}^{-1},$$

$$S = 496 \text{ km s}^{-1}.$$

The cosmological radial velocity of the centre of mass, cz_R, determined above differs insignificantly from the value (3324 km s^{-1}) given by Faber & Dressler (1976), but the velocity dispersion of 496 km s^{-1} is some 40% lower. This is mainly a consequence of the lack of mass weighting in the calculations of Faber & Dressler (and of Vidal & Peterson 1975). A fully rigorous computation would in fact yield a still lower estimate of S, since part of the measured dispersion arises from observational errors in the redshifts (cf. Materne 1974). Estimation of the confidence limits of the velocity dispersion is not straightforward; naive application of the χ^2 distribution implies limits for 68.3% confidence of $459 \leq S \leq 651$ km s^{-1}, but this neglects the uncertainties in the galaxy masses. The 68.3% confidence limits for the cosmological radial velocity cz_R have been calculated on the basis of the t-distribution, assuming error-free masses and a 10% uncertainty in the velocity v_o of the observer.

The downward revision of S from 771 km s^{-1} (the value adopted

for A1060 by Faber & Dressler 1976) to 496 km s^{-1} is of some consequence regarding correlations between S and other properties of clusters generally. The correlation between velocity dispersion and X-ray luminosity is a particularly relevant example, in connection with the evaluation of models of X-ray emission from clusters. Because A1060 has the lowest X-ray luminosity (L_x) of any Abell cluster yet observed, a large change in the estimate of the velocity dispersion (or in that of the L_x) of A1060 can alter appreciably the form of the correlation between L and S at low L_x (see, for example, Figure 5 of Dawe et al. 1977 or Figure 3, Vidal & Peterson 1975). Specifically, a more linear relationship between S and L_x results from the downward revision noted above.

It should be emphasised, however, that most (or all) of the previous determinations of the velocity dispersions in X-ray clusters (as opposed to nearby galaxy groups) have neglected the matter of mass-weighting of individual galaxies, usually in the absence of suitable photometry. If the masses of the galaxies observed in a cluster are appreciably unequal, this neglect may result in the velocity dispersion being overestimated, at least in a cluster dominated by a few bright and centrally located galaxies. It seems likely that the depth into the cluster luminosity function that is represented by each sample of redshifts is greater in nearby, poorer clusters such as A1060 than in richer and more distant clusters in which spectroscopic observations of faint members are not easily secured. Mass-weighting of the redshifts would then be essential for the derivation of comparative values of S, and this requires

optical photometry of the cluster members involved, in conjunction with realistic mass-to-light ratios.

Table 3.1

Particulars of UKST prism plate UJ4067P

Date exposed	4 - 5 April 1978
R.A. (1950)	$10^h\ 34^m$
Dec. (1950)	$-27^o\ 24'$
Emulsion	IIIa-J, hypersensitized
Grain type	Fine
Exposure (minutes)	35
Prism orientation (degrees)	180
Trailing	none

Table 3.2

The redshifts of 43 galaxies, determined by measurements of UKSTU prism plate UJ4067P. Notation is that used in Appendix II.

No.	Z	Suggested Membership	No.	Z	Suggested Membership
90	.00	A 1060	374	.10	
95	.02	A 1060	378	.10	
99	.00	A 1060	404	.05	
133	.00	A 1060	433	.08	C1 1037-260
136	.01	A 1060	449	.10	
157	.04		451	.05	C1 1030-269
169	.07		472	.04	
178	.09		496	.08	
179	.02	A 1060	509	.10:	
183	.00	A 1060	538	.08	C1 1037-260
220	.02	A 1060	563	.14	C1 1037-260?
236	.08	C1 1030-269	574	.06	
249	.05		579	.09	
268	.08	C1 1030-269	587	.07	C1 1037-260?
275	.07:		627	.07	
278	.09		742	.06	C1 1037-260
291	.07		775	.12	
318	.08		803	.06	C1 1030-269
319	.08		814	.07	
323	.09		848	.08	
352	.12		958	.09	C1 1037-260
364	.04				

Table 3.3

Compilation of radial velocities of galaxies in the field of A1060.

	VP	FD	No	α (1950.0) h m s	δ ° ' "	$cz_\odot$	s.e.	n	Identification	Refs
1	J		70	10 33 42.5	-27 14 59	(1)			A1033-2715	3,5
2	S		96	10 33 49.6	-27 11 39	4829	25	1		3
3	10	6	16	10 33 49.9	-26 54 09	3968	4	2	N3305	3,4
4	C	7	5	10 34 00.5	-27 10 43	3611	61	3	N3308	3,4,5
5		11	19	10 34 03.1	-26 44 23	4158	88	1		4
6	O		66	10 34 03.1	-27 19 20	2742	56	1		3
7		10	53	10 34 05.9	-27 03 34	3292	88	1		4
8	M		46	10 34 07.3	-27 13 29	4927	133	1		3
9	B	1	2	10 34 14.3	-27 15 31	4084	11	3	N3309	3,4,5
10	P		37	10 34 20.0	-27 18 03	4736	50	1	A1034-27A	5
11	A	2	1	10 34 21.5	-27 16 06	3650	41	4	N3311	2,3,4,5
12	L		61	10 34 23.4	-27 12 35	(2)				3,6
13	8		14	10 34 37.0	-27 55 01	2753	16	1		3
14	D	3	3	10 34 41.1	-27 18 18	2796	43	4	N3312	1,3,4,5
15	F		B	10 34 51.5	-27 25 24	2916(3)	120	1	N3314	3
16		8	24	10 34 55.5	-27 12 30	4836	4	2	A1034-27B	4,5
17		5	10	10 34 57.5	-26 55 55	3840	88	1		4
18	E	9	9	10 35 15.9	-27 20 01	3906	61	3	N3316	1,3,4
19	5	4	4	10 35 25.5	-26 49 12	3020	9	2		3,4
20	2		7	10 37 55.3	-27 30 57	3970	-	1		3

Column 1: running number; col. 2: VP = designation from Vidal & Peterson (1975); col. 3: FD = designation from Faber & Dressler (1977); col. 4: designation in Appendix II; cols. 5-10: precise epoch 1950 coordinates, ±2" (supersede approximations in Appendix II); col. 11: adopted weighted mean heliocentric velocity in km s^{-1}; col. 12: notes; col. 13: standard error in $cz_\odot$, km s^{-1}; col. 14: number of observations; col. 15: designation as in RC2; col. 16: references.

Notes

(1): $cz_\odot$ = 2389 ± 96 (s.d.)(Vidal & Peterson 1975); 4147 ± 50 (m.e.)(Sandage 1978). Refer to different galaxies? A1033-27 in RC2 is probably object 32, Appendix II.

(2): $cz_\odot$ = 2772 ± 59 (s.d.)(Vidal & Peterson 1975); 2280 ± ? (Fairall 1979).

(3): N3314 consists of two spiral galaxies superposed along line of sight.

References

1: Mayall & de Vaucouleurs (1962); 2: Peterson (1970); 3: Vidal & Peterson (1975); 4: Faber & Dressler (1977); 5: Sandage (1978); 6: Fairall (1979).

CHAPTER 4

PHOTOELECTRIC PHOTOMETRY

The most reliable method of calibration of photographic photometry of galaxies utilising the COSMOS measuring machine is shown, in chapter 5, to involve the comparison of the projected distributions of photographic and photoelectric intensities within suitable standard galaxies. The present chapter describes a series of multicolour and multiaperture photoelectric observations of sixteen galaxies in the field of A1060, carried out on the 1.0m and 0.5m reflectors at S.A.A.O., Sutherland in early 1978 for the purpose of plate calibration. The characteristics of the photoelectric systems are outlined, and an assessment is made of the photometric errors. The derivation of "total" magnitudes of galaxies from the photoelectric data is also discussed.

4.1 Instrumentation

The observations were secured between 31 January to 7 February 1978 with the St Andrews Photometer (StAP) on the S.A.A.O. 1.0m Elizabeth reflector, and during 28 March to 11 April 1978 initially with the 1.0m and StAP and later with the People's Photometer (PP) on the 0.5m reflector. The StAP and PP are single-channel pulse-counting photometers with EMI 6256A S11 photocathodes for UBV photometry operating at a nominal $-10^{o}C$; VBR response is catered for in the PP by an EMI 9659A extended S20 which functions optimally at $-25^{o}C$. The filter combinations applying to each of these systems is given in Table 4.1. Red leak across the Schott UG-2 filters defining the U wavebands is

assumed to be negligible (cf. Shao & Young 1965).

Trials were carried out to ascertain the behaviour of the photometric systems in their operational configurations. Short integrations performed as a star drifted centrally across the largest useful apertures in each of two mutually perpendicular directions confirmed that the response across the fields of the photocathodes was acceptably uniform. The dead time constants of the blue channels of the StAP and PP, which characterise the losses of counts caused by simultaneous arrival of photons, were determined to be 86 and 48 nanoseconds respectively; that of the red channel of the PP was approximately 30 ns.

Focal plane scales were estimated by timing the intervals between bisections of a star image by opposite edges of selected diaphragms with the telescopes stationary. A value of $13\overset{m}{.}8\ mm^{-1}$ was obtained for the 1.0m, in agreement with Corwin (1980), but a trend exists whereby smaller diaphragms give numerically larger plate scales. This effect may also be indicated in data from the 0.5m, for which a scale of $25.1\ mm^{-1}$ is adopted. The linear dimensions (S.A.A.O. and Corwin, private communications) and corresponding angular sizes of the 1.0m and 0.5m diaphragms are presented in Tables 4.2a and 4.2b. In general the tabulated values differ substantially from those quoted in the S.A.A.O. Facilities Handbook for 1977, and supersede them.

Multiaperture measurements of a standard star on the 1.0m telescope reveal a dependence of measured magnitude on diaphragm size caused by light being scattered out of the smaller apertures. For larger diaphragms the correction required was independent of seeing

and amounted to less than $0^m.01$ for apertures greater than 20 arc-seconds. The use of a 20" aperture to isolate the comparison stars therefore introduced negligible systematic error.

4.2 Observations and their Reduction

A single observation on the 1.0m or 0.5m represented the programmed filter sequence V, B, U, U, B, V, with 30-second integrations in each waveband, without recentring. Observations were alternated between each galaxy and one of a set of "sky holes" determined beforehand by reference to deep IIIa-J UK Schmidt plates to be free from contamination by field stars within apertures of interest down to a magnitude of B ≃ 20. All sky holes were at least 10 arcminutes distant from the nominal cluster centre (NGC 3311), beyond which any background glow of intracluster origin should be negligible. Typically 3 galaxy and 2 sky observations were made per selected object on any night; where a galaxy was measured on more than one night, averages were adopted.

The measurements were tied to the UBV system through the use of Cousins' (1973) photometric standards (expanded compilation, avaliable at S.A.A.O.), which were observed at least twice each night at dusk and dawn on the 0.5m and at least three times a night on the 1.0m. Linear transformation coefficients, with a non-linear correction in B-V, determined from measurements on the 1.0m have been used to reduce instrumental magnitudes to the UBV system. Data from the 0.5m have been reduced through linear and non-linear colour equations derived from observations with the blue and the red channels

of the PP separately. Throughout, mean extinction coefficients have been used.

Strictly, to obtain accurate galaxy photometry a correction for light scattered out of the smaller measuring diaphragms, which depends on the luminosity profile of the galaxy, should be taken into account. However since the main purpose of this photometry is to calibrate photographic plates where presumably a similar scattering function is already present, no attempt has been made to correct the photometry for this effect. It appears that only Weedman (1975) has applied corrections of this sort to his data.

In the course of the observations three aberrant stars were found, the implied colour indices of which differed by modest but consistent amounts from those listed by Cousins (1973). The correct indices and V magnitudes are listed in Table 4.4. A fourth star, E393, was also discrepant, but because the measurements were not repeated, the possibility of misidentification cannot be discounted. In addition, the star E336 may have a faint companion.

4.3 Results

The results of the photoelectric photometry are presented in Table 4.3. The galaxy designations in the first column of the table are those employed in Appendix II, which may be consulted to identify the galaxies in the Appendix I finding charts. In Table 4.3, for convenience, standard NGC designations are also given. Column (2) contains the morphological index, T, corresponding to the classification of the galaxy in the de Vaucouleurs (1959) system. Column (3)

lists the telescope aperture in metres, column (4) the diaphragm diameter in arcseconds, and the measured UBV magnitudes and colours are tabulated in columns (5) to (7). Column (8) notes the number of nights on which observations were repeated, where an asterisk indicates that a U-B value on one night was discarded (1.0m) or was not available during VBR photometry (0.5m). V-R colour indices from the latter and their repetition factors are given in columns (9) and (10).

The R band is in the Cape-Kron system (Bingham & Cousins 1974). At an effective wavelength of about 6500 Å the Cape-Kron R is some 450 Å shortward of Johnson's R band (e.g. Johnson 1966); in particular, direct comparison is precluded of the present V-R indices with those measured for galaxies in several southern clusters by Sandage (1975).

The internal accuracy of the photometry may be ascertained by the consistency of measurements from one night to the next. The mean absolute values, and their formal standard deviations, of 53 residuals in each colour from among the 1.0m photometry are

$$V : \langle|\Delta|\rangle = 0.012 \pm .013$$

$$B-V : \langle|\Delta|\rangle = 0.008 \pm .008$$

$$U-B : \langle|\Delta|\rangle = 0.020 \pm .020$$

In general the residuals are magnitude dependent and increase from about half the quoted value at V = 13 to twice the quoted value at V = 15 (Figure 4.1). Similar analysis of the 0.5m data on the brighter galaxies suggests that the mean internal errors of the 0.5m photometry

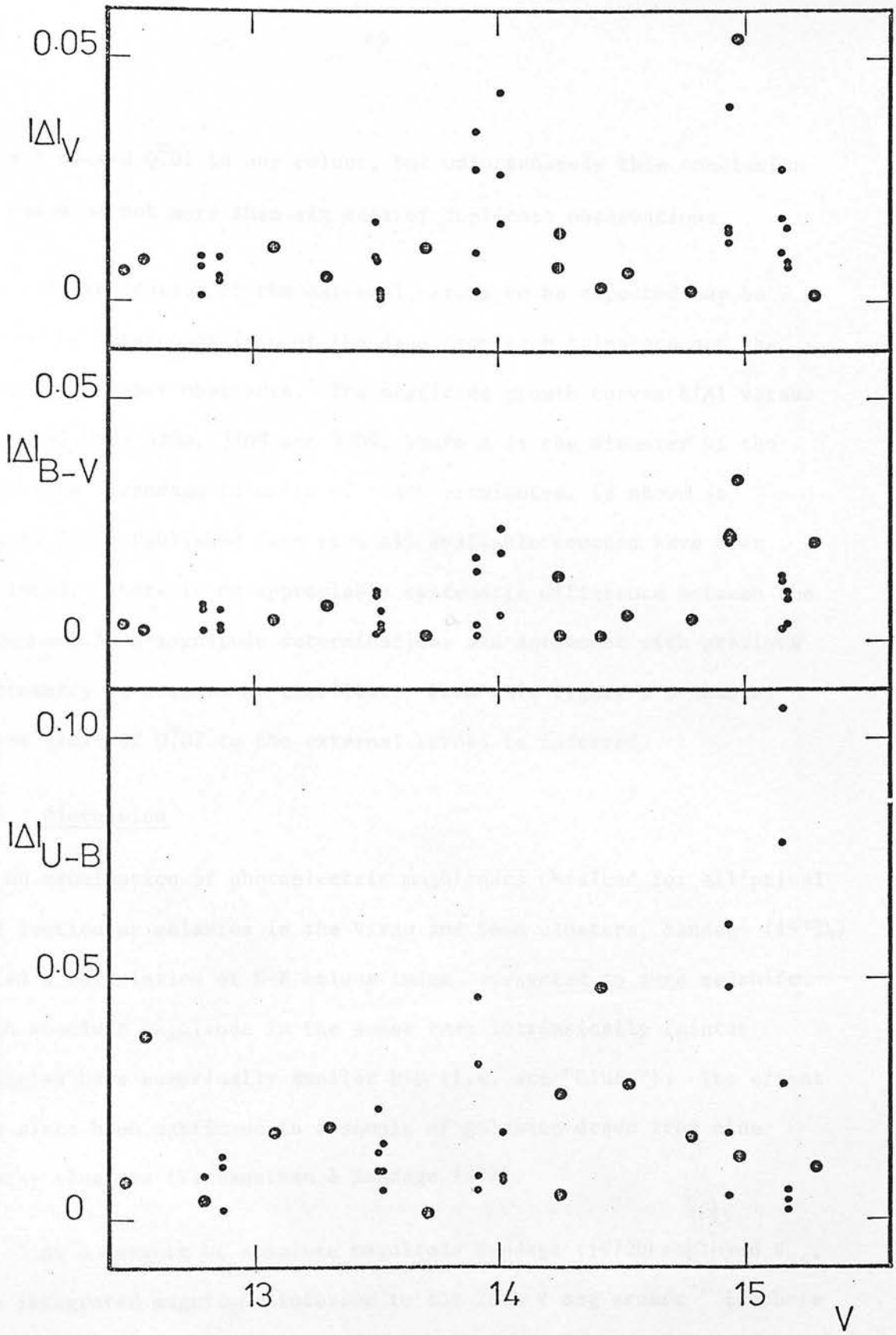

Figure 4.1

The dependence on observed V magnitude of the absolute values of the V, B-V, and U-B residuals from among the 1.0m photometry. Small dots are single points, large dots are double points.

do not exceed $0^m.01$ in any colour, but unfortunately this conclusion is based on not more than six sets of duplicate observations.

An indication of the external errors to be expected may be gained by intercomparison of the data from each telescope and the results of other observers. The magnitude growth curves B(A) versus log A of NGCs 3305, 3308 and 3309, where A is the diameter of the measuring diaphragm in units of tenth arcminutes, is shown in Figure 4.2. Published data from all available sources have been included. There is no appreciable systematic difference between the 1.0m and 0.5m B-magnitude determinations and agreement with previous photometry is seen to be excellent. From this figure a probable upper limit of $0^m.07$ to the external errors is inferred.

4.4 Discussion

In an examination of photoelectric magnitudes obtained for elliptical and lenticular galaxies in the Virgo and Coma clusters, Sandage (1972b) noted a correlation of U-B colour index, corrected to zero redshift, with absolute magnitude in the sense that intrinsically fainter galaxies have numerically smaller U-B (i.e. are "bluer"). The effect has since been confirmed in a sample of galaxies drawn from nine nearby clusters (Visvanathan & Sandage 1977).

As a measure of absolute magnitude Sandage (1972b) employed V_{26}, the integrated magnitude interior to the 26th V mag arcsec^{-2} isophote (adjusted to correspond to an object at the distance of the Coma cluster). In the absence of suitable photographic photometry V_{26} was estimated by means of a standard magnitude growth curve, originally

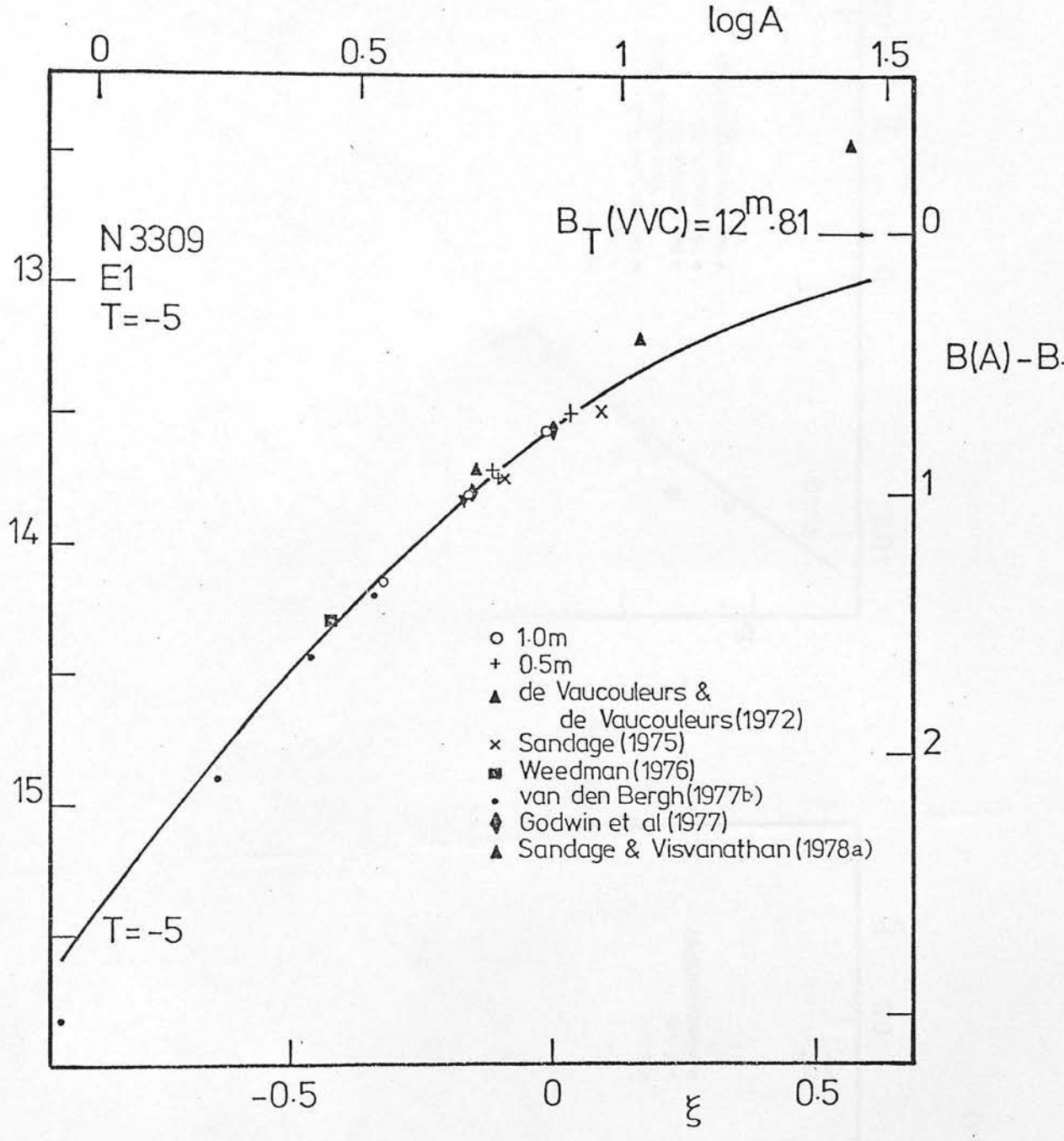

Figure 4.2 (in three parts)

B-magnitude growth curves of three NGC galaxies derived from all available photometry. ξ is the logarithm of the normalised aperture A/A_e, where A_e is that aperture containing half the total B luminosity of each galaxy.

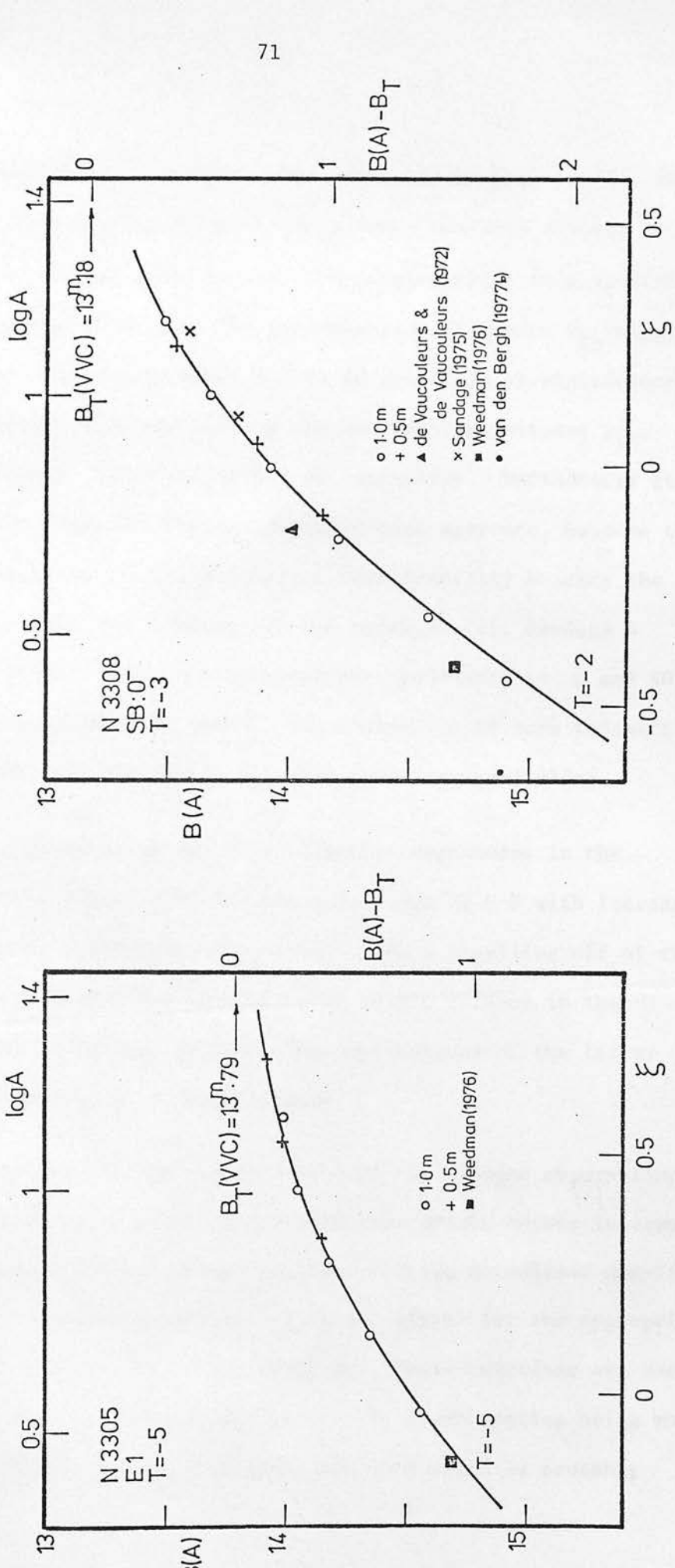

Figure 4.2 (continued)

defined by Humason et al. (1956) and revised by Sandage (1975), which was used to reduce photoelectric V magnitudes measured through diaphragms of various sizes to the values appropriate to a specific fractional galaxy diameter. The determination of metric V_{26} magnitudes of the galaxies listed in Table 4.3 is in principle straightforward, but it is expedient to use instead the isophotal magnitudes V_{25}^{c}, defined in chapter 5, as indicators of luminosity. Furthermore it is permissible to adopt U-B indices averaged over aperture, because the effective dimensions of the diaphragms used generally bracket the face-on major axis semidiameters of the galaxies (cf. Sandage & Visvanathan 1978a), and U-B colour-aperture gradients in E and SO galaxies are comparatively small. The correction to zero redshift (reddening the observed <U-B>) is taken from Sandage (1972b).

Within the range of the four brightest magnitudes in the Hydra I cluster, Figure 4.3 confirms a decrease of U-B with increasing V_{25} for galaxies fainter than $V_{25} \simeq 13.5$, and a levelling off of the relation at the bright end which is also weakly evident in the original study of Sandage (1972b). The implications of the latter result are discussed in a later chapter.

It is of interest to enquire how well the present observations are accommodated by standard galaxy magnitude growth curves in common use. In Figure 4.2 are featured the best-fitting normalised magnitude-aperture relations of de Vaucouleurs et al. (1976) for the appropriate morphological indices, T, of the galaxies. These functions are seen to represent the new observations very well, discrepancies being most apparent among previous photometry of NGC 3309 which is probably

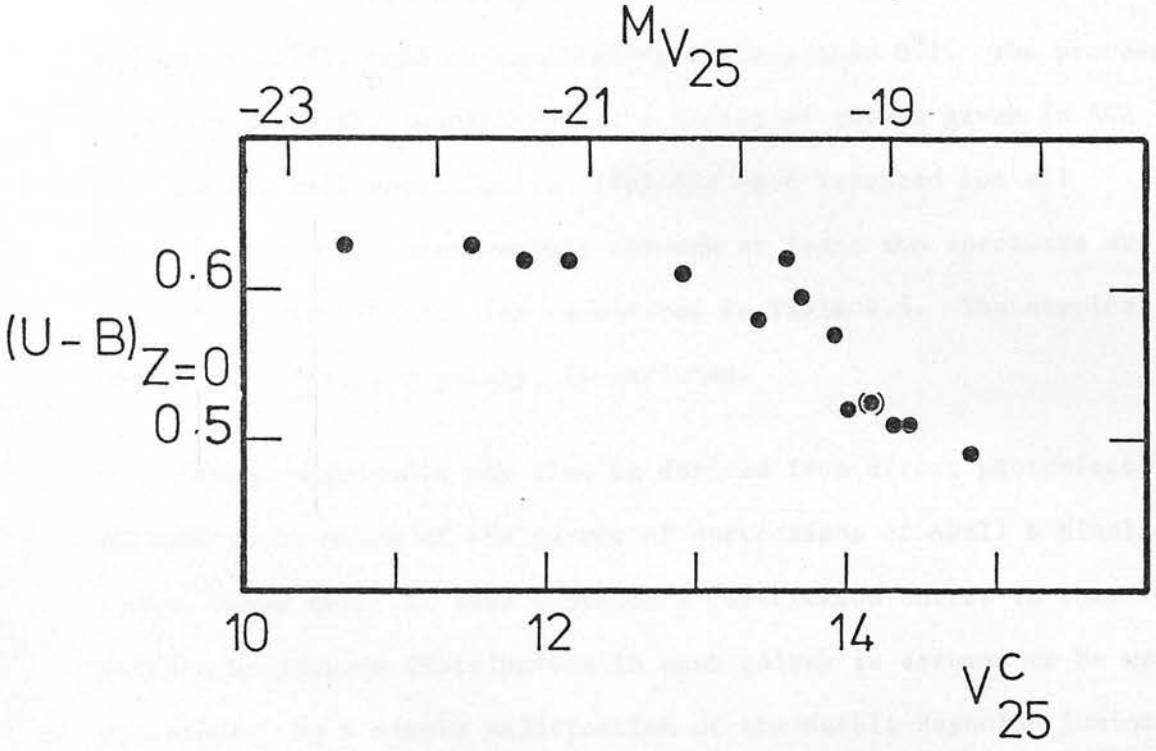

Figure 4.3

The correlation of U-B colour index, corrected to zero redshift, with isophotal magnitude. Parentheses distinguish the S0/a galaxy.

under-luminous at apertures less than 15 arcseconds because of the loss of scattered light, and conversely, affected by contamination of light from the halo of NGC 3311 and a 14th (B) magnitude star at apertures exceeding 56 arcsec. From the fits the "total" or asymptotic B magnitude (log A → ∞) of NGC 3309 is found to be $B_T(VVC) = 12^m.81$, with an uncertainty of less than $0^m.1$. The process of matching to the observations the family of curves given in RC2 (pp. 26-31, with approximation 17b) has been repeated for all galaxies for which measurements through at least two apertures are available, with the results summarized in Table 4.5. The atypical object NGC 3311, a D galaxy, is excluded.

Total magnitudes may also be derived from direct photoelectric photometry by means of the curves of corrections of Abell & Mihalas (1966, Table IV). In this instance a restriction enters in that the surface brightness distribution in each galaxy is assumed to be well represented by a simple modification of the Hubble-Reynolds luminosity profile; only different degrees of apparent ellipticity are distinguished. The prescription of Abell & Mihalas leads to the extrapolated values denoted by $B_T(AM)$ in Table 4.5.

Highly satisfactory fits to the present data, with the exception noted in Table 4.5, are obtained by both the above methods. The fundamental B_T magnitudes agree most closely for elliptical galaxies. The discrepancies of as much as half a magnitude between $B_T(AM)$ and $B_T(VVC)$ for the lenticulars and the transition spiral* reflect the departure of disk galaxies from the luminosity distribution law assumed by Abell & Mihalas. The likelihood that a similar systematic

* The optical appearance of this object is ambiguous and in fact the observed colours (Fig. 4.3) are consistent with those of a normal S0 or E.

error affects total magnitudes derived by the related procedure of "extrafocal" photographic photometry (Abell & Mihalas 1966) deserves consideration, particularly in studies of the radial distribution of galaxies of different luminosities within a cluster that exhibits marked segregation of galaxy types (cf. Abell 1977).

The reduction procedure employed by Sandage and collaborators to obtain V_{26} magnitudes suffers from an essentially equivalent drawback: photoelectric data must be fitted to a single magnitude growth curve without regard of the mean surface brightness, intrinsic ellipticity or precise morphological type of a galaxy. For objects of atypical light distribution (e.g. N3311), the procedure is acknowledged to be fallible (Sandage 1975; Schild & Davis 1979) and photographic surface photometry provides a more reliable method of deriving isophotal magnitudes V_{25} or V_{26}.

Table 4.1

Photomultiplier tubes and filter combinations.

	StAP blue	PP blue	PP red
photo-multiplier	EMI 6256A S11	EMI 6256A S11	EMI 9659A extended S20
V	2mm OG-515	2mm OG-302	3mm GG-495 +1mm BG-18
B	4mm GG-13 +1mm BG-12	4mm GG-13 +1mm BG-12	2mm OG-1 +2mm OG-23 +1mm BG-12
U	1mm UG-2	1mm UG-2	
R			2mm OG-570

Table 4.2a

Dimensions of diaphragms of the St Andrews Photometer on the 1.0m Elizabeth reflector.

Nominal aperture (arcseconds)	True aperture (mm)	True aperture (arcseconds)
5	0.378	5.1
7	0.637	8.8
10	0.758	10.4
14	1.115	15.3
20	1.509	20.9
28	2.188	30.1
40	3.088	42.6
56	4.329	59.6
80	6.128	84.6

Table 4.2b

Dimensions of single-hole (S) and double-hole (D) diaphragms of the People's Photometer on the 0.5m reflector. The blue (B) and red (R) channels of (D) diaphragms are distinguished. The qualifying colon indicates that measured horizontal and vertical diameter differ by more than two percent.

Nominal aperture (mm)	True aperture (mm)	True aperture (arcseconds)
0.32S	0.294:	7.4
0.63D(B)	0.636:	16.0
(R)	0.664	16.7
0.67D(B)	0.656	16.5
(R)	0.657:	16.5
0.73D(B)	0.652	16.4
(R)	0.639	16.0
1.0S	1.030	25.9
1.0D(B)	0.983	24.7
(R)	0.970	24.3
1.02D(B)	1.043	26.2
(R)	1.019:	25.6
1.141D(B)	1.371	34.4
(R)	1.352	33.9
1.5D(B)	1.404:	35.2
(R)	1.402	35.2
1.56D(B)	1.521	38.2
(R)	1.540	38.7
1.93D(B)	1.912	48.0
(R)	1.911	48.0
2.0S	1.970	49.4
2.0D(B)	2.017	50.6
(R)	2.014	50.6
2.02D(B)	2.018	50.7
(R)	2.024	50.8
3.0S	3.010	75.6
3.0D(B)	3.003	75.4
(R)	2.997	75.2
4.5S	4.486	113
4.5D(B)	4.372:	110
(R)	4.424	111
6.0S	6.017	151
6.0D(B)	6.006	151
(R)	5.961	150
8.0S	8.034	202
8.0D(B)	8.052	202
(R)	8.053	202
10.0S	9.999	251

Table 4.3

Photoelectric observations of galaxies in the Hydra I cluster.
For a guide to this table see the text.

Galaxy	T	Tel	Ap	V	B-V	U-B	n	V-R	n
1=N3311	-2	1.0	42.6	12.85	1.07	0.64	1		
		0.5	48.0	12.75	1.05	0.61*	2	0.63	1
		1.0	59.6	12.47	1.06	0.61	2		
		0.5	75.2	12.23	1.06		1	0.64	1
2=N3309	-5	1.0	20.9	13.08	1.07	0.65	2		
		1.0	30.1	12.75	1.06	0.58	1		
		0.5	33.9	12.63	1.09		1	0.62	1
		0.5	34.4	12.69	1.06	0.62	1		
		1.0	42.6	12.50	1.07	0.61	1		
		0.5	48.0	12.44	1.06	0.64*	2	0.65	1
4=I2597	-5	1.0	20.9	13.08	1.05	0.62	1		
		1.0	30.1	12.79	1.05	0.59	3		
		0.5	33.9	12.71	1.03		1	0.64	1
		1.0	42.6	12.55	1.04	0.63	2		
		0.5	48.0	12.48	1.04		1	0.63	1
5=N3308	-3	1.0	10.4	14.24	1.06	0.63	1		
		1.0	15.3	13.85	1.05	0.59	1		
		1.0	20.9	13.52	1.06	0.61	3		
		1.0	30.1	13.16	1.04	0.63	1		
		0.5	33.9	13.07	1.06		2	0.61	2
		1.0	42.6	12.86	1.06	0.61	3		
		0.5	48.0	12.82	1.05	0.59*	2	0.63	1
		1.0	59.6	12.62	1.04	0.61	1		
		0.5	75.2	12.50	1.04		1	0.67	1
		1.0	84.6	12.44	1.05	0.61*	1		
12=N3305	-5	1.0	20.9	13.50	1.06	0.60	3		
		1.0	30.1	13.30	1.05	0.59	2		
		1.0	42.6	13.13	1.05	0.59	1		
		0.5	48.0	13.11	1.04		1	0.59	1
		1.0	59.6	13.02	1.03	0.58	1		
		0.5	75.2	12.93	1.05		1	0.64	1
		1.0	84.6	12.95	1.04	0.63	1		
		0.5	111.0	12.89	1.04		1	0.67	1
22	-2	1.0	20.9	13.91	1.06	0.57	4		
		1.0	30.1	13.71	1.05	0.57	2		
		0.5	33.9	13.63	1.06		2	0.64	1
		0.5	48.0	13.51	1.04		2	0.66	1
24=N3315	-2:	1.0	20.9	14.25	1.08	0.59	2		
		1.0	30.1	13.97	1.07	0.66	1		

contd...

Table 4.3 (contd.)

Galaxy	T	Tel	Ap	V	B-V	U-B	n	V-R	n
31	-2	1.0	20.9	14.53	1.05	0.54	2		
		1.0	30.1	14.25	1.05	0.58	2		
		1.0	42.6	14.01	1.04	0.51	1		
38	-2	1.0	20.9	14.01	1.05	0.58	3		
		1.0	30.1	13.83	1.04	0.59	1		
		0.5	33.9	13.78	1.06		1	0.62	1
		0.5	48.0	13.70	1.04		1	0.64	1
56	-3	1.0	20.9	14.78	1.00	0.50	2		
60=N3307	1	1.0	20.9	14.93	1.00	0.44	4		
61	-5	1.0	20.9	14.41	0.99	0.51	2		
66	0:	1.0	20.9	15.15	1.00	0.54	3		
		1.0	30.1	14.97	0.98	0.49	2		
68	-5	1.0	20.9	14.76	1.01	0.50	1		
86	2	1.0	20.9	15.17	0.87	0.28	3		
92	-3	1.0	20.9	15.28	1.00	0.48	2		

Table 4.4

Corrections to the photometry of Cousins (1973, 1974) of stars in the Harvard E-regions. The last column records the number of nights during which each star was observed.

Star	V	B-V	U-B	n
E393	7.175	1.577	1.892	1
E491	6.843	-0.122	-0.527	2
E583	7.974	0.984	0.663	4
E607	8.788	0.120	0.098	2

Table 4.5

Extrapolated total magnitudes B_T of galaxies in the Hydra cluster. A less reliable determination is enclosed in parentheses.

Galaxy	Type	T	B_T(VVC)	B_T(AM)
2	E1	-5	12.80	12.65
4	E3	-5	(12.55)	12.70
5	SB:0$^-$	-3	13.20	12.75
12	E1	-5	13.80	13.80
22	S0^o	-2	14.35	14.15
24	S0:	-2:	14.45	13.90
31	S0	-2	14.60	14.10
38	S0 pec	-2	14.60	14.45
66	S0/a?	0?	15.75	15.35

CHAPTER 5

PHOTOGRAPHIC PHOTOMETRY

Early photographic photometry of galaxies involved the laborious construction of detailed two-dimensional luminosity profiles of single galaxies from repeated one-dimensional microphotometric scans (e.g. de Vaucouleurs 1948; Holmberg 1950, 1958). The high precision of magnitudes derived by this procedure more than justifies its continuing application (e.g. Fraser 1977, Kormendy 1977a) in studies of modest numbers of galaxies.

The relatively great speed and labour-saving potential of the new generation of rapid two-dimensional digitising microphotometers with auxiliary computers was nevertheless recognised by Jones et al. (1967), who describe numerical mapping techniques to extract, from data generated by these machines, useful photographic parameters of galaxies. Godwin (1976) has published abridged versions of these procedures which facilitate the processing by computer of the large numbers of images involved in studies of clusters. Independent data reduction schemes (e.g. Oemler 1976; Strom & Strom 1977, 1978a; MacGillivray & Dodd 1979) as well as adaptations of the Jones et al. or Godwin procedures (e.g. Okamura 1977, Carter & Dixon 1978, Green 1978) are now in widespread use.

In this chapter the derivation of isophotal magnitudes of several thousand galaxies in the field of A1060 by the analysis of measurements made by the COSMOS machine is described.

5.1 Plate Material

The photographic plates of the Hydra I cluster were taken with the UK 1.2m Schmidt telescope by members of the Schmidt Unit during 1975 and 1977. Details of the relevant plates are given in Table 5.1.

The emulsion-filter combinations are those routinely employed by UKSTU to imitate photographically the Johnson B and V photoelectric wavebands (Johnson & Morgan 1951, 1953). The resulting photographic responses cannot be expected to match precisely the effective wavebands of the photoelectric photometry secured for plate calibration, and such mismatching of bands could introduce errors of the photographic zeropoints which correlate with the colours of the calibrators involved. Those employed in this work (Table 4.3) represent too narrow a range of colour to indicate whether the effect is present, so negligible disparity of photoelectric and photographic wavebands is assumed by default.

All plates listed in Table 5.1 were measured on the COSMOS machine in either or both of two measurement modes (Table 5.2). A second B and a U-band plate were also measured, but were not processed to obtain magnitudes. Furthermore it proved unnecessary to calibrate the R plate photoelectrically. Calibration is considered in section 5.4.

COSMOS job number 254 was a pilot study involving the detailed examination of a small number of galaxies; the remaining jobs run under mapping mode each generated four magnetic tapes of data. One tape from job 301 was unfortunately corrupt and the remaining three

were used only to check the photometry of plate V3324.

5.2 Processing Techniques

The photographic photometry of galaxies undertaken in this study is of two types. The primary photometry is based on the application of modified Godwin (1976) routines to data generated by COSMOS in mapping-mode operation; the secondary photometry, of lower precision, is obtained from coarse-mode parameters output by the COSMOS hardware pattern analyser and is tied to the primary photometric system. The primary B and V systems are calibrated by photoelectric observations of standard galaxies (Chapter 4). Only V-band magnitudes are defined by the secondary photometry.

The principal virtue of the primary photometry lies in the ability of the adopted routines to handle most of the instances of overlapping images frequently found in the core regions of dense clusters of galaxies, and more generally within regions of enhanced density of field stars. At the galactic latitude of A1060 ($b \simeq 26^{o}$), the isophotes of brighter members are contaminated more often than not by light from neighbouring galaxies or superposed stars; such blends are not generally recognised for what they are by the COSMOS coarse-mode pattern analyser (now de-commissioned), and when assessing the secondary photometry this shortcoming must be accounted for.

During the course of the work several modifications to the processing routines of the primary photometry were introduced, and will be described in the following outline of the procedure.

The output from COSMOS in its mapping mode consists of arrays of up to 3200 x 3200 transmission readings representing an area of plate, and additional arrays of measurements across either or both step wedge calibrators impressed on the plate. This amount of data is obviously too large to be held in entirety in a computer core for random access, so subsamples of the main array are processed in instalments. To exploit more fully the computing power available in the present work, the original routines were uprated by 50% to handle individual grids of 316 x 316 picture elements. A subroutine was incorporated to generate the arrays.

A mesh of 44 x 44 integers, referred to as the "coarse" or "outer" grid, is first extracted to model the variation of the sky background in a chosen locality. The value of each array element represents the median of 15 x 15 transmission readings; the median is a more stable quantity than the mode and is less sensitive than the latter to biases in analogue-to-digital converters, although in the mean it lies slightly above the true sky level on account of the skewness of the distribution of transmissions.

Within this matrix of sky values, the 25% of all points encompassed by a specified interior square are removed. A two-dimensional third-order polynomial is then fitted to the reduced array by a process of repeated rejection of points more than β standard deviations distant from the most recent approximating surface, where on successive cycles β = 2, 2.25, 2.25, and 2.5. Only significant terms of this polynomial are retained after each cycle. Early exit is arranged if any cycle rejects no further points;

typically 12% of the points, mainly in the vicinity of bright images, are eliminated by this means. More than sufficient array elements remain at the conclusion of the process to define the final polynomial adequately, whereas the computational demands of coarse grid construction are more than offset by the greater speed of fitting a polynomial to fewer points (cf. Barbon et al. 1976).

A "fine" or "inner" grid interior to the coarse array and positioned over the effective hole in the latter is next constructed from 316 x 316 raw transmission readings. The relative geometry of coarse and fine grids is shown in Figure 5.1. This is a generalisation of Godwin's (1976) Figure ii in that the fine array is now permitted to take up any enclosed position relative to the coarse square, according to parameter values specified at execution time. The effect of this is to reduce the inaccessible border zone from 20% to 1% of the total area of the COSMOS scan. The relative dimensions of the grids employed satisfy the criterion of stability laid down by Jones et al. (1967) for third-order interpolation across the region of the inner grid, though it should be noted that extrapolation is invoked should one or more boundaries of inner and outer grids coincide. The interpolation procedure ensures that bright images contained entirely within the inner grid do not affect the local background determination.

Each pixel in the fine grid is transformed to a scale of relative intensity according to the Baker characteristic of the plate (section 5.3) and compared with the value of the background polynomial, likewise transformed, at the same position. In this way a grid of intensity

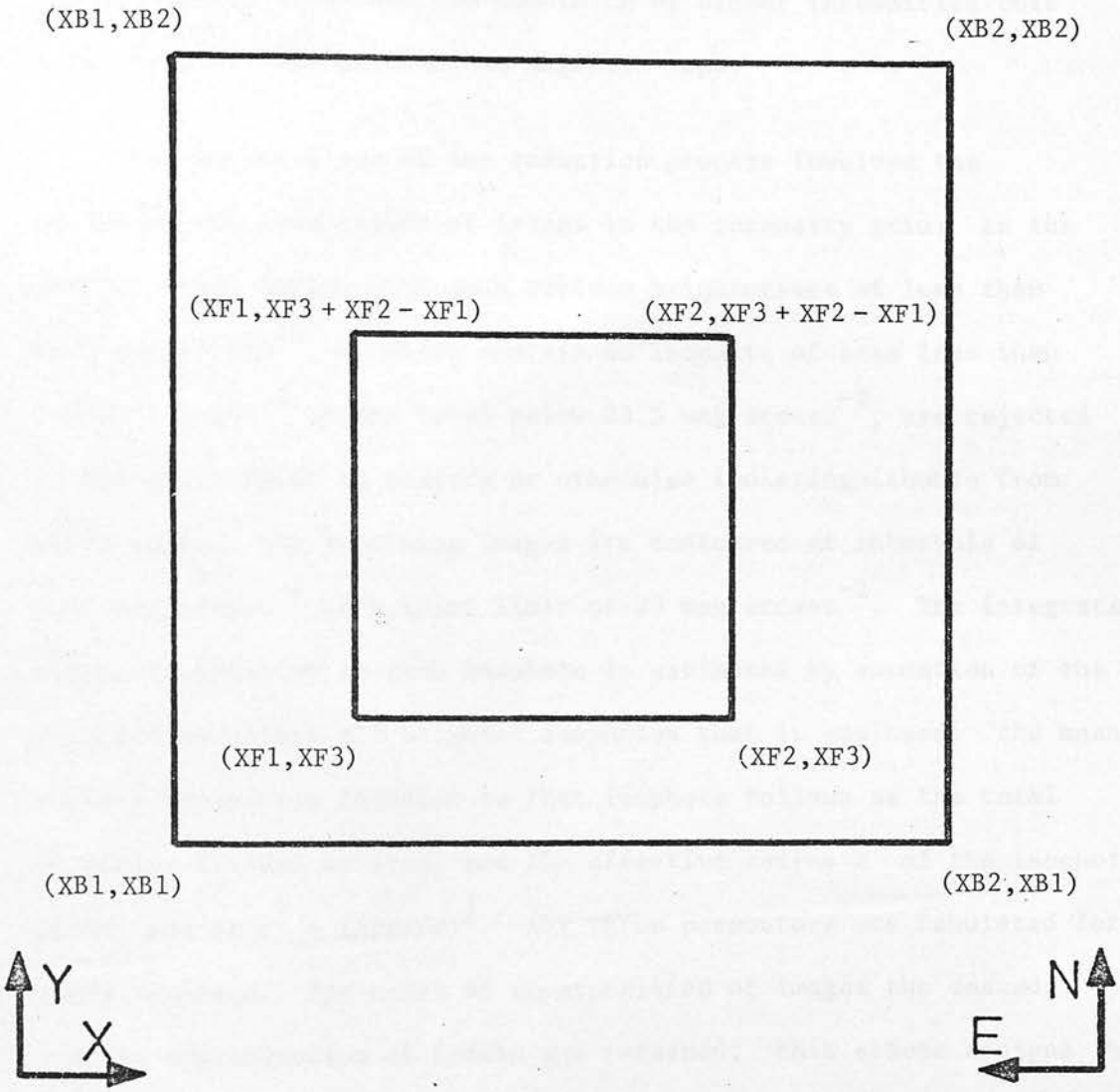

Figure 5.1

The relative geometry of the inner and outer grids.

readings expressed in units of the subtracted night sky background (de Vaucouleurs & Page 1962) is generated. After adjustments to the background level and the smoothing of higher intensities this array is stored temporarily on magnetic tape.

The second stage of the reduction process involves the selection and examination of images in the intensity grid. In the present study images with peak surface brightnesses of less than 23.5 mag arcsec^{-2}, or which contain an isophote of area less than 5.0625π arcsec^{2} at any level below 23.5 mag arcsec^{-2}, are rejected as being too faint to measure or otherwise indistinguishable from plate noise; the remaining images are contoured at intervals of 0.25 mag arcsec^{-2} to a faint limit of 25 mag arcsec^{-2}. The integrated magnitude interior to each isophote is estimated by summation of the intensities within all brighter isophotes that it encloses; the mean surface brightness interior to that isophote follows as the total intensity divided by area, and the effective radius r^* of the isophote is defined as $r^* = (\text{Area}/\pi)^{\frac{1}{2}}$. All three parameters are tabulated for every isophote. For cases of superposition of images the cascade overlap approximation of Godwin was retained; this scheme assigns the luminosity of succeeding (descending) isophotes to overlapping images in the ratio of the areas of their faintest unconnected isophotes. Since compact objects with steep brightness profiles have relatively large inner isophotes, superposed stars tend to become overluminous at the expense of galaxies in this photometry. Interactive picture processing schemes (e.g. Barbon et al. 1976, Strom & Strom 1977) are better equipped to handle superpositions, but final accuracy, about $\pm 0^{m}.25$, is never high.

Particular modifications were applied as follows. The calibration scheme was reworked to express the relationship between transmission and relative intensity in terms of a Baker characteristic (section 5.3). The coupling between the inner and outer grids was altered. The original method whereby the two sets of measurements were reduced to a common system by comparing transmissions round the perimeter of the inner grid with the values at corresponding positions in the outer grid was discarded as untenable because image contributions were present in one grid but not in the other. Instead a correction was applied to shift the mode of the frequency distribution of intensities in the inner grid to the zero level after the background was subtracted. Repeated checks showed that the variable skewness of the distribution caused by the presence of bright images within the inner grid was inconsequential compared to statistical uncertainties in the position of the mode arising from the quantisation of the transmission measurements. This, approximately 1% at the sky intensity, effectively limits the precision with which individual corrections can be determined, but by comparing the reductions of many grids the necessary adjustment was reckoned as +0.5% on average for the IIaD emulsions and +1.0% for the IIaO. The use of median transmission values to approximate the sky level thus results in a slight overestimate, as expected. These corrections were adopted for later reductions, and previous processing was repeated in cases of gross error. During reductions of plate B3028, every frame was examined individually before final zeropoint adjustments were made.

Numerical smoothing was effected in a contrary sense, to high intensities rather than to low. This reduced the number of cases in

which transmission fluctuations in the high-intensity domain produced spurious discrete peaks within the cores of authentic images; similar treatment of lower intensities, to reduce noise, was discontinued when surface brightness profiles were found to be altered.

Further necessary but trivial modifications included redefined functions and graphical instructions for the construction of isophotal maps. In addition a library of related programs was developed for the display and inspection of photometric data, descriptions of which are omitted.

5.3 Transformation to Intensities

On plates taken with the UK Schmidt telescope, guidance on the transformation of photometric measurements on some instrumental system is presently provided by a system of two step wedges. The prototype wedge consists of translucent metal film deposited on a glass base in seven contiguous steps of successively decreasing transparency; the second wedge is a photographic duplicate. In the telescope illuminating lamps leave photographic impressions of the wedges within two unexposed regions near the north and east edges of the plate masked off during the simultaneous sky exposure. Subsequent measurement of any plate by COSMOS in mapping mode operation includes a longitudual scan of at least one wedge impression.

A regrettable shortcoming of this arrangement that is conspicuous at shorter wavelengths is the faintness of the lamps deployed, in relation to the central surface brightnesses of the galaxies that register on the plate. As a result the impressions of the wedge

calibrators seldom exhibit opacitances as high as those measured in the cores of brighter images, unless the photographic emulsion saturates, as in the case of sky-limited IIIa-J plates. For IIaO, IIaD and 098 plates of representative exposure times, however, this problem is overshadowed by the effective upper limit to the dynamic range of the COSMOS measuring machine.

The relative intensity values corresponding to the steps of each wedge have been measured photoelectrically by Tritton (1977, UKSTU memorandum). The conflict between his figures and those of the less direct derivations of Dawe (1978 revision, privately circulated) is considered below.

Probably the most elegant expression empirically to relate the intensity of illumination to the density induced in the exposure was proposed by Baker (1925) and independently by de Vaucouleurs (1968). If RI denotes relative intensity and D optical density, the empirical Baker function or "generalised Sampson" transform is

$$RI = A(10^{D/B} - 1)^{n}$$

where A, B and n are constants. This relation also obtains as a limiting case of the Kaiser function (Honeycutt & Chaldu 1970) in the absence of saturation. It frequently offers a linear representation of the characteristic curve of a photographic emulsion, enabling calibrations to be constructed on the basis of few data points, but it is nevertheless fallible, as Barbon et al. (1976) have illustrated. The most satisfactory representation of a general characteristic curve may in fact involve a seven-parameter function (Tsubaki &

Engvold 1975). In particular, the breakdown of the linearity of the Baker function of densely exposed plates has led to the use of less wieldy alternatives (e.g. Schweizer 1976, Kormendy 1977a, Okamura 1977, Carter & Dixon 1978, Carter & Godwin 1979, Dufor et al. 1979), frequently polynomials in the opacitance $\omega = 10^{D/B} - 1$.

The expression for the opacitance appropriate to the COSMOS machine is $\omega = T_o/T - 1$, where T is transmission and T_o represents that of the chemical fog level. The enumeration of four parameters, including the small correction term in transmission that represents the reading for zero incident light intensity, is therefore required to define the Baker characteristic. Due to the established operational practice of adjusting the effective transmission range to ignore photographic intensities fainter than the minimum sky level, the value of T_o must be estimated by repeating the wedge measurements at different instrumental settings, or by relating the original wedge transmissions to the density readings recorded on, for example, a Joyce-Loebl isodensitometer or Macbeth densitometer. Both methods have been applied here to each determination.

An example of a wedge tracing is shown in Figure 5.2. At each position along the axis the recorded transmission is the mean of 128 samples laterally and may be non-integral. The appreciable non-uniformities of the wedge steps and the consequent difficulty of defining their mean levels constitute the principal limitation of the calibrations. Figure 5.3 shows the Baker functions for this wedge (north; upper) according to the relative intensity values supplied by Tritton and by Dawe. The greater linearity inherent in the former

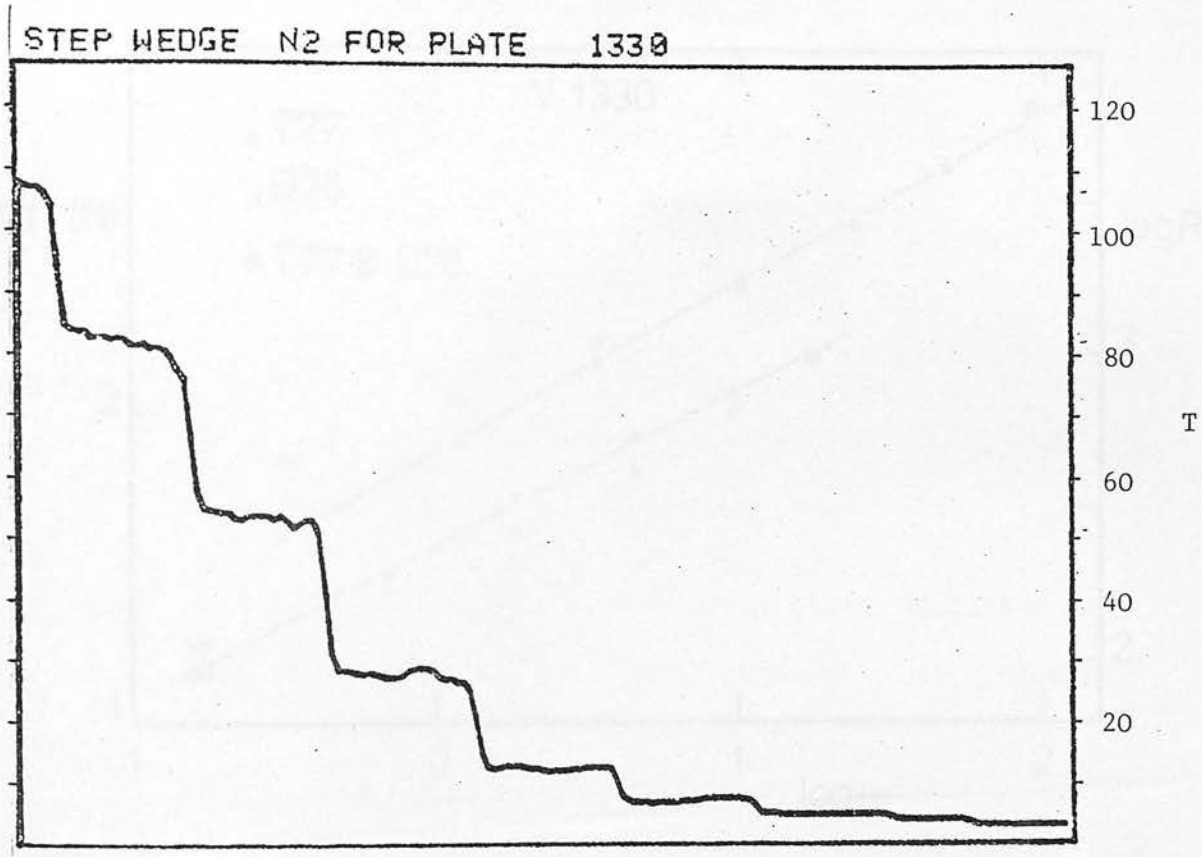

Figure 5.2

Example of a step wedge impression measured by COSMOS. The densest step level is lowermost. T denotes transmission.

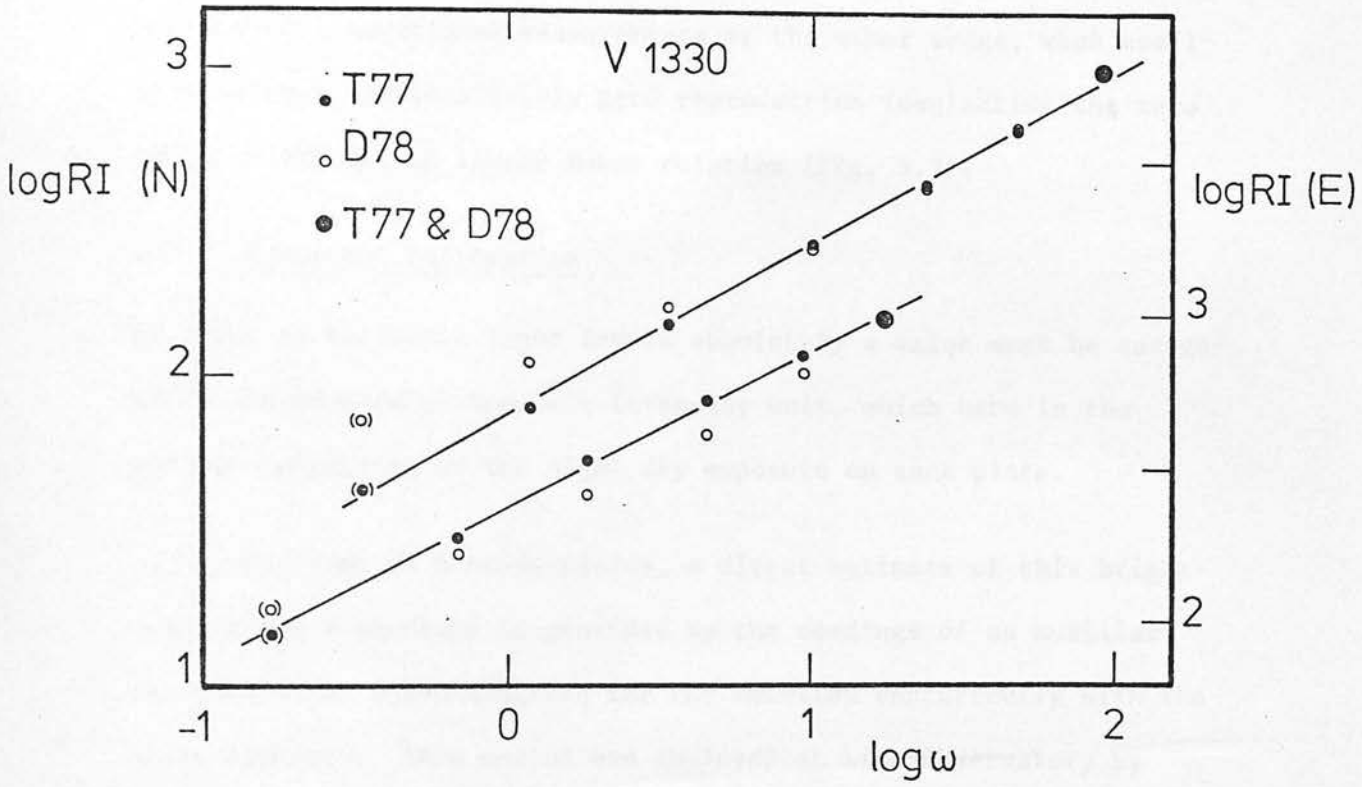

Figure 5.3

The Baker characteristic of plate V1330 as defined by the north step wedge (upper relation, left scale) and by the east step wedge (lower relation, right scale), using the relative intensity values of Tritton (T77) and of Dawe (D78). The lines are fits to Tritton's values; the upper relation was adopted. The zeropoints of the intensity scales are arbitrary.

calibration is also apparent in every other plate/filter combination so far investigated. For this reason the figures of Tritton were adopted provisionally, subject to confirmation*. Of the two wedges available, preference was normally given to the more densely exposed north wedge in order to maximise the range of opacitances thus calibrated; additional measurements of the other wedge, when available, always led to a fairly good reproduction (neglecting the zero point shift) of the linear Baker relation (Fig. 5.3).

5.4 Zeropoint Calibration

In order to calibrate light levels absolutely a value must be assigned to the adopted photometric intensity unit, which here is the surface brightness of the night sky exposure on each plate.

For some UK Schmidt plates, a direct estimate of this brightness in the B waveband is provided by the readings of an auxiliary sky photometer which monitors the sky emission concurrently with the plate exposure. This method was employed at Lick Observatory by Dressler (1978b). Unfortunately the original calibration of the UKST photometer in 1973 was in error by some +0.6 ± .16 magnitudes and the source is decaying at the rate of about $0^m.1$ year^{-1} (MacGillivray, private communication). The photometer does not define sky brightnesses in wavebands other than B.

Photoelectric stellar sequences have been shown (e.g. King & Hinrichs 1967, Kormendy 1973) to be capable of defining both the intensity scale and the zeropoint of a system of photographic measurements to an accuracy of $\sim 0^m.1$. One such sequence has been set up in

* The most recent estimates of the wedge intensities quoted by UKSTU (October 1979) take intermediate values.

the core of the Hydra I cluster by Smith & Weedman (1976). However in the present photometry exploitation of this sequence is seriously hampered by the lack of effective resolution of the spot scanner in the COSMOS machine, the restricted range of surface brightness that is measurable, and most fundamentally, due to the location of virtually all of the standard stars within regions exhibiting luminosity gradients caused by the proximity of very bright images.

The most satisfactory method of estimating the zeropoints has proved to be based on comparisons of integrated photographic magnitude profiles of standard galaxies with reference photoelectric profiles determined from multiaperture photometry. With suitable observations (Table 4.3) profiles can be defined over ranges of several tenths of arcminute, avoiding the effects of resolution and atmospheric seeing (cf. Carter 1979, Schweizer 1979) which dominate the central six arcseconds of images on Schmidt plates.

An example of a magnitude growth curve defined by photoelectric observations is plotted as circles in Figure 5.4. The total photoelectric intensity interior to various radii on a scale of arbitrary zeropoint may be found by interpolation and compared with the corresponding integrated photographic intensity obtained by simulated aperture photometry of the plate image (Fig. 5.5). If I^s denotes the zeropoint error in the total photographic intensity caused by saturation of transmission readings at the centre of the image, then at any radius r external to the saturated core of semidiameter r_{sat}

$$I_{pg}(\leq r) + I^s = \text{constant} \times I_{pe}(\leq r) \ , \quad r > r_{sat}$$

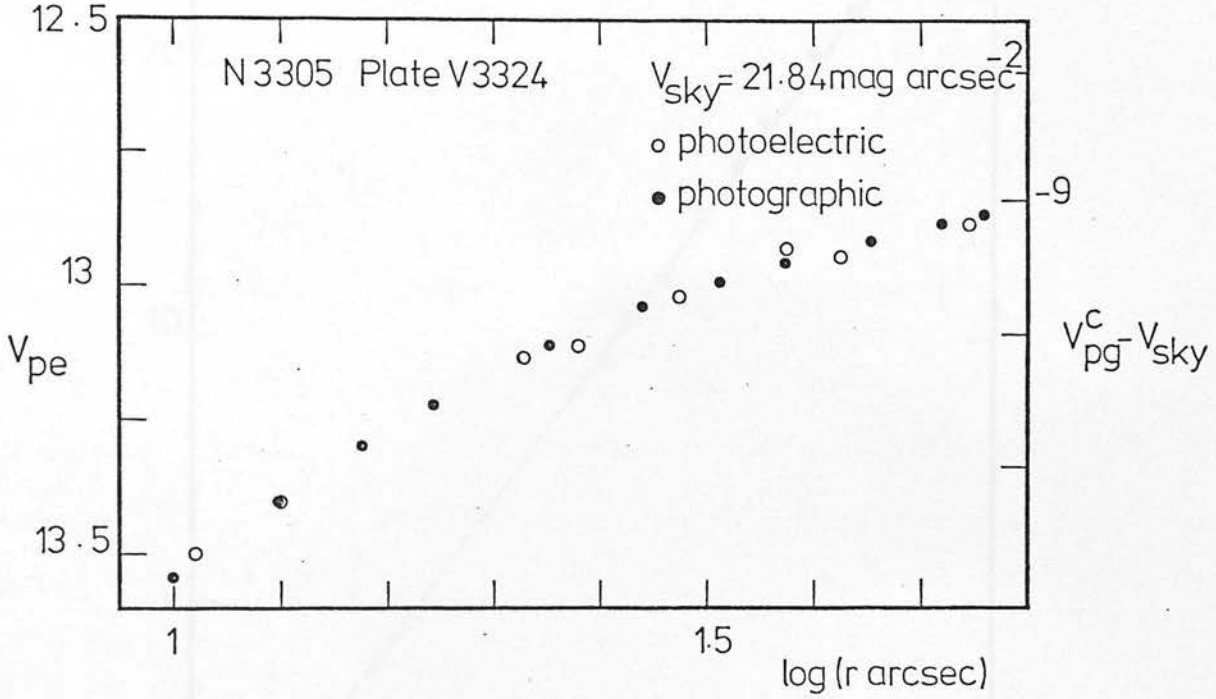

Figure 5.4

The optimally matched photoelectric (V_{pe}) and corrected photographic (V^c_{pg}) magnitude profiles of NGC 3305 in the V band.

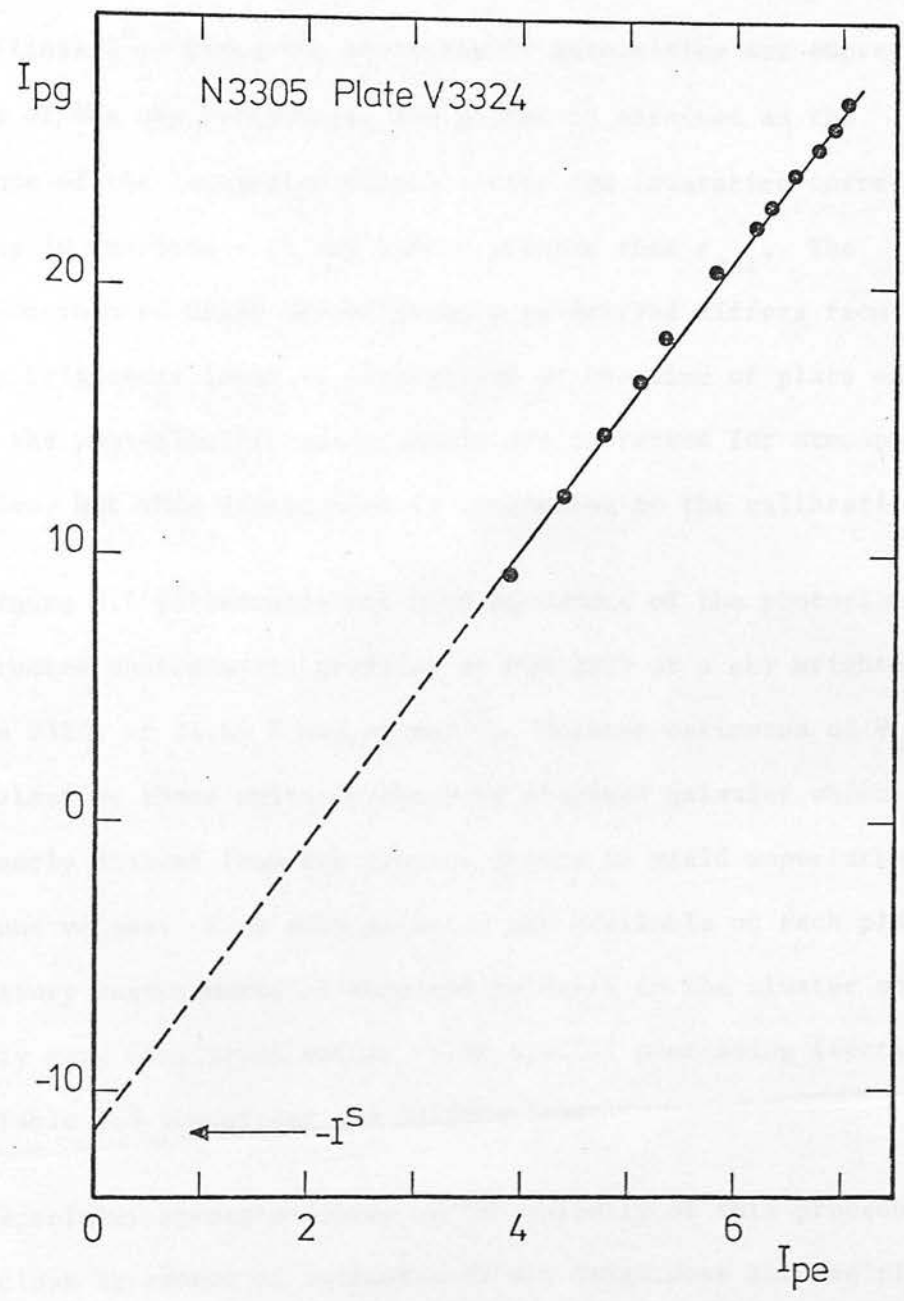

Figure 5.5

Plot of the integrated photographic intensity within simulated apertures centred on a plate image of N3305, versus corresponding photoelectric intensity (both shown in arbitrary units). I^s is a measure of the saturation of the photographic image.

which defines I^s. Since the photographic intensities are expressed in units of the sky brightness, the latter is obtained as the difference of the integrated photoelectric and saturation-corrected photographic magnitudes at any radius greater than r_{sat}. The extinction-reduced night sky brightness so derived differs from the true sky brightness local to that galaxy at the time of plate exposure because the photoelectric measurements are corrected for atmospheric extinction, but this distinction is immaterial to the calibration.

Figure 5.4 illustrates the good agreement of the photoelectric and corrected photographic profiles of NGC 3305 at a sky brightness on plate V3324 of 21.84 V mag arcsec^{-2}. Further estimates of V_{sky} are provided by those multiply-observed standard galaxies which are sufficiently distant from the cluster centre to yield unperturbed background values. Five such galaxies are available on each plate; confirmatory measurements of standard galaxies in the cluster core generally gave consistent values after special processing (section 5.5). Table 5.3 summarises the calibrations.

Especially strong evidence of the validity of this procedure is the close agreement of estimates of sky brightness for one plate that follow from independent measurements (Jobs 254 and 301). However the slope, m, of the relation in Figure 5.4 is not constant for galaxies on any one plate and empirically it is correlated with I^s, itself dependent on galaxy type (i.e. bulge to disk ratio) and magnitude (cf. Figs. 5.10-11). This would imply systematic errors in the calibrations of relative intensity, and that of plate B3028 in particular.

5.5 The Primary Photometry

The large angular extent of A1060 and the desirability of good resolution for the study of small images conspired to guarantee more data from a single plate than could be stored on one magnetic tape. The measurement of each plate was therefore carried out in four instalments, each involving one corner of a square region of 3.65 deg^2. In order to process the images inevitably split by internal boundaries, routines were devised to enable construction of a fifth tape from various combinations of the original four.

Straightforward computer analysis of four magnetic tapes would have involved the reduction of at least 484 individual frames each of 316^2 pixels, too many to contemplate. Accordingly, grids of data from plate V3324 were extracted only at locations which encompassed images suitable for photometry, so disregarding the 65% of unnecessary data. Galaxies were selected for study and later recovered on the basis of coarse-mode identifications (Chapter 2), and resulting photometric parameters were added to the master card file. The limiting magnitude of the photometry is therefore determined by the completeness of the three stages of detection, visual identification and selection of the coarse mode data, and by the surface brightness and magnitude requirements imposed during processing; ideally, the latter would dominate. Eleven objects with magnitudes in the range $16.2 < V_{25} < 17.9$, with no corresponding CM identifications, were discovered in the course of the primary photometry. The completeness limit, after including these objects, is considered to be $V_{25} = 17.0$.

The practical inconvenience of this piecemeal approach was

avoided in reductions of plate B3028, at some expense in resolution, through the ninefold increase in the areal dimensions of the inner grid afforded by 3 x 3 averaging in intensity. This permitted systematic and complete processing of the region scanned on the B plate. Finally, photographic photometry was also obtained from three data tapes of plate V1330, with and without intensity averaging.

The presence of the bright stars SAO 179041 (=BS 4162, V = 4.88) and SAO 179027, which seriously perturb the photographic sky background level local to the core of the cluster, dictated the following approach to image analysis of the central region. The geometry of Figure 5.1 was scaled up by a factor of 128/15 in absolute linear dimensions. Fully contained within the inner grid, the central images no longer affected the external background level; this simultaneously avoided the possible influence of intracluster luminosity concentrated near the cluster core. The luminosity profiles of the two bright stars were determined from diagonal cross-sections which avoided the diffraction spikes. Image analysis was then carried out as before within suitably positioned grids but with all intensity elements referred to the background polynomial determined from the giant external grid, and with both stellar luminosity profiles subtracted out of each matrix.

5.6 The Secondary Photometry

The secondary photometry is based on data generated by COSMOS in its coarse analysis mode. Among parameters that are output to describe every image is a measure of area, denoted A, in units of number of pixels, and a minimum transmission, T_{min}. A well-defined empirical

relation exists between the quantity log (A/T_{min}) and magnitude (cf. MacGillivray & Dodd 1979).

The original file of coarse mode parameters of galaxies (Chapter 2) refers to optical image characteristics in the R band, whereas V band CM parameters are required in order consistently to relate the secondary photometry to the primary V_{25} data. Extraction of the V band data was carried out by transforming the coordinates of all galaxies in the file to the system of the V plate. The identification procedure was built around a polynomial transformation routine devised by Mr J. Cooke.

The faintest 20% of the 0.15 million CM images detected on the V plate were attributable to emulsion faults such as grain clumping; all but 5% of the remainder were images of stars. The distribution of spurious images and stars is described by Poissonian statistics and these "images" have mean separation $\langle d \rangle$ = (surface density)$^{-\frac{1}{2}}$ = 740μm. The root-mean-square difference of the transformed and true positions of 46 faint reference stars distributed over the 22 square degrees was 11μm in each coordinate. The requirement that the maximum discrepancy of position should not exceed 250μm therefore permitted reliable image pairing even for large images with ill-defined centroids; this excludes, however, the very largest objects which did not record coherently during measurement of the V plate. A negligible number of generally very faint galaxies, 4% of the total, which were identified on the R plate were not detected on the V.

In Figure 5.6 the quantity log $(A/T_{min})_V$ derived from V band CM parameters is compared with the corresponding V_{25} magnitude from the

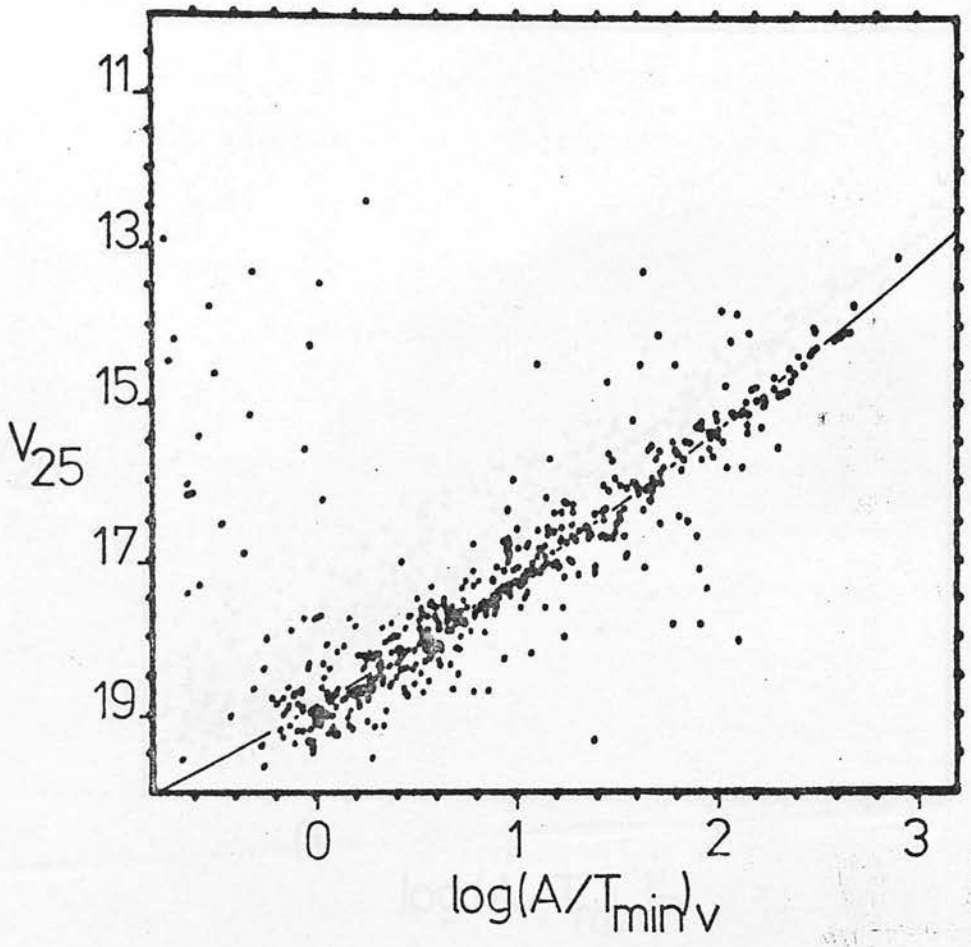

Figure 5.6

The correlation of the quantity log (image area/minimum transmission) derived from measurements of plate V1330, with isophotal V_{25} magnitude from V3324. The curve is the adopted mean relation.

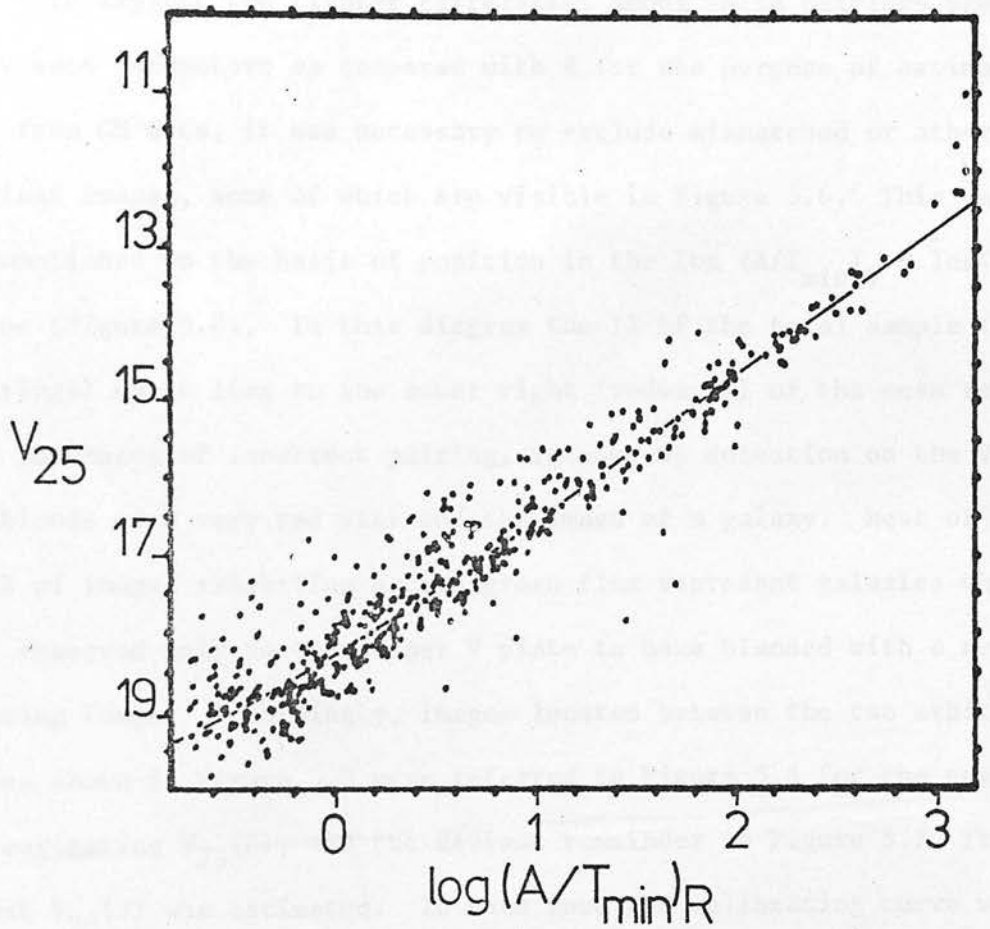

Figure 5.7

The correlation with V_{25} of the parameter $\log (A/T_{min})_R$, derived from measurements of a R band plate. Compare Figure 5.6.

primary photometry, where available. Good correlation exists among valid image pairings over a range of some 6 mag in V_{25}. The equivalent diagram based on R band parameters is shown in Figure 5.7.

To exploit the tighter correlation among valid pairings provided by V band parameters as compared with R for the purpose of estimating V_{25} from CM data, it was necessary to exclude mismatched or otherwise deviant images, some of which are visible in Figure 5.6. This was accomplished on the basis of position in the $\log (A/T_{min})_V - \log(A/T_{min})_R$ plane (Figure 5.8). In this diagram the 1% of the total sample (5287 pairings) which lies to the lower right (redwards) of the mean relation are instances of incorrect pairing, incoherent detection on the V plate, or blends of a very red star and the image of a galaxy. Most of the 3.3% of images exhibiting excess green flux represent galaxies which are observed only on the deeper V plate to have blended with a neighbouring image. Accordingly, images located between the two arbitrary lines shown in Figure 5.8 were referred to Figure 5.6 for the purpose of estimating $V_{25}(2)$, and the deviant remainder to Figure 5.7, from which $V_{25}(3)$ was estimated. In each case the calibrating curve was a polynomial of suitable order in $\log (A/T_{min})$ fitted after iterative rejection of discordant points.

In this manner crude V_{25} magnitudes on the primary system were obtained for all but 17 images for which primary $V_{25}(1)$ photometry was not already available. The remainder of cases was attributable to hardware processing errors. Visual estimates of the magnitudes of the brighter examples were substituted where necessary and these are listed at the end of Appendix II.

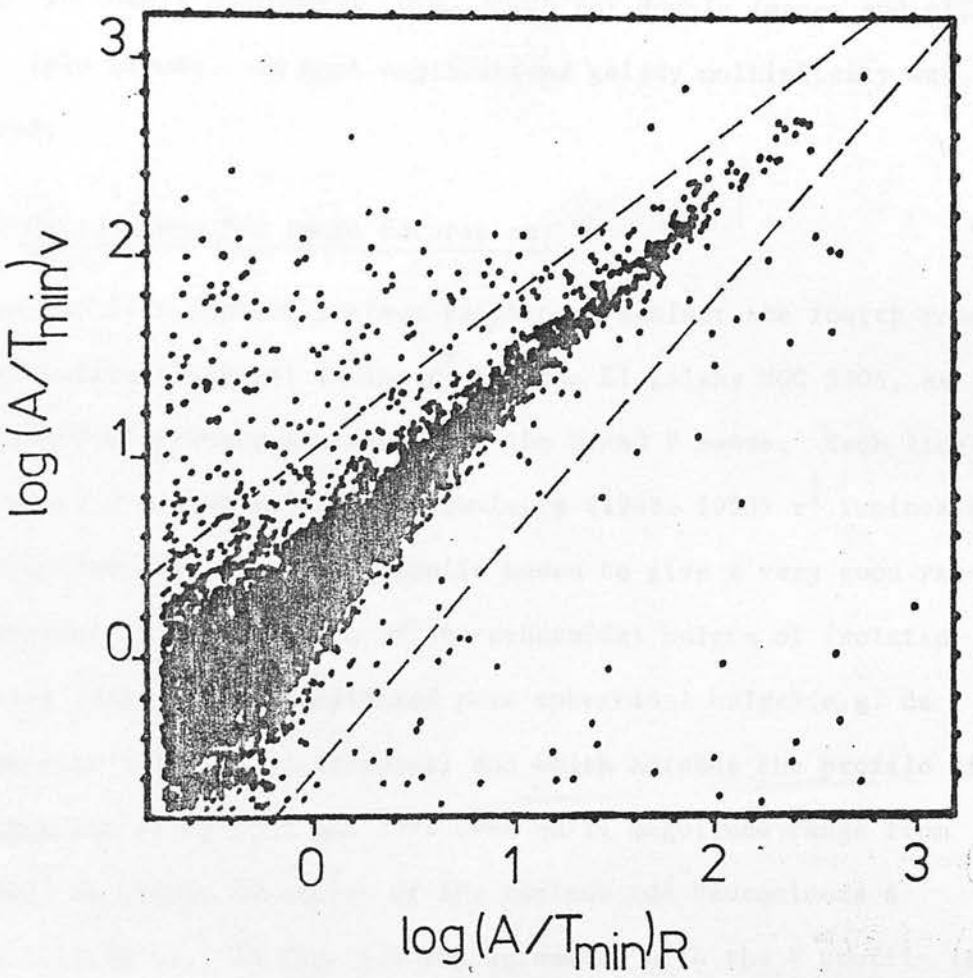

Figure 5.8

A plot of the quantity log(image area/minimum transmission) for galaxies on plate V1330 versus the same quantity measured on the R plate. Strong deviations from the mean sequence are mainly in the vertical direction and correspond to the discrepancies in Figure 5.6. The broken lines are taken to define the arbitrary limits of usefulness of the secondary V photometry.

Lastly, image blending present on both the R and (presumably) the V plate, as opposed to on the V plate only, was taken into account. It was simply assumed that each component of a blend contributed equally to the measured magnitude and a statistical correction applied to the secondary photometry, viz. $+0^{m}.75$ for double images and $+1^{m}.19$ for triple blends. In most applications galaxy multiplicity was ignored.

5.7 Corrections for Image Saturation

Figure 5.9 is a plot of surface brightness against the fourth root of the effective isophotal radius r^{*} for the E1 galaxy NGC 3305, as determined by primary photometry in the B and V bands. Each line represents a best-fitting de Vaucouleurs (1948, 1953) $r^{\frac{1}{4}}$ luminosity distribution law. This relation is known to give a very good representation of the profiles of the spheroidal bulges of isolated galaxies (ellipticals considered pure spheroidal bulge)(e.g. de Vaucouleurs 1977a for references) and which matches the profile of the standard elliptical NGC 3379 over an 11 magnitude range from $r \gtrsim 440''$ to within 10 arcsec of the nucleus (de Vaucouleurs & Capaccioli 1979). In Fig. 5.9 the agreement with the V profile is seen to be very good to within $r^{*} \simeq 9''.6$ after which the core saturates on plate V3324; galaxy number 4 (E3) and others reveal the same effect. On the more lightly exposed plate V1330 (Job no. 301) the threshold surface brightness of saturation is about $\mu_{V} = 20.5$ V mag arcsec^{-2}, corresponding to a transmission T of 17. On an earlier study of the same plate (Job no. 254) this threshold was T = 33; the improvement was brought about by modifications to the COSMOS spot

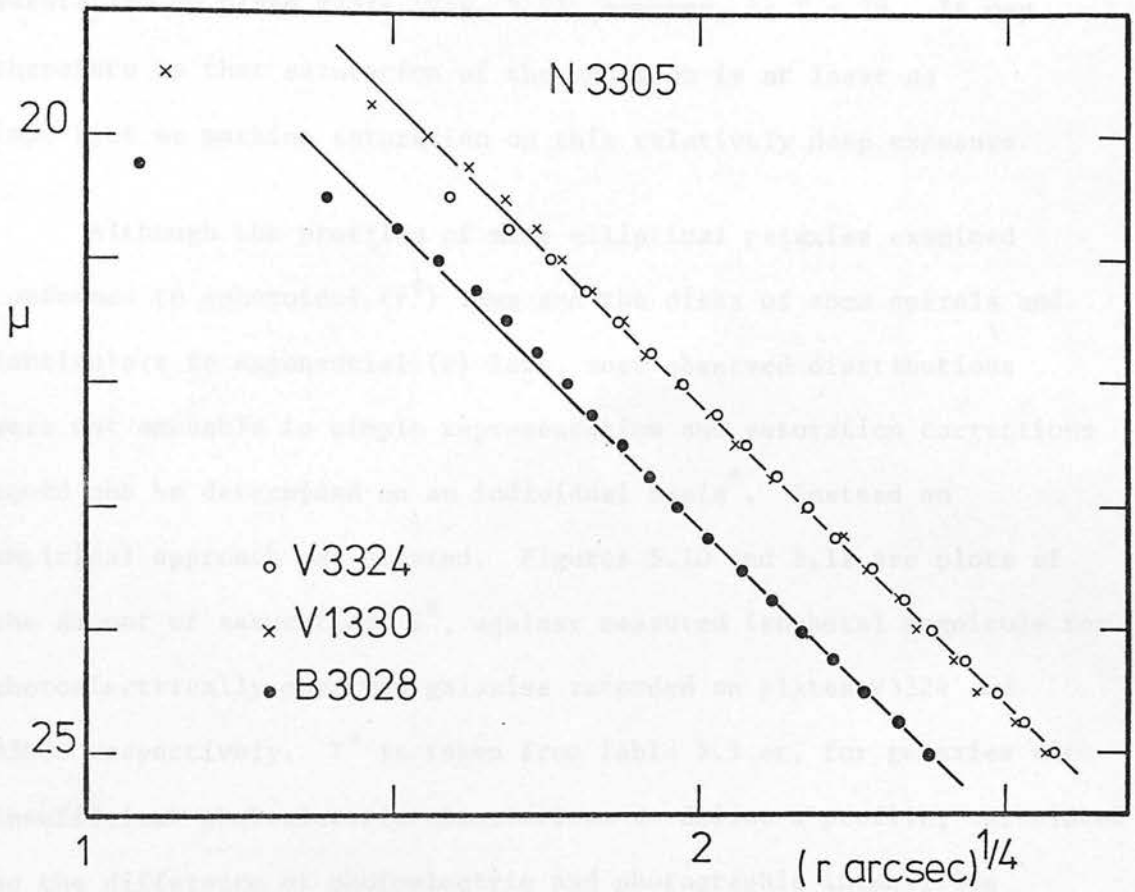

Figure 5.9

Surface brightness profiles of NGC 3305 from primary photographic photometry in the B and V bands. The $r^{\frac{1}{4}}$ law in μ_V represented by the uppermost line is fitted to the profile on plate V3324. The measured profile departs from this law shortwards of $r^{\frac{1}{4}} \simeq 1.76$ ($r^* \simeq 9''.6$).

scanning system during the intervening months. The threshold of saturation on plate V3324 (Fig. 5.9), however, is T = 29. It may therefore be that saturation of the emulsion is at least as important as machine saturation on this relatively deep exposure.

Although the profiles of many elliptical galaxies examined conformed to spheroidal ($r^{\frac{1}{4}}$) laws and the disks of some spirals and lenticulars to exponential (r) laws, most observed distributions were not amenable to simple representation and saturation corrections could not be determined on an individual basis*. Instead an empirical approach was adopted. Figures 5.10 and 5.11 are plots of the amount of saturation, I^s, against measured isophotal magnitude for photoelectrically observed galaxies recorded on plates V3324 and B3028 respectively. I^s is taken from Table 5.3 or, for galaxies with insufficient photoelectric observations to define a profile, calculated as the difference of photoelectric and photographic intensities (presuming a mean value of sky brightness as per Table 5.3). The exact magnitude corresponding to the saturation threshold ($I^s = 0$) for V3324 was taken as the median V_{25} ($= 15^m.75$) of all 22 galaxies with peak surface brightnesses in the range $20.75 \leq \mu_V \leq 21.0$, likely examples of incipient saturation. The photoelectric photometry, unfortunately, does not go faint enough to confirm this estimate. Note the correlation of the amount of saturation with relative central concentration of light, i.e. galaxy type (bulge-to-disk ratio), at fixed magnitude. The empirical curves outlined in the figures are defined, without regard to galaxy type, in polynomial form suitable

* The $r^{\frac{1}{4}}$ law which best fits the profile of N3305 (Fig. 5.9) leads to metric magnitudes which consistently exceed photoelectric values by $\sim 0^m.2$.

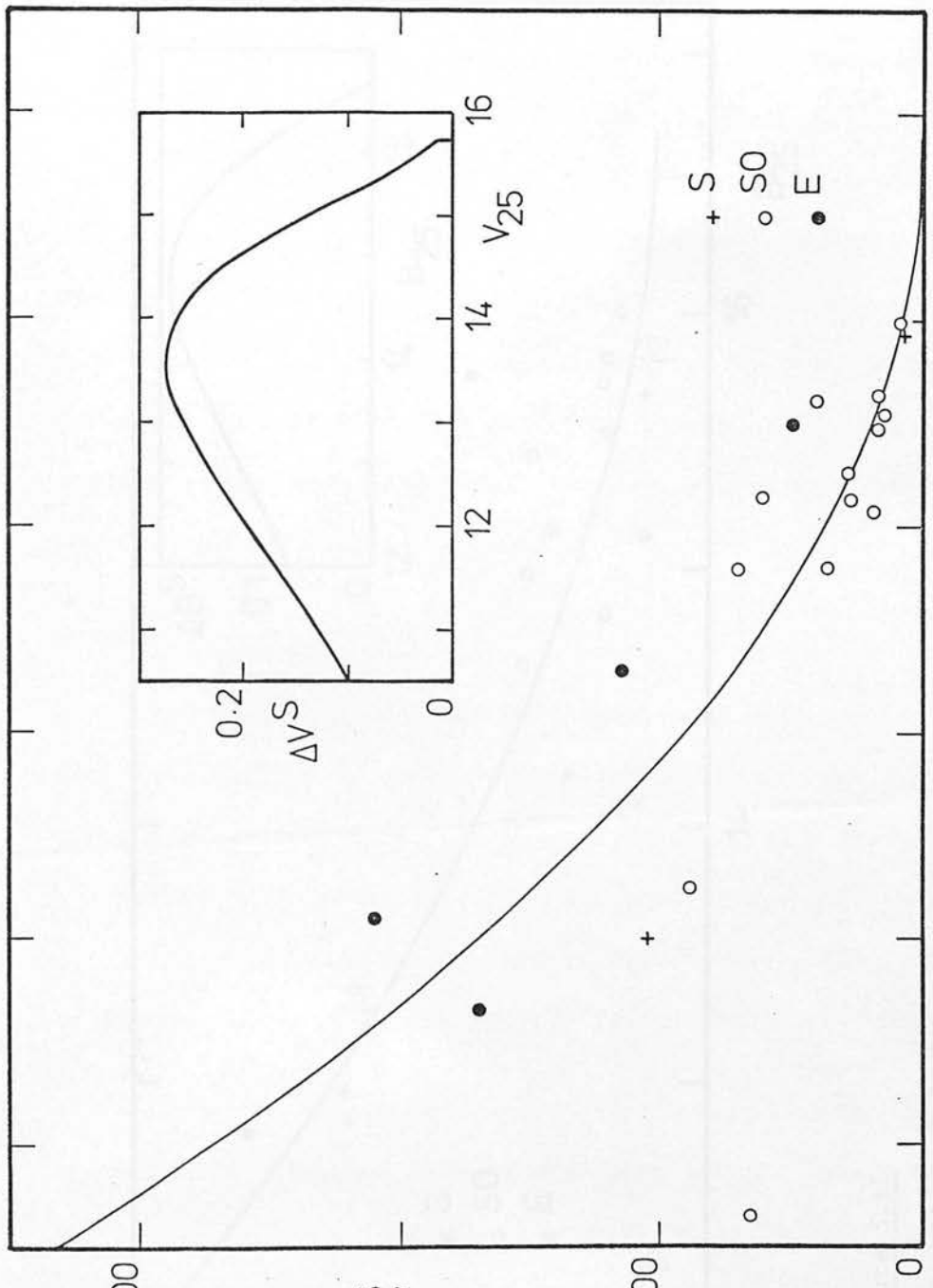

Figure 5.10

The relation between the amount of saturation in units of intensity, I_V^s, and isophotal magnitude as measured on plate V3324. Lenticular galaxies with relatively large bulges tend to lie above the mean line. The inset shows the curve of corrections to V_{25} magnitudes necessary to adjust V_{25} for saturation.

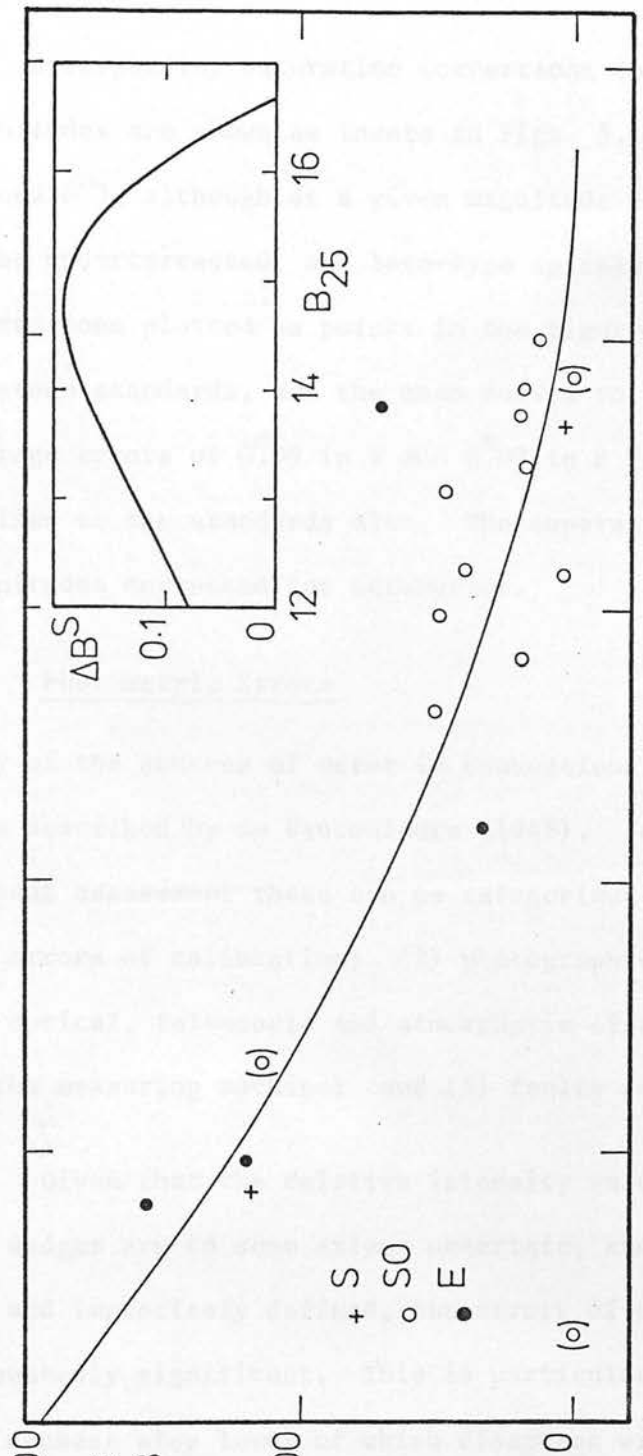

Figure 5.11

As for Figure 5.10 but with reference to plate B3028. Parentheses qualify particularly uncertain values.

for computer application:

$$I_V^s = 29884 - 3794.6\ V_{25} + 120.481\ V_{25}^2$$

$$I_B^s = 11437 - 1345.8\ B_{25} + 39.577\ B_{25}^2 .$$

The corresponding saturation corrections to the measured isophotal magnitudes are shown as insets in Figs. 5.10 and 5.11. These nowhere exceed $0^m.3$, although at a given magnitude elliptical galaxies tend to be undercorrected, and late-type spirals the opposite. The true corrections plotted as points in the figures were applied to the nineteen standards, and the mean curves to the rest of the photometry; average errors of $0^m.09$ in V and $0^m.07$ in B follow if the curves are applied to the standards also. The superscript c, as in V_{25}^c, denotes magnitudes corrected for saturation.

5.8 Photometric Errors

Many of the sources of error in conventional photographic photometry were described by de Vaucouleurs (1948). For the purpose of the present assessment these can be categorized simply as follows: (1) errors of calibration; (2) photographic non-uniformities; (3) optical, telescopic and atmospheric effects; (4) instabilities of the measuring machine; and (5) faulty reductions.

Given that the relative intensity values of the step levels of the wedges are to some extent uncertain, and that those levels are few and imprecisely defined, the errors of calibration involved are undoubtedly significant. This is particularly true of plate B3028, the densest step level of which disagrees with an extrapolation of

the linear Baker function defined by the rest of the wedge. The consequences are visible in Figure 5.9 as a systematic deviation of the B band radial surface brightness profile from an $r^{\frac{1}{4}}$ law at high intensities. Unfortunately there is no independent check of the B photometry.

Emulsion non-uniformities may be manifested as variations of the natural emulsion fog across a plate, or similar variation of the transfer characteristic. IIaO and IIaD emulsions are normally much more uniform than IIIa-J (cf. Carter & Dixon 1978). It is assumed here that the Baker functions determined for regions near the edges of the plates also apply within the scan areas, and that the background sky exposures dominate any variations of the emulsion fog.

Effects in category (3) include atmospheric haze and seeing, telescope guiding errors, and scattered light, diffraction, halation and vignetting. The unvignetted area on UK Schmidt plates is nominally $5^{\circ}.37$ in diameter; all galaxies within 1.5 Mpc of the centre of A1060 are located within this circle on the plates studied, and only the extreme corners of the CM scan area are affected. All plates have antihalation backing and, apart from a ghost ring of radius 340 arcseconds visible at the 24.5 V mag arcsec^{-2} level around the bright central star BS4162, optical and telescopic effects can safely be neglected. Atmospheric seeing causes loss of definition and a net outward transfer of illumination in an image, but the resulting diminution of isophotal magnitude becomes appreciable only for very small images below the completeness limit of the current photometry (Hoffman & Crane 1977). Atmospheric haze on these plates was also insignificant.

There is persuasive evidence, however, of large-scale transmission gradients across the north-east and especially south-east quarters of plate V3324. Small discontinuities at boundaries of scan areas tend to confirm that drift of the photometric zeropoint occurred during measurement of this plate. Independent photometry of the worst affected region could not be secured on plate V1330 because of the loss of one tape of data. There is no suggestion of similar drift in the measurements of B3028, and scans of one step wedge before and after measurement of the latter plate reproduce identically.

Figure 5.12 presents the plots of log r_{25}^{*}, the logarithms of the effective radius of the 25th V mag arcsec^{-2} isophote, against magnitude, for all galaxies with primary photometry, on each of three plates. The scatter of points is greater for plate V1330 than for V3324 principally because of the higher level of noise on the shorter exposure. Random fluctuations about the sky level are the result of emulsion granularity and the statistics of transmission measurement, and to a first approximation the amplitude of this noise can be represented by a gaussian of standard deviation 6% about the sky level on both V1330 and B3028, and 5.5% on V3324. Since the 25 V mag arcsec^{-2} isophote is only 5.4% above the sky level on plate V3324 and 4.7% above sky on V1330, the consequences of an error of 1 - 2% in the estimate of the sky level are serious (cf. Evans 1951, Fraser 1977). In fact, a 2% underestimate was found to result in a brightening of primary V_{25} magnitudes by $0^{m}.25$ on average on plate V3324. On B3028, on the other hand, the 25th B mag arcsec^{-2} isophote is 12.8% above the sky level, and in Figure 5.12 the scatter is obviously smaller.

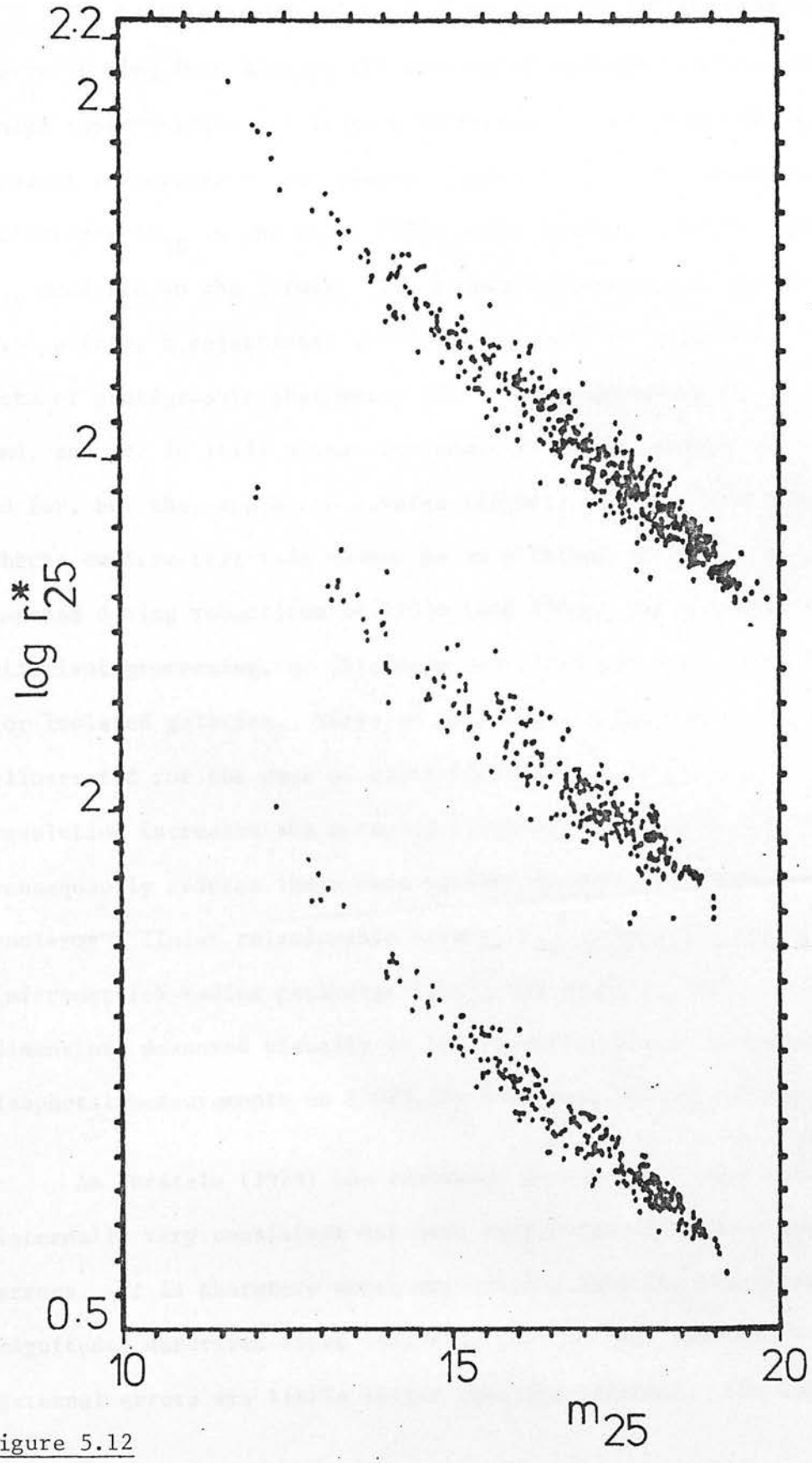

Figure 5.12

Plots of the logarithm of the isophotal radius against isophotal magnitude (V_{25} or B_{25} as appropriate) for plate V3324 (top), V1330 (centre) and B3028 (bottom). See text for discussion.

The best indicator of overall reliability of the primary photometry, taking into account all sources of systematic error other than image superposition and image saturation, is the comparison of independent reductions of two plates (Figure 5.13). The magnitude difference ΔV_{25} in the sense V3324 minus V1330 is plotted against the V_{25} measured on the former. The standard deviation of the differences (167 points, 8 rejections) is $0^m.18$, dependent on magnitude. The two sets of photographic photometry are in good agreement at the bright end, and are in still better agreement if image saturation is accounted for, but they appear to diverge slightly towards faint magnitudes. Checks confirm that this cannot be an artefact of areal contraction imposed during reductions of V1330 (and B3028) for the sake of efficient processing, as this does not alter the magnitudes derived for isolated galaxies. There is nevertheless the radius effect, illustrated for the case of plate B3028 in Figure 5.14(b): reduced resolution increases the measured isophotal radii of small images and consequently reduces their mean surface brightness. Figure 5.14(a) confirms a linear relationship between r_{25}^* from V3324 and the (micrometric) radius parameter $(ab)^{\frac{1}{2}}$, the geometric mean of semi-axis dimensions measured visually on IIIa-J survey plates (Chapter 2). Isophotal measurements on B3028, by contrast, deviate at small radii.

As Burstein (1979) has remarked, photographic photometry can be internally very consistent but have very large systematic external errors. It is therefore worth emphasising that the comparison of V_{25} magnitudes described above indicates that in this photometry, the external errors are little larger than the internal. The latter

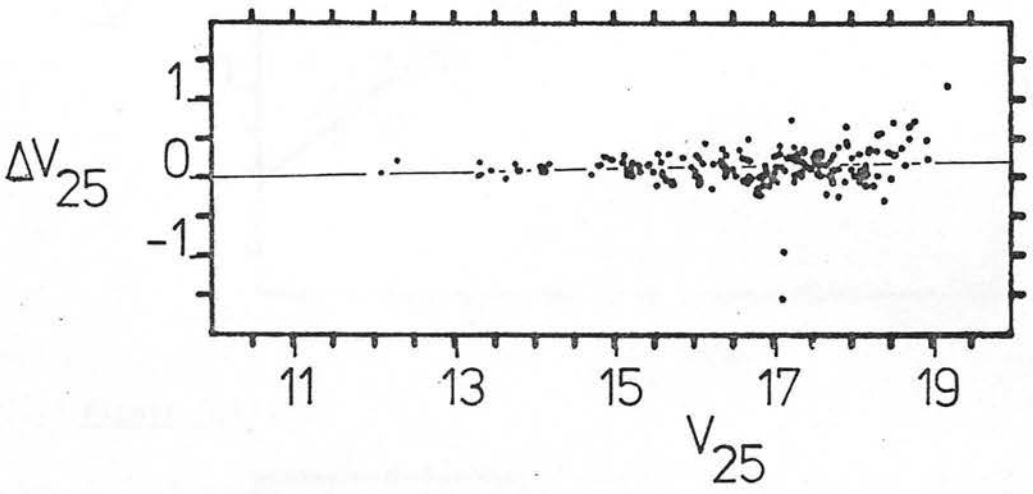

Figure 5.13

The difference of V_{25} magnitudes of galaxies as determined by primary photometry of two independent plates, plotted as a function of V_{25} measured on the deeper exposure. The latter is systematically fainter by $0^m.15$ at $V_{25} = 17$.

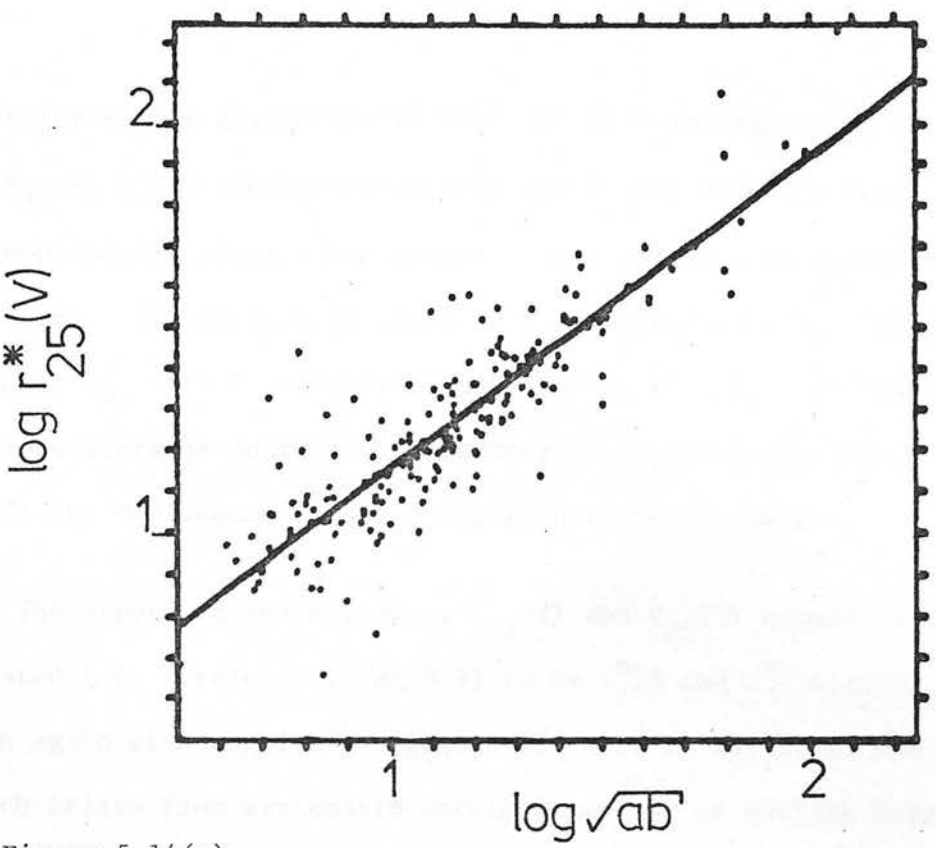

Figure 5.14(a)

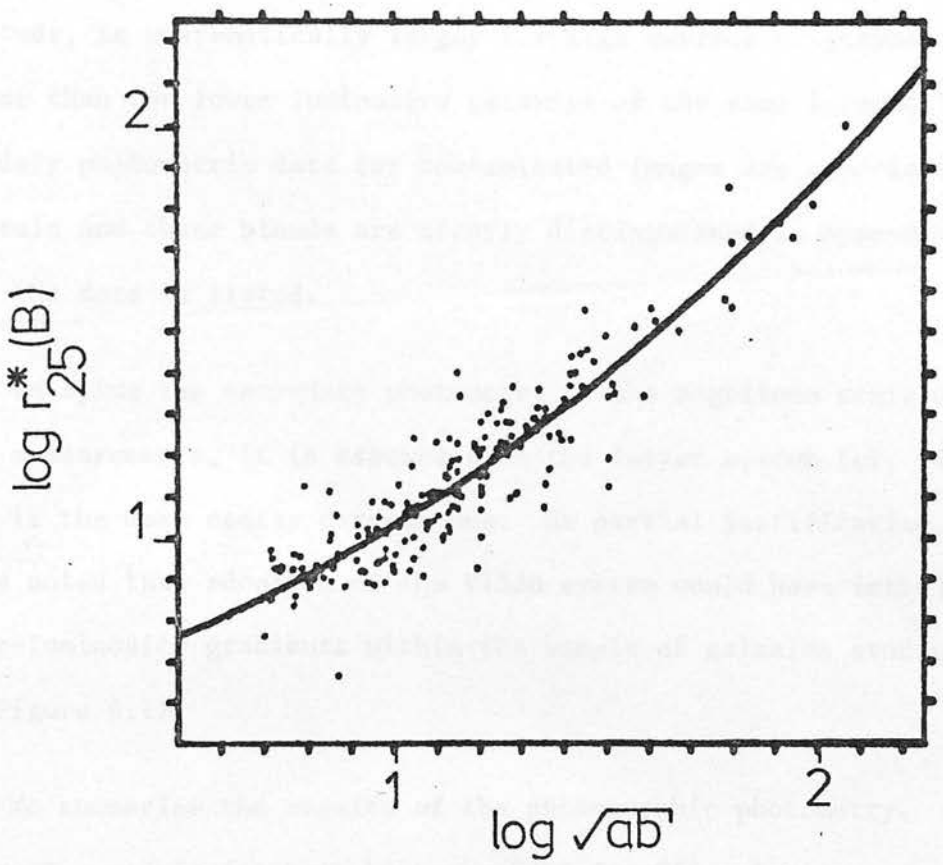

Figure 5.14(b)

Comparisons of photometric (ordinates) and micrometric (abscissae) dimensions of galaxies. Parameters a and b denote unadjusted semi-major and semiminor axis lengths in arcseconds respectively. The lower plot has been fitted by a parabola. See text for explanation.

uncertainties are generally $\pm 0^m.18/2^{\frac{1}{2}} = 0^m.13$ in the range $12 < V_{25}(1) < 19$, and less than this for $V_{25}(1)$ brighter than the completeness limit since accuracy progressively deteriorates faintwards. The saturation corrections applied where $V_{25} \leq 15.75$ and where $B_{25} < 16.7$ introduce uncertainties of approximately ±0.1, and image overlaps contribute a further ±0.2. Even so, there are grounds for confidence in the primary photographic data.

The errors in the secondary $V_{25}(2)$ and $V_{25}(3)$ magnitudes are estimated (cf. Figures 5.6 and 5.7) to be $0^m.25$ and $0^m.3$ respectively, though again with magnitude dependence. Part of the large scatter in each arises from systematic errors dependent on surface brightness: the measured quantity $\log(A/T_{min})$, and hence the implied magnitude, is systematically larger for high surface brightness systems than for lower-luminosity galaxies of the same isophotal m_{25}. Secondary photometric data for contaminated images are especially uncertain and these blends are clearly distinguished in Appendix II, where the data is listed.

In tying the secondary photometry to the magnitude scale of the V3324 measurements, it is assumed that the latter system (cf. Figure 5.13) is the more nearly correct one. As partial justification, it may be noted that adoption of the V1330 system would have introduced colour-luminosity gradients within the sample of galaxies studied (cf. Figure 6.1).

To summarise the results of the photographic photometry, primary B_{25} magnitudes have been obtained for 266 galaxies and

$V_{25}(1)$ magnitudes for 524 galaxies located within a square region of area 3.65 degree^2 centred on the Hydra I cluster. In addition, secondary estimates of V_{25} for over 5000 galaxies found in a larger region 21.8 degree^2 in area are derived. The collated V band photometry is the basis of the first determination of the luminosity function of Hydra I and the surface distribution of luminosity within it, and B magnitudes provide supplementary information on the integrated colours of its members.

Table 5.1

Plate Material

Plate No	3028	1330	3324	1347
Date exposed	10-11 April 1977	20-21 March 1975	5-6 July 1977	23-24 March 1975
R.A. (1950)	$10^h\ 34^m$	$10^h\ 34^m$	$10^h\ 34^m$	$10^h\ 34^m.5$
Dec. (1950)	$-27^\circ\ 24'$	$-27^\circ\ 30'$	$-27^\circ\ 24'$	$-27^\circ\ 22'.5$
Filter	GG385	GG495	GG495	RG630
Emulsion	IIaO	IIaD	IIaD	098-04
Grain type	medium	medium	medium	coarse
Exposure (minutes)	20	12	60	10
Equivalent photo-electric waveband*	B	V	V	R

* Adopted in the text as prefixes for plate numbers.

Table 5.2

COSMOS Measurements

Plate No	Date measured	COSMOS Job No	Mode	Spot FWHM(μm)	Increment size(μm)	Area measured (sq. degrees)
3028	22 Mar 1979	333	MM	32	16	3.65
1330	31 Jan 1977	222	CM	25*	16	21.86
1330	17 Aug 1977	254	MM	25*	16	0.91
1330	19 Nov 1978	301	MM	32	16	3.65
3324	30 May 1978	287	MM	32	16	3.65
1347	3 Feb 1977	222	CM	25*	16	21.86

* Nominally 8μm. This was replaced by a new 8μm spot scanner installed during 1978.

Table 5.3

Zeropoint Calibrations

Job No	Galaxy	m	I^s/I_{sky}	m_{sky}	Δ
287	4	5.67	2100	21.88	.05
287	12	5.45	1150	21.84	.01
287	22	5.48	690	21.85	.02
287	31	5.02	190	21.77	-.05
287	38	5.29	610	21.81	-.02
Mean sky brightness, plate V3324				= 21.83 ± .02 (s.e.)	
254	12	4.51	780	21.66	-.03
254	22	4.75	480	21.69	.00
254	38	4.75	495	21.69	.00
301	4	5.20	1190	21.79	.10
301	12	4.59	450	21.66	-.03
301	31	4.47	50	21.63	-.06
Mean sky brightness, plate V1330				= 21.69 ± .02 (s.e.)	
333	4	1.41	600	22.87	.10
333	12	1.23	170	22.72	-.05
333	22	1.36	255	22.83	.06
333	31	1.15	20	22.62	-.15
333	38	1.28	245	22.76	-.01
Mean sky brightness, plate B3028				= 22.77 ± .04 (s.e.)	

Column 1: COSMOS job number; col. 2: galaxy designation; col. 3: slope in arbitrary units of linear regression between integrated photographic and photoelectric intensities (Fig. 5.5); col. 4: total photographic saturation in units of sky intensity $arcsec^{-2}$; col. 5: estimated sky brightness; col. 6: the deviation, estimated sky less mean sky brightness.

CHAPTER 6

PHOTOMETRIC AND OPTICAL DATA ASSESSED

6.1 Correlation of Colour with Morphological Type

Accurate photoelectric aperture photometry of galaxies (of which Table 4.3 is an unrepresentative sample) reveals a clear correlation of integrated colour with morphological type (e.g. de Vaucouleurs 1961a) due to the differing stellar compositions of galaxies of different stages within the revised Hubble classification system. Such a correlation should exist in the present photographic photometry also.

In Figure 6.1 the corrected colour indices $B_{25}^{c} - V_{25}^{c}$ are plotted against V magnitude, for all galaxies in the field of A1060 which have photometry in each waveband and morphological classifications. Strictly, this colour index lacks rigorous physical justification inasmuch as B_{25}^{c} and V_{25}^{c} refer to light emission interior to different and unrelated isophotes; the correct procedure is to form a colour index in which the magnitude in one waveband is contrasted with the effective magnitude interior to a disk of the same dimensions in the second band (e.g. Austin, Godwin & Peach 1975). This, however, is impracticable here because of the manner of data compilation, and in either case the results are affected by image superpositions and overlaps. Figure 6.1 does reveal that on the crude definition of B-V colour index, spiral and irregular galaxies are on average $0^{m}.25$ bluer than lenticulars and ellipticals of

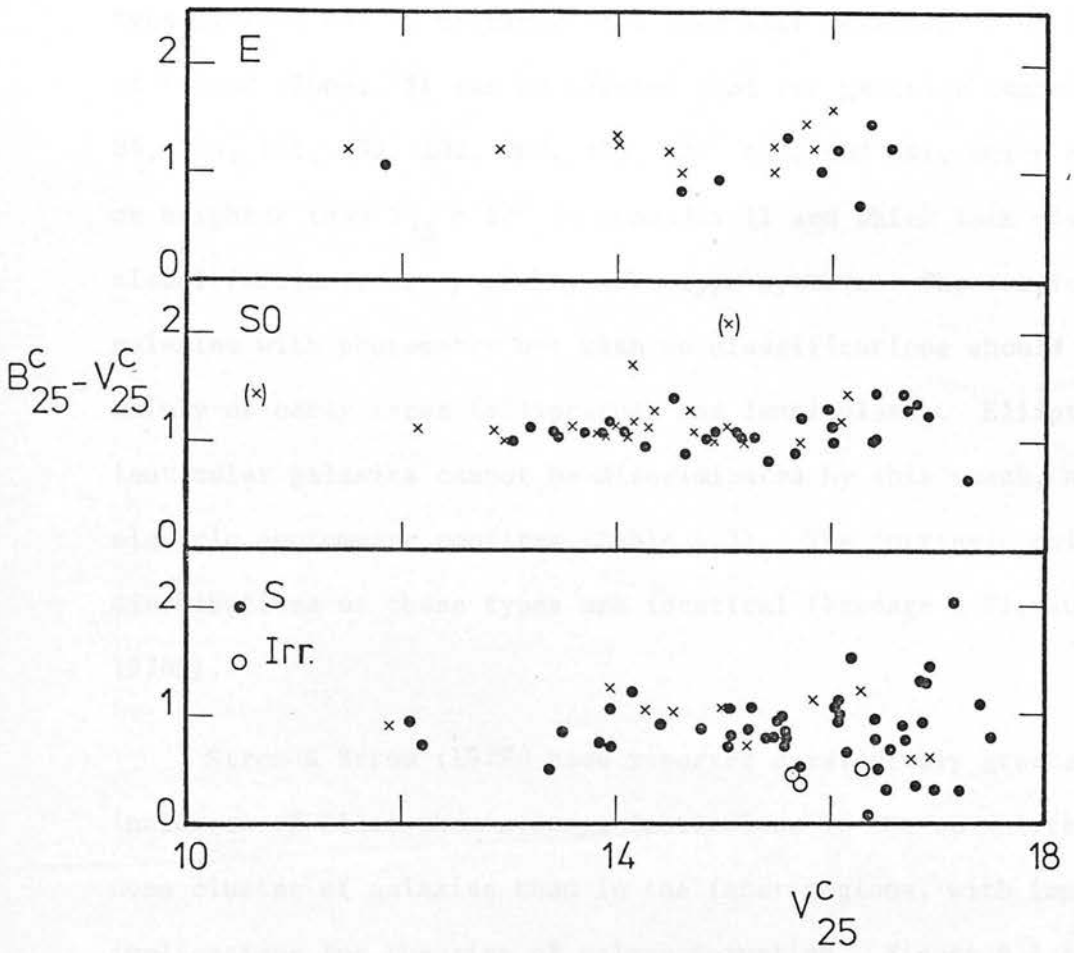

Figure 6.1

Plots of B-V colour index versus V_{25} magnitude for elliptical (E), lenticular (S0), spiral (S) and irregular (Irr) galaxies in the field of A 1060. Crosses represent systems within 0.25 Mpc of the adopted cluster centre, and filled circles those beyond 0.25 Mpc, as seen in projection. Galaxies nearer to the cluster centre tend to be less blue and S and Irr galaxies more blue than other types.

Parentheses enclose less certain values.

comparable V_{25}. The latter types comprise 76% of all galaxies with measured $B-V \geq 1.0$, whereas 81% of those systems with $B-V < 1.0$ are spiral or irregular (late-type*) galaxies. Thus, in spite of significant intermingling of colour indices of the two groups, late-type systems can be distinguished with fair reliability on the basis of colour alone. It can be deduced that the galaxies numbers 14, 33, 84, 104, 115, 132, 202, 207, 324, 427, 448, and 481, which are listed as brighter than $V_{25} = 17^m$ in Appendix II and which lack visual classifications, are probably late-type systems. The remaining galaxies with photometry but with no classifications should consist mainly of early types (ellipticals and lenticulars). Elliptical and lenticular galaxies cannot be discriminated by this means, as photoelectric photometry confirms (Table 4.3). The intrinsic colour distributions of these types are identical (Sandage & Visvanathan 1978b).

Strom & Strom (1979b) have reported a relatively greater incidence of bluer-than-average lenticulars in the outskirts of the Coma cluster of galaxies than in the inner regions, with important implications for theories of galaxy formation. Figure 6.1 suggests that the same trend exists among lenticular galaxies identified, in projection, near the Hydra I cluster. The same inference, however, would also be drawn regarding E and S systems; it is more likely that the V magnitudes determined for galaxies in the cluster core are brighter than they should be, either because of incomplete subtraction of light scattered from the two red field stars, SA0179027

* A misappropriated term as used in the Hubble and the de Vaucouleurs classification systems. In reality, young stellar populations characterise spiral and S and Irr galaxies; cf. the Yerkes system (Morgan 1958).

and SA0179041, or because of contamination of luminosity from the halo of NGC 3311, or both. The blue magnitudes would have been less affected since they refer to brighter isophotal levels, so accounting for the net reddening of B-V. The demonstration (or otherwise) of radial segregation of lenticular galaxies in A1060 according to colour probably will be possible only if a further programme of direct photoelectric photometry, which avoids many of the large uncertainties inherent in the photographic method, is carried out.

6.2 The Luminosity Function

In constructing the V-band luminosity function of the cluster, attention is restricted to galaxies within the conical volume of cross-sectional diameter 3 Mpc at the assumed distance of Hydra I (Δ = 40 Mpc). A histogram of these galaxies collected in $0^m.2$ bins represents the differential luminosity function as contaminated by non-members (Figure 6.2). This sample is dominated by faint galaxies (85% of the measured magnitudes lie in the range $17.0 < V_{25} \leq 19.8$), but interest is concentrated on those brighter than the limit at which appreciable incompleteness sets in. Figure 6.3 illustrates the effect of statistically correcting for non-members assuming a homogeneous distribution of field galaxies corresponding to a surface density of 19 galaxies degree^{-2} at $V_{25} = 17^m.0$ (Chapter 2). The dip at $V_{25} \simeq 15.8$ in the shaded histogram may well be a statistical artefact of the correction; this apart, the essential form of the function is preserved although most galaxies fainter than $V_{25} = 16$ are assigned to the field.

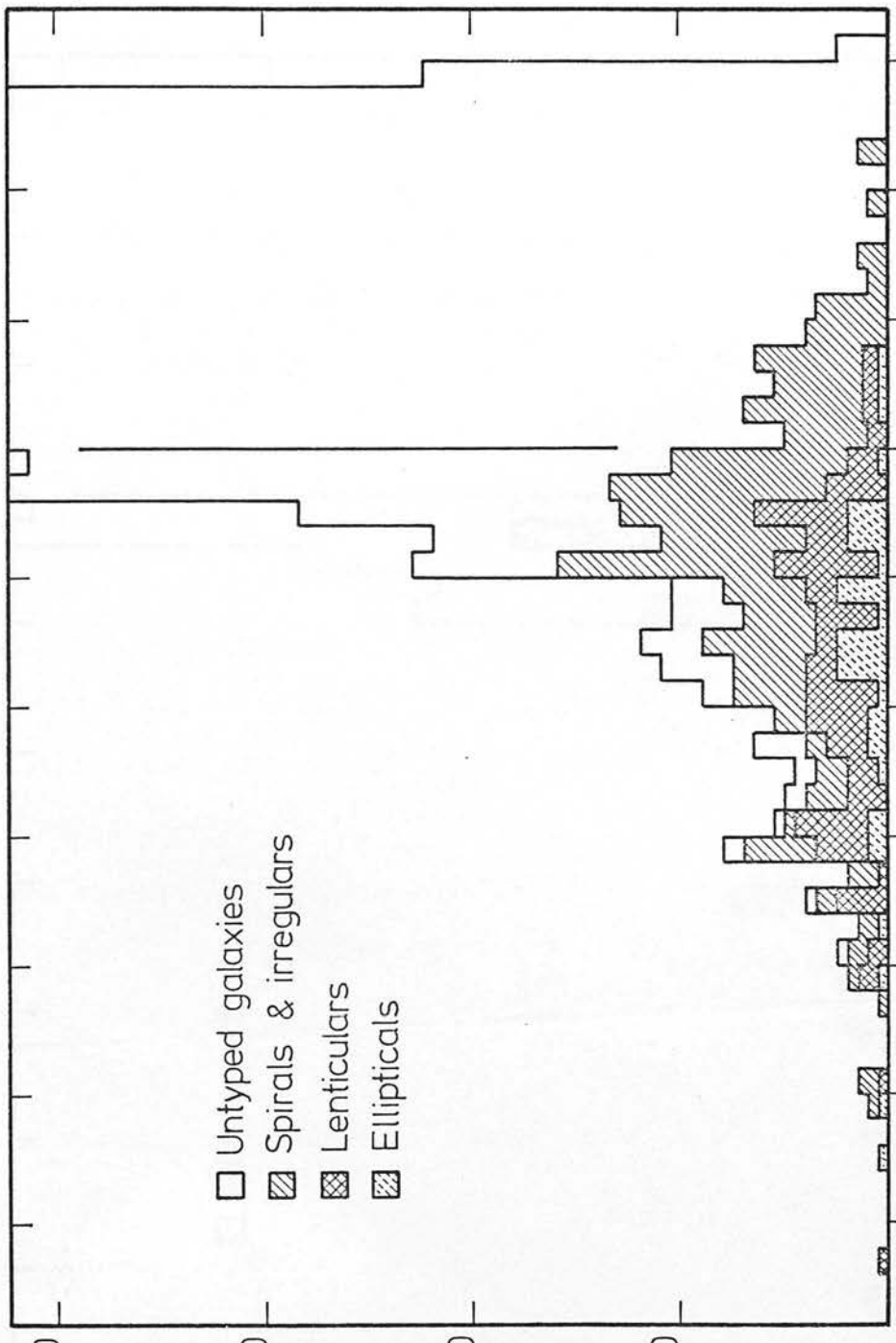

Figure 6.2

The differential luminosity function of the cluster, uncorrected for the field contribution. The vertical line marks the limit of completeness. There are 87 galaxies in $16.6 < V_{25} \leq 16.8$.

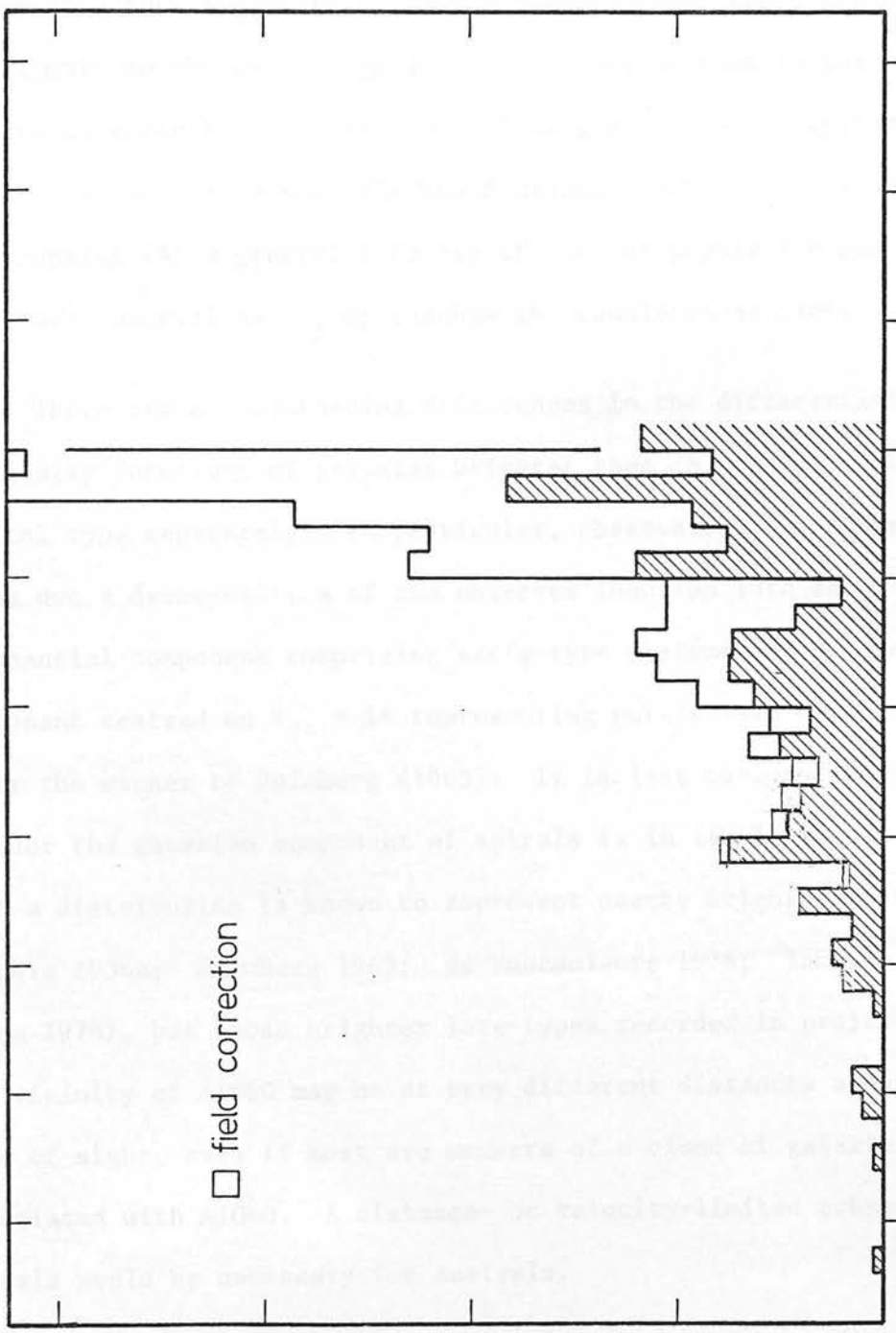

Figure 6.3

The differential luminosity function statistically corrected for the field assuming a homogeneous distribution of non-members corresponding to 19 galaxies degree^{-2} at V_{25} = 17.0.

The basic features of the distribution are (1) a high-luminosity "toe" ($V_{25} \leq 12.2$) consisting of bright representatives of all main morphological types; (2) a local maximum in the numbers of early-type and (less convincingly) late-type systems near $V_{25} = 14$; (3) a possible broad minimum around $V_{25} \simeq 14.5$, interrupting (4) a general increase of cluster population per magnitude interval as V_{25} approaches the completeness limit.

There are no outstanding differences in the differential luminosity functions of galaxies brighter than 16^m for each morphological type separately. In particular, observation (2) above rules out a decomposition of the observed function into an exponential component comprising early-type systems and a gaussian component centred on $V_{25} = 14$ representing purely late-type galaxies, after the manner of Holmberg (1969). It is less obvious, however, whether the gaussian component of spirals is in itself precluded. Such a distribution is known to represent nearby bright spirals well (Hubble 1936a; Holmberg 1969; de Vaucouleurs 1974; Tammann & Kraan 1978), but those brighter late-types recorded in projection in the vicinity of A1060 may be at very different distances along the line of sight, even if most are members of a cloud of galaxies associated with A1060. A distance- or velocity-limited subsample of spirals would be necessary for analysis.

The form of the field-corrected differential luminosity function for all galaxy types, Figure 6.3, is similar to that of the Coma cluster (Godwin & Peach 1977), which exhibits a pronounced minimum following a local peak in numbers of galaxies of intermediate

luminosity. As Godwin & Peach point out, these features cannot be accounted for on any smoothly rising analytic representation of the function. The correspondence between the cluster functions appears to be close despite the relative deficiency of elliptical galaxies in Hydra I and the much higher proportion of spirals.

The logarithmic cumulative luminosity function of A1060 before and after adjustment for the inclusion of non-members is shown in Figure 6.4. Except at the bright end, the corrected data is well represented by two straight lines of slopes 0.60 ± 0.05 and 0.235 ± 0.005. The intersection at $V_{25}^{*} = 14.08$ corresponds to the local maximum in the differential luminosity function.

Abell (1962, 1965, 1975) has obtained adequate bilinear representations of the luminosity functions of several clusters in the manner of Figure 6.4, and has suggested (Abell 1972; Bautz & Abell 1973) that the discontinuity or "knee" in the functions occurs at a similar absolute magnitude in all clusters. Austin, Godwin & Peach (1975) quote a mean absolute dispersion of only $0^{m}.15$ in the position of the knee in the functions of nine clusters, which supports the impression of universality. The observed V_{25}^{*} of Hydra I is readily placed on their system by the prescription $H_o = 50$ km s^{-1} Mpc^{-1}, $q_o = +1$, K-correction $K_V = 0^{m}.02$ (cf. Sandage 1973b), galactic absorption $A_V = 0^{m}.13$ (Sandage 1973a), redshift $z(A1060) = 0.0113$ (Chapter 3), and a correction of $-0^{m}.2$ to convert V_{25}^{*} to a total magnitude. The result is $M_{V_{25}^{*}} = -20.42$, which differs markedly from the average $\langle M_{V_{25}^{*}} \rangle = -21.16 \pm 0.15$ reported by Austin, Godwin &

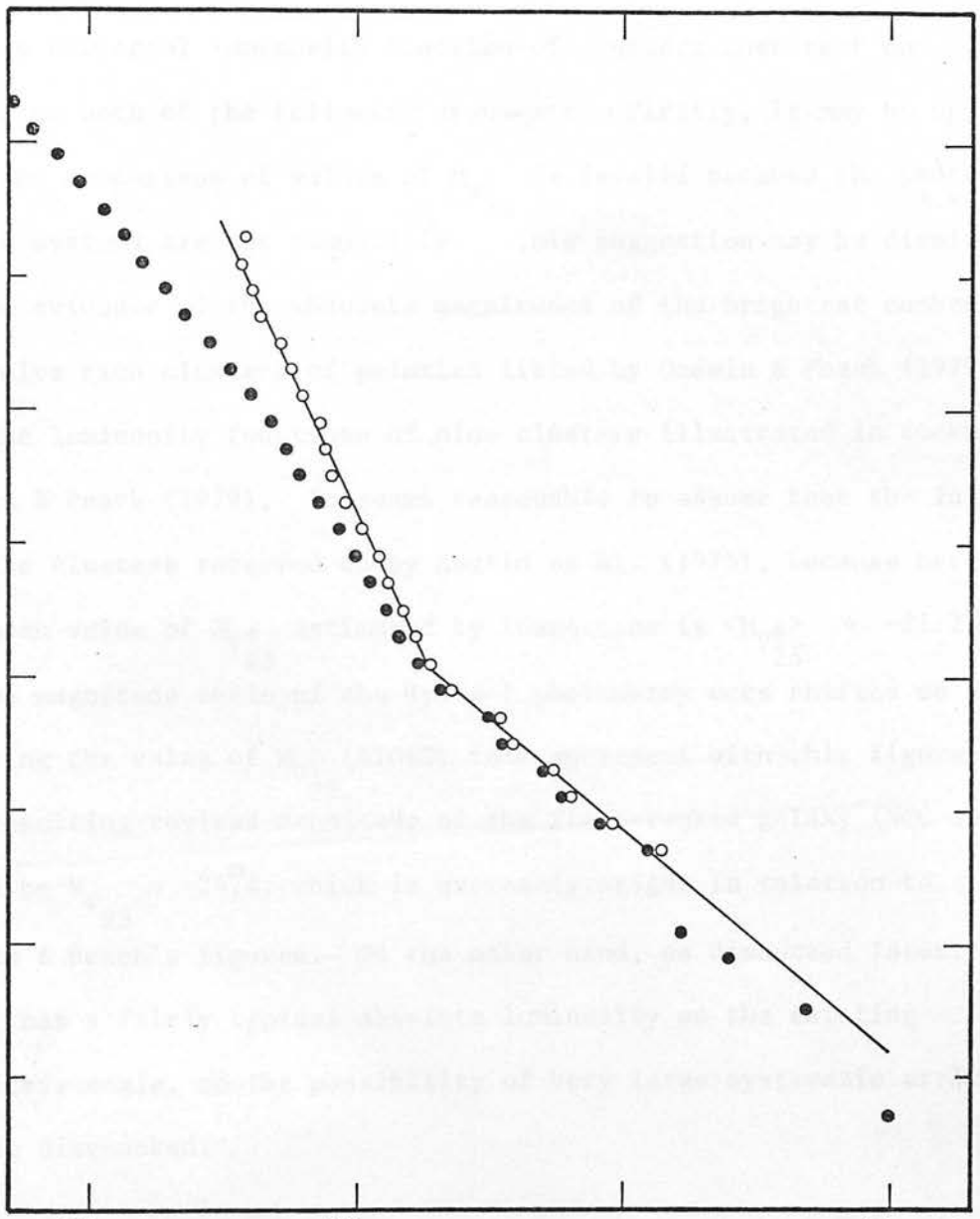

Figure 6.4
The logarithmic cumulative luminosity function of A 1060 . Filled circles are totals uncorrected for the field, open circles are corrected totals. The two lines which best represent the corrected data faintwards of V_{25} = 12.5 are illustrated.

Peach (1975). An exploratory reduction of the size of the A1060 sample, by changing the radius of the projected boundary from 1.5 Mpc to 0.6 Mpc, did not alter V^*_{25} or the corrected slopes of the function.

Any attempt to reconcile the above figures with the notion of a truly universal luminosity function of clusters must rest on either or both of the following arguments. Firstly, it may be opined that the comparison of values of $M_{V^*_{25}}$ is invalid because the photometric systems are not compatible. This suggestion may be dismissed on the evidence of the absolute magnitudes of the brightest members of twelve rich clusters of galaxies listed by Godwin & Peach (1979), and the luminosity functions of nine clusters illustrated in Bucknell, Godwin & Peach (1979). It seems reasonable to assume that the latter are the clusters referred to by Austin et al. (1975), because here the mean value of $M_{V^*_{25}}$ estimated by inspection is $\langle M_{V^*_{25}} \rangle = -21.2 \pm 0.1$. If the magnitude scale of the Hydra I photometry were shifted so as to bring the value of $M_{V^*_{25}}$ (A1060) into agreement with this figure, the resulting revised magnitude of the first-ranked galaxy (NGC 3311) would be $M_{V_{25}} = -24^m.4$, which is extremely bright in relation to Godwin & Peach's figures. On the other hand, as discussed later, N3311 has a fairly typical absolute luminosity on the existing magnitude scale, so the possibility of very large systematic errors can be discounted.

The second argument would be that a difference of $0^m.74$ in $M_{V^*_{25}}$ is not a significant discrepancy. The numerical simulations of Dressler (1978a) provide some support for this view. Dressler constructed several thousand model clusters each representing, in

effect, a random selection or "statistical fluctuation" from an infinite population of galaxies conforming exactly to the Schechter (1976) formulation of a universal luminosity function. He found many instances in which the characteristic magnitude M^* estimated by analysis of a model with the assumed population of an Abell richness class 0 or 1 cluster differed by more than $0^m.5$ from that used to define the Schechter function on which the model was based. These deviations tended to be much smaller in richer clusters. Although M^* in Schechter's definition is not equivalent to the discontinuity in Abell's integrated function, statistically they should behave in much the same way. Since A1060 is a richness class 1 cluster whereas six of the aforementioned nine clusters have richnesses $R \geq 2$, the value of $M_{V_{25}}^*$ for A1060 does not contradict the universal-function hypothesis.

A more severe challenge to the idea of universality is the marked inconsistency of the slopes of the bright and faint ends of the luminosity functions constructed by Bucknell et al. (1979) and Dressler (1978b). Among the former sample, there exists at least one cluster which bears only crude resemblance to an Abell function. In the case of A1060 (Figure 6.4) the gradient of the bright-end segment is less steep than the average slope, 0.75, determined by Abell (1975) for four different clusters, and agreement would deteriorate further if the brightest members of Hydra I were afforded due weight in the line fitting. These misgivings acknowledged, it is nonetheless striking how well a linear approximation does fit the data over a range of nearly three magnitudes in V_{25}, from the position

of the knee at $14^{m}.1$ down to the completeness limit of the photographic photometry. The confirmation that the numbers of galaxies in the cluster increase exponentially to this limit is significant, and consideration is given in the next chapter as to whether this relation continues to still fainter limits. Linear extrapolation of Figure 6.4 to $V_{25} = \infty$ would imply that 90% of the galaxian luminosity contained within the 25th V mag arcsec^{-2} isophote is represented by systems brighter than $V_{25} = 17$.

Introducing the notation M_n for the absolute V_{25} magnitude of the n-th brightest cluster member, and M^* for that magnitude corresponding to the knee of the integrated function, the difference $M_1 - M^*$ for A1060 is $3^{m}.3$, which is larger than that of any of the clusters in the sample of Bucknell et al. except possibly A426. The dependence, if any, of this differential on cluster richness and composition is very relevant in relation to the use of both M_1 (strictly, the equivalent metric magnitude) (e.g. Sandage 1973b) and M^* (e.g. Abell 1978) as standard candles for the determination of distance, and it may also be intimately related to secular changes in the distribution of luminosity in a cluster (e.g. Ostriker 1977). Coincidentally, A426 (the Perseus cluster) is the only other distance class 0 association in the Abell (1958) catalogue, though it is more populous and flattened in outline and possesses two unusual characteristics: an unique radial distribution of members of different morphological types (Melnick & Sargent 1977), and a very luminous first-ranked Seyfert galaxy. This latter fact is partly responsible for the large $M_1 - M^*$ of A426, and from an uncompromising viewpoint it

would seem surprising that the $M_1 - M^*$ of A1060 is similar. The statistical uncertainties demonstrated by Dressler (1978a) would, however, be compounded with photometric errors affecting M_1, rendering $M_1 - M^*$ liable to large illusory fluctuations from cluster to cluster. For possible underlying trends to be revealed clearly, photographic photometry of still more clusters is required.

6.3 Optical Properties of the Brightest Member

The remarkable contrast of the luminosity distributions of the two brightest, centrally located galaxies in Hydra I (e.g. van den Bergh 1977b; Disney & Wall 1977; Fairall 1979) is well shown by an iso-transmission contour plot of the core of the cluster (Figure 6.5). This chart was generated from COSMOS measurements of the CTIO 4m prime focus plate number 995 detailed in Table 7.1.

The dominant galaxy, NGC 3311, forms an optical binary with the second-ranked elliptical NGC 3309 which north precedes it by 100 arcseconds. The luminosity distributions of the two galaxies appear to overlap from a level much brighter than the 25 V mag arcsec^{-2} limiting isophote of the photographic photometry, but in view of the lack of serious distortion of N3309, this is thought to be mainly an effect of projection.

Assessment of Figure 6.5 is complicated by the fact that many extraneous sources of luminosity contribute to and influence the visible isophotes (see below). Nonetheless, the relatively great extent of the halo of N3311 is obvious. Inspection also shown that the iso-transmission contours representing successively fainter light levels

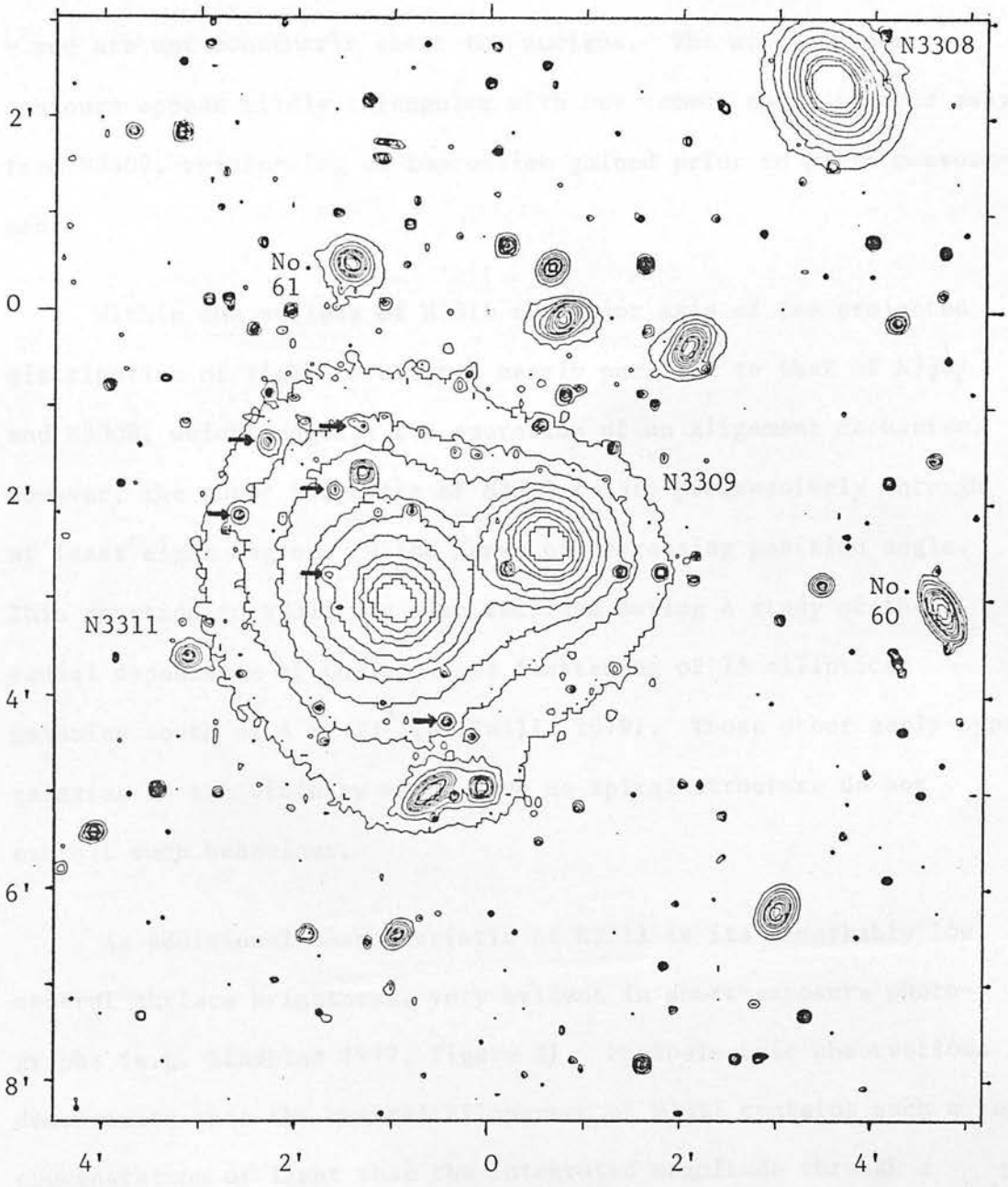

Figure 6.5

An isotransmission contour plot of the core of A1060. N3311 (left) and N3309 form the central binary, and N3308 is at the top right. The horizontal arrows identify six faint galaxies visible in projection in the halo of N3311.

within N3311 do not take the form of simple ellipses - compare N3308 - and are not concentric about the nucleus. The middle-order contours appear mildly triangular with one common apex directed away from N3309, reinforcing an impression gained prior to plate measurement.

Within the nucleus of N3311 the major axis of the projected distribution of light is aligned nearly parallel to that of N3309 and N3308, which suggests the operation of an alignment mechanism. However, the outer isophotes of N3311 rotate progressively through at least eight degrees in the sense of decreasing position angle. This rotation in N3311 was also recorded during a study of the radial dependence of the apparent flattening of 75 elliptical galaxies south of $\delta = -23^{\circ}$ (di Tullio 1979). Those other early-type galaxies in the vicinity which have no spiral structure do not exhibit such behaviour.

An additional characteristic of N3311 is its remarkably low central surface brightness, very evident in short-exposure photographs (e.g. Lindblad 1977, Figure 2). Photoelectric observations demonstrate that the central kiloparsec of N3311 contains such a low concentration of light that the integrated magnitude through a 5-arcsecond aperture at the nucleus is $\sim 1^{m}.5$ fainter than the corresponding nuclear magnitude of N3309 (van den Bergh 1977b), although no doubt part of the effect can be attributed to the absorption lane or dark cloud discovered at the very centre of N3311 by Lindblad (1977) and his collaborators.

The radial surface brightness profile of N3311 in the B and V wavebands has been derived from photographic surface photometry of plates V3324 and B3028 rather than the IIIa-J exposure depicted in part in Figure 6.5. Such 4m telescope plates suffer from severe field non-uniformities (see: Harris & Smith 1976; Rose 1979) which here are impossible to disentangle from the very extensive luminosity gradients associated with the many bright images in the small field. On the more uniform Schmidt plates only image overlaps require treatment. Cross-sections of selected galactic nuclei were taken at intervals of $\pi/4$ in position angle within grids of intensity values from which both the profiles of stars BS4162 and SA0179027 and the sky background had been subtracted (cf. Section 5.5). The mean B and V profiles of N3311 corrected for superpositions of discrete sources are shown in Figure 6.6. At high intensities (filled circles) the curves are defined by the results of numerical processing, and by cross-sections at fainter levels (open circles). The straight line at the upper right of the figure represents the critical inverse-square decline of projected intensity with radius, r, that must be attained or exceeded as $r \to \infty$ if the integrated luminosity is to converge. The observed gradients are shallower than this out to about 60 kpc; on the crude representation Intensity $\propto r^{-\alpha}$, the exponent α takes the value 1.55 over the interval $10 \lesssim r \lesssim 40$ kpc in the V band and 1.85 over $16 \lesssim r \lesssim 70$ kpc of the B profile. Clearly $\alpha < 2$, though the difference between the two values of α is not significant (photoelectric aperture photometry reveals that it is the V profile which is steeper). The gradient beyond 50 kpc is ill-defined on account of limited sampling, superposed images, deteriorating

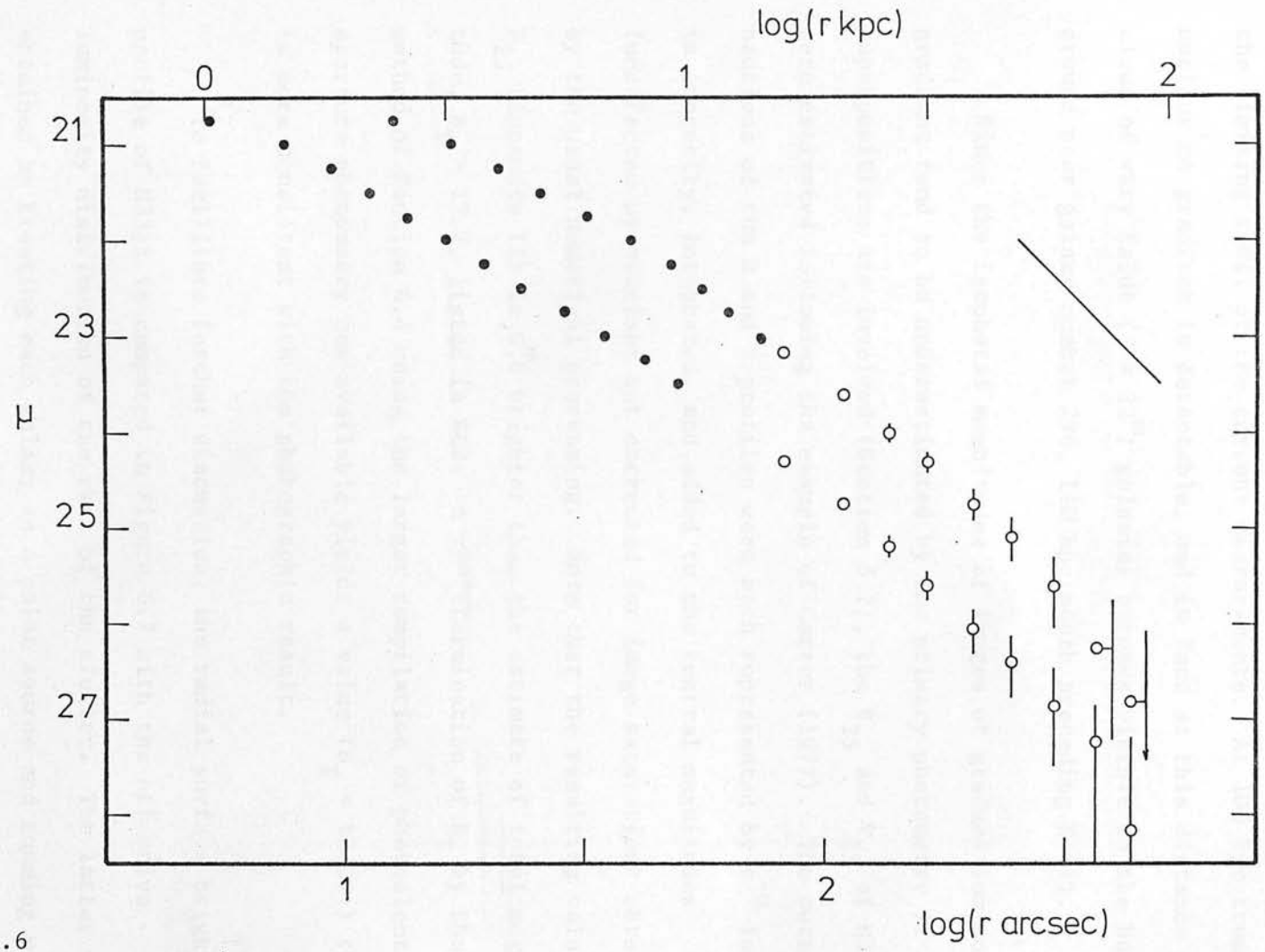

Figure 6.6

The surface brightness profiles of N3311 in the V (upper) and B wavebands. The straight line represents an inverse-square dependence of projected intensity with radius. The error bars correspond to an uncertainty of ±1% in the subtracted background level.

signal-to-noise ratios and the limitations of the background modelling. Nevertheless, the indications are that the condition for convergence of total luminosity is met - that is, $\alpha > 2$ - near the limiting radii of the current measurements. At 100 kpc from the nucleus no gradient is detectable, and in fact at this distance a cloud of very faint ($J \simeq 22^m$) galaxies becomes visible in the background near galaxy number 296, 110 kpc south preceding N3311.

Since the isophotal magnitudes of images of gradual luminosity gradient tend to be underestimated by the primary photometry if superpositions are involved (Section 5.2), the B_{25} and V_{25} of N3311 were estimated following the example of Carter (1977). The outer sections of the B and V profiles were each represented by $r^{-\alpha}$ laws in intensity, integrated, and added to the central magnitudes (unaffected by overlaps but corrected for image saturation) obtained by the usual numerical processing. Note that the resulting value of B_{25} (Appendix II) is $0^m.6$ brighter than the estimate of <u>total</u> magnitude, $B_T = 12.7$, listed in RC2. A re-determination of B_T by the method of Section 4.4 using the larger compilation of photoelectric aperture photometry now available yields a value ($B_T = 12.06$:) that is more consistent with the photographic result.

To facilitate further discussion, the radial surface brightness profile of N3311 is compared in Figure 6.7 with the effective luminosity distribution of the rest of the cluster. The latter was obtained by treating each galaxy as a point source and summing within rings centred on N3311 (itself excluded) the isophotal luminosities of all galaxies brighter than $V_{25} = 17$, with appropriate adjustment

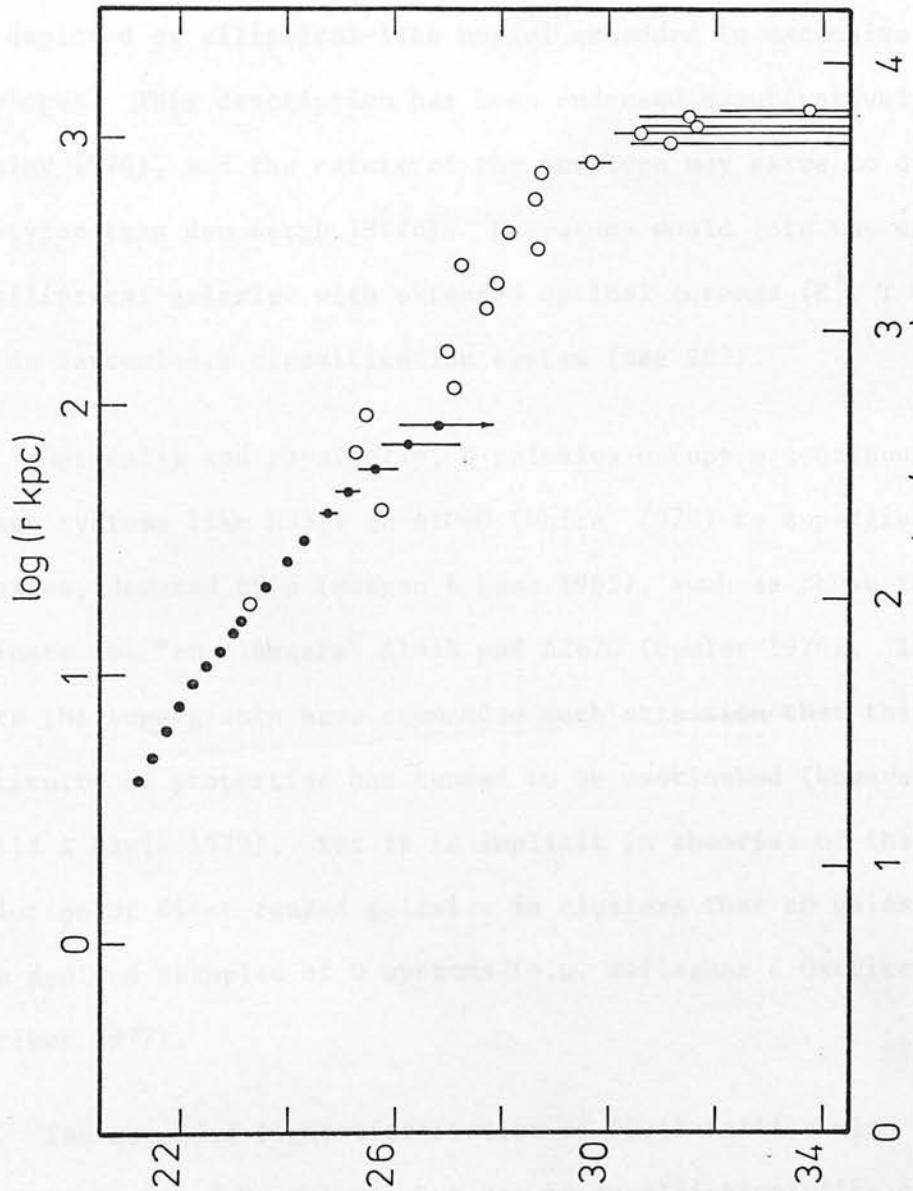

Figure 6.7

The projected radial profile of N3311 (filled circles) compared with the profile of the cluster (open circles).

for the integrated light of the proportion of non-members at each magnitude predicted by the field correction of Section 2.5.

6.4 The Nature and Evolution of N3311

White (1978) has assigned N3311 to the class of objects known as D galaxies (Morgan 1958; Matthews, Morgan & Schmidt 1964). These are depicted as elliptical-like nuclei embedded in extensive envelopes. This description has been endorsed quantitatively (Oemler 1976), and the nature of the envelope may serve to distinguish sub-types (van den Bergh 1977c). D systems would join the category of elliptical galaxies with extended optical coronae (E^+, T = -4) in the de Vaucouleurs classification system (see RC2).

Optically and physically, D galaxies occupy a continuum from modest systems like N3311 in A1060 (White 1978) to supergiant D galaxies, denoted cD's (Morgan & Lesh 1965), such as those that dominate the "cD clusters" A1413 and A2670 (Oemler 1974). In recent years the supergiants have commanded such attention that this continuity of properties has tended to be overlooked (however, see Schild & Davis 1979). Yet it is implicit in theories of the evolution of first-ranked galaxies in clusters that cD galaxies are more evolved examples of D systems (e.g. Gallagher & Ostriker 1972; Ostriker 1977).

The extended light distribution of N3311 tallies with one characteristic of D systems, but has it an elliptical-like core? The classification of N3311 as lenticular might suggest so. However, its central surface brightness is singularly low among the giant

early-type members of this cluster, which contradicts the proposal (Godwin & Peach 1979) that brighter galaxies in rich clusters exhibit higher central surface brightnesses than fainter systems. Oemler (1976) states that cD galaxies possess exceptionally bright cores. Presumably this refers to the integrated light contained within the core radius, which - although it cannot directly be measured in N3311 due to saturation effects - increases with the scale length of the luminosity distribution, and the latter is large for N3311. The core luminosity of N3311 should be comparable to that of N3309, and neither seems abnormally luminous.

Comparison with other nearby clusters provides a better perspective. Godwin & Peach (1979) have listed the isophotal magnitudes $M_{V_{25}}$ of the three brightest members of each of twelve rich clusters of galaxies, obtained by a programme of photographic surface photometry (Bucknell, Godwin & Peach 1979). Their data are not corrected for cosmological affects (see, for example, Green 1978), so only the two nearest clusters, Virgo I and A426, may straightforwardly be compared with A1060. The isophotal radii, r^{*}_{25} of the brightest members of the respective clusters are 43 kpc (N4486 = M87) and 41 kpc (N1275); adopting the distance scale used by Godwin & Peach (H_o = 50 km s^{-1} Mpc^{-1}), the equivalent dimensions are 78 kpc for N3311 and 39 kpc for N3309. On the extinction law of Sandage (1973a), the $M_{V_{25}}$ magnitudes of N3311 and N3309 are $-23^{m}.6$ and $-22^{m}.8$ respectively, both intermediate relative to those objects of the same rankings in the other two clusters.

These results suggest that the dimensions of N3311 are anomalously large for its luminosity, a fact reflected in its low surface brightness. There is ample additional evidence that supports the picture of N3311 as a relatively extended system. Photoelectric aperture photometry matched to RC2 magnitude growth curves (cf. Chapter 4) indicates that half of the B-band emission from this galaxy comes from a region 131 arcsec in diameter, as compared to only 46 arcsec in the case of N3309. The measurements of di Tullio (1979) imply that at a surface brightness level corresponding to the faintest detectable isophote on ESO (B) films, N3311 is at least twice the size of its bright companion. The photoelectric data of Sandage (1973b) would indicate that the absolute metric V magnitude of N3311 interior to a standard diameter of 86 kpc is not significantly lower than the average for a large sample of brightest galaxies in clusters, contrary to expectation if its mean surface brightness is in fact unusually low. This inference, however, is mistaken, because the metric magnitude of N3311 was derived by Sandage on the erroneous assumption of conformity to universal linear dimensions shared by all first-ranked galaxies in clusters (Sandage 1972a).

It is obvious from the previous section that N3311 is a highly disturbed stellar system. Its bloated appearance and asymmetric light distribution strongly suggest that during the recent (the previous $\sim 10^9$ year) evolution of the galaxy, strong dynamical interactions occurred between N3311 and other mass concentrations in the cluster. In this possible interpretation,

some of the kinetic energy of the intruding masses has been absorbed in dynamical heating of the stellar velocity distribution in N3311, reducing the negative binding energy of the galaxy and inducing it to expand. This hypothesis would be favoured by the discovery of concentrations of mass in the vicinity of N3311 which show properties that might be associated with gravitational perturbations.

Plausible candidates for such systems are compact galaxies. Fairall (1978b) has suggested that these are formed when the outer regions of normal galaxies are stripped away by tidal forces; and in particular, he speculates (Fairall 1979) that the extremely compact elliptical object number 61 in the Hydra cluster, located near N3311 and to its north (Figure 6.5), is the nuclear remnant of a giant elliptical galaxy that was largely denuded by N3311 during a previous encounter. However, the observed colours of galaxy 61 do not support this hypothesis. On the evidence of colour-aperture gradients in normal ellipticals, an intact and isolated elliptical core should be measurably more red than an entire galaxy of the same total luminosity; there is no indication that this is true of galaxy number 61 (see Figure 4.3).

A more likely explanation for the distension of N3311 is suggested by the presence of several fainter early-type galaxies which appear to be companions of the giant. As indicated in Figure 6.5, five of these small systems are located to the north-east of N3311, superposed on its halo and within 26 kpc of the nucleus as seen in projection. There is no similar clustering of faint galaxies in the halo of N3309. The strongly localised distribution of the

small systems near N3311 must affect its gravitational potential, perturbing stellar orbits and contributing to the global asymmetry. If these companions are acually immersed in the envelope of the giant, dynamical friction will operate, causing the captives to spiral towards the nucleus as they lose energy. The optical properties of the N3311 system are consistent with the theory of cluster evolution by galactic accretion and cannibalism (Ostriker & Tremaine 1975; Ostriker & Hausman 1977; Ostriker 1977; Hausman & Ostriker 1978).

This course of evolution presumes the initial existence of a "seed" galaxy within what was to become the Hydra I cluster, which began to interact with and to pillage its fellow cluster members. Such a system might have been a bright galaxy that initially dominated a subcluster of galaxies of low internal velocity dispersion. All known examples of D and cD galaxies occur within local density enhancements inside rich or poor clusters (White 1978), and within such associations gravitational encounters that might promote the formation of a D galaxy are likely to be relatively frequent. On an alternative scheme (Gallagher & Ostriker 1972), the observed D system was formed as tidal debris, liberated during galaxy collisions and interactions, gradually accumulated in the potential well at the centre of the cluster: no progenitor or "seed" was involved. At least four readily testable predictions follow from the debris hypothesis (e.g. Richstone 1976): the starcloud would have the same relatively blue colour as the outer regions of normal ellipticals; it would have no colour gradients from centre to rim; it should be

centrally located in the cluster, and its radial surface density distribution would be similar to, or somewhat steeper than, the radial luminosity profile of the cluster itself.

Photographic photometry confirms that N3311 satisfies the latter condition (Figure 6.7), and it has already been remarked in Chapter 2 that this galaxy is close to the centre of maximum number density in the cluster. The remaining requirements of the debris hypothesis, however, are clearly contradicted by photoelectric aperture photometry. The face-on intrinsic U-B colour of N3311 extrapolated to infinite aperture $[(U-B)^{o}_{T}]$ is not appreciably bluer than those of the normal elliptical galaxies N3305 and N3309; the figures are $0^{m}.48$, $0^{m}.49$ and $0^{m}.50$ for the three systems respectively. Moreover both the B-V and U-B colour indices of N3311 become progressively bluer through increasing apertures, in the same sense and perhaps more markedly than in the case of its companion, N3309. Since N3311 approximates so closely at the present epoch to the stellar composition and population gradients of a normal early-type giant, its formation entirely from tidal debris can be ruled out.

In the cannibalism hypothesis the dominant galaxy evolves towards the properties of a starpile, as distinct from always having existed as one (cf. Gallagher & Ostriker 1972). As captive galaxies disintegrate and lose their identity in the giant system, the integrated colour of the latter should gradually tend towards the mean colour of the galaxies consumed. Numerical simulations (Hausman & Ostriker 1978) indicate that much of the accreted material would have existed as galaxies with magnitudes close to M^{*}, the

characteristic magnitude or turnover point in the logarithmic integrated luminosity function (cf. Figure 6.4). These galaxies are less bright than the giant systems and hence should be bluer according to the colour-magnitude relation (Figure 4.3). The fact that N3311 itself is not relatively blue in comparison with N3309 and N3305 implies that N3311 cannot have accreted very many fainter galaxies during its past evolution.

However if it is accepted that N3311 is the only member of A1060 to be growing at the expense of lesser galaxies, a difficulty of interpretation does arise regarding the trends visible in the colour-magnitude diagram, Figure 4.3. Assuming that a linear colour-magnitude relation as observed by Sandage (1972b) applies initially to all unevolved early-type galaxies in clusters, Hausman & Ostriker (1978) predict a gradual flattening of this relation among bright galaxies as they proceed to digest faint companions. Near-equality of the colour of bright galaxies as seen in Figure 4.3 could have resulted, on this hypothesis, only if all of the galaxies on this plateau behave in the manner suggested for N3311.

Recent work by Michard (1979a,b) indicates, nonetheless, that too much should not be made of this apparent failure of the cannibalism hypothesis to account for the presence of a marked horizontal branch in the colour-magnitude diagram for A1060 in the absence of evidence that cannibalism is rife in the cluster. Michard has reported that early-type galaxies in each of many nearby groups and clusters exhibit different intrinsic U-B colours from those found in other groups. Within each cluster, galaxies separate into distinct

sequences and two separate colour-magnitude correlations are observed: bright galaxies populate the nearly horizontal branch; faint galaxies obey a steeper relation. These sequences also segregate in other planes, for example in the total magnitude-surface brightness plane, although insufficient photoelectric observations exist to confirm this in the case of A1060. The subject of the evolution of the colour indices of galaxies is clearly more complex than has hitherto been supposed, and further studies of colour-magnitude correlations are required.

It is tempting to speculate that N3311, uniquely among galaxies in the Hydra I cluster, is evolving towards the characteristics of a supergiant cD system. At present it most likely represents a transitionary stage between elliptical galaxies with some indication of tidally distended haloes (Kormendy 1977b), and classic D galaxies such as N4874 in the Coma cluster.

6.5 Peculiar Galaxies

NGC 3312 in the Hydra I cluster is a large early-type spiral which appears to be in the process of losing its interstellar dust and gas. It is highly distorted, laced with sharp dust lanes, and there are condensations or filaments to the south-west of the galaxy which may have been stripped from the disk (Gallagher 1978). The asymmetry of the disturbance discourages the idea that internal activity in N3312 is responsible, and the apparently greater stability of the stellar component as compared to the gaseous is likewise difficult to account for on a tidal interaction picture. The most natural explanation for

the appearance of N3312 is that it is being scoured of its interstellar material by the ram-pressure effect of its motion through an intracluster gas (cf. Gunn & Gott 1972).

Gallagher (1978) has remarked that there exist other "anaemic" or gas-poor spirals (van den Bergh 1976) besides N3312 in the core of Hydra I. Inspection of the prime focus plates taken with the CTIO 4m telescope reveals two particularly interesting candidates, both of which show evidence of structural perturbations. The first is the peculiar spiral galaxy number 60 = N3307, located 5 arcminutes west of N3309/N3311. N3307 appears to have narrow, bright and well-defined arms which are strongly warped relative to a plane. On the available 4m plates no Population I tracers (O, B-star complexes, HII regions) are visible in the arms, which suggests that no recent star formation has occurred; this absence is one symptom of gas loss. The optical characteristics of N3307 are those of the smooth-arm spiral galaxies (Strom, Jensen & Strom 1976) whose existence in several other X-ray emitting clusters has been reported by Wilkerson, Strom & Strom (1977).

The second unusual system and possibly a better example is the galaxy number 43, which is also classified as a peculiar spiral. It has a diffuse, low-surface-brightness arm which encircles the nucleus and may formerly have closed in on itself; the presence of a second main arm is uncertain. Apart from knotty condensations on the inside of the first arm, most internal structure in the arm has been obliterated. The inner boundary of this arm is sufficiently sharp, on the south side of the nucleus, to reveal a possible narrow inner (detached?)

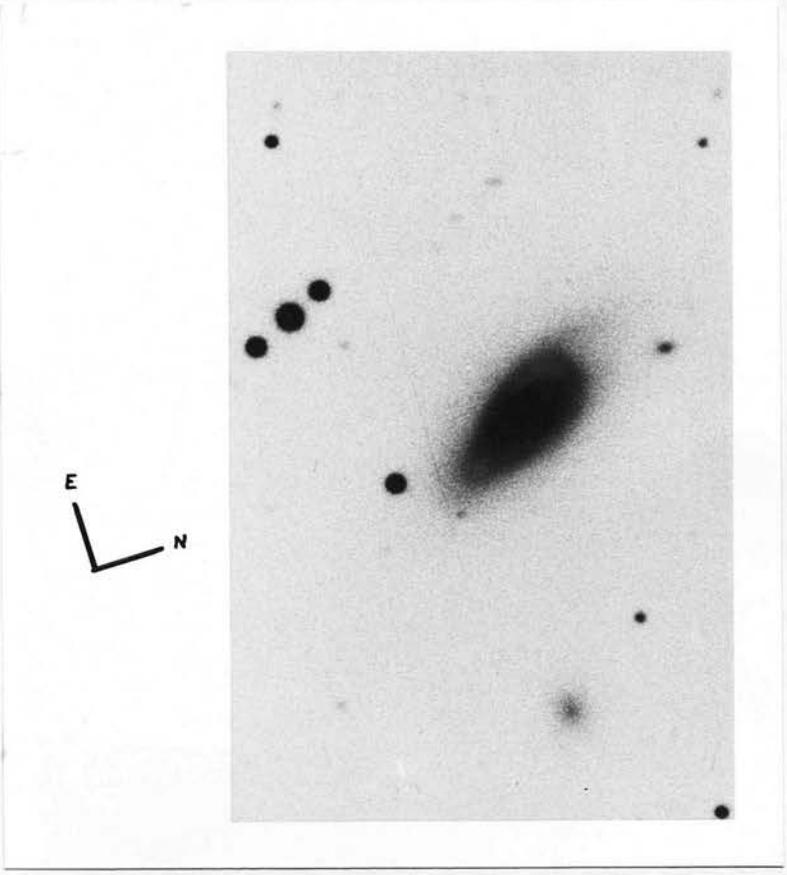

Left: the smooth-arm spiral galaxy no. 60 = N3307. Enlargement of plate no. 641 taken by M.G. Smith at the prime focus of the 4m reflector at CTIO (see page 169 for further details).

Scale 1.26 arcsec mm^{-1}.

Seeing <1 arcsec.

Right: the peculiar system no. 43, as recorded on plate no. 641.

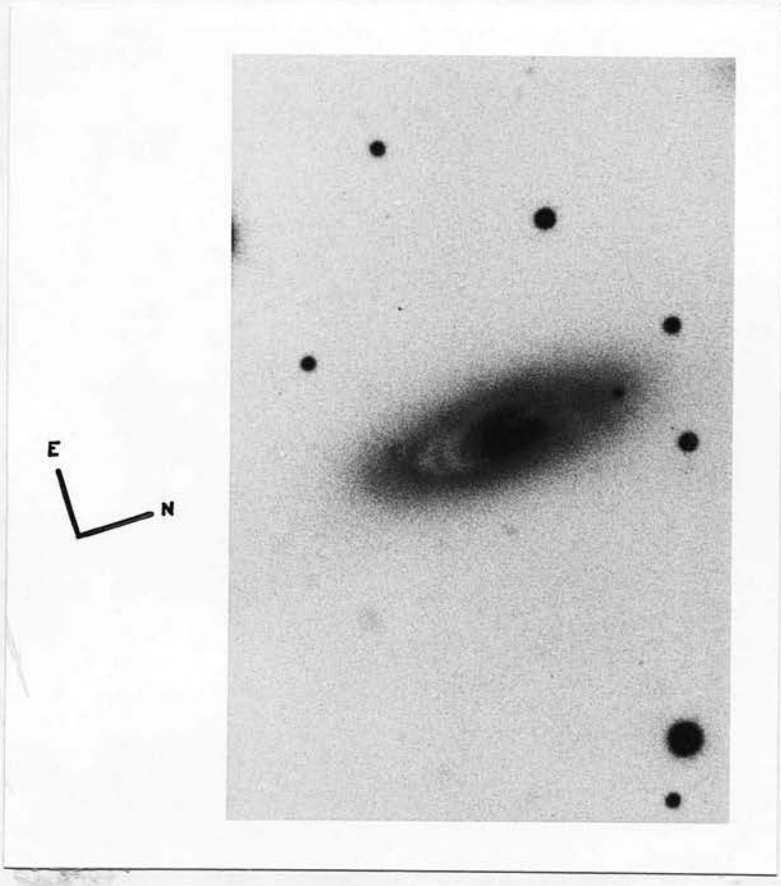

arm of the galaxy; on the north side the arm dissolves chaotically. In addition a prominent absorption lane trails across the northern half of the nuclear region, nearly parallel to the long axis.

If the interpretation of these systems as disturbed spirals is correct, and star-forming events in their disks have ceased, their integrated colours should be anomalously red relative to normal spirals. A comparison of the photoelectric colour indices of N3307 and the normal barred spiral number 86, which is of very similar stage in the revised Hubble classification system, shows that N3307 is indeed redder (Table 4.3), and at the same time less red than a S0. This single observation is, therefore, consistent with the belief that there exist disk galaxies in A1060 which have lost, or are currently losing, a substantial fraction of their gas. Since ram-pressure stripping would be most efficient in the core of a cluster where the mean density of the pervading medium is highest, it is worth noting that the three galaxies mentioned are all within a projected distance of 0.2 Mpc of the centre of A1060.

Only one possible and very dubious instance has been discovered of a spiral system in this cluster in which gas loss has already proceeded to extremes. This is galaxy number 112, a fainter "lenticular" with a small bulge-to-disk ratio and a very smooth envelope. Inspection of CTIO plate 995 leaves a persistent impression of two small, weak arms in the immediate region of the nucleus, in which it bears some resemblance to IC 2951 in A1367 (Strom & Strom 1979b), a smooth-arm spiral in which the arms have almost disappeared and which is otherwise visually indistinguishable from a S0. However,

the arms are not revealed on the shorter-exposure plate number 641; UKST photographs have insufficient resolution to reveal the structure.

Since at least two of the three disturbed spirals - N3312 and number 43 - appear to be currently losing their gas, the stripping of these systems may have begun only recently (a few 10^9 years ago). Gas shed by evolving stars in the galaxies would tend to replenish each interstellar medium (e.g. Faber & Gallagher 1976), probably to the extent of rendering such systems invulnerable to stripping over most of their lives (Gisler 1979). The era of gas depletion may have begun when gas injection rates dropped sharply. As the galaxies leave the stripping regime due to their peculiar motions through the cluster, gas-poor character could be maintained through the internal sweeping action of galactic winds driven by supernovae (Matthews & Baker 1971; Johnson & Axford 1971; Bregman 1978).

Whether such systems will eventually evolve into bona fide lenticulars is a question open to dispute. Such transmutations could in principle explain why so many SOs and so few spirals are observed in the central regions of Hydra I; it would also account for the lower proportion of spiral galaxies generally in higher-luminosity X-ray clusters (Bahcall 1977b; Tytler & Vidal 1978) in which the intracluster medium is most likely denser and gas stripping consequently more efficient. However, in the apparent absence (in A1060) of ancient spiral relics which more nearly resemble SOs, it is doubtful whether sufficient time has elapsed for many conversions to have run to completion in A1060. Furthermore, many SOs are situated too far from the centre of any rich cluster for external ram

pressure to have been effective. They are likewise too far from the dense cores of clusters for collisions between the spiral and other galaxies (Spitzer & Baade 1951) to be a viable alternative explanation for the formation of the SOs (see Sandage & Visvanathan 1978b for a review).

To summarise, the distinctive features of the three spiral systems (low rates of star formation in the spiral arms, structural distortion, generally "anaemic" appearance and in the one case measured, reddening of the system) suggests strongly that in the core of A1060, an era of gas stripping has recently begun. The present nature of these candidate "lenticulars" in A1060 could be clarified by HI-line observations of gas abundance and further photoelectric photometry.

CHAPTER 7

DWARF GALAXIES IN A1060

7.1 Definition and Review

Dwarf galaxies - a term extended, in the present context, to the most extreme examples of miniature galaxies, including the "pygmy" and "gnome" categories of Zwicky (1971) - represent the faintest and least well delineated region of the spectrum of galaxian luminosities. Like the transition between giant systems and normally bright galaxies, the separation of normal galaxies from dwarfs is to some extent arbitrary; de Vaucouleurs (1975) suggests the definition M_{B_T} (dwarf) $\geq$ -16.0. Systems fainter than absolute magnitude M_{B_T} = -15 probably do not contribute significantly to the total mass density of a cluster (Reaves 1967).

The absolute number of these low-luminosity, and presumably low-mass, galaxies is uncertain, even within the nearest 3×10^3 Mpc^3 (Tammann & Kraan 1978). There exist strong logical arguments (Arp 1965) and observational evidence (e.g. Sandage, Tammann & Yahil 1979) which suggest that at all distances there remain low surface brightness galaxies that are not catalogued. Arp (1965) pointed out that the log L : log R plane, where L and R represent the total luminosities and radii of different classes of object, is everywhere populated where it is detectable and that there is no justification for supposing that systems of lower surface brightness do not exist. The omission, as distance increases, of a growing proportion of intrinsically faint galaxies in a sample selected to a limiting

apparent magnitude shifts the observed distribution of absolute magnitudes in the sample towards brighter values (Sandage, Tammann & Yahil 1979).

An important corollary of dynamical relaxation of clusters over long timescales is the radial segregation of galaxies according to mass; for as equipartition of energy is achieved, the less massive galaxies assume a higher velocity dispersion and a relatively broader quasi-equilibrium distribution. Many studies have been pursued which test directly or indirectly for the presence of observable segregation in clusters (Zwicky 1942, 1956; Rudnicki 1963, 1967; Kwast 1966; Rudnicki & Baranowski 1966a,b; Rood 1969; Bahcall 1972, 1973c; Noonan 1971, 1974; MacGillivray et al. 1976b, and others), but most of these have either lacked photometric calibration or involved clusters so distant that genuine dwarfs were unobservable. Moreover the difficulty of distinguishing faint galaxies from intrinsically brighter systems at greater distances has sometimes led to equivocal or even contradictory conclusions (cf. Zwicky 1956, Noonan 1974). It does appear that in rich regular clusters segregation in the expected sense is observed (see Bahcall 1977a), but competing evolutionary effects, which are discussed later, complicate the picture.

The number of moderately rich groups of galaxies that are near enough for their dwarf members to be observationally accessible is limited. Jones & Jones (1978) list sixteen candidates, populous and otherwise. Reaves (1967) has examined the distribution of dwarf galaxies associated with the most amenable systems, namely the Virgo

(Reaves 1956, 1977a) and Fornax (Reaves 1964) clusters; Hodge and his collaborators (Hodge 1959, 1960; Hodge, Pyper & Webb 1965) have also investigated faint objects in the Fornax cluster. The next nearest dense groupings that are comparably rich are Pegasus, Centaurus I and Hydra I.

The structural properties of dwarf galaxies are diverse (e.g. Reaves 1977a,b; Webster et al. 1979), but a dwarf may be one of three general types: dwarf elliptical; dwarf spiral or irregular; or of a species exemplified by IC3475 in the Virgo cluster (Reaves 1977b). Hodge (1971), however, does not recognise the latter as a distinct class, whereas van den Bergh (1959) distinguishes dwarf spirals from Magellanic irregulars. Low surface brightness is the most common visual characteristic of dwarfs, collectively. For example, the Sculptor and Fornax dwarf elliptical members of the Local Group (Shapley 1939) have peak surface brightnesses of only $24.0 \pm .5$ B mag arcsec^{-2}; this figure would be 17 or less for giant galaxies. The surface brightnesses and optical appearances of galaxies vary with distance (van den Bergh notes that IC3475 types are more easily identified when relatively distant than when nearby and completely resolved into stars).

Besides Sculptor and Fornax, other local dwarf ellipticals - N147, N185, N205 and N221=M32 - and the representative dwarf irregulars N6822 and IC1613 (see also Fisher & Tully 1979) are readily visible on Palomar Observatory Sky Survey (POSS) and Southern Sky Survey plates. The detection on POSS plates of the dwarf systems identified in the Coma cluster by Reaves (1966) and

Rood & Baum (1967), each of whom had access to prime focus plates from the 5.1m Hale telescope, poses a greater challenge: as an illustration, M32 at the distance of the Coma cluster ($\mu \simeq 34\overset{m}{.}1$) would have an apparent magnitude $B_T = 19\overset{m}{.}2$ and a standard angular diameter D(0) of 3 arcseconds. Most of the dwarfs are indistinguishable from stellar images and emulsion defects.

On the new deep IIIa-J surveys, however, dwarf systems in the Virgo I (Δ = 12.5 Mpc) and Fornax I (Δ = 17 Mpc, de Vaucouleurs 1977b) clusters are more conspicuous. Thirty-nine of the fifty objects discovered by Hodge et al. (1965) in the latter cluster lie within ESO/SRC Field No 358 on the basis of their epoch 1950 positions, and all but six of those found by Reaves (1964). Inspection of high quality survey film revealed that seven of those objects described by Hodge et al. as similar in appearance to dwarf elliptical galaxies (their designations 6, 9, 11, 22, 37, 38 & 41) are in fact spiral or irregular galaxies; two listed as irregulars (numbers 5 & 39) are probably misclassified, and a further two (29 & 35) are not visible on the film copy. Additional dwarf-like objects exist that are not tabulated by Hodge et al. The survey of Reaves exhibits comparatively greater homogeneity, but includes some late-type galaxies which rather than being members of Fornax I, are probably intrinsically brighter systems in the background. In less than twenty cases do the independent surveys agree on the selection of a given galaxy. The contention of Reaves that the discovery of dwarf galaxies under favourable circumstances is a matter of recognition rather than detection, therefore, receives support; a more striking illustration

is the disclosure (Fisher & Tully 1975) that only 15% of the DDO "dwarf" systems catalogued by van den Bergh (1959, 1966) are true dwarfs on the de Vaucouleurs definition. Identification problems will be greatly alleviated when redshifts surveys of the nearer clusters become available (see Jones & Jones 1978). In the meantime, purely optical criteria must be used.

7.2 Selection Procedure

For the purpose of locating dwarf members of the Hydra I cluster, deep IIIa-J reject survey plates were examined for objects which were visually comparable to the Virgo and Fornax dwarfs discovered by Reaves and others. This approach is important, because unlike Reaves (e.g. 1977a), no use is made of the apparent surface distribution of like systems, relative to that of normal galaxies, as an indicator of association of those systems with the cluster. Hence, conclusions regarding the true surface distribution of dwarfs remain valid.

The COSMOS machine was not engaged for the detection and measurement of dwarfs because the relevant regions of the photographic plates were appreciably vignetted; the eye is a more reliable detector within confused regions of multiple luminosity gradients, and moreover the high density of star images ($\sim$500 cm^{-2} with $J \leq 22^m$ would have taxed any automatic star sorting routine. The procedure was to insert a metal-on-glass graticule in the design of a labelled 10 x 10 grid behind one eyepiece of a binocular microscope through which each plate was viewed. The position of every recognisable

galaxy was marked on a reproduction of the grid scaled to give a convenient twenty times magnification of the plate (3.4 arcsec mm^{-1}). Stepping down successive columns while recording galaxies in this manner, a composite chart of a region 1.8 $degree^2$ in area and centred on the Hydra cluster was generated. Registration was later restored by matching the individual grids to the coordinate system defined by COSMOS coarse-mode measurements. Candidate dwarfs were emphasized on the charts.

Opportunity to verify these identifications was subsequently provided by two prime focus IIIa-J plates obtained on the 3.8m reflector at CTIO. Their particulars are summarised in Table 7.1. On plate 995, which displays the central 0.7 $degrees^2$ of the cluster at superior resolution and to a slightly brighter limiting magnitude than do the sky-limited Schmidt plates, all of the more plausible dwarf galaxy candidates were recovered and five additional faint examples were also found. Such disagreement as there was essentially concerned image structure, as emulsion granularity is relatively more serious at the scale of the Schmidt plates.

The probable dwarf systems discovered in projection within the central region of the Hydra I cluster are listed in Table 7.2. Those galaxies within the central field of plate 995 (group A) are set apart from the systems which are outside this field and visible only on the UKST plate (group B). The least persuasive identifications, i.e., the smallest and faintest images noted, are not included. The systems exhibit much variety of form, and the notes in Table 7.2 supply an abbreviated description of their more obvious optical

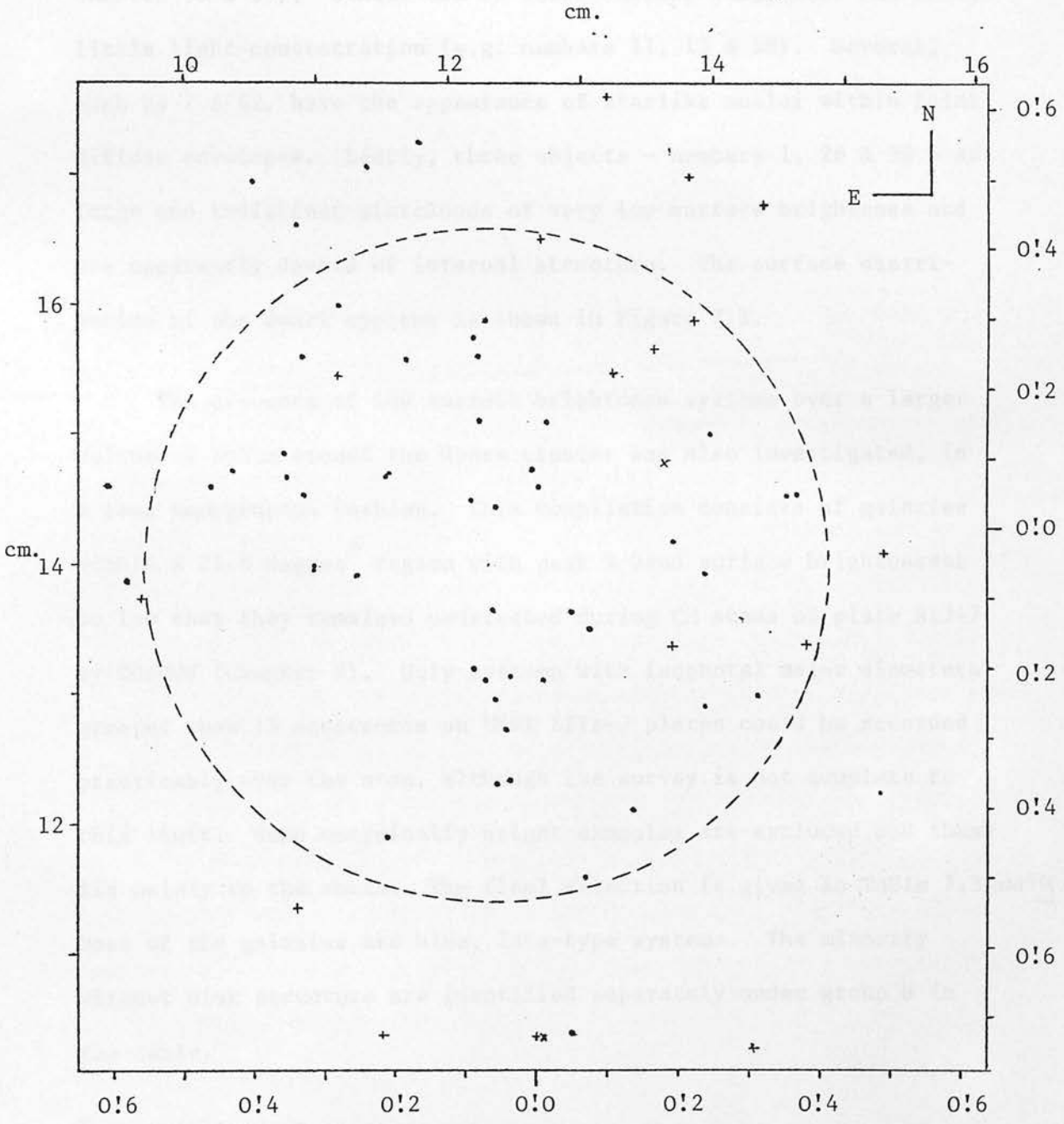

Figure 7.1

The surface distribution of dwarf galaxies (dots: Table 7.2) and low surface brightness systems ('plus' symbols: Table 7.3) near the centre of A1060. Crosses distinguish the two galaxies listed in Table 7.2 which may have spiral structure. The approximate area covered by plate 995 ("central region") is shown by the dotted circle.

characteristics. Some dwarfs are fairly compact, relatively bright and have significant central concentration of luminosity (e.g. numbers 33 & 39); others are of lower surface brightness and reveal little light concentration (e.g. numbers 11, 13 & 38). Several, such as 7 & 42, have the appearance of starlike nuclei within faint diffuse envelopes. Lastly, three objects - numbers 1, 28 & 36 - are large and indistinct starclouds of very low surface brightness and are apparently devoid of internal structure. The surface distribution of the dwarf systems is shown in Figure 7.1.

The presence of low surface brightness systems over a larger volume of space around the Hydra cluster was also investigated, in a less homogeneous fashion. This compilation consists of galaxies within a 21.8 degree^2 region with peak R-band surface brightnesses so low that they remained undetected during CM scans of plate R1347 by COSMOS (Chapter 2). Only systems with isophotal major diameters greater than 15 arcseconds on UKST IIIa-J plates could be recorded practicably over the area, although the survey is not complete to this limit. Some untypically bright examples are excluded and these lie mainly to the south. The final selection is given in Table 7.3 and Fig. 7.2. Most of the galaxies are blue, late-type systems. The minority without disk structure are identified separately under group B in the table.

7.3 Magnitude Estimates

To estimate the apparent magnitudes of the dwarf systems listed in Table 7.2 it is necessary to advance indirect arguments. Firstly,

it can be appreciated immediately that the observation that the brightest members of the system of globular clusters associated with NGC 3311 (cf. Figure 2, Smith & Weedman 1976) are not visible on the Schmidt plates constrains the limiting magnitude to $J < 23^{m}.5$. More usefully, the number counts of galaxies of all types within the 1.8 degree^2 may be compared with empirical number versus apparent limiting magnitude relations derived from other photometrically calibrated number counts (e.g. Shane 1975, Karachentsev & Kopylov 1977, Tyson & Jarvis 1979, MacGillivray & Dodd 1980). The 2866 galaxies recorded represent a density of 1570 degree^{-2}, of which about 1300 degree^{-2} are not Hydra cluster members; according to the compilation of Karachentsev & Kopylov, this surface density is typically reached at approximately $J = 21^{m}.6$, equivalent to an apparent magnitude of $22^{m}.0$ after extinction ($A_B = 0^{m}.38$, RC2). The relation of Tyson & Jarvis (1979) would indicate the limit $J \simeq 21^{m}.3$ or $21^{m}.8$ on the basis of their empirical extinction law, and Shane's $J > 22^{m}$ with extrapolation. Three qualifications of these figures are necessary: density fluctuations (greatly exceeding the statistical) due to largescale clustering of galaxies are liable to vitiate such comparisons; patchy galactic obscuration (e.g. Holmberg 1974, Sandage 1976) is unpredictable to a certain extent; and inconsistencies remain regarding the mean rate of increase of the number of galaxies with magnitude.* It is also uncertain whether the effective limiting magnitude for detection is the same for diffuse systems as for compact images. For instance, a disk of uniform apparent

* Shane (1975) and Karachentsev & Kopylov (1977) find $\log N(\leq m_J)$ to increase progressively more slowly at faint m; Tyson & Jarvis (1979) report a constant $d \log N(\leq m_J)/dm_J = 0.41$ in $17^{m} < J < 24^{m}$, but Kron (1977) quotes a constant Euclidean slope of 0.6 in the blue to $B = 24^{m}$.

surface brightness μ_J = 25 mag arcsec^{-2} would have an integrated magnitude J = $20^m.3$ interior to 10 arcseconds diameter; such an object would probably have been detected. Having regard of all clues, a limiting magnitude of $21^m.0$ is adopted. While obviously uncertain, this figure is insensitive to the allowance made for the local excess of galaxies represented by A1060 itself, because of the steep increase of the number of field galaxies per magnitude interval at this limit.

As for the galaxies of Table 7.3, their effective radii are about 15 arcseconds in the mean at the visual limiting isophote on survey plates. By reference to Figures 5.14(b) and 5.12, a normally luminous system of this size would have a blue magnitude B_{25} = 16.4, corresponding to V_{25} = 15.6 for late-type galaxies of group A. Since by definition the latter were missed during a survey complete to $V_{25} \simeq 17^m.0$, these galaxies are at least one magnitude fainter than normal systems of comparable size.

7.4 Results

It is evident from Tables 7.2 and 7.3 that there are relatively few low-luminosity spiral and irregular galaxies in the cluster core and a preponderance in the outer regions. Figure 7.2 presents the surface distribution of the late-type systems over the 21.8 degree^2 studied. The weak clustering in the general vicinity of the cluster suggests association, but few are found in the core itself. Because of their comparatively large angular dimensions, it seems unlikely that most of the systems can be distant; they probably form part of a cloud of late-type galaxies surrounding the core of earlier types

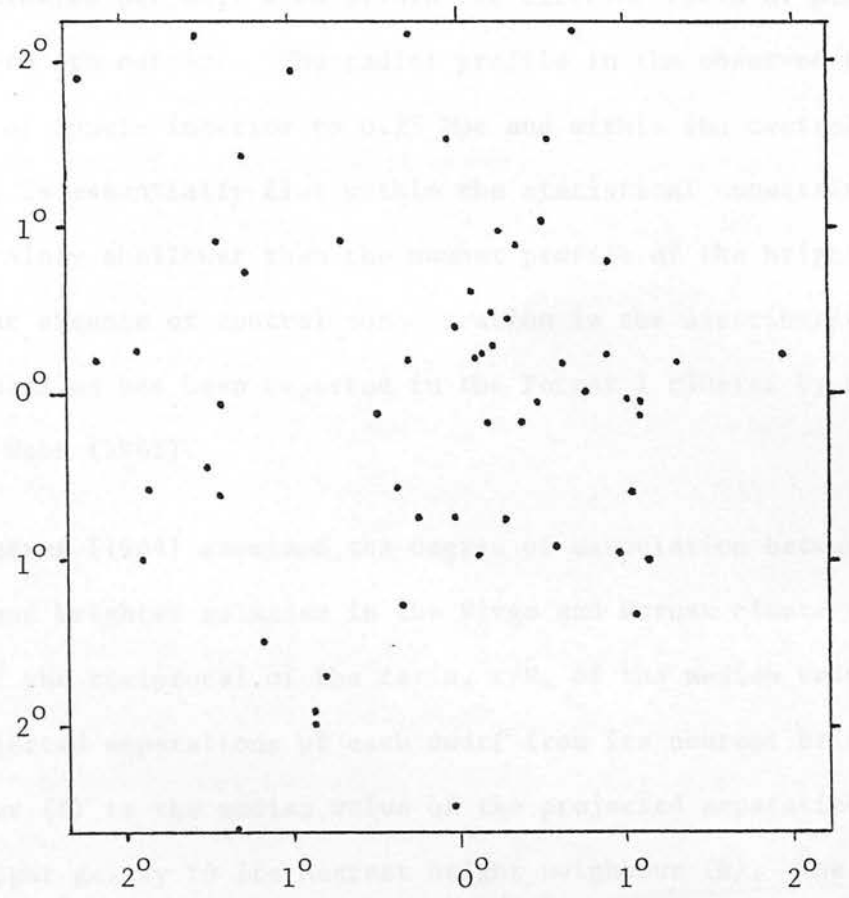

Figure 7.2

The surface distribution of the low surface brightness galaxies listed in Table 7.3. There is some suggestion that these systems are associated with A1060. Compare with Figures 2.7 - 2.9.

(compare with Figures 2.7 - 2.9).

In the inner regions of Hydra I there are appreciably more dwarf galaxies per unit area within the circular field of plate 995 than there are outside. The radial profile in the observed number density of dwarfs interior to 0.25 Mpc and within the central circle, however, is essentially flat within the statistical uncertainties, and certainly shallower than the number profile of the bright members. A similar absence of central concentration in the distribution of dwarf galaxies has been reported in the Fornax I cluster by Hodge, Pyper & Webb (1965).

Reaves (1964) examined the degree of association between dwarfs and brighter galaxies in the Virgo and Fornax clusters by means of the reciprocal of the ratio, r/R, of the median value of the projected separations of each dwarf from its nearest bright neighbour (r) to the median value of the projected separations of each bright galaxy to its nearest bright neighbour (R). The dimensionless quantity R/r is independent of the density (and the distance) of the cluster; if the dwarfs are located preferentially in the vicinity of giant galaxies, R/r would exceed unity. Adopting the criterion $M_{V_{25}} < -18^{m}.0$ as an arbitrary definition of a bright galaxy, the data here indicate that R/r(A1060) = (43 kpc)/(45 kpc) = 1.0. For comparison, this ratio is 1.0 for Virgo I and 0.6 for the Fornax cluster (Reaves 1964). Combined with the result R/r(A1656) = 0.8 implied by figures given by Rood & Turnrose (1968) pertaining to Reaves' (1966) Coma cluster dwarfs, this is convincing evidence that in general, dwarf systems in the central regions of rich clusters are not satellites of giant galaxies.

The morphology of the faint dwarf systems near the centre of A1060 is noteworthy. The scarcity or absence of dwarf spirals and irregulars parallels the situation in Virgo I (Reaves 1977a,b). The diffuse systems within A1060 with sharp nuclei are similar to some of Reaves' Virgo dwarfs, which may be the same systems as the "nucleated dwarfs" described by Romanishin, Strom & Strom (1977). These types are also visible in the Fornax cluster, yet they have no counterparts in the Local Group. Strom & Strom (1978b) have also reported higher-luminosity versions of nucleated dwarfs in the Perseus cluster (A426), but they find none in A262, A1367 and A1656. A possible inference is that the composition of the local dwarf population varies from cluster to cluster.

The distributions of the apparent ellipticities, $e = 10(1 - d/D)$, of the "early-type" and "late-type" dwarfs listed in Tables 7.2 and 7.3(A) respectively are not significantly different at the 20% level in the Kolmogorov-Smirnov test. There are appreciable numbers of elongated ($e > 3$) systems among early as well as late types (although individually, estimates of e are imprecise). Hodge (1971) notes that dwarf ellipticals in the Local Group have quite high ellipticities; a good example is the Carina dwarf galaxy recently discovered by Cannon et al. (1977). The term applied to such systems by some authors, "dwarf spheroidal", is unfortunate.

Altogether 51 faint galaxies have been identified in the central 0.73 degree^2 of A1060 in the approximate magnitude range $17.5 < V_{25} < 21.0 - \langle B_{25} - V_{25} \rangle - A_V$, i.e. $17.5 < V_{25} < 20.4$ (Figure 7.1). A linear extrapolation of the Abell-type luminosity function

defined by galaxies brighter than $V_{25} = 17.0$ (Figure 6.4) would predict an average of 64 galaxies to each 0.73 degree^2 interior to a radius of 1.5 Mpc. This shortfall of observed numbers relative to prediction is probably significant, for two reasons. Firstly, it would be an exceptional optical survey of intrinsically faint systems that was not to some degree contaminated by normally luminous galaxies; the precedents are not encouraging. Secondly, the actual surface density of galaxies towards the cluster centre ought certainly to be higher than the average predicted by a luminosity function for a much larger area. The force of this argument is only partially diminished by the lack of observable central concentration of the identified dwarfs.

It is possible, nevertheless, that the incorrect conclusion may be drawn, because of the strong bias that favours selection of low surface brightness members of Hydra I. Small compact ellipsoidals undoubtedly exist, but are extremely difficult to identify at the distance of A1060 by appearance alone (though the compacts in the halo of N3311 are exceptions, the evidence is circumstantial). The importance of the omission of these types of galaxies cannot be assessed until integrated colours or redshifts are determined, a technically ambitious undertaking that demands the best equipment. The facts presented in this Chapter provide sufficient grounds for questioning whether the numbers and the distribution of poor stellar systems really represent a logical continuation of the properties of the larger systems. There is in fact evidence of a breakdown of a bilinear luminosity function at faint magnitudes in the Coma cluster

(Abell 1977), but the sense of the departure is entirely contrary to that implied here for A1060, and appears to be better determined. The issue is still open, and comparable studies of other nearby clusters would be worthwhile.

Table 7.1

Details of the prime focus plates from the 4m reflector at CTIO

Plate No	641	995
Date exposed	16-17 Feb. 1975	10-11 April 1975
R.A. (1975)	$10^h35^m.7$	$10^h35^m.7$
Dec. (1975)	$-27^\circ23'$	$-27^\circ23'$
Filter	GG385	GG385
Emulsion	IIIa-J	IIIa-J
Grain type	fine	fine
Exposure (minutes)	45	60
Equivalent photo-electric waveband*	"J"	"J"

* "J" is a UKSTU designation for a IIIa-J/GG385 combination and is unrelated to the Johnson J photoelectric waveband at wavelength 1.25μm.

Table 7.2

A list of probable dwarf galaxies in A1060. The "central region" is defined by the dotted circle in Figure 7.1.

No	X	Y	α (1950.0) h m s	δ ° ' "	D	d	Notes
A. Galaxies within central region							
1	146400	145400	10 32 38.5	-27 10 12	21	21	F
2	145700	145300	10 32 42.0	-27 10 19	11	9	F,U
3	143500	130050	10 32 52.8	-27 27 24	11	6	U
4	139950	150170	10 33 11.0	-27 04 53	8	7	
5	139500	129200	10 33 13.0	-27 28 22	13	8	F
6	139400	139300	10 33 13.6	-27 17 04	7	6	B
7	137050	141800	10 33 25.5	-27 14 16	11	11	F,pn
8*	136400	147900	10 33 28.7	-27 07 23	19	9	B
9	134000	121150	10 33 40.7	-27 37 24	11	10	
10	130600	135200	10 33 57.9	-27 21 40	11	9	
11	130300	115750	10 33 59.3	-27 43 27	13	6	
12	129200	136400	10 34 05.0	-27 20 20			pn
13	127350	151000	10 34 14.4	-27 03 59	11	6	
14	126900	131200	10 34 16.6	-27 26 09	11	7	F
15	126700	146050	10 34 17.6	-27 09 31	11	9	
16	126300	147350	10 34 19.6	-27 08 04	11	6	
17	124640	123350	10 34 27.9	-27 34 53	30	12	
18	124500	131350	10 34 28.7	-27 25 59	15	9	F,pn
19	124100	127300	10 34 30.7	-27 30 31	9	7	B,pn
20	123520	123080	10 34 33.6	-27 35 11	34	13	
21	123432	129560	10 34 34.1	-27 27 59	18	15	B,pn
22	123350	144400	10 34 34.5	-27 11 22	9	7	B,pn
23	123250	136450	10 34 35.0	-27 20 16	9	6	F
24	122699	158856	10 34 37.8	-26 55 11	11	11	B,pn
25	122600	131100	10 34 38.3	-27 26 16	7	4	
26	122250	151100	10 34 40.0	-27 03 52	10	9	U
27	122150	156150	10 34 40.5	-26 58 13	10	7	
28	121900	157500	10 34 41.8	-26 56 42	26	24	F
29	121750	131900	10 34 42.6	-27 25 22	10	6	B
30	121600	144900	10 34 43.3	-27 10 49	15	6	F

contd....

Table 7.2 (contd.)

No	X	Y	α (1950.0) h m s	δ ° ' "	D	d	Notes
31	116800	155900	10 35 07.4	-26 58 30	9	9	F,pn
32	115440	146880	10 35 14.4	-27 08 32	8	7	
33	115362	119064	10 35 14.9	-27 39 44	10	10	B
34	115130	146640	10 35 15.9	-27 08 48	10	10	
35	112800	138950	10 35 27.6	-27 17 28	14	8	pn
36	111650	159950	10 35 33.2	-26 53 57	23	13	F
37	109700	139650	10 35 43.2	-27 16 40	7	5	
38	109700	139300	10 35 43.2	-27 17 04	13	7	
39	108900	145250	10 35 47.2	-27 10 24	10	8	B
40	108850	156000	10 35 47.5	-26 58 22	11	9	F,U
41	107700	146650	10 35 53.2	-27 08 50	11	6	F
42	107500	148400	10 35 54.2	-27 06 52	10	10	F,pn
43	103500	147000	10 36 14.3	-27 08 26	10	7	
44	102000	145750	10 36 21.9	-27 09 49	10	8	B
B. Galaxies outside central region							
45	152500	122600	10 32 06.9	-27 35 38	20	13	B
46	129200	103900	10 34 04.8	-27 56 43	11	9	F
47*	126600	103700	10 34 18.0	-27 56 56	13	8	
48	117690	172690	10 35 02.8	-26 39 40	20	17	
49	113900	170700	10 35 21.9	-26 41 53	13	11	F
50	108600	166300	10 35 48.6	-26 46 48	19	13	B,U
51	105200	173000	10 36 05.6	-26 39 17	21	10	B
52	95700	138900	10 37 01.7	-27 09 17	11	8	U

Column 1: running number (an asterisk indicates that weak spiral structure in the galaxy is visible); cols. 2 & 3: coordinates in the system of the Appendices, in microns; cols. 4 - 9: epoch 1950 coordinates; col. 10: micrometric major-axis diameter, arcseconds; col. 11: minor axis diameter; col. 12: optical characteristics (see key).

Key to symbols B = relatively bright F = very faint
pn = point nucleus U = uncertain morphological type

Table 7.3

A list of low surface brightness systems in a region of 21.8 degree^2 centred on A1060.

No	X	Y	α (1950.0) h m s	δ ° ' "	D	d	Notes
A.	Disk or irregular systems						
1	232390	155800	10 25 26.7	-26 57 38	26	23	
2	198185	153420	10 28 18.4	-27 00 49	15	13	
3	188720	89520	10 29 01.9	-28 12 20	30	27	
4	186085	140510	10 29 18.7	-27 15 24	27	20	p
5	185960	136810	10 29 19.2	-27 19 33	30	20	
6	184720	72170	10 29 21.4	-28 31 48	23	20	
7	183230	111900	10 29 30.9	-27 47 22	34	27	
8	182380	141880	10 29 37.4	-27 13 55	26	19	F
9	178240	92980	10 29 55.3	-28 08 35	37	23	
10	175860	185900	10 30 12.2	-26 24 39	17	12	
11	175400	156210	10 30 13.01	-26 57 56			
12	168360	143950	10 30 47.4	-27 11 38	27	20	
13	164460	260530	10 31 11.4	-25 01 11	30	17	
14	161140	153770	10 31 24.1	-27 00 42	28	22	
15	158879	94490	10 31 33.8	-28 07 03	37	17	
16	156900	225470	10 31 47.4	-25 40 30	20	13	
17	154510	199590	10 31 59.1	-26 09 28	34	27	
18	152950	141005	10 32 05.1	-27 15 03	27	20	
19	147180	133940	10 32 34.1	-27 22 59	23	23	
20	146215	191244	10 32 40.3	-26 18 51	15	14	
21	143790	167480	10 32 51.7	-26 45 28	27	15	B
22	143100	102600	10 32 54.2	-27 58 04	18	15	
23	141960	195800	10 33 01.3	-26 13 47	40	17	
24	138790	158810	10 33 16.7	-26 55 11	30	13	
25	138190	169860	10 33 19.9	-26 42 49	40	34	p
26	136960	133800	10 33 25.7	-27 23 10	40	34	
27	135680	156690	10 33 32.4	-26 57 33	32	23	F
28	133840	91380	10 33 41.1	-28 10 38	20	13	F
29	132640	154880	10 33 47.7	-26 59 35	20	15	
30	132400	176000	10 33 49.0	-26 35 57	34	27	

contd...

Table 7.3 (contd.)

No	X	Y	α (1950.0) h m s	δ ° ' "	D	d	Notes
31	127140	165120	10 34 15.4	-26 48 08	34	27	
32	126600	103700	10 34 18.0	-27 56 52	15	8	
33	126020	10370	10 34 20.7	-29 41 18	26	10	B
34	124320	225500	10 34 29.6	-25 40 35	27	13	
35	115040	103730	10 35 16.7	-27 56 49	40	34	F
36	112300	259400	10 35 28.9	-25 02 34	20	16	
37	111696	154500	10 35 33.0	-27 00 01	27	20	
38	109720	75930	10 35 44.0	-28 27 55	47	40	p?
39	108540	113610	10 35 49.5	-27 45 45	31	22	
40	101570	137420	10 36 24.4	-27 19 05	37	20	
41	90460	192560	10 37 18.5	-26 17 19	37	34	
42	85000	53190	10 37 50.7	-28 53 15	34	20	B
43	82080	37330	10 38 06.1	-29 10 58	17	13	
44	81210	42160	10 38 10.5	-29 05 33	27	20	
45	74880	247690	10 38 34.2	-25 15 28	27	23	
46	65130	64040	10 39 32.0	-28 40 54	40	17	
47	60000	182270	10 39 51.2	-26 28 33	32	21	
48	59040	220140	10 39 53.8	-25 46 10	23	17	
49	56570	3700	10 40 18.8	-29 48 20	34	10	
50	52340	140670	10 40 32.2	-27 15 00	26	15	
51	51950	111030	10 40 36.0	-27 48 10	34	34	
52	50830	192340	10 40 36.4	-26 17 10	26	21	
53	48140	120530	10 40 54.7	-27 37 29	26	17	B
54	44700	258500	10 41 02.9	-25 03 01	60	47	p
55	29330	112960	10 42 30.3	-27 45 39	17	15	B
56	27420	89960	10 42 41.9	-28 11 21	21	11	B
57	25750	157600	10 42 56.8	-29 34 20	40	34	
58	13910	154140	10 43 44.4	-26 59 17	17	12	
59	8000	245000	10 44 05.3	-25 17 30	67	30	

contd...

Table 7.3 (contd.)

No	X	Y	α (1950.0) h m s	δ ° ' "	D	d	Notes
B. Elliptical or spheroidal systems							
60	144660	54440	10 32 45.45	-28 51 57	28	20	
61	117690	172690	10 35 02.8	-26 39 40	20	17	
62	89520	89140	10 37 26.6	-28 13 03	17	12	
63	85170	42200	10 37 50.2	-29 05 33	19	15	F
64	39890	158040	10 41 33.6	-26 55 23	36	11	

Columns: as for Table 7.2

Key to symbols B = relatively bright F = faint
p = peculiar

CHAPTER 8

CONCLUDING REMARKS

It is appropriate in this last chapter to review the facts that have been gleaned in this work and elsewhere concerning A1060, and to consider its present state and possible past and future evolution. Before recapitulating, the dynamics of the cluster will be considered in relation to the observed luminous mass.

8.1 The Mass-to-Light Ratio

There are two methods by which the mass of a cluster might be determined, two other approaches to the problem having proved untenable (see Zwicky 1937). The first is to approximate the total mass of a cluster by the sum of the masses of the member galaxies, as estimated from their internal dynamics (rotation curves) or intrinsic luminosities given 'conventional' mass-to-light ratios. The second procedure involves the virial theorem for an ensemble of interacting point masses, and was first applied to the determination of cluster mass by Zwicky (1933).

Derivation of the virial theorem is straightforward: from Newton's laws, the force on the i^{th} galaxy whose coordinates with respect to the centre of mass of the system are $\underline{r}_i$ i $\underline{F}_i = m_i \ddot{\underline{r}}_i$; taking the scalar product with $\underline{r}_i$ and summing over i,

$$2T + \sum \underline{F}_i \cdot \underline{r}_i = \tfrac{1}{2}\ddot{I}$$

where I is the moment of inertia and T the kinetic energy of the

system. A number of assumptions are then made. Firstly, $\underline{F}_i$ consists solely of an (internal) gravitational force; thus $\sum \underline{F}_i . \underline{r}_i = \Omega$, yielding the theorem. If, secondly, the cluster is assumed to be in a steady state,

$$2\langle T \rangle + \langle \Omega \rangle = 0,$$

the "static virial". Thirdly, a smooth mass distribution is assumed in introducing the following approximations for T and Ω:

$$2T = \sum m_i \dot{r}_i^2 = M\sigma^2$$

$$\Omega = -G \sum_{\text{pairs}} \frac{m_i m_j}{r_{ij}} = \frac{Gm\, m\, n(n-1)}{2R'} \simeq \frac{-GM^2}{2R'}$$

where σ^2 is the variance of the space velocities and $2R' = R$ is the mean of the individual space separations r_{ij}, both mass-weighted.

In practice it is necessary to estimate R in terms of the <u>projected</u> separations (Limber & Matthews 1960) or the distribution of galaxies on the sky (Schwarzschild 1954), and ξ in terms of the radial velocity dispersion S: $\sigma^2 = \xi S^2$. ξ may take any value from $\xi = 1$, in which near-radial velocities predominate and only galaxies found near the cluster core are sampled, to $\xi = 3$, if the velocity field is everywhere isotropic. An additional uncertainty of a factor of two is introduced if the requirement that the cluster must be in a steady state is relaxed to the point where the cluster is on the verge of instability and the total energy $T + \Omega$ is zero. The (static) virial

theorem thus predicts that

$$M = \xi S^2 R/G$$

where $\frac{1}{2} \lesssim \xi \leq 3$ and M is the mass of the cluster.

The value of R for A1060 is uncertain. Strip counts of the distribution of prominent galaxies within an area of 100 degree^2 that includes A1060 (Section 6.2) lead to the estimate, $R_m = 4.0$ Mpc by Schwarzschild's (1954) method. This is much larger than the value $R_m = 1.75$ Mpc ($H_o = 85$ km s^{-1} Mpc^{-1}) that has been derived for the Centaurus cluster by Dawe, Dickens & Peterson (1977), although it is less than that of the Coma cluster, for which $R_m = 5.2$ Mpc on this distance scale (Rood et al. 1972). On the other hand, a fit of a de Vaucouleurs $r^{\frac{1}{4}}$ luminosity distribution law to the radial profile of the effective surface brightness of the cluster (the latter is shown in Figure 6.7) furnishes an estimate of the effective radius, $r_e = 0.53$: Mpc, which is very much smaller than R_m. The r_e derived in this manner is also applicable to virial theorem estimates of mass, in analogy to mass estimates for individual galaxies (as outlined in Young 1976).

Despite the fact that the fit of the luminosity profile of the cluster to an $r^{\frac{1}{4}}$ law breaks down beyond 0.9 Mpc, it is felt that the r_e so derived is more representative of the size of Hydra I than is R_m. Only in the former case are the luminosities of the individual cluster members implicitly taken into account in the fit. Moreover, the core radius of this cluster is unusually small (Section 2.4).

Nevertheless, in view of the uncertainty regarding which value of R is more appropriate, it is preferable to adopt the compromise of Green (1978). He expresses virial properties in terms of the parameter χ, where

$$\chi = \frac{3S^2}{GL} = \frac{M}{L}\frac{1}{R} .$$

Here L is the optical luminosity of the cluster and the factor, 3, is the adopted value of ξ.

A fair estimate of L may be obtained by summation of the luminosities of bright galaxies, and a linear extrapolation of the faint-end slope of the field-corrected luminosity function shown in Figure 6.4 to $V_{25} = \infty$. (As suggested in Chapter 7, the numbers of galaxies in the cluster may not continue to increase with magnitude faintwards of 17^m at this exponential rate, but even if the assumption holds they contribute only 10% of the total V_{25} luminosity of the galaxies). Subtracting $0^m.2$ from the total magnitude corresponding to the integrated luminosity defined above, to account for the light emission from those regions of the galaxies of surface brightness less than 25 V mag arcsec^{-2}, the corrected total luminosity of A1060 (out to a projected radius of 1.5 Mpc) is $L = 1.26 \times 10^{12} L_\odot$. With $S = 496$ km s^{-1}, $\chi(\text{A1060}) = 136\ M_\odot L_\odot^{-1}\ \text{Mpc}^{-1}$.

Where R = 1 Mpc, the mean mass-to-light ratio of the galaxies in the cluster would be $136\ M_\odot L_\odot^{-1}$, roughly an order of magnitude larger than that which was assumed for elliptical galaxies for the purpose of mass-weighting of velocities in the determination of S (Chapter 3). Thus, the longstanding puzzle of the "hidden mass" in groups of

galaxies arises once again. A recent and careful review of current evidence (Faber & Gallagher 1979) favours the existence of such dark matter, although the question of what physical form it takes remains unresolved. If it was divided among the galaxies, more equipartition of energy would be expected than is observed; theoretical time scales for the mutual accretion and merging of galaxies would also become embarrassingly small - as indeed they may be already (cf. the high frequency of multiply-nucleated first-ranked galaxies in clusters that has been reported by Rood & Leir 1979). Conversely, however, if galaxies are only minute perturbations in the overall mass distribution in each cluster, it would be surprising to observe cannibalism proceeding at all.

Nonetheless, it should be emphasised that the magnitude of the apparent mass discrepancy in A1060 is not especially serious. If (i) $R = r_e \simeq 0.5$ Mpc, the value of χ is halved; (ii) if near-radial velocities predominate in the cluster ($\xi \simeq 1$), a further factor-of-three reduction is appropriate. The central binary might be efficient at throwing cluster galaxies into radial orbits (cf. the binary model of the Coma cluster proposed by Byrd & Valtonen 1979); (iii) if significant gravitational binding energy is locked up in cluster binaries, this would mimic the effect of hidden mass (Wesson & Lermann 1977; Ozernoy & Reinhardt 1979). To investigate the latter two points, more radial velocities of members are required.

8.2 The Evolutionary State of A1060

In order to assist rapid evaluation, the main characteristics of the

Hydra I cluster are summarised in Table 8.1.

One of the more surprising results of the previous chapters is the degree of compactness of the core of this cluster; on the Emden sphere model the core radius of the number density distribution of galaxies is less than 100 kpc, one-third - or less - that of many other Abell clusters (Section 2.4). This core is highly symmetric, with an axial ratio of 0.9, and is aligned roughly parallel to the axis defined by the four bright and centrally located NGC galaxies (six if N3314 and N3316 are included). There are no statistically significant secondary maxima in the number density profile within 1.5 Mpc of the centre of the cluster, and the fit to an idealised unbounded isothermal sphere is good (but not necessarily physically significant). There are several recognisable groups of galaxies located within 5^{o} of the centre of A1060, including Klemola 13 at an angular separation of only 0.8 Mpc, but no clear evidence has been revealed that might suggest physical association of Hydra I with other major galaxy groupings that are visible in the same region, namely the Hydra cloud and the Antlia group. To check this finding it may be necessary to investigate, on the basis of redshift data, the spatial structure of a region at least as large as that illustrated in Figure 2.1 (cf. Einasto, Joeveer & Saar 1980).

The changes in the relative proportions of different types of galaxies with distance from the centre of A1060 is very marked; a comparable tendency for galaxies of different luminosity to segregate radially has not been confirmed, although the two brightest galaxies are centrally located in the cluster. It is difficult to account for

the radial segregation of spirals and SO galaxies entirely in terms of ram-pressure transmutation of the former type into the latter, since the possible examples of active transformation that have been found appear to represent only the early stages of the process. This finding may favour "independent formation" theories of the creation of lenticular galaxies over those which interpret these systems as spirals, less gas.

The luminosity function of the Hydra I cluster has been defined over a range of more than six magnitudes. The composite function for all galaxy types is similar in form to that of the Coma cluster (A1656, BM type II, RS type B), notwithstanding the differences in the relative proportions of galaxies of each type in the classified samples of members of each cluster. In both cases, the differential luminosity function exhibits an excess of numbers near the bright end followed by a local minimum (A426, as it happens, also exhibits the latter feature). On the other hand, the work of Dressler (1978b) and possibly of Bucknell et al. (1979) suggests significant variation of the overall forms of the luminosity functions of rich clusters.

The cannibalism hypothesis predicts that as a cluster of galaxies evolves, the absolute magnitude (M^*) corresponding to the turnover point of the logarithmic cumulative luminosity function will gradually shift faintwards due to the proportionately greater depletion rate for members that have magnitudes close to M^*. Bucknell et al.'s (1979) data imply that it does not; so the apparently untypical value of M^* determined here for A1060 is more likely a statistical artefact than a consequence of evolution.

It was argued in Chapter 6 that the shallow slope of the (U - B) colour-magnitude correlation for the brighter members of A1060 could not be a consequence of widespread accretion of galaxies as implied by the Ostriker model. Michard's (1979a,b) work could be interpreted as evidence that the stellar composition of bright galaxies in clusters differs from the composition of the faint, though no explanation is ventured as to why this should be so.

Whilst the inconsistencies as regards A1060 suggests the need for some revision of the theory of evolution via galactic cannibalism, the positive aspects of the model deserve emphasis. Dynamical friction accounts in an attractive manner for the optical properties of N3311, the largest and brightest galaxy. In other, "cD" clusters, the presence of so-called "reverse" segregation (Dressler 1978b, Green 1978) - in which a deficiency of moderately bright galaxies exists in the cluster core, contrary to the expected consequences of dynamical relaxation through two-body encounters - is understandable in terms of galactic accretion, as is the observed tendency of many cD galaxies to align in sympathy with the galaxy distribution in their clusters. The importance of dynamical friction in spherical clusters has been stressed by White (1976a), and by Binney (1977) in the more general case of aspherical clusters.

The apparently normal integrated colours and colour gradients of N3311 imposes a strong limit on the amount of stellar debris that it could in principle have accreted, assuming that the accretion hypothesis is valid. On the evidence of this observation, and its optical characteristics, N3311 is regarded as a D system in the early stages of evolution.

The existence and properties of three anaemic spiral galaxies in the Hydra I cluster was discussed in Section 6.5. It was proposed that these systems are being depleted of their interstellar gas by the ram-pressure effect of their motion through an intracluster medium (the presence of the latter seems to be implied by observations of diffuse X-ray emission from the cluster). This, too, is believed to represent the early stages of a transitory phase.

On the evidence of the preceding, it is thought that A1060 is relatively young in dynamical terms. It seems entirely possible that N3311 will eventually evolve into a cD supergiant, at the expense of other members of the cluster; the compactness of the cluster core could encourage and accelerate this process. One other consequence of dynamical friction, as A1060 evolves (cf. Binney 1977) should be an increase in the flattening of the distribution of the bright galaxies at the centre of the cluster. Ultimately they may agglomerate into an enormous cD system.

8.3 Comparison with Other Clusters

The most striking single difference between A1060 and other nearby clusters for which compositions are quite well determined is the absence of spatial (as opposed to radial) segregation of different morphological types of galaxies. In the Centaurus I cluster (HMS 1247 - 4102: Dawe, Dickens & Peterson 1977; Fairall 1978a) - within which spiral S0 and elliptical galaxies are present in proportions similar to those in A1060 - the spiral galaxies form an elongated and irregular distribution which contrasts with the more centrally

concentrated cloud of early types, and these clouds are ∿0.3 Mpc apart (if H_o = 85 km s^{-1} Mpc^{-1}).

The Virgo cluster has long been considered the classic example. de Vaucouleurs (1961b; see also de Vaucouleurs & de Vaucouleurs 1973) has interpreted this system as a superposition of a nearer cloud of early-type galaxies and a more distant cloud of spirals. Recent HI-profile observations (Helou, Salpeter & Krumm 1979), however, indicate that these clouds are concentric; in which case Virgo I would more nearly resemble Hydra I, although the latter cluster is more regular. Spiral galaxies located in the Virgo I cluster are already known to be deficient in neutral hydrogen (Davies & Lewis 1973), and it has been suggested that the gas loss is proceeding in the present era (Butcher & Oemler 1978).

Finally, in the Fornax cluster (G53 in the list of de Vaucouleurs, 1975) the most luminous galaxy, N1316, is located in a clump of mostly lenticulars and spiral galaxies; the next four brightest are in or near a larger concentration of mostly early types (Welch, Chincarini & Rood 1975).

The theme will not now be elaborated on because further details regarding two of the clusters, Centaurus and Fornax, are lacking. Comment will be limited to two remarks. Firstly, whilst it may be risky and irresponsible to generalise on the basis of so few examples, the features of the Centaurus and Fornax clusters may appear to favour White's (1976b) model of the formation of rich clusters, in which subclustering of galaxies develops rapidly during the expansion

of the initial cloud and anisotropies persist on recollapse. Secondly, the correspondence of some properties of Virgo I and Hydra I is close enough to warrant further investigation.

8.4 The Way Ahead

The necessity and importance of further work on many aspects of the properties of the Hydra I cluster has been emphasised time and again in the preceding chapters.

The most immediately useful additional data on Hydra I that might be secured are redshifts for a larger sample of galaxies, so as better to elucidate the structure, velocity dispersion, and membership of A1060. It would also appear to be important to obtain HI-line observations of spiral and lenticular galaxies in the cluster. Observational programmes along these lines are already underway (Richter 1979, private communication).

In addition, spectrographic studies of the halo of N3311 would enable the velocity dispersion of stellar orbits in the outer regions of this galaxy to be estimated; a low value would rule out the presence of a massive envelope of luminous matter consisting of material stripped from other cluster members, the existence of which is already doubtful on photometric grounds.

The detailed study of nearby clusters of galaxies is only just beginning. A truly vast amount of research remains to be done, involving many disciplines and aimed towards a common goal: comprehension of the physical universe and our place within it.

Table 8.1

Summary of the properties of the Abell 1060 = Hydra I cluster

Property		Reference
1. Position		
equatorial (1950.0)	$\alpha = 10^h34^m17^s \pm 6^s$	
	$\delta = -27^\circ17' \pm 1'$	*
galactic	$l = 269\overset{\circ}{.}6$	
	$b = +26\overset{\circ}{.}5$	*
supergalactic	$SGL = 139\overset{\circ}{.}3$	
	$SGB = -37\overset{\circ}{.}6$	*
2. Identification as X-ray source		
3rd UHURU catalogue	3U 1044-30	Giacconi et al. (1974)
4th UHURU catalogue	4U 1033-26	Forman et al. (1978)
2nd Ariel V catalogue	2A 1033-270	Cooke et al. (1978)
3. X-ray luminosity	$L_x \simeq 2 \times 10^{43}$ erg s^{-1}	Gursky & Schwartz (1977), Bahcall (1977a)
4. Redshift		
heliocentric	$z_o = 0.01221 \pm 0.00042$(s.e.)	*
cosmological	$z_R = 0.01131 \pm 0.00043$(s.e.)	*
5. Velocity dispersion	$S \equiv \langle v_G^2 \rangle^{\frac{1}{2}} = 496$ km s^{-1}	*
	(= 771 km s^{-1}	adopted by Faber & Dressler (1976))
6. Distance	$\Delta = 40.5(1 \pm 0.10:)$ Mpc	de Vaucouleurs (1977b)
	(= 40 Mpc adopted)	
	(= 68 Mpc if $H_o = 50$ km s^{-1} Mpc^{-1})	
geometric distance modulus	$\mu_o = 33\overset{m}{.}0 \pm 0\overset{m}{.}2$	de Vaucouleurs (1977b)
galactic absorption	$A_B = 0\overset{m}{.}38$ ($A_V = 0\overset{m}{.}28$)	RC2
	$A_B = 0\overset{m}{.}16$ ($A_V = 0\overset{m}{.}12$)	Sandage (1973a)
K-correction	$K_V = 0\overset{m}{.}02$	Sandage (1973b)

Table 8.1 (contd.)

Property		Reference
7. Size		
core radius	R_c = 0.08 Mpc (= 0.14 Mpc if $H_o = 50$ km s^{-1} Mpc^{-1})	*
effective radius	r_e = 0.53: Mpc (= 0.90: Mpc if $H_o = 50$)	*
visible extent	= 2 - 3.5 Mpc (= 3.5 - 6 Mpc if $H_o = 50$)	*
8. Shape		
axial ratio	0.87 ± 0.02	*
at position angle (galaxies $V_{25} < 17$)	121^o	*
9. Composition		
<1.5 Mpc radius, $V_{25} < 15$: E:SO:S & Irr	= 15%:46%:39% (14 unclassified, total 102)	*
$\lesssim$3.5 Mpc radius, E:SO:S & Irr	= 6%:13%:81% (87 unclassified, total 459)	*
10. Luminosity distribution		
isophotal V magnitude at discontinuity in log. integrated luminosity function	$M_{V^*_{25}} \equiv M^* = -19.2$ ($V^*_{25} = 14.08$)	*
isophotal V magnitude of first-ranked galaxy (N3311)	$M_1 = -22.6$ ($V_{25,1} = 10.65$)	*
magnitude difference between first and second-ranked galaxies:		
isophotal, V-band	$\lvert M_1 - M_2 \rvert = 0.85$	*
total, B-band	$\lvert B_{T,1} - B_{T,2} \rvert = 0.74$:	*

Table 8.1 (contd.)

Property			Reference
11. Mass-to-light ratio	$\chi \equiv \frac{M}{L}\frac{1}{R} = 136\ M_{\odot} L_{\odot}^{-1} \mathrm{Mpc}^{-1}$		*
12. Classification			
Bautz-Morgan	BM =	III	Bautz & Morgan (1970)
Rood-Sastry	RS =	C	Rood & Sastry (1971)
Bahcall		Intermediate	*
Other		spiral cluster	Melnick & Sargent (1977)

* denotes present study

APPENDIX I

FINDING CHARTS OF GALAXIES

The first four of the following charts record all galaxies near A1060 of $V_{25}^{c} < 17.0$ (i.e., those galaxies with photographic magnitudes interior to the 25th V mag arcsec^{-2} isophote, corrected for saturation effects and for image overlaps, brighter than 17^{m}). Each chart represents a different quarter of a region of total area 21.8 degree^{2} approximately).

The fifth chart depicts systems brighter than $V_{25} = 17.5$ in the central zone of the cluster. The area shown is approximately 0.87 degree^{2}.

Where the orientation and apparent (micrometric) axis dimensions of a galaxy are known, these are indicated; otherwise each galaxy is represented by a circular disk of area proportional to the luminosity corresponding to the V_{25}^{c}. Galaxies listed in the Appendix II Supplement are represented by filled circles (not to scale).

Axes are in the rectangular coordinate system of Appendix II and are labelled in centimetres (1 cm = 671.4 arcseconds).

North is to the top, east to the left.

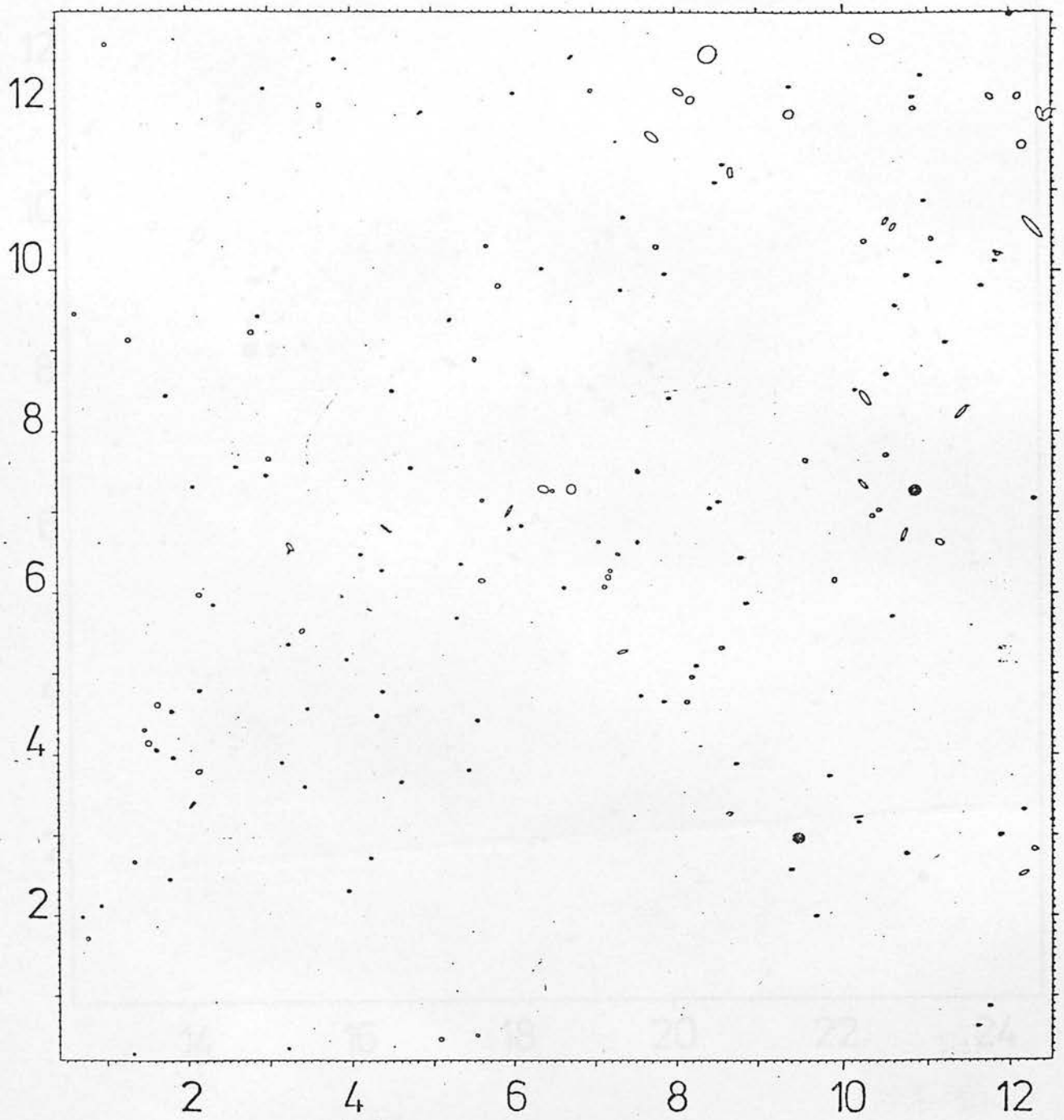

South east; $V_{25} < 17.0$

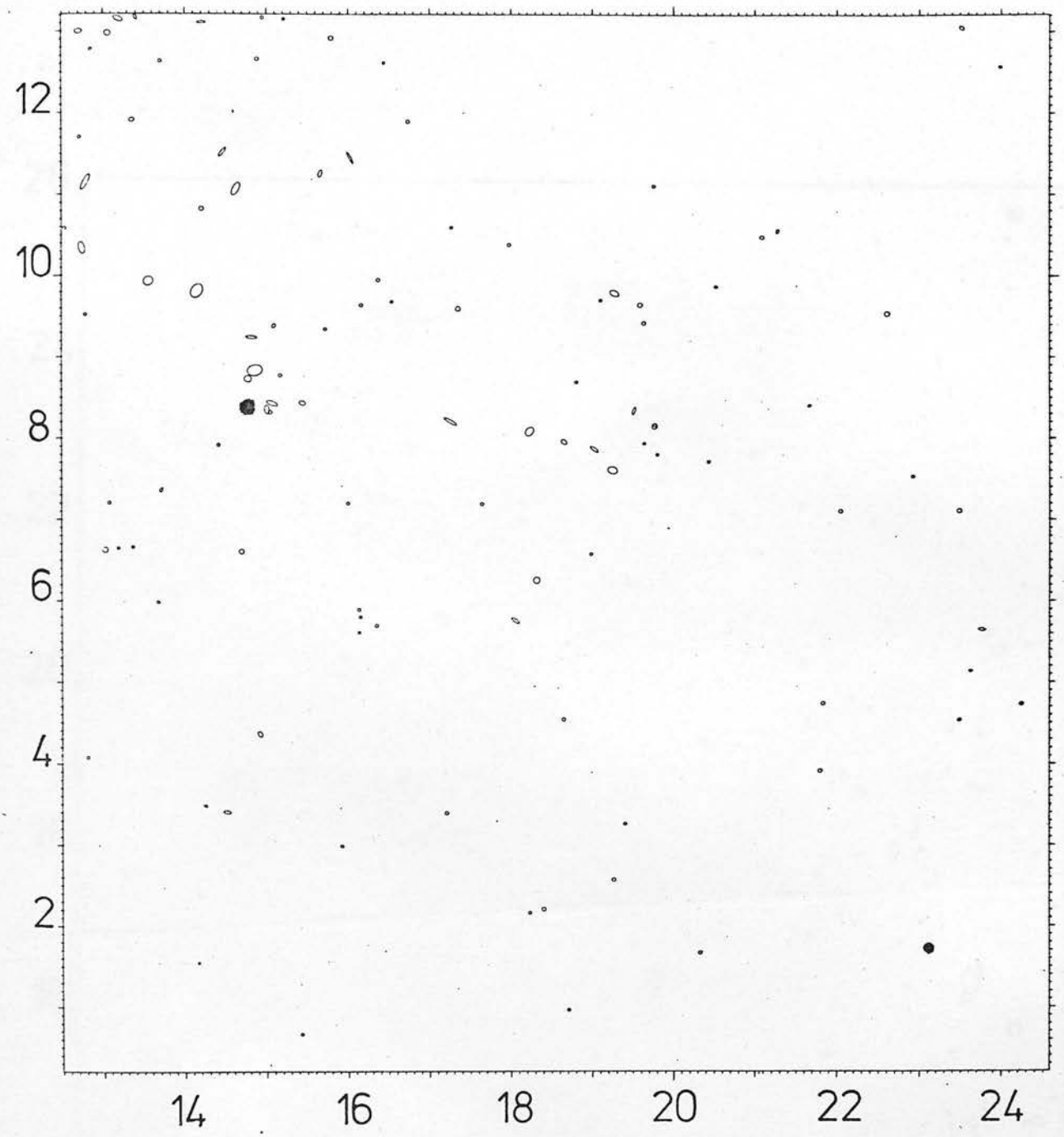

South west; $V_{25} < 17.0$

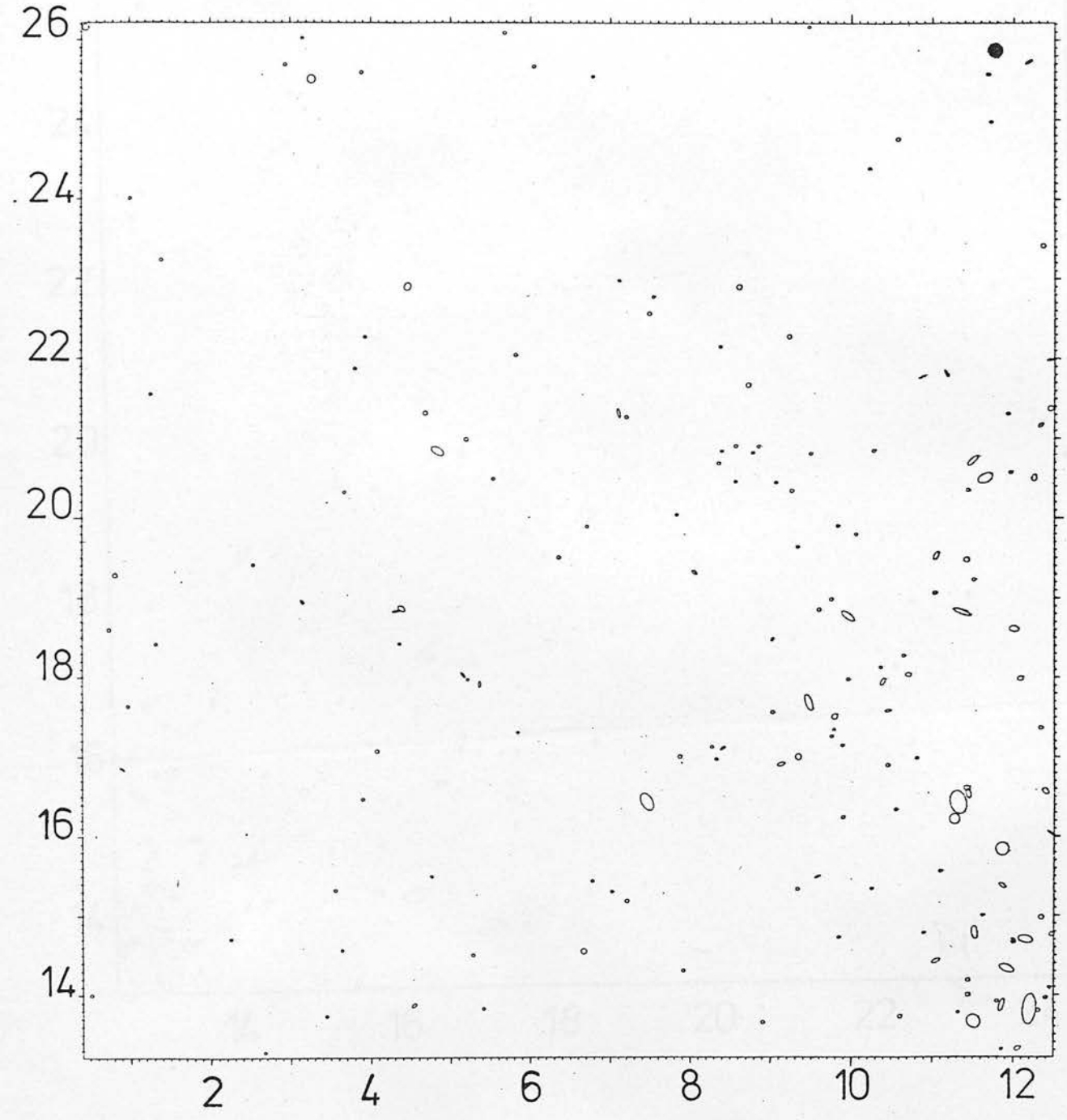

North east; $V_{25} < 17.0$

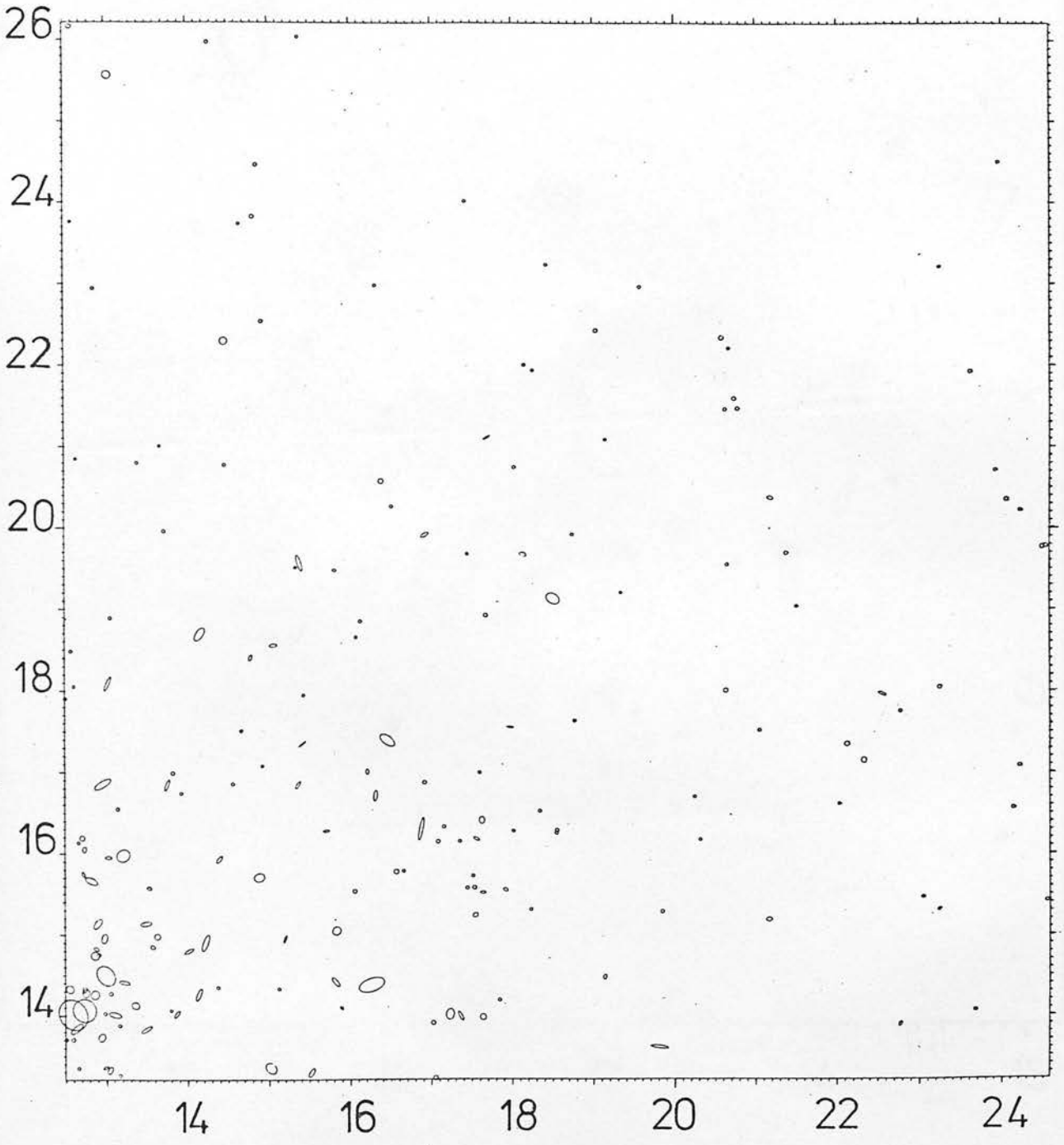

North west; $V_{25} < 17.0$

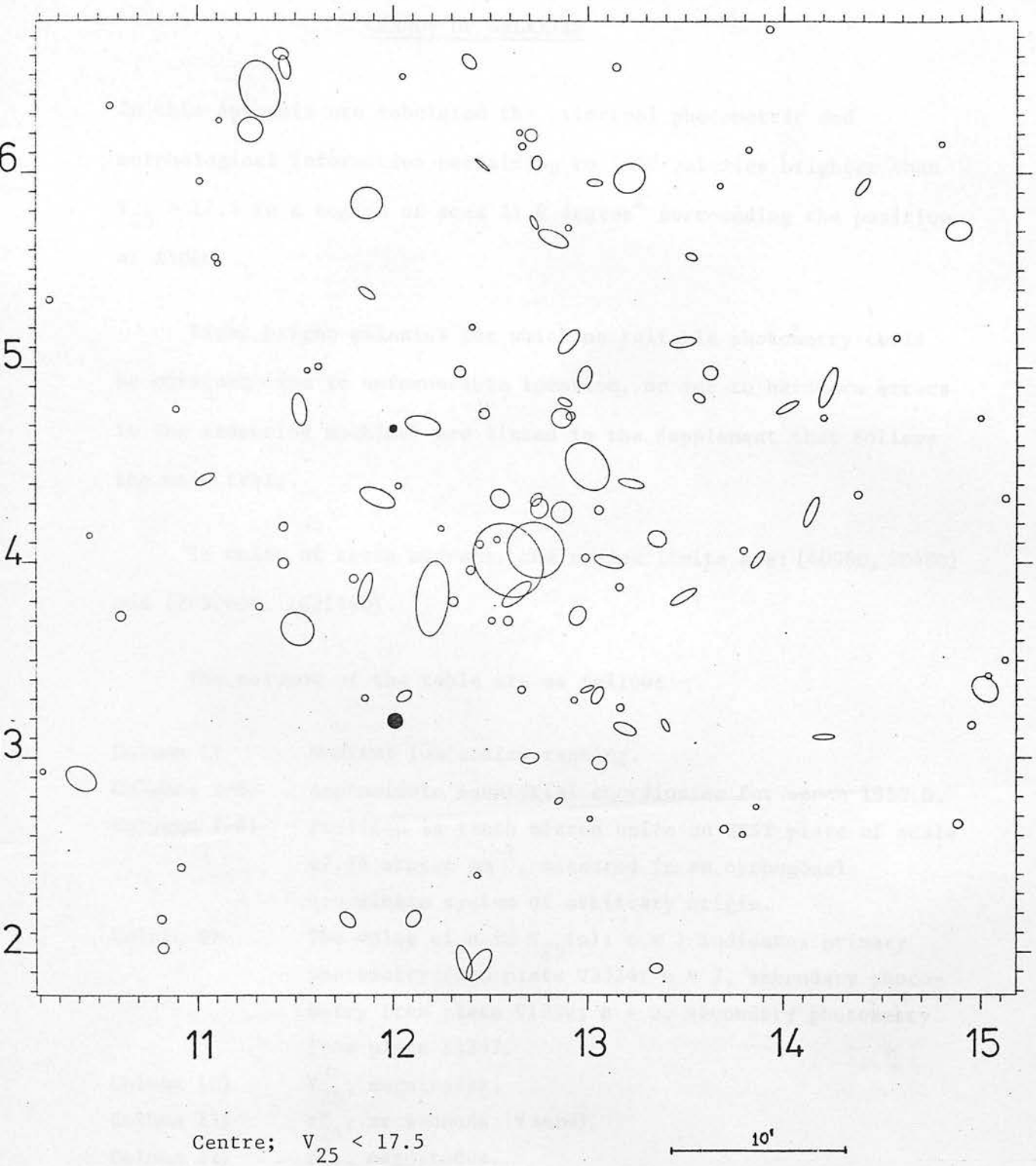
6
5
4
3
2
11
12
13
14
15
Centre; V_{25} < 17.5
10'

APPENDIX II

CENSUS OF GALAXIES

In this Appendix are tabulated the principal photometric and morphological information pertaining to 1000 galaxies brighter than $V_{25} = 17.5$ in a region of area 21.8 degree^2 surrounding the position of A1060.

Eight bright galaxies for which no reliable photometry could be obtained (due to unfavourable location, or due to hardware errors in the measuring machine) are listed in the Supplement that follows the main table.

In units of tenth microns, the region limits are: (40960, 20480) and (2457600, 2621440).

The columns of the table are as follows:-

Column 1)	Nominal luminosity ranking.
Columns 2-6)	Approximate equatorial coordinates for epoch 1950.0.
Columns 7-8)	Position in tenth micron units on UKST plate of scale 67.14 arcsec mm^{-1}, measured in an orthogonal coordinate system of arbitrary origin.
Column 9)	The value of n in $V_{25}(n)$: n = 1 indicates primary photometry from plate V3324; n = 2, secondary photometry from plate V1330; n = 3, secondary photometry from plate R1347.
Column 10)	V_{25}^{c}, magnitudes.
Column 11)	r_{25}^{*}, arcseconds (V band).
Column 12)	B_{25}^{c}, magnitudes.
Columns 13+)	Morphological classification in the revised Hubble classification system (e.g. de Vaucouleurs 1959). If the image is a blend, this is noted thus: m G n S = m galaxies + n stars (last column).

Standard designations of brighter galaxies:

Galaxy No	RNGC	IC	MCG	Anon.
1	3311		-4-25-36	
2	3309		-4125-34	
3	3312	629	-4-25-39	
4		2597	-4-25-51	
5	3308		-4-25-32	
6	3285		-4-25-19	
7	3336		-5-25-36	
9	3316		-4-25-46	
12	3305		-4-25-31	
20	3285B		-4-25-22	
24	3315		-4-25-43	A1034-27B; A1034-2712
32			-4-25-25	A1033-27
34	3285A		-4-25-15	
37				A1034-27A; A1034-2718
42			-5-25-32	A1037-27
60	3307		-4-25-29	
70				A1033-2715
A	3313		-4-25-44	
B	3314		-4-25-41	

The MCG gives designations for further galaxies in this field.

RNGC = Revised New General Catalogue of Nonstellar Astronomical Objects (Sulentic & Tifft 1973).

IC = Index Catalogue of Nebulae (Dreyer 1895); Second Index Catalogue of Nebulae and Clusters of Stars (Dreyer 1908).

MCG = Morphological Catalogue of Galaxies (Vorontsov-Velyaminov, Krasnogorskaja & Arkipova 1962-8).

Anon = as in the Second Reference Catalogue of Bright Galaxies (de Vaucouleurs, de Vaucouleurs & Corwin 1976), and Sandage (1978).

Listed below are the saturation-corrected isophotal magnitudes of nineteen galaxies for which photoelectric photometry is available. These photoelectric standards defined the photographic saturation corrections of section 5.7. The magnitudes given here supersede the values in the main table (overleaf).

The magnitudes in the main table have been adjusted on the basis of the mean curves of corrections shown in Figures 5.10 and 5.11.

Galaxy No	V_{25}^{c}	B_{25}^{c}	
1	10.65	12.11	r_{25}^{*} = 237:"
2	11.50	12.73	
3	11.88	12.79	
4	11.83	12.89	
5	12.13	13.25	
12	12.91	14.13	
22	13.41	14.49	
24	13.58	14.75	
31	13.92	15.11	
37	13.91	14.97	
38	13.69	14.79	
46	14.01	15.18	
56	14.28	15.41	
61	13.99	15.27	
63	14.36	15.67	
66	14.16	15.86	
68	14.41	15.57	
86	14.77	15.65	
92	14.82	15.87	

ID NO	R.A. (1950.0) H	M	S	DEC. °	′	X	Y		V25	R25	B25	TYPE		
1	10	34	21.	-27	16.1	1259050	1401380	1	10.86	170.57	12.26	S	D	
2	10	34	14.	-27	15.5	1273120	1406690	1	11.48	119.56	12.73	E1		
3	10	34	41.	-27	18.3	1220150	1381700	1	11.81	89.54	12.78	SA	PEC	
4	10	35	25.	-26	49.1	1132000	1643000	1	11.89	85.72	12.89	E3		
5	10	34	1.	-27	10.7	1299590	1449510	1	12.05	84.40	13.26	SB	D	
6	10	31	16.	-27	11.9	1626200	1437520	1	12.07	71.66	13.02	S	PEC	
7	10	37	52.	-27	30.7	840575	1269465	1	12.19	58.16	12.92	SAB(RS)		
8	10	38	39.	-26	48.7	746000	1644000	1	12.67	50.75		SA (S)		
9	10	35	16.	-27	20.1	1151170	1366130	1	12.85	56.59	13.97	SB	D	1G1S
10	10	34	58.	-26	55.6	1186375	1584305	1	12.93	50.01	13.93	SB	D	1G1S
11	10	32	26.	-28	14.0	1486165	883340	1	13.02	47.78	14.03	S	D	
12	10	33	50.	-26	54.2	1321090	1597460	1	13.04	44.11	14.08	E1		
13	10	33	2.	-28	3.1	1414628	981442	1	13.05	43.78	13.96	SB (R)		
14	10	34	37.	-27	55.0	1227351	1054049	1	13.05	39.77	13.90			
15	10	31	7.	-26	38.1	1646010	1739725	1	13.19	44.44	14.32	S	D	
16	10	29	26.	-26	18.5	1849845	1913090	3	13.21			E3		
17	10	35	8.	-26	3.4	1165235	2030520	3	13.23			SAB(R)	PEC	1G1S
18	10	36	11.	-27	28.6	1041075	1289375	1	13.37	37.63	13.87	S		
19	10	34	3.	-26	44.3	1296295	1685380	1	13.46	39.20	14.49	S	D	
20	10	32	19.	-27	23.5	1502040	1335250	1	13.49	38.57		SAB(R)		
21	10	36	58.	-26	34.9	947000	1769000	1	13.49	36.35	14.33	SAB(RS)		
22	10	34	29.	-27	39.4	1244195	1193320	1	13.52	31.97	14.51	S	D	
23	10	34	43.	-27	8.4	1215320	1470260	1	13.53	33.17	15.17	S	D	
24	10	34	55.	-27	12.5	1192110	1433335	1	13.53	33.17	14.69	S	D	
25	10	33	3.	-26	23.7	1415600	1869270	3	13.55			SB	D	
26	10	35	27.	-26	51.4	1127280	1622075	1	13.55	33.21	14.27			2G0S
27	10	38	28.	-27	42.2	771150	1166780	3	13.58			S	D	
28	10	40	47.	-25	59.2	483985	2084225	2	13.67			SAB(S)		
29	10	36	20.	-28	18.5	1026040	843260	1	13.76	24.62		SB		
30	10	36	33.	-26	22.7	995870	1877750	3	13.80			SA		
31	10	32	26.	-26	57.1	1488590	1570480	1	13.81	32.53	15.01	SB	D	
32	10	32	59.	-27	6.1	1422320	1490105	1	13.81	27.06	14.91	S	D	SP
33	10	32	38.	-27	49.0	1462370	1106905	1	13.82	26.85	14.53			
34	10	30	27.	-27	15.9	1722959	1401155	1	13.83	32.86	14.58	SB (R)		
35	10	33	32.	-28	1.8	1355420	993280	1	13.84	33.54	14.93	SB	D	1G1S
36	10	39	20.	-28	31.0	671565	729880	3	13.84			SA		
37	10	34	19.	-27	18.0	1263505	1384105	1	13.87	37.58	15.03	S	D	SP
38	10	34	33.	-27	39.3	1236540	1194685	1	13.88	25.69	14.86	S	D	PEC
39	10	34	11.	-27	48.1	1278480	1115410	1	13.92	25.94	14.98			SP
40	10	35	22.	-26	22.2	1136752	1382575	3	13.92			S		SP 1G1S
41	10	30	46.	-26	50.3	1687600	1630400	1	13.94	25.04	15.01	S		SP
42	10	37	4.	-27	39.1	937819	1195369	1	13.94	33.10	14.66	SB (RS)		
43	10	35	15.	-27	7.5	1152390	1478465	1	13.95	33.75	15.21	S		PEC
44	10	34	10.	-26	57.7	1282100	1566170	1	13.98	35.04	15.33	E6		
45	10	30	38.	-28	30.9	637265	729810	2	13.99			S	D	
46	10	34	7.	-27	13.4	1286375	1426010	1	14.01	38.03	15.33	SB (RS)	D	
47	10	34	13.	-27	57.2	1274180	1034290	1	14.03	25.29	15.03	S	D	
48	10	34	48.	-27	43.5	1215660	1156730	1	14.07	30.88	15.16(R)	SB (R)	D	
49	10	29	34.	-28	22.1	1822810	808535	3	14.12			SB (S)	D	
50	10	42	2.	-25	6.9	326580	2550575	2	14.12			E2		

ID NO	R.A. (1950.0) H	M	S	DEC. °	′	″	X	Y		V25	R25	B25	TYPE			
51	10	34	7.	-27	8.	0	1286485	1474270	1	14.13	38.30	15.86	SA	D		
52	10	31	33.	-27	4.	5	1583600	1504060	2	14.14		15.37	SAB(RS)			
53	10	34	5.	-27	3.	6	1290105	1513530	1	14.16	29.76	15.34	SA	D		
54	10	28	42.	-28	27.	3	1924480	761030	3	14.17			E3			1G2S
55	10	32	2.	-26	13.	8	1538210	1956900	3	14.18					SP	
56	10	34	58.	-27	17.	7	1185740	1386805	1	14.24	27.35	15.42	SB (S)	D		
57	10	33	59.	-25	6.	8	1304105	2556770	2	14.26			SB (R)		PEC	
58	10	35	16.	-26	1.	0	1150200	2072535	2	14.26			S			
59	10	38	3.	-27	37.	1	819065	1212505	1	14.26	28.43	15.22	S	D		
60	10	33	55.	-27	16.	2	1310785	1400970	1	14.27	26.80	15.32	SA (RS)		PEC	
61	10	34	23.	-27	12.	5	1254965	1432940	1	14.27	34.56	15.66	E1			
62	10	38	11.	-27	36.	0	804525	1222570	1	14.29	19.94	15.24				1G2S
63	10	34	13.	-27	13.	1	1275180	1428080	1	14.32	35.12	15.73	SA (RS)	D		
64	10	35	21.	-28	20.	6	1140245	824890	2	14.36					SP	
65	10	32	48.	-25	43.	3	1446240	2230050	3	14.37			S			1G1S
66	10	34	3.	-27	19.	3	1294615	1378155	1	14.40	35.34	15.77	S	O		
67	10	34	50.	-26	24.	5	1200920	1861305	2	14.41		15.34	S (R)			
68	10	34	1.	-27	5.	5	1298300	1495345	1	14.43	27.74	15.62				
69	10	41	5.	-25	36.	1	446555	2290320	2	14.45			S	D		1G1S
70	10	33	43.	-27	14.	9	1335480	1412570	1	14.47	27.21	15.69	E2			
71	10	37	39.	-27	47.	2	867670	1122800	1	14.52	26.01	15.94	SB	D		
72	10	28	43.	-28	3.	0	1926420	978260	2	14.53			S	D		
73	10	33	3.	-27	13.	3	1413940	1426270	1	14.53	23.04	15.56	S			
74	10	28	17.	-27	20.	2	1980615	1360530	2	14.54			S		SP	
75	10	32	15.	-28	18.	6	1507295	842660	1	14.58	22.34				SP	
76	10	32	30.	-28	15.	2	1477630	872835	1	14.61	23.53	15.44	E1			
77	10	33	36.	-27	3.	5	1348775	1513490	1	14.61	25.50	15.62	E6			
78	10	33	59.	-26	30.	5	1302525	1808895	1	14.62	24.55	15.51	S	D		
79	10	35	18.	-26	47.	8	1144715	1654045	1	14.65	22.99	15.61				
80	10	33	51.	-27	25.	3	1318945	1315225	1	14.67	26.69	15.96	S	D		
81	10	35	35.	-28	38.	7	1114325	663585	2	14.68			SB (R)	D		
82	10	44	20.	-24	59.	0	46010	2615850	2	14.69			S	D		
83	10	33	36.	-27	18.	2	1348985	1382965	1	14.71	21.84	15.81	S	D	SP	
84	10	31	38.	-27	11.	5	1582355	1441150	1	14.72	18.72	15.63				
85	10	30	24.	-28	20.	9	1725545	820535	3	14.74						
86	10	34	46.	-27	36.	7	1210405	1217225	1	14.74	21.85	15.58	SB (RS)			
87	10	35	56.	-28	37.	6	1071867	673696	2	14.77			S			
88	10	29	29.	-28	42.	5	1831440	625925	2	14.80						
89	10	32	18.	-28	19.	5	1501075	834920	2	14.80						
90	10	31	53.	-27	24.	1	1552520	1329630	1	14.81	21.13	15.84	S	D		
91	10	31	14.	-26	45.	8	1631605	1671235	1	14.84	20.68	15.88	S	D	SP	
92	10	35	3.	-27	36.	8	1176630	1216855	1	14.84	22.79	15.93	SB (R)	D		
93	10	41	11.	-26	21.	1	433440	1887210	2	14.89			E4			
94	10	42	17.	-28	38.	5	326680	657835	2	14.89			S	D		
95	10	30	9.	-26	49.	0	1762435	1541100	2	14.90		16.00(R)	S (R)	D		
96	10	33	59.	-27	11.	7	1322255	1440330	1	14.90	22.83	15.91	S	D	SP	
97	10	36	21.	-28	30.	5	1023105	736370	2	14.90			S	D		
98	10	35	38.	-26	14.	4	1104750	1952860	2	14.91			S			
99	10	30	7.	-27	16.	3	1763860	1397600	2	14.93		15.87	E0			
100	10	32	29.	-27	5.	3	1352795	1497765	1	14.98	22.59	16.05	SB (RS)			

ID NO	R.A. (1950.0) H	M	S	DEC. °	′	″	X	Y		V25	R25	B25	TYPE			
101	10	37	4.	-26	42	5	933865	1700435	1	14.99	24.16	16.04	(R)SB (RS)			
102	10	43	43.	-29	5	3	152575	415180	3	14.99			S	D		
103	10	34	43.	-29	24	7	1216440	252585	2	15.01			SB (R)			
104	10	33	23.	-26	44	4	1375590	1684415	1	15.02	17.13	15.94			SP	
105	10	34	31.	-26	47	5	1239010	1656975	1	15.02	20.99	15.72	S			
106	10	33	58.	-27	23	8	1304715	1332525	1	15.03	29.21	17.15	S	D		
107	10	33	57.	-27	27	7	1305880	1297655	1	15.03	21.50	16.17	SB (R)	D		
108	10	34	33.	-26	3	4	1225340	2050810	2	15.03			E3			
109	10	39	50.	-28	34	0	594280	707360	2	15.04					SP	
110	10	32	28.	-28	9	5	1481845	924115	1	15.05	20.56	16.11	S			
111	10	36	41.	-26	36	9	979430	1751275	1	15.05	18.67	15.86	SB (S)			
112	10	34	15.	-27	27	5	1270320	1300090	1	15.07	25.20	16.21	S	D		
113	10	35	19.	-26	47	0	1142725	1661000	1	15.11	23.04	16.21	S	D		
114	10	32	47.	-27	44	0	1445790	1152115	1	15.13	17.57	15.43				2GOS
115	10	36	2.	-27	54	9	1058890	1055120	2	15.14		15.80				
116	10	36	11.	-26	32	0	1039835	1795200	1	15.14	23.09	16.18	S	D		
117	10	39	19.	-27	9	8	666960	1454915	2	15.14			S	D	SP	
118	10	34	28.	-25	53	7	1244820	2137735	2	15.17			SA			
119	10	35	39.	-27	11	5	1104260	1442690	1	15.19	15.88	16.17	SB (R)	D		
120	10	38	50.	-28	53	5	733215	528885	2	15.19			S			
121	10	35	7.	-27	54	0	1050095	1062520	2	15.20						1G1S
122	10	33	59.	-28	38	8	1302855	662670	2	15.21			S	D		
123	10	30	21.	-27	16	2	1736280	1398855	1	15.22	20.54	16.07	S			
124	10	33	9.	-27	7	3	1401800	1479965	1	15.22		15.94	S			1G1S
125	10	43	42.	-29	0	1	163565	462545	2	15.23			S			
126	10	31	27.	-27	44	3	1602440	1144370	1	15.25	19.18	16.32	S		SP	
127	10	32	51.	-26	54	6	1439610	1593050	1	15.27	19.47	16.32	S	D		
128	10	28	15.	-28	21	2	1976350	815200	2	15.28			E3			
129	10	30	45.	-26	9	9	1692235	1991490	2	15.28			S			
130	10	26	13.	-26	40	1	2233355	1714755	2	15.29			E1			
131	10	38	58.	-28	43	2	716110	620910	3	15.29			E2			
132	10	34	15.	-26	51	7	1270870	1619185	1	15.31	15.74	16.02				1G1S
133	10	35	19.	-26	14	9	1142405	1947820	2	15.31			E0			
134	10	31	55.	-28	18	6	1544610	842650	1	15.32	16.67		S			
135	10	34	43.	-27	23	9	1205630	1331930	1	15.32	18.94	16.41				1G1S
136	10	28	54.	-28	24	5	1901965	786785	2	15.33					SP	
137	10	40	18.	-28	43	5	560030	616535	2	15.34			E4			
138	10	43	17.	-29	9	4	213685	379765	2	15.37			SAB(R)			
139	10	29	13.	-28	23	5	1865040	795730	2	15.38						
140	10	29	45.	-26	12	4	1812950	1967680	2	15.38						
141	10	37	15.	-26	43	5	912985	1691430	1	15.38	15.76	16.17	S			
142	10	31	46.	-27	47	0	1566245	1124800	1	15.39	17.06	16.22	SB	D		
143	10	37	39.	-25	36	5	861245	2290325	2	15.39			S		PEC	
144	10	34	53.	-27	0	3	1186570	1538080	1	15.40	17.97	16.48				
145	10	42	39.	-28	8	3	279395	922860	2	15.40						1G1S
146	10	29	32.	-28	40	2	1805040	570220	2	15.41			S	(P)		
147	10	31	12.	-26	2	5	1633855	2057410	2	15.41			S	D		
148	10	38	54.	-25	54	1	710170	2132040	2	15.43			S		SP	
149	10	34	26.	-29	21	3	1229100	202695	2	15.44			SA	(R)		1G1S
150	10	32	22.	-29	4	1	1492130	436220	2	15.45			SA			

ID NO	R.A. (1950.0) H	M	S	DEC. °	′	″	X	Y		V25	R25	B25	TYPE			
151	10	33	17.	-27	16	.0	1386840	1402015	1	15.45	15.23	16.43				
152	10	34	46.	-26	31	.6	1208895	1790825	1	15.45	21.66		E2			
153	10	32	18.	-26	25	.2	1505925	1855400	2	15.46		16.26	S			
154	10	34	14.	-27	12	.6	1273575	1432490	1	15.46	21.25	16.73	E3			
155	10	34	14.	-26	53	.3	1273710	1605100	1	15.47	19.63	16.49	E3			
156	10	32	42.	-29	14	.8	1451285	340735	2	15.49					PEC	
157	10	35	55.	-26	31	.0	1071645	1803915	1	15.50	19.09	16.45	SA			
158	10	40	3.	-28	2	.8	581245	931015	3	15.50			S			1G1S
159	10	25	53.	-28	5	.2	2260100	953780	2	15.53					SP	
160	10	30	12.	-27	2	.2	1754440	1523695	1	15.53	13.03	16.51	SB			1G1S
161	10	32	33.	-28	39	.0	1469755	660350	2	15.55						
162	10	34	22.	-25	0	.2	1258090	2516095	2	15.55			SB		PEC	
163	10	43	55.	-28	9	.6	129585	913195	2	15.55						
164	10	32	2.	-26	44	.3	1536550	1684450	1	15.56	14.61	16.41	S			1G1S
165	10	31	1.	-26	56	.2	1656840	1577440	1	15.57	18.98	16.27	S		PEC	
166	10	33	42.	-27	39	.6	1335320	1191720	1	15.57	20.78	16.89	E3			
167	10	34	33.	-27	5	.3	1234350	1497910	1	15.57	27.41	17.62			SP	
168	10	26	24.	-26	37	.9	2212705	1734670	2	15.58			SB (S)			
169	10	27	10.	-27	2	.3	2116685	1518285	2	15.58			E3			
170	10	30	20.	-28	5	.4	1734625	959145	1	15.58	18.72	16.36				
171	10	43	14.	-28	45	.0	214480	598025	2	15.58			S			
172	10	42	10.	-28	50	.2	340850	553760	2	15.59			SA			
173	10	37	34.	-25	50	.3	872635	2167285	2	15.60						
174	10	37	43.	-29	16	.1	864770	327870	2	15.61			E3			
175	10	36	20.	-27	56	.8	1024485	1037200	1	15.62	19.57	16.85				
176	10	30	35.	-27	24	.7	1704729	1322436	1	15.63	20.92	16.08	IRR			
177	10	36	38.	-28	43	.8	990105	617610	2	15.63			S			
178	10	28	26.	-28	4	.6	1957865	964145	2	15.64			S			
179	10	31	39.	-27	28	.2	1579360	1291995	1	15.66	13.76	16.55	S			
180	10	34	33.	-25	30	.9	1235315	2341670	2	15.67			S			
181	10	38	25.	-27	57	.5	775485	1030105	2	15.67			SB (R)			
182	10	44	9.	-26	15	.9	81505	1928595	2	15.67			SA			
183	10	28	29.	-28	19	.1	1950990	834245	2	15.68					SP	
184	10	24	26.	-26	10	.3	2452090	1977825	2	15.69			S			
185	10	27	44.	-25	42	.3	2058120	2233995	3	15.69						
186	10	26	3.	-26	30	.9	2255675	1796570	2	15.70			SA			1G1S
187	10	27	13.	-26	4	.3	2118060	2037185	2	15.70			S (R)			
188	10	35	50.	-27	38	.4	1082655	1202485	1	15.70	12.05	16.69				1G1S
189	10	32	60.	-27	26	.2	1420370	1310985	1	15.71	17.09	16.07	IRR			
190	10	33	59.	-26	54	.4	1303250	1595025	1	15.71	15.52	16.71	S			
191	10	34	58.	-27	58	.7	1185905	1020550	1	15.71	17.32	16.22	S			
192	10	32	59.	-27	51	.8	1420395	1082610	1	15.72	20.64	16.95	S			
193	10	40	43.	-29	47	.2	508429	46438	2	15.72			SA			
194	10	27	39.	-26	30	.3	2062705	1800955	2	15.76						1G1S
195	10	34	27.	-27	7	.7	1246735	1476435	3	15.76		17.23	E1			
196	10	40	51.	-25	53	.3	468630	2131300	2	15.76						
197	10	42	30.	-28	26	.4	300475	766240	2	15.76			SB			
198	10	41	17.	-28	36	.2	442382	680310	2	15.78			S		SP	
199	10	41	54.	-27	37	.3	362235	1205440	2	15.79						1G1S
200	10	33	22.	-27	6	.3	1357015	1484870	1	15.83	15.77	17.06	E3			

ID NO	R.A. (1950.0) H	M	S	DEC. °	′	X	Y		V25	R25	B25	TYPE			
201	10	34	6.	-27	7.0	1288130	1482525	1	15.83	16.74	16.97	SB (S)			
202	10	35	19.	-27	16.3	1144085	1399785	1	15.83	17.43	16.66				
203	10	36	56.	-28	27.2	955580	765710	2	15.83			S	D		
204	10	24	51.	-28	48.5	2376155	564735	2	15.84			SB		PEC	
205	10	44	5.	-27	28.6	101765	1279370	2	15.84			SB	D	PEC	
206	10	25	5.	-28	32.2	2348470	710680	2	15.85			S			
207	10	30	38.	-27	17.1	1702165	1390700	1	15.86	12.15	16.46				1G1S
208	10	34	42.	-25	5.1	1217915	2572655	2	15.86			S		SP	
209	10	36	3.	-28	26.5	1049795	772395	2	15.86			E1			
210	10	39	1.	-28	44.5	711480	600040	2	15.87			E1			
211	10	24	23.	-25	10.4	2448665	1976680	2	15.88			S		SP	
212	10	37	9.	-25	43.5	922260	2227350	2	15.88						1G1S
213	10	34	34.	-25	56.0	1233000	2117000	3	15.89			SB (R)			1G1S
214	10	35	1.	-27	19.3	1061345	1372520	1	15.89	15.25	16.91	E0			
215	10	35	15.	-28	34.9	1034330	697055	2	15.91						1G1S
216	10	41	7.	-27	17.2	453695	1386900	2	15.92			S			
217	10	40	29.	-25	57.6	519600	2098995	2	15.94			S	D		
218	10	25	10.	-27	25.7	2351740	1304890	2	15.95			SB (S)			
219	10	34	34.	-26	38.6	1233340	1736575	1	15.96	17.02		S		SP	
220	10	30	12.	-26	51.6	1755755	1618015	1	15.97	16.19	17.27	S	D		
221	10	32	31.	-25	26.2	1481565	2383020	2	15.97						1G1S
222	10	34	35.	-27	18.5	1230800	1380210	1	15.98	21.32	17.58	E2			
223	10	38	10.	-29	0.5	812130	467250	2	15.98			S			
224	10	44	23.	-29	32.4	75595	171560	2	15.98			SAB			
225	10	40	23.	-26	31.9	536105	1792055	2	16.00			S			
226	10	29	22.	-29	27.8	1839915	221050	2	16.01						1G1S
227	10	31	19.	-26	42.5	1621590	1700735	1	16.01	15.99	17.02	S	D	SP	
228	10	32	32.	-26	26.9	1478100	1840700	1	16.01	16.13	17.15	S	D		
229	10	37	43.	-28	53.1	854760	533850	2	16.01			S	D		
230	10	28	52.	-27	10.6	1913960	1446925	2	16.02						
231	10	36	12.	-28	34.1	1041960	704220	2	16.02						
232	10	38	13.	-26	42.4	787015	1700980	1	16.02	11.30					1G1S
233	10	24	50.	-26	4.0	2405680	2035100	2	16.03						
234	10	55	40.	-27	56.6	1104040	1039740	1	16.03	16.40	17.10	SA			
235	10	38	57.	-28	42.3	718640	628915	2	16.03			SB			
236	10	30	13.	-26	58.3	1753185	1557960	1	16.04	17.14	17.23	E1			
237	10	39	5.	-27	35.5	696245	1224645	2	16.04			SA			
238	10	34	21.	-27	19.6	1259045	1370435	1	16.05	19.49	17.34				
239	10	38	52.	-27	2.7	720660	1518680	2	16.05			S			
240	10	30	36.	-26	52.0	1708345	1614775	2	16.06		17.20(R)	SB			
241	10	31	27.	-26	59.0	1605920	1552360	1	16.06	17.70	17.00	S			
242	10	36	3.	-26	36.1	1045920	1758375	1	16.06	14.82	17.07	S		SP	
243	10	40	21.	-28	12.9	551905	889385	2	16.06			S	D		2GOS
244	10	32	14.	-28	7.9	1509340	936080	1	16.07	12.42	17.07	SB			
245	10	35	55.	-29	21.3	1075020	278310	2	16.07						
246	10	32	10.	-27	5.6	1519855	1494620	1	16.08	16.60	17.10	S		SP	
247	10	29	14.	-25	41.6	1903410	2242590	2	16.09					SP	
248	10	29	54.	-26	58.6	1791720	1555390	2	16.09			SA			
249	10	30	7.	-26	20.3	1766955	1892815	2	16.09			S	D		
250	10	33	24.	-26	58.6	1352935	1557360	1	16.09	15.62	17.29	S	D		

ID NO	R.A. (1950.0) H	M	S	DEC. °	′	″	X	Y		V25	R25	B25	TYPE			
251	10	44	23.	-28	5.8		63325	945370	3	16.09			SB (RS)			
252	10	32	25.	-27	31.2		1488415	1266005	1	16.11	14.16	17.03				1G1S
253	10	27	36.	-25	50.7		2073450	2159170	2	16.12			SB			
254	10	37	7.	-26	5.1		925305	2034905	2	16.12						
255	10	39	32.	-28	31.2		648130	727835	2	16.12						
256	10	33	40.	-27	25.5		1339330	1317055	1	16.13	13.26	17.14				
257	10	34	14.	-26	56.7		1272365	1574355	1	16.13	16.66	17.58	S		D	
258	10	43	21.	-29	14.0		204950	338585	2	16.13			S		SP	
259	10	41	23.	-26	41.2		407925	1707375	2	16.14						1G1S
260	10	31	45.	-26	50.7		1571325	1627375	1	16.15	13.42	16.80	SB			
261	10	38	35.	-25	40.2		748665	2256665	2	16.15			S		D	
262	10	38	39.	-28	28.5		752185	751755	3	16.15			SB		PEC	
263	10	25	23.	-26	29.9		2324570	1805030	2	16.16			S			
264	10	40	12.	-27	57.2		566615	1030715	2	16.16			SA			
265	10	40	17.	-28	32.4		560815	715585	2	16.16			S		SP	1G2S
266	10	43	50.	-29	3.5		147605	431545	2	16.16			E4			
267	10	27	11.	-27	55.0		2107855	1047465	2	16.17			SA			
268	10	30	8.	-26	59.0		1763815	1552015	2	16.17		17.70	S			
269	10	35	19.	-27	14.2		1144225	1418440	1	16.17	15.53	17.41				
270	10	27	34.	-25	52.0		2077770	2146945	2	16.18						1G1S
271	10	32	16.	-28	19.8		1505035	831430	3	16.18						
272	10	38	5.	-28	57.1		813325	497710	2	16.18			S			
273	10	44	13.	-26	23.5		73905	1860110	2	16.18			SB (S)			
274	10	36	1.	-25	15.8		1058015	2475815	2	16.19			S			
275	10	38	8.	-26	16.4		804505	1932900	2	16.19			SA (R)			
276	10	40	33.	-26	30.5		515375	1803865	2	16.19			S		D SP	
277	10	34	5.	-27	7.8		1291085	1475285	1	16.20	19.85	17.94				
278	10	26	19.	-28	32.5		2204290	710760	2	16.21						
279	10	26	29.	-29	8.2		2179485	392235	2	16.21			S		D	1G1S
280	10	33	53.	-27	13.2		1305530	1427225	1	16.21	20.65	17.89				
281	10	41	15.	-26	21.5		431295	1883965	2	16.21					SP	
282	10	25	14.	-25	46.4		2361355	2192685	2	16.22						1G1S
283	10	27	3.	-26	11.8		2137470	1969235	2	16.22			S		SP	
284	10	28	24.	-28	7.0		1962430	941585	2	16.22						
285	10	28	39.	-29	23.6		1925850	257685	2	16.22			S		D	
286	10	34	28.	-25	46.9		1244985	2198795	2	16.22			S		PEC	
287	10	34	37.	-28	32.7		1227745	717420	2	16.22						
288	10	36	51.	-26	21.3		959520	1886000	2	16.22			SA			
289	10	33	19.	-26	42.3		1382588	1699057	1	16.23	20.77					
290	10	36	25.	-29	16.7		1018025	323545	3	16.23					SP	
291	10	30	44.	-26	43.3		1691760	1687910	1	16.24	12.87					
292	10	34	57.	-29	19.4		1187930	300310	2	16.24					SP	
293	10	32	29.	-25	19.1		1486240	2446620	2	16.25			SB			1G1S
294	10	34	31.	-27	16.7		1239730	1396320	1	16.25	17.48	17.53				
295	10	35	51.	-27	36.7		1081325	1217210	1	16.25	12.93	16.94	E5			1G1S
296	10	34	1.	-27	23.5		1299400	1335730	1	16.26	15.37	17.48				
297	10	35	15.	-26	17.7		1151670	1223280	2	16.26						
298	10	37	25.	-28	40.6		878135	645370	2	16.26			S			
299	10	43	38.	-29	1.0		180140	454190	2	16.27			E0			
300	10	25	43.	-27	16.4		2277415	1389285	2	16.28			S			

ID NO	R.A. (1950.0) H	M	S	DEC. °	′	″	X	Y		V25	R25	B25	TYPE			
301	10	28	16.	-27	1.	4	1984730	1527955	2	16.28						
302	10	32	53.	-25	2.	3	1426815	2597285	2	16.28						1G1S
303	10	35	1.	-27	17.	2	1179780	1391895	1	16.28	16.03	16.78	RING			
304	10	35	13.	-26	5.	1	1144100	2035355	2	16.28						1G1S
305	10	35	32.	-25	48.	3	1116945	2181615	2	16.28			S		SP	
306	10	40	32.	-27	38.	5	485995	1196095	2	16.28						
307	10	30	24.	-29	14.	7	1720428	330769	2	16.29			SB (R)			
308	10	32	25.	-25	40.	6	1492185	2254400	2	16.29						
309	10	36	7.	-28	15.	3	1050325	872400	1	16.29	14.44	16.80	IRR			
310	10	39	33.	-26	14.	2	635035	1951250	2	16.31			E4			
311	10	43	33.	-29	7.	4	181805	396855	2	16.31						
312	10	29	22.	-26	50.	3	1354805	1628525	2	16.32			E2			
313	10	35	55.	-28	1.	6	1074080	994460	2	16.33		16.39	SB (S)			
314	10	41	25.	-29	2.	0	430670	440485	2	16.33			E5			
315	10	39	52.	-28	40.	1	727950	640320	2	16.34			SB			
316	10	42	13.	-26	20.	0	314615	1895265	2	16.34			SB			
317	10	29	11.	-29	1.	5	1864150	455050	2	16.35			S			1G1S
318	10	30	32.	-26	50.	0	1715670	1633155	1	16.35	13.74	17.80	E2			
319	10	37	27.	-27	20.	1	891155	1365170	1	16.35	13.99	17.78				
320	10	43	53.	-29	21.	3	134520	267365	2	16.35						
321	10	33	24.	-28	30.	6	1371520	735930	2	16.36			SA			
322	10	24	42.	-26	46.	3	2414165	1556360	2	16.37			S			
323	10	26	23.	-28	58.	9	2133155	474535	2	16.37			E2			
324	10	30	52.	-27	39.	6	1673395	1189600	1	16.37	11.36	17.17				
325	10	31	10.	-28	1.	6	1636740	993815	1	16.37	8.50	17.14				1G1S
326	10	33	25.	-26	9.	5	1371890	1996135	2	16.37						
327	10	36	3.	-26	43.	8	1045495	1689855	1	16.37	16.89	17.36	S			
328	10	24	21.	-26	59.	0	2454495	1542060	2	16.38			SB			
329	10	32	10.	-28	14.	7	1517240	876940	1	16.38	14.12	17.48				
330	10	43	43.	-29	6.	4	162075	405870	2	16.38						
331	10	29	48.	-27	56.	5	1797240	1037460	2	16.39						
332	10	40	3.	-25	0.	5	567700	2608660	2	16.39						1G1S
333	10	41	31.	-25	6.	0	388430	2558930	2	16.39						
334	10	27	43.	-29	33.	5	2032335	167275	2	16.40			S			
335	10	35	39.	-26	19.	5	1102920	1906640	2	16.40					SP	
336	10	36	25.	-26	51.	1	989695	1624320	1	16.40	14.57	17.43	S			
337	10	37	5.	-27	1.	2	932900	1533790	1	16.40	15.88	17.16	SA			
338	10	37	20.	-26	36.	2	902695	1756845	1	16.40	13.78	17.35	SB (S)			
339	10	24	33.	-26	40.	5	2421925	1708165	2	16.41						
340	10	42	13.	-25	4.	7	293875	2568835	2	16.41						
341	10	30	17.	-26	58.	4	1744450	1557530	1	16.42	14.54	17.88	S			
342	10	37	51.	-26	41.	2	840795	1711030	1	16.42	11.09	16.91	S			
343	10	39	17.	-27	30.	9	672250	1266185	2	16.43			SB			
344	10	40	22.	-29	2.	8	553500	444185	2	16.43			S			1G1S
345	10	27	2.	-27	54.	1	2126735	1054820	3	16.44						
346	10	30	4.	-28	32.	2	1764185	719210	2	16.44			S			
347	10	38	53.	-26	47.	8	1314685	1654640	1	16.44	12.09	16.63				2G1S
348	10	40	25.	-29	46.	7	553150	51530	2	16.44			E2			
349	10	27	42.	-25	32.	2	2062345	2145945	2	16.46						1G1S
350	10	29	52.	-26	36.	1	1796920	1755895	2	16.46						

ID NO	R.A. (1950.0) H	M	S	DEC. D	'	X	Y		V25	R25	B25	TYPE			
351	10	38	50.	-25	54.6	719720	2127040	2	16.46			SA	(S)		
352	10	38	50.	-25	54.6	719720	2127040	2	16.46						
353	10	41	45.	-29	26.4	395680	230955	2	16.46			E3			
354	10	41	45.	-27	31.0	380710	1262430	2	16.46						
355	10	39	58.	-25	45.8	581775	2204845	2	16.47			SA	(S)		
356	10	34	3.	-25	36.2	1285145	2294425	2	16.48						
357	10	35	4.	-29	43.1	1174465	82015	2	16.48						1615
358	10	37	54.	-28	33.7	840640	706625	2	16.48						1625
359	10	38	47.	-27	53.4	735425	1066115	2	16.48						
360	10	39	26.	-28	44.6	661950	608040	2	16.48			S	(R)		
361	10	28	15.	-28	21.0	1976920	816665	3	16.49			S		□	
362	10	33	5.	-27	31.5	1369975	1263425	1	16.49	12.89	18.22				2605
363	10	34	1.	-27	16.0	1298635	1402785	1	16.49	14.82	18.04				
364	10	40	29.	-27	10.2	527870	1450045	2	16.49			S		□	
365	10	31	20.	-28	5.1	1615830	962950	2	16.50		17.07				
366	10	39	45.	-25	5.4	604330	2566630	2	16.50			E0			
367	10	29	50.	-26	0.5	1802660	2074770	2	16.51			S			
368	10	31	9.	-28	49.1	1634950	569530	2	16.51						1615
369	10	34	24.	-27	54.5	1252945	1058605	1	16.51	13.74	16.80	S			
370	10	42	19.	-28	52.0	323865	537085	2	16.51						
371	10	43	15.	-28	58.2	214350	479990	2	16.51						
372	10	25	52.	-26	33.3	2277660	1775390	2	16.53			S		□	
373	10	29	57.	-27	13.9	1784310	1410825	2	16.53						
374	10	32	22.	-27	25.5	1495245	1316720	1	16.53	11.66	17.76	E1			
375	10	36	43.	-26	20.4	974815	1898890	2	16.53			S		□	
376	10	41	1.	-28	27.3	473385	755635	2	16.53			S			
377	10	27	30.	-26	13.5	2064550	1955110	2	16.54						1615
378	10	28	35.	-25	35.5	1957165	2296230	2	16.54			S		□	
379	10	32	51.	-27	12.3	1437350	1434935	2	16.54		17.73				
380	10	35	46.	-27	33.7	1091840	1243900	1	16.54	10.61	17.65				
381	10	39	4.	-28	38.3	704540	664675	2	16.54						
382	10	40	13.	-26	3.1	553245	2049650	2	16.54			S			SP
383	10	29	22.	-26	50.7	1854325	1625225	2	16.55			S		□	
384	10	31	59.	-26	38.7	1542205	1735119	1	16.55	13.76	17.21	S			SP
385	10	37	5.	-29	23.9	940240	256750	2	16.55						1615
386	10	40	26.	-28	7.4	521240	938815	2	16.55			SB		□	
387	10	42	34.	-28	6.6	287640	942855	2	16.55						
388	10	34	23.	-27	15.2	1244425	1409530	1	16.56	15.19					
389	10	43	32.	-28	17.4	174625	844140	2	16.56			SA			
390	10	32	48.	-26	0.4	1446725	2077655	2	16.57						
391	10	41	12.	-28	17.1	450845	850890	2	16.57						1615
392	10	43	35.	-25	31.8	1399950	2323575	2	16.57			SB			
393	10	44	29.	-27	14.9	51650	1400055	2	16.57			E2			
394	10	32	42.	-26	44.2	1456300	1585705	1	16.58	11.07	17.61				
395	10	33	53.	-26	21.5	1305750	1869000	2	16.58						
396	10	34	13.	-27	23.5	1266000	1335300	1	16.58	12.26		E2			
397	10	37	42.	-25	58.8	856630	2056210	2	16.58						
398	10	38	40.	-28	38.4	752030	664395	2	16.58			S		□	
399	10	39	52.	-28	36.0	609455	684125	2	16.58						SP
400	10	40	0.	-28	36.4	593580	680595	2	16.58			E6			

ID NO	R.A. (1950.0) H	M	S	DEC. °	′	X	Y		V25	R25	B25	TYPE
+01	10	33	52.	-27	17.6	1316215	1387810	1	16.59	15.36	17.58	
+02	10	33	52.	-27	24.5	1316545	1326190	1	16.59	17.64	18.29	
+03	10	27	13.	-26	36.2	2104350	1751930	2	16.60			E3
+04	10	29	33.	-26	47.7	1833730	1652370	2	16.60			S
+05	10	31	20.	-28	46.9	1613265	589080	2	16.60			
+06	10	31	40.	-26	14.7	1581475	1947720	2	16.60			S PEC
+07	10	35	9.	-28	3.1	1164440	981410	1	16.60	14.01	17.84	
+08	10	41	21.	-28	58.7	437700	479575	2	16.60			SA
+09	10	42	43.	-26	14.3	253290	1941200	2	16.60			
+10	10	29	46.	-25	46.4	1815175	2209395	2	16.61			
+11	10	31	6.	-26	6.0	1651440	2026280	2	16.61			
+12	10	31	24.	-26	21.3	1612795	1885020	2	16.61			SR
+13	10	31	42.	-28	8.4	1572285	933650	1	16.61	11.07	17.60	
+14	10	34	52.	-26	2.7	1196530	2057640	2	16.61			SB (S)
+15	10	38	21.	-28	1.3	785760	996485	2	16.61		18.09	
+16	10	40	23.	-29	9.7	543465	382035	2	16.61			
+17	10	41	46.	-26	4.3	367480	2032590	2	16.61			1G1S
+18	10	43	55.	-25	23.1	101410	2400305	3	16.61			
+19	10	24	42.	-26	5.4	2422635	2022000	2	16.62			1G1S
+20	10	33	55.	-28	32.3	1307740	720475	2	16.62			1G1S
+21	10	36	26.	-28	17.5	1013655	852950	1	16.62	10.56		S
+22	10	24	57.	-25	59.9	2391820	2071340	2	16.63			
+23	10	25	25.	-27	0.5	2324320	1531140	2	16.63			SB (R)
+24	10	34	22.	-26	26.1	1256980	1848175	2	16.63			
+25	10	35	53.	-26	28.3	1065690	1827990	1	16.63	14.95	17.86	
+26	10	29	15.	-26	9.6	1873790	1991985	2	16.64			
+27	10	36	52.	-25	59.4	958000	1549675	1	16.64	12.76	17.19	
+28	10	29	33.	-27	1.3	1823085	1530875	2	16.65			
+29	10	30	22.	-25	23.9	1742305	2401835	2	16.65			
+30	10	32	43.	-28	24.4	1441215	791300	2	16.65			1G1S
+31	10	34	15.	-27	42.0	1271345	1170500	1	16.65	10.53	17.66	
+32	10	34	54.	-25	54.4	1192835	2131155	2	16.65			
+33	10	37	52.	-26	1.2	835320	2069535	2	16.65			2G0S
+34	10	40	31.	-28	1.2	534155	636775	2	16.65			S D
+35	10	41	55.	-27	0.7	355695	1532235	2	16.65			
+36	10	42	31.	-28	28.7	296980	745760	2	16.65			
+37	10	44	20.	-29	27.9	93285	212280	2	16.65			S SP
+38	10	28	19.	-27	48.2	1974920	1110065	2	16.66			SP
+39	10	30	22.	-26	51.9	1735010	1515215	2	16.66			1G1S
+40	10	35	5.	-25	6.8	1168025	2557265	2	16.66			
+41	10	37	20.	-26	25.9	902290	1848845	2	16.66		17.55	S
+42	10	37	27.	-25	58.9	885290	2090480	2	16.66			
+43	10	39	54.	-27	35.9	600400	1220835	2	16.66			2G1S
+44	10	41	37.	-26	47.9	390020	1647010	2	16.66			
+45	10	44	3.	-26	34.3	97425	1764090	2	16.66			1G1S
+46	10	32	4.	-25	1.5	1537910	2504025	2	16.67			
+47	10	36	23.	-26	11.3	1005575	1960045	2	16.67			1G1S
+48	10	36	23.	-26	31.7	996020	1797985	1	16.67	10.14	17.51	
+49	10	37	57.	-26	41.0	827360	1713355	1	16.67	10.60	18.11	S D
+50	10	42	10.	-29	11.3	343300	361005	2	16.67			SP

ID NO	R.A. (1950.0) H	M	S	DEC. °	′	″	X	Y		V25	R25	B25	TYPE			
+51	10	30	14.	-26	56.	7	1751565	1572425	2	16.68						
+52	10	31	27.	-28	32.	3	1600150	719645	2	16.68			SB			
+53	10	33	42.	-26	0.	1	1338639	2080086	2	16.68						
+54	10	36	43.	-26	39.	7	975551	1726333	1	16.68	11.98	17.43	S		SP	
+55	10	25	3.	-27	14.	3	2367210	1406690	2	16.69			S			
+56	10	31	15.	-25	35.	6	1631870	2298050	2	16.69			S			
+57	10	32	14.	-27	12.	5	1512300	1432970	1	16.69	11.74	18.21				
+58	10	34	10.	-29	7.	3	1280860	408010	2	16.69						
+59	10	34	25.	-29	17.	4	1248864	318124	2	16.69			S			
+60	10	36	15.	-25	59.	6	1027785	2084815	2	16.69			SB			
+61	10	43	45.	-26	25.	6	132150	1842310	2	16.69			E1			
+62	10	24	59.	-25	17.	6	2395815	2450295	3	16.70						
+63	10	25	3.	-29	1.	0	2348770	453460	2	16.70						
+64	10	25	35.	-26	58.	3	2304235	1546475	2	16.70						
+65	10	30	7.	-25	56.	4	1769222	2111255	2	16.70					SP	
+66	10	33	14.	-26	45.	5	1392800	1674065	1	16.70	12.02	18.24				
+67	10	34	11.	-28	6.	4	1273500	952040	1	16.70	8.63		S			1G1S
+68	10	38	17.	-27	12.	7	791020	1430565	1	16.70	12.76	17.99	S	D		
+69	10	39	15.	-26	9.	3	670155	1990100	2	16.70						
+70	10	40	23.	-27	17.	8	541040	1382515	2	16.70						
+71	10	41	33.	-28	39.	7	411585	648390	2	16.70						
+72	10	30	57.	-26	56.	1	1665795	1578350	1	16.71	11.23	18.01				
+73	10	35	47.	-25	49.	2	1087200	2177470	2	16.71			S		SP	
+74	10	36	24.	-29	17.	4	1018460	317175	2	16.71						
+75	10	41	30.	-29	21.	9	422825	271410	2	16.71						
+76	10	29	31.	-29	28.	4	1822840	216555	2	16.72						
+77	10	34	13.	-26	52.	4	1266255	1613465	1	16.72	10.79	17.80				
+78	10	34	26.	-26	32.	5	1250150	1790505	1	16.72	10.99	17.86				
+79	10	38	24.	-29	0.	4	783795	467980	2	16.72			SB	D		
+80	10	32	37.	-26	36.	9	1466830	1750940	1	16.73	12.15	17.86				
+81	10	34	60.	-27	58.	4	1182485	1023495	1	16.73	12.10	17.28				
+82	10	36	37.	-26	40.	9	988990	1714960	2	16.73		17.87				
+83	10	29	5.	-29	41.	7	1870764	96731	3	16.74			SAB			
+84	10	36	33.	-26	10.	1	982906	1990670	2	16.74			S		PEC	
+85	10	44	32.	-29	29.	3	69855	196545	2	16.74						
+86	10	29	12.	-26	35.	2	1876025	1763775	2	16.75			SB (S)			
+87	10	34	23.	-26	53.	4	1245625	1603840	1	16.75	12.03	17.34	S		SP	
+88	10	41	33.	-25	47.	4	380735	2187635	2	16.75						1G1S
+89	10	43	37.	-29	24.	4	177330	245435	2	16.75			S	D		
+90	10	27	58.	-26	45.	5	2024190	1670095	2	16.76						
+91	10	29	49.	-26	50.	5	1801365	1627855	2	16.76						
+92	10	30	10.	-26	42.	4	1759440	1699920	3	16.76						
+93	10	33	26.	-28	46.	0	1367710	598315	2	16.76			IRR			1G1S
+94	10	34	3.	-27	29.	9	1284975	1278005	2	16.76		17.95				
+95	10	34	20.	-26	30.	9	1260550	1805360	1	16.76	14.93					
+96	10	37	44.	-27	46.	1	857150	1132450	1	16.76	11.09	18.03				
+97	10	38	30.	-28	59.	6	755470	476750	2	16.76						
+98	10	39	13.	-26	59.	9	677570	1543995	2	16.76						
+99	10	24	46.	-27	31.	0	2398790	1257320	2	16.77			SB (S)			
500	10	29	5.	-28	15.	3	1879790	868820	2	16.77						

ID NO	R.A. (1950.0) H	M	S	DEC. °	′	″	X	Y		V25	R25	B25	TYPE			
501	10	31	30.	-29	19	4	1592190	298675	2	16.77						1G1S
502	10	36	4.	-28	48	3	1057855	572805	2	16.77						1G1S
503	10	35	25.	-27	18	8	1131760	1377635	2	16.78		17.78				
504	10	35	32.	-28	11	0	1120120	911120	2	16.78		17.11	SB (R)			
505	10	35	35.	-26	58	7	1109330	1556340	1	16.78	12.54	18.13	SB	D		
506	10	37	32.	-28	47	0	884320	500360	2	16.78			S			
507	10	38	4.	-28	55	5	823245	511705	2	16.78			S	D		
508	10	27	39.	-28	1	9	2051320	986755	2	16.79			S			
509	10	33	20.	-27	15	5	1379615	1406490	1	16.79	13.05	18.73				
510	10	36	56.	-25	59	9	949240	2081320	2	16.79						
511	10	42	8.	-29	0	9	346691	458196	2	16.79			SB			
512	10	42	25.	-29	8	4	315245	390805	2	16.79						
513	10	42	41.	-27	23	5	2672250	1327430	2	16.79						
514	10	43	17.	-28	30	1	207205	731355	2	16.79			S	D		
515	10	27	54.	-26	51	4	2031245	1617205	2	16.80						
516	10	31	39.	-26	32	0	1543335	1794960	1	16.80	14.34					
517	10	34	25.	-27	19	6	1250625	1370530	1	16.80	15.10					3G0S
518	10	35	12.	-29	45	9	1159890	63065	2	16.80						
519	10	43	44.	-25	50	6	125525	2155455	2	16.80						
520	10	44	2.	-29	48	5	132885	28610	2	16.80						
521	10	27	42.	-28	26	0	2042715	771390	2	16.81			S			
522	10	30	24.	-27	54	3	1726525	1058530	2	16.81		17.93				1G1S
523	10	36	55.	-25	0	0	947180	2617000	2	16.81						
524	10	38	19.	-28	18	5	790753	842763	2	16.81						
525	10	24	25.	-28	58	5	2424175	473545	2	16.82						
526	10	24	35.	-28	58	6	2423790	472520	2	16.82						
527	10	32	9.	-27	25	7	1521285	1315115	1	16.82	11.36	18.13	S		SP	
528	10	34	43.	-29	15	8	1216525	331880	2	16.82						
529	10	28	51.	-28	4	0	1909325	969425	2	16.83						
530	10	28	55.	-28	38	9	1898155	657945	2	16.83						
531	10	31	19.	-28	47	9	1615115	580080	2	16.83						1G1S
532	10	25	35.	-28	27	5	2291545	753375	2	16.84						
533	10	28	32.	-29	15	8	1939260	327010	2	16.84			E1			
534	10	29	32.	-25	32	5	1842440	2323740	2	16.84						
535	10	30	19.	-26	12	4	1744310	1960275	2	16.84						
536	10	35	50.	-26	42	3	1081405	1698830	1	16.84	12.94	18.49				
537	10	37	38.	-29	9	2	873055	390350	2	16.84			SB (S)			
538	10	37	42.	-26	3	8	856300	2046470	2	16.84						
539	10	37	51.	-25	44	9	837555	2215430	2	16.84						
540	10	42	50.	-28	27	4	260000	756140	2	16.84			SA (S)			
541	10	32	39.	-25	27	2	1465040	2374310	2	16.85						
542	10	36	2.	-28	5	8	1060715	957215	1	16.85	11.08	17.77	S			
543	10	36	19.	-27	1	2	1025300	1534365	2	16.55		18.04				
544	10	40	34.	-28	48	7	529100	570250	2	16.85			SB			
545	10	41	31.	-25	43	0	393315	2227180	2	16.85			S	D		1G1S
546	10	31	55.	-29	45	4	1543031	66537	2	16.86						
547	10	36	3.	-24	50	0	1055840	1634190	1	16.86	11.17	17.98				
548	10	37	4.	-26	13	0	932535	1966520	2	16.86						
549	10	42	2.	-27	18	5	344580	1373090	2	16.86			E4			
550	10	44	7.	-26	43	1	90120	1685050	2	16.86			S		SP	

ID NO	R.A. (1950.0) H	M	S	DEC. °	′	″	X	Y		V25	R25	B25	TYPE			
551	10	31	1.	-28	4.	5	1653495	967385	1	16.87	9.51	17.54				
552	10	32	55.	-29	13.	9	1424935	348580	2	16.87						
553	10	36	13.	-26	30.	0	1036745	1812945	1	16.87	12.16	18.17	S			
554	10	37	49.	-28	32.	3	850870	714695	2	16.87						1G1S
555	10	39	1.	-27	1.	4	702025	1530660	2	16.87						
556	10	39	33.	-28	0.	4	634850	1002700	2	16.87						
557	10	41	13.	-26	26.	1	435590	1842935	2	16.87			S		SP	
558	10	28	14.	-28	25.	1	1979645	780400	2	16.88						
559	10	38	19.	-26	8.	4	782445	2004810	2	16.88						1G1S
560	10	41	20.	-28	42.	0	437210	628785	2	16.88			S			
561	10	26	28.	-26	46.	2	2203205	1661200	2	16.89						
562	10	29	40.	-25	47.	1	1825665	2193720	2	16.89						
563	10	37	50.	-25	59.	5	839285	2084565	2	16.89						
564	10	43	43.	-29	6.	2	161130	407470	2	16.89					SP	1G1S
565	10	31	27.	-26	24.	0	1607615	1865560	2	16.90						1G1S
566	10	37	55.	-26	42.	3	832760	1697960	1	16.90	11.23	18.55				
567	10	43	1.	-27	7.	4	224831	1470478	2	16.90			SB	D		
568	10	26	40.	-28	18.	0	2165870	840695	2	16.91						
569	10	31	35.	-27	15.	1	1589490	1409200	1	16.91	9.80	18.35	S			
570	10	32	24.	-26	41.	3	1492600	1707615	1	16.91	11.89	17.93				
571	10	33	42.	-28	38.	4	1336520	666000	2	16.91						
572	10	35	4.	-25	13.	5	1171755	2497405	2	16.91						
573	10	35	35.	-27	59.	3	1113040	1010210	1	16.91	13.55	18.14	S	D		
574	10	40	55.	-26	59.	0	475020	1549655	2	16.91			S	D		
575	10	42	17.	-28	39.	2	325105	651635	2	16.91					SP	
576	10	26	56.	-26	19.	1	2149835	1903755	2	16.92						
577	10	31	7.	-27	31.	6	1643945	1261785	1	16.92	8.60	18.02				
578	10	35	10.	-27	5.	0	1161835	1500455	1	16.92	11.82	17.52	SB (S)			
579	10	38	32.	-25	37.	8	753865	2277750	2	16.92						
580	10	25	33.	-25	32.	1	2324085	2321740	2	16.93						
581	10	28	55.	-25	56.	6	1914600	2108540	2	16.93						
582	10	33	50.	-28	38.	6	1318885	664545	2	16.93						
583	10	34	58.	-27	24.	0	1185385	1330960	2	16.93		18.50				
584	10	36	39.	-27	8.	1	984320	1472720	2	16.93		18.19				
585	10	36	51.	-29	30.	4	968100	201000	2	16.93			S			
586	10	39	9.	-25	6.	9	677650	2553910	2	16.93						
587	10	37	17.	-26	3.	9	906260	2045305	2	16.94			(R)SB (S)			
588	10	38	48.	-28	3.	5	731960	976175	2	16.94						
589	10	42	24.	-29	48.	2	322480	35155	2	16.94					PEC	
590	10	42	29.	-27	34.	9	294005	1226190	2	16.94			SB			
591	10	32	4.	-26	14.	5	1533390	1951315	2	16.95						
592	10	35	0.	-27	59.	7	1101605	1012055	1	16.95	10.84					
593	10	35	46.	-27	7.	5	1089515	1478445	1	16.95	8.59					
594	10	36	42.	-26	38.	7	978300	1734915	1	16.95	10.89	18.16				
595	10	41	10.	-29	11.	3	460710	366675	3	16.95			S			
596	10	24	57.	-28	54.	2	2362605	512785	2	16.96						
597	10	33	23.	-25	57.	8	1366679	2101059	2	16.96						
598	10	36	12.	-29	11.	0	984165	374900	2	16.96						
599	10	37	1.	-27	35.	3	937315	1229695	2	16.96		17.26	S		SP	
600	10	37	49.	-27	48.	5	847910	1110135	1	16.96	11.75	18.07				

ID NO	R.A. (1950.0) H	M	S	DEC. °	′	″	X	Y		V25	R25	B25	TYPE
501	10	38	53.	-25	35.	5	710740	2298025	2	16.96			
502	10	42	7.	-25	1.	0	315015	2602215	2	16.96			
503	10	34	22.	-25	27.	0	1258365	2376360	2	16.97			SB (S)
504	10	36	13.	-25	19.	9	1022345	2439160	2	16.97			SB
505	10	41	51.	-27	9.	2	364065	1456500	2	16.97			
506	10	27	40.	-25	43.	8	2066918	2221102	2	16.98			
507	10	27	41.	-25	43.	3	2066900	2221000	2	16.98			S SP
508	10	28	45.	-26	17.	5	1933095	1920685	2	16.98			
509	10	31	20.	-28	50.	0	1613400	561120	2	16.98			
510	10	37	31.	-25	59.	7	877875	2082780	2	16.98			
511	10	39	59.	-26	38.	3	584460	1731380	2	16.98			S
512	10	40	30.	-26	31.	2	521170	1797330	2	16.98			
513	10	28	23.	-28	23.	5	1963315	793990	2	16.99			
514	10	34	19.	-25	59.	5	1263790	2085080	2	16.99			
515	10	35	44.	-27	51.	3	1094990	1087200	1	16.99	10.04	18.09	
516	10	41	43.	-28	54.	2	394035	518660	2	16.99			
517	10	43	5.	-28	46.	4	231575	585865	2	16.99			
518	10	24	55.	-26	7.	1	2394720	2007135	2	17.00			SB 1G1S
519	10	25	37.	-26	30.	5	2307475	1799885	2	17.00			
520	10	29	32.	-29	28.	1	1820690	218455	2	17.00			
521	10	30	33.	-28	41.	2	1705445	639480	3	17.00			S SP
522	10	31	51.	-27	18.	5	1557610	1378635	2	17.00		18.84	
523	10	32	24.	-28	33.	8	1487995	706840	2	17.00			
524	10	33	33.	-29	34.	3	1352255	166235	2	17.00			1G1S
525	10	35	22.	-26	18.	9	1137340	1912220	2	17.00			
526	10	36	40.	-25	34.	1	978810	2312630	2	17.00			
527	10	39	40.	-27	44.	3	629080	1141625	2	17.00			
528	10	40	23.	-29	2.	9	552470	443160	3	17.00			
529	10	31	31.	-26	7.	7	1599650	2011890	2	17.01			
530	10	34	24.	-27	14.	9	1253295	1411925	1	17.01	12.42		
531	10	34	43.	-25	59.	7	1205215	2083965	2	17.01			
532	10	40	13.	-28	36.	1	569190	582795	2	17.01			
533	10	42	13.	-25	9.	2	303750	2528650	2	17.01			
534	10	43	11.	-28	56.	1	222540	499195	2	17.01			
535	10	43	39.	-29	8.	2	169765	389605	2	17.01			SP
536	10	25	1.	-26	23.	3	2381095	1862485	2	17.02			SB (S)
537	10	28	53.	-28	15.	9	1895460	863265	2	17.02			
538	10	30	5.	-26	13.	5	1772550	1958880	2	17.02			
539	10	31	23.	-26	46.	3	1601960	1666960	2	17.02			
540	10	31	35.	-28	24.	7	1584750	788040	2	17.02			
541	10	31	55.	-25	17.	7	1555400	2458345	2	17.02			
542	10	32	0.	-28	11.	5	1536520	905260	1	17.02	10.58	17.38	
543	10	32	34.	-26	5.	4	1474910	2032420	2	17.02			
544	10	34	4.	-27	24.	1	1292725	1330060	1	17.02	16.20		
545	10	37	54.	-26	14.	1	832050	1952965	2	17.02			
546	10	40	15.	-25	49.	3	548205	2168545	2	17.02			
547	10	40	45.	-28	38.	5	505965	660540	2	17.02			
548	10	42	49.	-29	27.	3	270815	216305	2	17.02			
549	10	27	1.	-25	10.	2	2149400	2520325	2	17.03			
550	10	32	13.	-27	22.	7	1503565	1342095	1	17.03	9.49	18.51	

ID NO	R.A. (1950.0) H	M	S	DEC. °	′	X	Y		V25	R25	B25	TYPE			
551	10	33	0.	-27	7.9	1420070	1474475	2	17.03						
552	10	33	15.	-29	19.2	1385630	301455	2	17.03						
553	10	35	40.	-26	54.4	1101320	1595550	1	17.03	11.12	18.09				
554	10	37	53.	-26	1.0	833205	2071030	3	17.03						
555	10	24	29.	-26	9.0	2447355	1989300	2	17.04						
556	10	30	24.	-28	2.3	1727090	986980	1	17.04	10.57					
557	10	33	27.	-29	13.0	1364100	357305	3	17.04						
558	10	27	3.	-25	17.8	2133800	2452305	2	17.05						
559	10	27	49.	-26	52.5	2041000	1606535	2	17.05						
560	10	27	55.	-28	15.3	2016810	867330	2	17.05						
561	10	29	49.	-25	55.9	1805685	2115825	2	17.05						
562	10	32	42.	-26	5.7	1459030	2020985	2	17.05						
563	10	38	23.	-26	40.8	766870	1715060	1	17.05	10.75					
564	10	40	4.	-28	43.8	587380	614295	2	17.05						
565	10	40	45.	-27	3.4	494820	1510380	2	17.05						
566	10	41	45.	-28	50.1	390545	555140	2	17.05						
567	10	25	18.	-27	8.2	2339665	1461675	2	17.06						
568	10	29	3.	-27	7.1	1881360	1478750	2	17.06						
569	10	29	23.	-27	32.1	1840320	1255855	2	17.06						
570	10	29	37.	-27	36.3	1821290	1213605	2	17.06						
571	10	29	43.	-28	44.5	1803460	608595	2	17.06						
572	10	30	28.	-29	46.2	1711415	58215	2	17.06						
573	10	31	58.	-27	5.5	1543475	1495635	1	17.06	10.91	19.03				
574	10	38	10.	-26	16.9	801825	1928560	2	17.06					SP	
575	10	40	2.	-27	56.3	585510	1038730	2	17.06						
576	10	25	11.	-26	9.4	2362765	1987675	2	17.07			S		SP	
577	10	33	14.	-28	43.5	1390245	620190	2	17.07						
578	10	34	40.	-28	6.5	1220710	951635	1	17.07	11.24	18.18				
579	10	35	51.	-28	30.3	1081720	738675	2	17.07			S-B	D		
580	10	37	12.	-28	29.5	924315	745305	2	17.07						
581	10	38	45.	-27	40.8	737905	1170510	3	17.07			S			
582	10	42	3.	-29	41.4	361845	96055	2	17.07			S	D		
583	10	33	50.	-26	25.9	1301625	1849860	2	17.08						260S
584	10	37	45.	-26	1.6	849275	2065895	2	17.08						
585	10	38	5.	-27	32.5	815360	1253575	2	17.08						
586	10	40	25.	-25	57.5	528935	2100075	2	17.08						
587	10	25	30.	-29	23.1	2293840	256220	2	17.09			S-B			
588	10	29	35.	-29	20.7	1814290	284660	2	17.09						
589	10	29	55.	-28	3.9	1784345	971975	2	17.09						
590	10	30	19.	-28	3.7	1736820	974320	1	17.09	8.47	18.00				
591	10	30	57.	-25	26.9	1672280	2375755	2	17.09						1G1S
592	10	31	31.	-27	1.5	1598715	1530380	1	17.09	11.25					
[illegible]	10	34	[illegible]	-27	40.3	1215540	1106930	1	17.09	9.47	17.87				
[illegible]	10	34	48.	-29	4.4	1205730	434335	2	17.09						
[illegible]	10	36	33.	-26	21.3	976480	1890315	2	17.09						
[illegible]	10	38	54.	-25	19.3	708653	2443144	2	17.09			S			
[illegible]	10	39	30.	-28	34.4	652090	690955	2	17.09						
[illegible]	10	40	0.	-28	38.8	594535	659280	3	17.09						
[illegible]	10	40	51.	-26	22.9	478690	1871795	2	17.09			S-B			
700	10	27	12.	-28	52.9	2098250	529365	2	17.10			S			

ID NO	R.A. (1950.0) H	M	S	DEC. °	′	″	X	Y		V25	R25	B25	TYPE		
701	10	27	40.	-25	52.	6	2066240	2141800	2	17.10					
702	10	29	52.	-27	8.	4	1793510	1467785	2	17.10					
703	10	33	20.	-26	52.	5	1382015	1612095	1	17.10	8.79	18.49		SP	
704	10	34	42.	-27	46.	9	1216750	1126205	1	17.10	10.54	18.34			
705	10	37	5.	-25	57.	1	929645	2106080	2	17.10					
706	10	38	56.	-28	45.	5	719430	600530	2	17.10					
707	10	33	45.	-28	39.	0	1329385	660475	2	17.11					
708	10	36	34.	-28	34.	8	997425	697735	2	17.11					
709	10	28	29.	-27	50.	6	1954825	1089305	2	17.12					
710	10	29	3.	-26	7.	3	1897840	2013125	2	17.12					
711	10	29	7.	-25	31.	6	1893020	2332165	2	17.12					
712	10	31	40.	-25	5.	0	1582950	2036190	2	17.12					
713	10	31	60.	-27	34.	5	1538370	1236730	2	17.12					
714	10	32	42.	-27	3.	3	1456975	1515305	1	17.12	7.39				
715	10	38	44.	-25	21.	4	728270	2424385	2	17.12				SP	
716	10	42	5.	-28	8.	8	345520	924285	2	17.12					
717	10	43	10.	-29	7.	8	226155	394660	2	17.12					
718	10	24	47.	-28	13.	3	2389995	879175	2	17.13					
719	10	31	52.	-26	5.	8	1558375	2028450	2	17.13					
720	10	37	24.	-26	57.	2	895135	1569465	1	17.13	9.40				
721	10	27	31.	-25	10.	4	2089320	2519560	2	17.14					
722	10	28	55.	-25	10.	4	1918425	2521810	2	17.14					
723	10	29	47.	-28	5.	5	1799350	957080	2	17.14					
724	10	30	40.	-28	14.	4	1694810	879015	1	17.14	11.70				
725	10	36	28.	-28	8.	3	1008770	935180	1	17.14	9.89	19.18	S	SP	
726	10	38	2.	-26	52.	2	818550	1613100	1	17.14	8.57	18.28			1615
727	10	43	36.	-27	25.	5	159020	1307645	2	17.14					
728	10	27	57.	-27	17.	0	2021175	1388065	2	17.15					
729	10	28	38.	-25	13.	7	1947740	1955030	2	17.15					
730	10	34	6.	-26	57.	0	1289665	1571705	1	17.15	11.11	18.45			
731	10	34	25.	-26	21.	2	1251610	1891855	2	17.15					
732	10	34	29.	-27	34.	2	1243070	1239640	1	17.15	10.57	18.37			
733	10	38	59.	-25	38.	4	699850	2271890	2	17.15			S	SP	
734	10	40	33.	-26	18.	9	504705	1907855	2	17.15			S		
735	10	41	59.	-29	0.	5	364525	461220	2	17.15			S	SP	
736	10	28	15.	-26	10.	7	1994135	1980900	2	17.16					
737	10	31	30.	-25	24.	4	1605650	2399030	2	17.16					
738	10	38	2.	-26	33.	9	817795	1776845	1	17.16	8.81	17.98			
739	10	42	18.	-27	4.	9	310965	1494235	2	17.16					
740	10	24	29.	-25	9.	1	2457240	2525655	2	17.17					
741	10	36	43.	-26	4.	5	974750	2040430	3	17.17					
742	10	37	56.	-26	1.	4	828720	2067850	2	17.17					2605
743	10	38	28.	-26	49.	0	766580	1642000	1	17.17	9.10				
744	10	40	25.	-29	37.	4	552480	134715	2	17.17			S		
745	10	40	46.	-26	25.	7	489200	1847455	2	17.17					
746	10	43	23.	-26	3.	0	172090	2000430	2	17.17					
747	10	43	56.	-29	2.	5	134930	439675	2	17.17					
748	10	44	13.	-29	7.	7	103230	393065	2	17.17					
749	10	27	35.	-25	24.	7	2079090	2391560	2	17.18					
750	10	28	24.	-29	5.	8	1955740	416610	2	17.18					

ID NO	R.A. (1950.0) H	M	S	DEC. °	′	″	X	Y		V25	R25	B25	TYPE		
751	10	32	29.	-26	4.5		1483600	2039360	2	17.18					
752	10	34	30.	-27	2.8		1240580	1520670	1	17.18	8.21	17.95			1G1S
753	10	34	49.	-27	11.9		1202750	1439295	3	17.18					
754	10	37	50.	-25	57.2		840085	2104935	2	17.18					
755	10	37	56.	-25	45.1		826625	2212975	2	17.18					
756	10	38	32.	-28	46.4		767145	592565	2	17.18					
757	10	42	55.	-28	45.2		250470	597130	2	17.18					1G1S
758	10	43	48.	-29	4.8		152530	419605	2	17.18					
759	10	28	1.	-26	39.4		2017660	1724710	2	17.19					
760	10	29	57.	-26	12.5		1789010	1966921	2	17.19			SA		
761	10	30	9.	-25	34.3		1766690	2308675	2	17.19			S	J	
762	10	33	20.	-27	31.8		1379235	1260665	1	17.19	9.31	18.77			
763	10	34	14.	-27	47.7		1272140	1119465	1	17.19	9.21	18.21			
764	10	35	26.	-26	22.9		1129390	1876740	2	17.19			SB (S)		
765	10	36	25.	-28	14.9		1014380	875905	2	17.19		17.49	SA		
766	10	29	20.	-27	54.6		1854065	1054145	2	17.20					
767	10	30	49.	-25	50.2		1686520	2167395	2	17.20					
768	10	28	37.	-26	49.9		1945430	1531745	2	17.21					
769	10	33	18.	-29	1.8		1382735	457040	3	17.21					
770	10	34	13.	-26	51.5		1264905	1620445	1	17.21	7.45	18.15			2G0S
771	10	37	45.	-28	2.5		857360	985775	1	17.21	8.09	18.07			
772	10	39	42.	-25	37.6		613795	2278375	2	17.21			E4		
773	10	43	1.	-25	1.7		207035	2594480	2	17.21			S		
774	10	25	13.	-28	26.7		2336495	760335	2	17.22					
775	10	32	14.	-27	21.8		1512215	1350175	1	17.22	9.93				
776	10	32	30.	-25	16.5		1483605	2468910	2	17.22					
777	10	38	13.	-28	32.7		794295	715585	2	17.22					
778	10	43	18.	-28	57.5		209695	486275	2	17.22					
779	10	25	15.	-25	35.5		2358540	2290390	3	17.23					
780	10	33	34.	-28	39.0		1350865	660700	2	17.23					
781	10	34	48.	-26	48.3		1204775	1649370	1	17.23	9.96	18.46			
782	10	35	53.	-25	25.8		1063480	2387015	2	17.23			S	PEC	
783	10	36	17.	-26	10.4		1027055	1988055	2	17.23			SB		
784	10	37	56.	-25	45.5		827485	2209985	2	17.23					
785	10	42	58.	-26	31.4		225370	1792240	2	17.23					
786	10	31	18.	-29	1.3		1617020	460290	2	17.24					1G1S
787	10	35	28.	-29	37.4		1128050	138445	2	17.24					2G1S
788	10	43	25.	-26	8.8		168995	1993640	2	17.24					
789	10	24	44.	-28	30.8		2391725	722065	2	17.25					1G1S
790	10	28	15.	-28	1.7		1981345	989645	2	17.25					
791	10	34	4.	-28	40.2		1293505	650280	2	17.25					
792	10	39	32.	-26	36.3		638145	1753715	2	17.25					
793	10	41	5.	-26	21.6		450465	1883505	2	17.25					
794	10	25	54.	-28	8.0		2257580	926790	3	17.26			IRR		
795	10	33	21.	-25	26.2		1360225	2382220	2	17.26					
796	10	33	31.	-25	26.3		1361115	2382355	2	17.26					
797	10	34	51.	-29	23.1		1200645	266435	2	17.26					
798	10	35	21.	-26	18.1		1119715	1919075	2	17.26					
799	10	35	36.	-25	59.1		1110620	1553295	1	17.26	10.68	18.26		SP	
800	10	24	21.	-29	24.7		2427455	239425	2	17.27					

ID NO	R.A. (1950.0) H	M	S	DEC. °	′	″	X	Y		V25	R25	B25	TYPE	
301	10	24	43.	-27	12	1	2397990	1425925	2	17.27				1G1S
302	10	28	33.	-29	15	7	1937445	320465	2	17.27				
303	10	30	14.	-26	58	2	1750055	1559025	1	17.27	9.95			
304	10	32	5.	-27	14	5	1528775	1414795	1	17.27	10.03	17.90	SB	D
305	10	32	15.	-28	12	9	1507410	893740	1	17.27	10.47	18.44		
306	10	34	25.	-28	20	3	1252225	823740	2	17.27				
307	10	36	43.	-26	38	8	975675	1733685	1	17.27	10.33	18.17		
308	10	44	30.	-29	33	5	75305	162000	2	17.27			SB	
309	10	24	37.	-29	11	5	2398770	357885	2	17.28				SP
310	10	25	1.	-29	24	4	2350200	243305	2	17.28			S	
311	10	25	15.	-27	5	5	2343250	1485095	2	17.28			S	
312	10	42	60.	-29	6	2	246400	409145	2	17.28				
313	10	42	55.	-26	40	5	234530	1710300	2	17.28				
314	10	43	34.	-25	41	6	147015	2236015	2	17.28				
315	10	24	32.	-28	51	0	2412160	541465	2	17.29			E2	
316	10	26	4.	-27	23	6	2245740	1325955	2	17.29				
317	10	27	9.	-28	54	1	2103560	510730	2	17.29				
318	10	27	36.	-26	4	3	2072770	2037340	2	17.29			S	
319	10	28	33.	-28	12	2	1944640	896195	2	17.29				
320	10	29	13.	-27	32	5	1869565	1251365	2	17.29				
321	10	29	21.	-27	32	0	1853510	1256000	2	17.29				
322	10	35	0.	-28	52	3	1182500	537965	2	17.29				
323	10	36	16.	-28	12	3	1031890	894715	1	17.29	7.58	18.13		
324	10	38	23.	-26	21	3	776135	1889350	2	17.29				
325	10	38	53.	-26	44	6	716510	1680450	2	17.29				
326	10	39	34.	-26	27	3	633245	1834115	2	17.29				
327	10	40	14.	-28	2	3	563280	984590	2	17.29				
328	10	41	55.	-29	25	3	375390	240620	2	17.29				
329	10	42	23.	-29	46	2	314000	52630	3	17.29				1G1S
330	10	30	33.	-28	43	3	1706500	620115	2	17.30				
331	10	31	56.	-25	16	0	1552735	2474235	2	17.30				
332	10	37	9.	-28	58	1	930645	489155	2	17.30			S	
333	10	38	33.	-25	29	4	750875	2352760	2	17.30				
334	10	38	57.	-27	53	5	714740	1064790	2	17.30				
335	10	40	47.	-28	56	0	505075	504710	2	17.30				
336	10	24	31.	-26	39	3	2438300	1718390	2	17.31				
337	10	31	0.	-28	40	0	1652410	650675	2	17.31				
338	10	32	30.	-26	52	2	1480035	1614815	1	17.31	8.10	18.65		
339	10	35	33.	-28	51	4	1118775	549725	2	17.31				
340	10	36	33.	-25	1	6	992310	2602650	2	17.31				
341	10	38	19.	-25	50	5	781575	2164495	3	17.31				
342	10	39	4.	-27	52	4	700130	1074915	2	17.31				
343	10	39	3.	-27	53	6	703150	1064005	2	17.31				
344	10	39	4.	-28	45	0	705510	504765	2	17.31				
345	10	27	31.	-25	50	5	2084160	2161135	2	17.32				
346	10	32	20.	-27	7	9	1499405	1474050	1	17.32	8.97	18.47		
347	10	37	11.	-26	52	7	921450	1609980	1	17.32	9.21	18.33		
348	10	43	34.	-25	51	8	147370	2144675	2	17.32				
349	10	27	40.	-26	51	1	2058600	1618905	2	17.33				
350	10	29	23.	-27	7	1	1851470	1478720	2	17.33				

ID NO	R.A. (1950.0) H	M	S	DEC. °	′	″	X	Y		V25	R25	B25	TYPE	
351	10	31	19.	-26	55	7	1621690	1582605	1	17.33	9.16			
352	10	32	5.	-25	14	9	1533760	2483590	2	17.33				
353	10	37	21.	-26	58	6	900440	1556630	1	17.33	9.07			
354	10	43	12.	-29	17	3	224120	309780	2	17.33				
355	10	43	41.	-26	17	4	138420	1916125	2	17.33				
356	10	43	41.	-26	17	5	138640	1914995	2	17.33				
357	10	30	34.	-25	31	4	1717665	2335110	2	17.34				
358	10	30	30.	-28	37	2	1711840	679150	2	17.34				
359	10	36	9.	-27	14	7	1045625	1413720	1	17.34	10.81			
360	10	39	35.	-27	20	5	635555	1359375	2	17.34				
361	10	43	46.	-29	42	5	161865	82420	2	17.34				
362	10	28	12.	-29	26	0	1976585	236050	2	17.35				
363	10	34	17.	-27	42	4	1267025	1166755	1	17.35	8.05	17.97		
364	10	35	44.	-28	27	0	1095580	768305	3	17.35			S	SP
365	10	36	21.	-27	28	2	1021280	1292955	1	17.35	9.05			
366	10	36	41.	-28	44	7	985690	609265	2	17.35				
367	10	42	11.	-28	40	1	338330	643720	2	17.35				
368	10	44	24.	-29	14	7	83365	329665	2	17.35				1G1S
369	10	27	33.	-28	5	9	2053630	950410	2	17.36				
370	10	27	51.	-26	47	7	2037320	1650210	2	17.36				
371	10	31	47.	-29	2	7	1560105	447785	2	17.36				
372	10	34	39.	-27	14	3	1224605	1417535	2	17.36				
373	10	38	24.	-26	47	3	775885	1657240	1	17.36	10.55			
374	10	38	45.	-27	43	8	737300	1151645	2	17.36			S	
375	10	41	28.	-26	36	0	406895	1753815	2	17.36				
376	10	27	40.	-26	10	7	2063505	1980540	2	17.37				
377	10	33	27.	-25	54	5	1367565	1593780	1	17.37	6.90			1G1S
378	10	34	10.	-29	1	5	1280680	459400	2	17.37			S	
379	10	35	23.	-26	42	5	1125600	1701925	1	17.37	10.11	18.45	S	
380	10	39	9.	-29	49	7	699865	26275	2	17.37				
381	10	40	3.	-26	44	6	578085	1679065	2	17.37				
382	10	42	29.	-27	14	3	290055	1409750	2	17.37				
383	10	43	27.	-29	25	5	195960	236025	2	17.37			SB (S)	
384	10	28	22.	-25	28	3	1984650	2360865	2	17.38				
385	10	30	26.	-26	23	6	1729080	1868430	3	17.38				
386	10	33	58.	-26	0	9	1305505	2072860	2	17.38				
387	10	35	27.	-26	35	8	1127350	1761700	2	17.38				
388	10	41	4.	-28	40	4	468735	642965	2	17.38			S	
389	10	43	34.	-26	59	0	158255	1544260	2	17.38				
390	10	24	11.	-27	17	1	2457285	1379835	2	17.39				1G1S
391	10	29	55.	-27	55	9	1784940	1042940	2	17.39				
392	10	31	32.	-27	34	3	1593215	1238095	3	17.39		15.94		
393	10	35	35.	-26	50	9	1111235	1626730	1	17.39	8.60	18.39		
394	10	37	17.	-27	50	2	911105	1096035	2	17.39		17.56		
395	10	39	26.	-28	44	6	779355	608975	2	17.39				
396	10	41	23.	-27	4	7	420840	1497625	2	17.39				
397	10	44	15.	-25	14	9	67285	1937170	2	17.39				
398	10	31	7.	-28	40	2	1639550	648565	2	17.40				
399	10	31	6.	-28	40	2	1640625	648435	2	17.40				
400	10	31	50.	-28	38	3	1555160	666445	2	17.40				

ID NO	R.A. (1950.0) H	M	S	DEC. °	′	″	X	Y		V25	R25	B25	TYPE		
201	10	34	1.	-27	45	3	1298175	1140530	1	17.40	9.60				
202	10	37	27.	-26	4	4	886195	2041055	3	17.40					
203	10	40	23.	-25	43	3	530175	2226985	2	17.40					
204	10	40	49.	-28	37	0	498735	673900	2	17.40					
205	10	41	11.	-26	20	9	438820	1889015	3	17.40					
206	10	41	51.	-26	50	0	363835	1539157	2	17.40			S		
207	10	24	34.	-26	19	9	2434640	1891630	2	17.41			S		
208	10	26	27.	-25	24	9	2195850	2300090	2	17.41					
209	10	29	56.	-27	55	9	1782345	1043775	2	17.41					
210	10	34	24.	-25	50	0	1253235	2170600	2	17.41					
211	10	35	34.	-26	21	7	1112825	1887260	2	17.41					
212	10	35	42.	-27	54	6	1099680	1057600	1	17.41	10.31				
213	10	37	33.	-27	5	5	877385	1495000	1	17.41	8.65				
214	10	40	27.	-27	2	7	532465	1517115	2	17.41			SA		
215	10	40	37.	-27	36	4	514130	1215725	2	17.41			S		
216	10	43	32.	-28	6	1	174245	944870	2	17.41					
217	10	24	21.	-27	54	1	2443700	1049795	2	17.42			S		
218	10	26	39.	-28	24	5	2167065	783175	2	17.42					
219	10	27	1.	-26	24	2	2139000	1858845	2	17.42					1G1S
220	10	28	53.	-29	20	8	1887390	283655	2	17.42					1G2S
221	10	32	28.	-28	39	7	1480085	654110	2	17.42					
222	10	33	51.	-25	47	4	1319660	2193650	2	17.42					
223	10	33	59.	-26	7	3	1302930	2015985	2	17.42					
224	10	40	33.	-25	59	5	502840	2081370	2	17.42					
225	10	42	36.	-25	56	7	264920	2103165	2	17.42					
226	10	42	46.	-27	7	3	256375	1472500	2	17.42			S		
227	10	44	17.	-28	49	3	92650	557370	2	17.42					1G1S
228	10	44	37.	-28	44	2	52495	602225	2	17.42					
229	10	28	10.	-26	47	0	1998840	1657065	3	17.43					
230	10	31	9.	-28	45	2	1635595	1604225	2	17.43					
231	10	33	17.	-27	30	2	1386075	1274970	1	17.43	7.33			SP	
232	10	33	16.	-28	30	6	1386985	735935	2	17.43					
233	10	33	40.	-25	26	3	1343420	2382440	2	17.43					
234	10	34	0.	-27	30	9	1301035	1268860	2	17.43					
235	10	34	13.	-29	14	6	1264055	343110	2	17.43					
236	10	34	34.	-25	44	0	1232365	2224100	2	17.43					1G1S
237	10	36	3.	-28	26	6	1053180	771550	2	17.43					
238	10	36	44.	-28	28	4	978405	754905	2	17.43			E2		
239	10	37	47.	-25	56	5	845595	2111165	2	17.43					
240	10	39	2.	-29	22	9	710840	266100	2	17.43					
241	10	39	21.	-28	43	6	671230	616455	2	17.43			S		
242	10	39	22.	-29	27	2	673365	226940	2	17.43					1G1S
243	10	41	15.	-29	0	2	449405	466830	2	17.43					
244	10	27	19.	-25	48	2	2108035	2181380	2	17.44					
245	10	28	2.	-26	39	4	2015115	1724470	3	17.44					
246	10	28	5.	-28	44	8	1995480	603485	2	17.44					
247	10	28	15.	-28	21	3	1972530	809825	2	17.44					
248	10	28	50.	-29	47	3	1901455	46180	2	17.44					
249	10	29	37.	-26	11	1	1829705	1979185	2	17.44					1G1S
250	10	37	6.	-29	12	3	936095	362915	2	17.44					

ID NO	R.A. (1950.0) H	M	S	DEC. °	′	X	Y		V25	R25	B25	TYPE	
351	10	40	33.	-28	35.3	529350	6889665	2	17.44				
352	10	41	51.	-28	44.6	377620	6904860	2	17.44			SP	
353	10	42	1.	-27	30.8	348740	12663515	2	17.44				
354	10	43	31.	-26	58.2	163640	15516695	2	17.44				
355	10	28	23.	-28	21.9	1953925	8008840	2	17.45				
356	10	29	30.	-25	34.5	1846720	2306710	2	17.45				
357	10	35	13.	-27	5.2	1156260	14908455	1	17.45	9.72			
358	10	37	50.	-25	58.7	839575	2091275	2	17.45				2GOS
359	10	37	56.	-29	14.3	839663	3445550	2	17.45			SB	
360	10	38	58.	-28	40.9	715970	6416550	2	17.45				
361	10	43	44.	-25	8.9	121160	2528240	2	17.45				
362	10	44	11.	-29	1.7	106440	4467705	2	17.45				
363	10	24	45.	-28	35.6	2389130	6790715	2	17.46				
364	10	28	43.	-27	31.1	1929840	12630755	2	17.46				
365	10	30	32.	-29	14.7	1704895	3397555	2	17.46			SP	
366	10	31	19.	-28	48.4	1615155	5756305	2	17.46				1G1S
367	10	40	55.	-26	43.0	471195	16922755	2	17.46				
368	10	42	14.	-28	40.7	331230	6384555	2	17.46				1G1S
369	10	24	50.	-26	3.0	2406745	20435805	2	17.47				
370	10	25	25.	-29	40.1	2183905	1060005	2	17.47				
371	10	26	36.	-28	40.9	2170115	6363355	2	17.47			SP	
372	10	28	45.	-25	58.0	1934565	20958705	3	17.47				
373	10	34	27.	-28	36.8	1247760	5805605	2	17.47				
374	10	36	31.	-26	23.5	999725	18707105	2	17.47				
375	10	38	50.	-25	40.0	717015	22582705	2	17.47				
376	10	41	46.	-25	43.7	364025	22205105	2	17.47				
377	10	27	20.	-26	42.6	20997005	16947405	2	17.48				
378	10	31	35.	-28	27.7	1584385	7607555	2	17.48				
379	10	33	9.	-26	22.6	1403045	18795155	2	17.48				
380	10	34	1.	-29	40.4	1297960	1124905	2	17.48				
381	10	35	21.	-26	5.4	11393205	20330005	2	17.48				
382	10	37	50.	-26	32.3	840580	17917805	1	17.48	7.02	18.69		
383	10	40	24.	-29	47.3	554650	465155	2	17.48				
384	10	40	30.	-27	24.3	527455	12238205	2	17.48				
385	10	42	17.	-26	39.0	310145	17256105	2	17.48				
386	10	43	39.	-28	46.2	166215	5866905	2	17.48				
387	10	26	13.	-25	32.0	22340555	2324130	2	17.49				
388	10	26	30.	-27	22.7	2194245	13347905	2	17.49				
389	10	26	52.	-26	54.2	2153425	15902205	2	17.49				
390	10	26	52.	-26	54.3	2153705	15894405	2	17.49				
391	10	27	53.	-29	39.4	2012525	1156155	3	17.49				
392	10	29	7.	-25	39.9	1892410	22580155	2	17.49			SB (S)	
393	10	31	50.	-27	19.3	1558710	13722855	2	17.49		18.28	S	
394	10	34	12.	-25	5.3	1277670	25703005	2	17.49				
395	10	35	26.	-29	19.3	1131320	2958555	2	17.49				
396	10	36	11.	-29	36.4	1045205	1437755	2	17.49				
397	10	37	27.	-28	17.9	873485	9465005	2	17.49				
398	10	37	37.	-27	15.4	870065	14069355	1	17.49	8.31	19.00		
399	10	39	39.	-27	45.5	630640	11386655	2	17.49				
1110	10	43	43.	-28	18.4	154210	8344405	2	17.49				

SUPPLEMENT

	R.A. (1950.0) h m s	Dec. ° ′			V_{25}	R_{25}	B_{25}	Type	Comments
A	10 35 02	-25 03.5	1177000	2586000				SB(r)	420" x 370:"
B	10 34 52	-27 25.4	1200985	1319185	12.72			S	= Two spirals superposed
C	10 32 30	-28 19.5	1477000	834600	~13.2			SB(s)	160" x 107", largest in Klemola 13
D	10 35 50	-28 31.5	1084500	727900	~13.9			SBO:	87" x 74"
E	10 37 01	-29 19.5	948000	298000				SB(rs)	94:" x 50"
F	10 25 20	-29 32.5	2311000	172500				SB(rs)	70:" x 47:"
G	10 34 51	-27 08.6	1199800	1469000	~15.5			E:	~0!4 np ✱ (BS 4162)
H	10 35 17	-27 20.4	1149410	1363090	16.0	13.5			24" sf and sup. N3316

ACKNOWLEDGEMENTS

To my supervisors, Drs M.T. Brück and R.S. Stobie, I proffer warm thanks for encouragement and advice when I needed it, and for patience and forbearance when sometimes it seemed that I didn't.

Harvey MacGillivray and Harold Corwin Jr may have influenced this work more than I immediately realise. I am very grateful to them both. My appreciations, also, to them and to my supervisors for constructive criticism of parts of this thesis.

Mrs J. Shand skilfully handled the typewriting, and Mrs M. Fretwell prepared most of the diagrams.

Thanks is due to the Director and to several members of the staff of SAAO for hospitality and assistance and for various kindnesses shown to me while I was a visitor there.

I am indebted to: the Photographic Laboratories of the Royal Observatory, Edinburgh; R.D. Cannon and the U.K. Schmidt Telescope Unit for the loan of UKST plates, and Harvey, M.G. Smith and E.B. Newell in connection with plates taken at CTIO; Bill Zealey and Graham Smith for measuring them on COSMOS; John Cooke for occasional advice on computer graphics; and Ralph Martin for trouble-shooting in respect of the computer links. Data processing was carried out on the ICL 1906A and, later, on the twin IBM 360/195s and IBM 3032 at the Rutherford Computer Laboratory.

Finally, though words hardly suffice, I would like to thank my parents. They made all the right decisions nineteen to fourteen years ago.

REFERENCES

Non-standard abbreviations are listed below (for other commonly used abbreviations and prefixes, consult Table 1.1):

A & Ap	Astronomy & Astrophysics
AJ	Astronomical Journal
Ap J	Astrophysical Journal
Mem. RAS	Memoirs of the Royal Astronomical Society
MNASSA	Monthly Notices of the Astronomical Society of Southern Africa
MNRAS	Monthly Notices of the Royal Astronomical Society
PASP	Publications of the Astronomical Society of the Pacific

Abadi, H.I., & Edmunds, M.G., 1978. A & Ap 70, 189.

Abell, G.O., 1958. Ap J Supp. 3, 211.

Abell, G.O., 1962. IAU Symp. 15, 213.

Abell, G.O., 1965. A. Rev. Astr. Ap. 3, 1.

Abell, G.O., 1972. IAU Symp. 44, 341.

Abell, G.O., 1975. in Stars & Stellar Systems 9, eds. A. Sandage, M. Sandage & J. Kristian (Chicago: Univ. Chicago Press), p. 601.

Abell, G.O., 1977. Ap J 213, 327.

Abell, G.O., 1978. IAU Symp. 79, 253.

Abell, G.O., & Mihalas, D.M., 1966. AJ 71, 635.

Allen, C.W., 1973. Astrophysical Quantities, 3rd ed. (Univ. London, Athlone Press), p. 292.

Ames, A., 1923. Harvard Circs. No. 257.

Arigo, R., Czuhai, K., Hubbard, E., Noerdlinger, P., & Wisner, K., 1978. Ap J 223, 410.

Arp, H.C., 1965. Ap J 142, 402.

Austin, T.B., Godwin, J.G., & Peach, J.V., 1975. MNRAS 171, 135.

Austin, T.B., & Peach, J.V., 1974. MNRAS 167, 437.

Baade, W., 1928. Astr. Nach. 233, 66.

Bahcall, N.A., 1972. Ap J 177, 550.

Bahcall, N.A., 1973a. Ap J 180, 699.

Bahcall, N.A., 1973b. Ap J 183, 783.

Bahcall, N.A., 1973c. Ap J 186, 1179.

Bahcall, N.A., 1974. Ap J 187, 439.

Bahcall, N.A., 1975. Ap J 198, 249.

Bahcall, N.A., 1977a. A. Rev. Astr. Ap. 15, 505.

Bahcall, N.A., 1977b. Ap J 218, L93.

Bahcall, N.A., 1979. Ap J 232, 689.

Baier, F.W., 1976. Astr. Nach. 297, 295.

Baker, E.A., 1925. Proc. R.S. Edin. 45, 166.

Barbon, R., Benacchio, L., & Capaccioli, M., 1976. Mem. S.A.It., 47, 263.

Bautz, L.P., & Abell, G.O., 1973. Ap J 184, 709.

Bautz, L.P., & Morgan, W.W., 1970. Ap J 162, L149.

van den Bergh, S., 1959. Publ. David Dunlap Obs. 2, 145.

van den Bergh, S., 1966. AJ 71, 922.

van den Bergh, S., 1976. Ap J 206, 883.

van den Bergh, S., 1977a. Vistas Astr. 21, 71.

van den Bergh, S., 1977b. Ap J 212, 317.

van den Bergh, S., 1977c. PASP 89, 746.

Bingham, R.G., & Cousins, A.W.J., 1974. MNASSA 33, 15.

Binney, J., 1977. MNRAS 181, 735.

Braid, M.K., & MacGillivray, H.T., 1978. MNRAS 182, 241.

Bregman, J.N., 1978. Ap J 224, 768.

Brown, G.S., 1974. Ph.D Thesis, Univ. of Texas at Austin (= Univ. Texas Publ. Astron. No. 11, 1978).

Bruzual, A.G., & Spinrad, H., 1978. Ap J 220, 1.

Bucknell, M.J., Godwin, J.G., & Peach, J.V., 1979. MNRAS 188, 579.

Burstein, D., 1979. AAS Photo-Bull. 20, 6.

Butcher, H., & Oemler, A., 1978. Ap J 226, 559.

Byrd, G.G., & Valtonen, M.J., 1979. Ap J 230, 655.

Cannon, R.D., Hawarden, T.G., & Tritton, S.B., 1977. MNRAS 180, 81P.

Carter, D., 1977. MNRAS 178, 137.

Carter, D., 1979. MNRAS 186, 897.

Carter, D., & Dixon, K.L., 1978. AJ 83, 574.

Carter, D., & Godwin, J.G., 1979. MNRAS 187, 711.

Cooke, B.A., Ricketts, M.J., Maccacaro, T., Pye, J.P., Elvis, M., Watson, M.G., Griffiths, R.E., Pounds, K.A., McHardy, I., Maccagni, D., Seward, F.D., Page, C.G., & Turner, M.J.L., 1978. MNRAS 182, 489.

Cooke, J.A., Emerson, D., Nandy, K., Reddish, V.C., & Smith, M.G., 1977. MNRAS 178, 687.

Corwin, H.G., Jr., 1980. MNRAS, in press.

Cousins, A.W.J., 1973. Mem. RAS 77, 223.

Cousins, A.W.J., 1974. MNASSA 33, 149.

Davies, R.D., & Lewis, B.M., 1973. MNRAS 165, 231.

Davis, M., & Geller, M.J., 1976. Ap J 208, 13.

Dawe, J.A., Dickens, R.J., & Peterson, B.A., 1977. MNRAS 178, 675.

Disney, M.J., & Wall, J.V., 1977. MNRAS 179, 235.

Dressler, A., 1978a. Ap J 222, 23.

Dressler, A., 1978b. Ap J 223, 765.

Dressler, A., 1978c. Ap J 226, 55.

Dreyer, J.L.E., 1888. Mem. RAS 49, 1.

Dreyer, J.L.E., 1895. Mem. RAS 51, 185.

Dreyer, J.L.E., 1908. Mem. RAS 59, 105.

Dufor, R.J., van den Bergh, S., Harvel, C.A., Martins, D.H., Schiffer, F.H., III, Talbot, R.J., Jr., Talent, D.L., & Wells, D.C., 1979. AJ 84, 284.

Duus, A., & Newell, B., 1977. Ap J Supp. 35, 209.

Einasto, J., Joeveer, M., & Saar, E., 1980. Nature 283, 47.

Emden, R., 1907. Gaskugeln (Leipzig: Teubner).

Evans, D.S., 1951. MNRAS 111, 526.

Faber, S.M., & Dressler, A., 1976. Ap J 210, L65.

Faber, S.M., & Dressler, A., 1977. AJ 82, 187.

Faber, S.M., & Gallagher, J.S., 1976. Ap J 204, 365.

Faber, S.M., & Gallagher, J.S., 1979. A. Rev. Astr. Ap. 17, 135.

Fairall, A.P., 1978a. MNRAS 183, 59P.

Fairall, A.P., 1978b. Observatory 98, 1.

Fairall, A.P., 1979. MNASSA 38, 24.

Fall, S.M., Geller, M.J., Jones, B.J.T., & White, S.D.M., 1976. Ap J 205, L121.

Felten, J.E., 1977. AJ 82, 861.

Fisher, J.R., & Tully, R.B., 1975. A & Ap 44, 151.

Fisher, J.R., & Tully, R.B., 1979. AJ 84, 62.

Forman, W., Jones, C., Cominsky, L., Julien, P., Murray, S., Peters, G., Tananbaum, H., & Giacconi, R., 1978. Ap J Supp. 38.

Fraser, C.W., 1977. A & Ap Supp. 29, 161.

Freeman, K.C., 1976. in Galaxies, by K. Freeman, R.B. Larson & B. Tinsley (Geneva Observatory).

Gallagher, J.S., 1978. Ap J 223, 386.

Gallagher, J.S., & Ostriker, J.P., 1972. AJ 77, 288.

Giacconi, R., Murray, S., Gursky, H., Kellogg, E., Schreier, E., Matilsky, T., Koch, D., & Tananbaum, H., 1974. Ap J Supp. 27, 37.

Gisler, G.R., 1979. Ap J 228, 385.

Godwin, J.G., 1976. Rep. Dept. Astr. Oxford, 1.

Godwin, J.G., & Peach, J.V., 1977. MNRAS 181, 323.

Godwin, J.G., & Peach, J.V., 1979. Nature 277, 364.

Green, M.R., 1978. Ph.D Thesis, Univ. of Oxford.

Gunn, J.E., & Gott, J.R., III, 1972. Ap J 176, 1.

Gursky, H., & Schwartz, D.A., 1977. A. Rev. Astron. Ap. 15, 541.

Harris, W.E., & Smith, M.G., 1976. Ap J 207, 1036.

Harrison, E.R., & Noonan, T.W., 1979. Ap J 232, 18.

Hausman, M.A., & Ostriker, J.P., 1978. Ap J 224, 320.

Hawley, D.L., & Peebles, P.J.E., 1975. AJ 80, 477.

Helou, G., Salpeter, E.E., & Krumm, N., 1979. Ap J 228, L1.

Herschel, J., 1864. Phil. Trans.

Herschel, W., 1784. Collected Works 1, 157 (London: RS and RAS, 1912).

Hickson, P., 1977. Ap J 217, 16.

Hodge, P.W., 1959. PASP 71, 28.

Hodge, P.W., 1960. PASP 72, 188.

Hodge, P.W., 1971. A. Rev. Astr. Ap. 9, 35.

Hodge, P.W., Pyper, D.M., & Webb, C.J., 1965. AJ 70, 559.

Hoffman, A.A., & Crane, P., 1977. Ap J 215, 379.

Holmberg, E., 1946. Medd. Lunds Astr. Obs. (II), No. 117.

Holmberg, E., 1950. Medd. Lunds Astr. Obs. (II), No. 128.

Holmberg, E., 1958. Medd. Lunds Astr. Obs. (II), No. 136.

Holmberg, E., 1969. Ark. Astr. 5, 305.

Holmberg, E., 1974. A & Ap 35, 121.

Honeycutt, R.K., & Chaldu, R.S., 1970. AAS Photo-Bull. 2, 14.

Hubble, E.P., 1936a. Ap J 84, 158.

Hubble, E.P., 1936b. Ap J 84, 270.

Humason, M.L., Mayall, N.U., & Sandage, A.R., 1956. AJ 61, 97.

Ives, J.C., & Sanford, P.W., 1976. MNRAS 176, 13P.

Johnson, H.L., 1966. A. Rev. Astron. Ap. 4, 193.

Johnson, H.E., & Axford, W.I., 1971. Ap J 165, 381.

Johnson, H.L., & Morgan, W.W., 1951. Ap J 114, 522.

Johnson, H.L., & Morgan, W.W., 1953. Ap J 117, 313.

Jones, J.E., & Jones, B.J.T., 1978. MNRAS 184, 327.

Jones, W.B., Obitts, D.L., Gallet, R.M., & de Vaucouleurs, G., 1967.
Publ. Dept. Astr. Univ. Texas at Austin (II), Vol. I, No. 8.

Karachentsev, I.D., & Kopylov, A.I., 1977. Sov. Astron. Letts. 3, 130.

King, I.R., 1966. AJ 71, 64.

King, I.R., & Hinrichs, E.L., 1967. PASP 79, 226.

Klemola, A.R., 1969. AJ 74, 804.

Kormendy, J., 1973. AJ 78, 255.

Kormendy, J., 1977a. Ap J 214, 359.

Kormendy, J., 1977b. Ap J 218, 333.

Kron, R., 1977. in The Evolution of Galaxies and Stellar Populations, eds. B.M. Tinsley & R.B. Larson (New Haven: Yale Univ. Obs.), p. 334.

Kron, G.E., & Shane, C.D., C.D., 1974. Ap. Space Sci. 30, 127.

Kwast, T., 1966. Acta. Astron. 16, 45.

Limber, D.N., & Matthews, W.G., 1960. Ap J 132, 286.

Lindblad, P.O., 1977. The Messenger No. 10, 20.

MacGillivray, H.T., Martin, R., Pratt, N.M., Reddish, V.C., Seddon, H., Alexander, L.W.G., Walker, G.S., & Williams, P.R., 1976a. MNRAS 176, 265.

MacGillivray, H.T., Martin, R., Pratt, N.M., Reddish, V.C., Seddon, H., Alexander, L.W.G., Walker, G.S., & Williams, P.R., 1976b. MNRAS 176, 649.

MacGillivray, H.T., & Dodd, R.J., 1979. MNRAS 186, 743.

MacGillivray, H.T., & Dodd, R.J., 1980. Preprint.

Materne, J., 1974. A & Ap 33, 451.

Matthews, W.G., & Baker, J.C., 1971. Ap J 170, 241.

Matthews, T.A., Morgan, W.W., & Schmidt, M., 1964. Ap J 140, 35.

Mayall, N.U., & de Vaucouleurs, A., 1962. AJ 67, 363.

Melnick, J., & Sargent, W.L.W., 1977. Ap J 215, 401.

Messier, C., 1781. in Conn. des Temps pour 1784 (Paris), p. 227.

Michard, R., 1979a. A & Ap 74, 206.

Michard, R., 1979b. A & Ap 79, 337.

Morgan, W.W., 1958. PASP 70, 364.

Morgan, W.W., 1961. Proc. Nat. Acad. Sci. 47, 905.

Morgan, W.W., & Lesh, J.R., 1965. Ap J 142, 1364.

Nandy, K., 1979. IAU Colloq. 47.

Nandy, K., Reddish, V.C., Tritton, K.P., Cooke, J.A., & Emerson, D., 1977. MNRAS 178, 63P.

Neyman, J., & Scott, E.L., 1952. Ap J 116, 144.

Noonan, T.W., 1971. AJ 76, 765.

Noonan, T.W., 1972. AJ 77, 134.

Noonan, T.W., 1973. AJ 78, 26.

Noonan, T.W., 1974. AJ 79, 358 (erratum: AJ 80, 252, 1975).

Oemler, A., Jr., 1974. Ap J 194, 1.

Oemler, A., Jr., 1976. Ap J 209, 693.

Okamura, S., 1977. Ann. Tokyo Astr. Obs. (II), Vol. XVI, No. 3.

Ostriker, J.P., 1977. in The Evolution of Galaxies and Stellar Populations, eds. B.M. Tinsley & R.B. Larson (New Haven: Yale Univ. Obs.), p. 369.

Ostriker, J.P., & Hausman, M.A., 1977. Ap J 217, L125.

Ostriker, J.P., & Tremaine, S.D., 1975. Ap J 202, L113.

Peach, J.V., & Beard, J.M.C., 1969. Ap. Letters 4, 205.

Peterson, B.A., 1970. AJ 75, 695.

Pratt, N.M., 1977. Vistas Astr. 21, 1.

Quintana, H., 1979. AJ 84, 15.

Reaves, G., 1956. AJ 61, 69.

Reaves, G., 1964. AJ 69, 556.

Reaves, G., 1966. PASP 78, 407.

Reaves, G., 1967. in Modern Astrophysics, ed. M. Hack (Paris: Gauthier-Villars), p. 337.

Reaves, G., 1977a. PASP 89, 620.

Reaves, G., 1977b. in The Evolution of Galaxies and Stellar Populations, eds. B.M. Tinsley & R.B. Larson (New Haven: Yale Univ. Obs.)., p. 39.

Richstone, D.O., 1976. Ap J 204, 642.

Romanishin, W., Strom, K.M., & Strom, S.E., 1977. Bull. AAS 9, 347.

Rood, H.J., 1969. Ap J 158, 657.

Rood, H.J., 1979. Ap J 233, 21.

Rood, H.J., & Baum, W.A., 1967. AJ 72, 398.

Rood, H.J., & Dickel, J.R., 1978. Ap J 224, 724.

Rood, H.J., & Leir, A.A., 1979. Ap J 231, L3.

Rood, H.J., Page, T.L., Kintner, E.C., & King, I.R., 1972. Ap J 175, 627.

Rood, H.J., & Sastry, G.N., 1971. PASP 83, 313.

Rood, H.J., & Turnrose, B.E., 1968. Ap J 152, 1057.

Rose, J.A., 1979. Ap J 231, 10.

Rudnicki, K., 1963. Acta. Astr. 13, 230.

Rudnicki, K., 1967. Astr. Zh. 44, 77 (= Sov. Astron. 11, 59, 1967).

Rudnicki, K., & Baranowski, M., 1966a. Acta. Astra. 16, 55.

Rudnicki, K., & Baranowski, M., 1966b. Acta. Astra. 16, 65.

Sandage, A., 1961. The Hubble Atlas of Galaxies (Washington: Carnegie Inst. of Washington).

Sandage, A., 1972a. Ap J 173, 485.

Sandage, A., 1972b. Ap J 176, 21.

Sandage, A., 1973a. Ap J 183, 711.

Sandage, A., 1973b. Ap J 183, 731.

Sandage, A., 1975. Ap J 202, 563.

Sandage, A., 1976. PASP 88, 367.

Sandage, A., 1978. AJ 83, 904.

Sandage, A., & Hardy, E., 1973. Ap J 183, 743.

Sandage, A., & Tammann, G.A., 1976. Ap J 207, L1.

Sandage, A., Tammann, G.A., & Yahil, A., 1979. Ap J 232, 352.

Sandage, A., & Visvanathan, N., 1978a. Ap J 223, 707.

Sandage, A., & Visvanathan, N., 1978b. Ap J 225, 742.

Sastry, G.N., 1968. PASP 80, 252.

Schechter, P., 1976. Ap J 203, 297.

Schild, R., & Davis, M., 1979. AJ 84, 311.

Schwarzschild, M., 1954. AJ 59, 273.

Schweizer, F., 1976. Ap J Supp. 31, 313.

Schweizer, F., 1979. Ap J 233, 23.

Scott, E.L., 1962. IAU Symp. 15, 269.

Shane, C.D., 1975. in Stars & Stellar Systems 9, eds. A. Sandage, M. Sandage & J. Kristian (Chicago: Univ. Chicago Press), p. 647.

Shane, C.D., 1956. AJ 61, 292.

Shane, C.D., & Wirtanen, C.A., 1954. AJ 59, 285.

Shane, C.D., & Wirtanen, C.A., 1967. Publ. Lick Obs. 22, 1.

Shane, C.D., Wirtanen, C.A., & Steinlin, U., 1959. AJ 64, 197.

Shao, C.-Y., & Young, A.T., 1965. AJ 70, 726.

Shapley, H., 1933. Proc. Nat. Acad. Sci. 19, 591.

Shapley, H., 1939. Nature 142, 715.

Shapley, H., & Ames, A., 1932. Harvard Coll. Obs. Ann. 88, 41.

Sharov, A.S., 1959. Astr. Zh. 36, 807 (= Sov. Astr. 3, 784, 1960).

Smith, M.G., & Weedman, D.W., 1976. Ap J 205, 709.

Soneira, R.M., & Peebles, P.J.E., 1977. Ap J 211, 1.

Spitzer, L., Jr., & Baade, W., 1951. Ap J 113, 413.

Strom, S.E., Jensen, E.B., & Strom, K.M., 1976. Ap J 206, L11.

Strom, K.M., & Strom, S.E., 1977. in The Evolution of Galaxies and Stellar Populations, eds. B.M. Tinsley & R.B. Larson (New Haven: Yale Univ. Obs.), p. 239.

Strom, K.M., & Strom, S.E., 1978a. AJ 83, 73.

Strom, S.E., & Strom, K.M., 1978b. AJ 83, 732.

Strom, K.M., & Strom, S.E., 1978c. AJ 83, 1293.

Strom, S.E., & Strom, K.M., 1978d. Ap J 225, L93.

Strom, S.E., & Strom, K.M., 1978e. IAU Symp. 77, 69.

Strom, S.E., & Strom, K.M., 1979a. AJ 84, 1091.

Strom, S.E., & Strom, K.M., 1979b. Sci. Am. 240, 56.

Sulentic, J.W., & Tifft, W.G., 1973. Revised New General Catalogue (RNGC)(Tucson: Univ. Arizona Press).

Tammann, G.A., & Kraan, R., 1978. IAU Symp. 79, 71.

Thompson, L.A., 1976. Ap J 209, 22.

Tifft, W.G., 1974. IAU Symp. 58, 243.

Tsubaki, T., & Engvold, O., 1975. AAS Photo-Bull. 9, 17.

di Tullio, G.A., 1979. A & Ap Supp. 37, 591.

Tyson, J.A., & Jarvis, J.F., 1979. Ap J 230, L153.

Tytler, D., & Vidal, N.V., 1978. MNRAS 182, 33P.

de Vaucouleurs, G., 1948. Ann. d'Ap. 11, 247.

de Vaucouleurs, G., 1953. MNRAS 113, 134.

de Vaucouleurs, G., 1956a. Mem. Comm. Obs. No. 13.

de Vaucouleurs, G., 1956b. Vistas Astr. 2, 1584.

de Vaucouleurs, G., 1959. Handbuch der Physik, 53, 311.

de Vaucouleurs, G., 1961a. Ap J Supp. 5, 233.

de Vaucouleurs, G., 1961b. AJ 66, 629.

de Vaucouleurs, G., 1968. Appl. Opt. 7, 1513.

de Vaucouleurs, G., 1971. PASP 83, 113.

de Vaucouleurs, G., 1974. IAU Symp. 58.

de Vaucouleurs, G., 1975. in Stars & Stellar Systems 9, eds. A. Sandage, M. Sandage & J. Kristian (Chicago: Univ. Chicago Press), p. 557.

de Vaucouleurs, G., 1977a. in The Evolution of Galaxies and Stellar Populations, eds. B.M. Tinsley & R.B. Larson (New Haven: Yale Univ. Obs.), p. 43.

de Vaucouleurs, G., 1977b. Nature 266, 126.

de Vaucouleurs, G., & Capaccioli, M., 1979. Ap J Supp. 40, 699.

de Vaucouleurs, G., & Page, J., 1962. Ap J 136, 107.

de Vaucouleurs, G., & de Vaucouleurs, A., 1964. Reference Catalogue of Bright Galaxies (RC1)(Austin: Univ. Texas Press).

de Vaucouleurs, G., & de Vaucouleurs, A., 1972. Mem. RAS 77, 1.

de Vaucouleurs, G., & de Vaucouleurs, A., 1973. A & Ap 28, 109.

de Vaucouleurs, G., de Vaucouleurs, A., & Corwin, H.G., Jr., 1976. Second Reference Catalogue of Bright Galaxies (RC2)(Austin: Univ. Texas Press).

Visvanathan, N., & Sandage, A., 1977 Ap J 216, 214.

Vorontsov-Velyaminov, B.A., Krasnogorskaja, A., & Arkipova, V.P., 1962-8. Morphological Catalogue of Galaxies (MCG; in four volumes)(Moscow).

Waters, S., 1873. MNRAS 33, 558.

Webster, B.L., Goss, W.M., Hawarden, T.G., Longmore, A.J., & Mebold, U., 1979. MNRAS 186, 31.

Weedman, D.W., 1975. Ap J 195, 587.

Weedman, D.W., 1976. Ap J 203, 6.

Welch, G.A., Chincarini, G., & Rood, H.J., 1975. AJ 80, 77.

White, R.A., 1978. Ap J 226, 591.

White, S.D.M., 1976a. MNRAS 174, 19.

White, S.D.M., 1976b. MNRAS 177, 717.

Wilkerson, M.S., Strom, S.E., & Strom, K.M., 1977. Bull. AAS 9, 649.

Yahil, A., & Vidal, N.V., 1977. Ap J 214, 347.

Young, P.J., 1976. AJ 81, 807.

Zwicky, F., 1933. Helv. Phys. Acta. 6, 110.

Zwicky, F., 1937. Phys. Rev. 51, 290 & 679.

Zwicky, F., 1941. Proc. Nat. Acad. Sci. 27, 264.

Zwicky, F., 1942. Proc. Nat. Acad. Sci. 28, 355.

Zwicky, F., 1956. PASP 68, 331.

Zwicky, F., 1957. Morphological Astronomy (Berlin: Springer-Verlag).

Zwicky, F., 1971. Catalogue of Selected Compact Galaxies and of Post-Eruptive Galaxies (Zurich: L Speich Zuerich).

Zwicky, F., Herzog, E., Wild, P., Karpowicz, M., & Kowal, C.T., 1961-8. Catalogue of Galaxies and of Clusters of Galaxies (CGCG; in six volumes)(Pasadena: California Institute of Technology).